Alma Mater Studiorum – Università di Bologna

DOTTORATO DI RICERCA
IN
INGEGNERIA CIVILE, AMBIENTALE E DEI MATERIALI

Ciclo XXVIII

Settore Concorsuale di afferenza: 08A3

Settore Scientifico Disciplinare: ICAR/04

USE OF INDUSTRIAL RECLAIMED FILLER TO MODIFY ASPHALT MIXTURE AND BINDER PERFORMANCES

Advanced rheological performance evaluation and 3D DEM Modeling of bituminous binders and mastics

Presentata da: DOTT. ING. FRANCESCO MAZZOTTA

Coordinatore Dottorato

PROF. ING. ALBERTO LAMBERTI

Relatore

PROF. ING. GIULIO DONDI

Co-Relatore

DOTT. ING. CESARE SANGIORGI

Esame finale anno 2016

ABSTRACT

The mechanical performance of an asphalt mixture is largely dependent on the properties of its constituents and by the way they reciprocally interact in the bituminous layer. In particular, the stress-strain response of the road pavements is closely related to the rheological behavior of the bituminous binder and of its interaction with the finest part of the lytic skeleton. Therefore, it is important to study in the laboratory by means of advanced rheological tests, how mastics (Bitumen-Filler Systems) and mortars (Bitumen-Filler-Sand Systems) react to dynamic loads and thermal stresses. Moreover, the understanding of the contacts mechanisms within the bitumen-filler system, through 3D micro-mechanical models, should allow for a deeper analysis of the mastic rheological behavior. Based on these considerations, in a socio-economic context in which it is necessary to reduce the environmental impact caused by the construction and maintenance of transportation infrastructures, bituminous mastics containing different reclaimed fillers from the industrial production wastes were studied. For this purpose, advanced rheological tests have been first validated and then implemented and combined with the 3D DEM models development. Results showed that the methods used to study the bituminous mastics and mortars allowed to understand the effects due to the addition of innovative and recycled fillers within the mixtures blend, highlighting as these can increase the asphalt mixture performance during its service life.

ABSTRACT ITALIANO

Le prestazioni meccaniche di una miscela di conglomerato bituminoso dipendono in gran parte dalle proprietà dei materiali che la compongono e dalle modalità con cui interagiscono reciprocamente. In particolare, la risposta tenso-deformativa delle sovrastrutture stradali è strettamente legata al comportamento reologico del legante bituminoso ed all'interazione che questo ha con la parte più fine dello scheletro litico. Risulta pertanto di fondamentale importanza studiare in laboratorio, attraverso test reologici avanzati, come mastici (sistema Bitume-Filler) e mortar (sistema di Bitume-Filler-Sabbia) reagiscono alle sollecitazioni dinamiche e termiche imposte. Inoltre la comprensione dei meccanismi di contatto del sistema bitume-filler attraverso modelli micro-meccanici in 3D permette di approfondire l'analisi del comportamento reologico del mastice. Sulla base di tali considerazioni, e in un contesto socio-economio in cui è necessario ridurre l'impatto ambientale causato dalla costruzione di nuove infrastrutture, con i metodi precedentemente descritti, si sono studiati mastici bituminosi contenenti filler da recupero industriale. A tale scopo sono stati prima validati e poi implementanti test reologici avanzati, associati allo sviluppo di modelli 3D. I metodi validati ai fini dello studio del comportamento reologico dei mastici e dei mortar bituminosi, hanno consentito di studiare gli effetti apportati dall'aggiunta di filler innovativi all'interno della miscela, evidenziando quanto questi possano incrementare le prestazioni in opera della misce

TABLE OF CONTENTS

LIST OF FIGURES

LIST OF TABLES

1. INTRODUCTION

The analysis of the flexible pavements response to the stresses imposed by heavy vehicles and temperature change, starts from the rheological study of the bituminous mastics. In fact, the bituminous matrix influences the stress-strain response of the pavement structure in terms of fatigue cracking at low temperatures (high load frequency) and permanent deformations, with consequent rutting phenomenon, at high operating temperatures (low load frequencies). The Filler - Bitumen interaction increases the mastic stiffness, improving the mixture shear-stress response at high operating temperatures; in this conditions, in fact, the bitumen exhibits a deformation response predominantly viscous and its rheological behavior tends to a non - Newtonian fluid. In recent years research has therefore focused its attention on the study and design of bituminous mixtures that were able to optimize the amount and type of filler, searching for high performance standards and reusing waste materials, in order to reduce the environmental impact. In this context, the following work places its bases on the use and the optimization of industrial reclaimed filler able to give to the mixture higher performance than those produced using common mineral filler. In particular, in this thesis bituminous mastics containing three different types of fillers will be studied:

- waste fillers from bleaching clays used for the decoloring process in the food industry;
- rubbery fillers from the mechanical shredding of end of life tires .

The aim of this thesis is also to implement innovative research methods that combine the laboratory rheological evaluation with the 3D numerical modeling of the laboratory tests, in order to better understand the micro-mechanical response of asphalt concrete. Part of the asphalt multiscale model approach will be here used; this approach is fundamental to understand the rheological phenomena, through volumetric study of individual components, morphological identification and mechanical properties analysis in the different size scales (bitumen, cement and mortar) (Figure I.1)

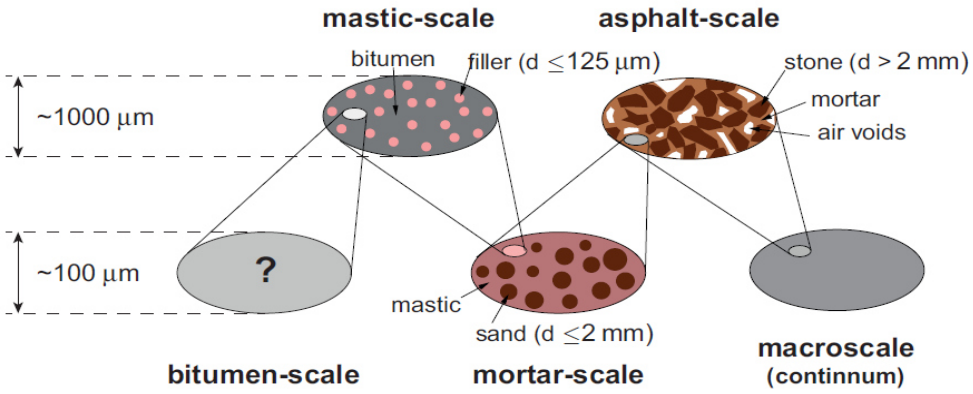

Figure I.1 Asphalt mixture multiscale Analysis

Therefore, the micromechanical analysis associated to rheological analysis at different scales of size, it will allow to analyze the interaction and the role of each mixture constituent material. Through this study will be possible to identify the optimum combination to improve the asphalt layer performance. In particular, with reference to the experimental analysis in the laboratory, binders and the bituminous mastics will be tested using a Dynamic Shear Rheometer (DSR) in different testing configurations. This device is able, through the application of a sinusoidal dynamic load, to simulate the load conditions to which the bitumen matrix is subjected during its service life. Fundamental rheological parameters of the studied mastic will be extrapolated with dynamic tests in linear viscoelastic range and creep tests with different load mode.

In the first analysis, standardized bitumen test will be validated on bituminous mastics containing traditional mineral filler and, in the second analysis the same methods will be applied on mastics containing the industrial reclaimed fillers. With regard to the modelling, the Discrete particle Element Method (DEM) considers particles as distinct interacting bodies, and it is an excellent tool to investigate the micromechanical behavior of mastics. Interactions between particles are considered to be a dynamic process with states of equilibrium developing whenever the internal forces are in equilibrium. Contact forces and displacements of an assembly are found by tracing the movements of individual particles. A commercial three-dimensional DEM code called Particle flow code (PFC), developed by Itasca Consulting Group, was used in this study. In PFC3D, particles are spheres that move independently and interact at contact points. The adoption of micromechanical three-dimensional discrete element approach, will be used to assess the real time-dependent behavior of asphalt mastics

and to predict its performance through the better understanding of its internal interaction. In this way Frequency Sweep Test will be simulated and the numerical results will be compared with the experimental ones. Figure I.2 shows the thesis experimental program.

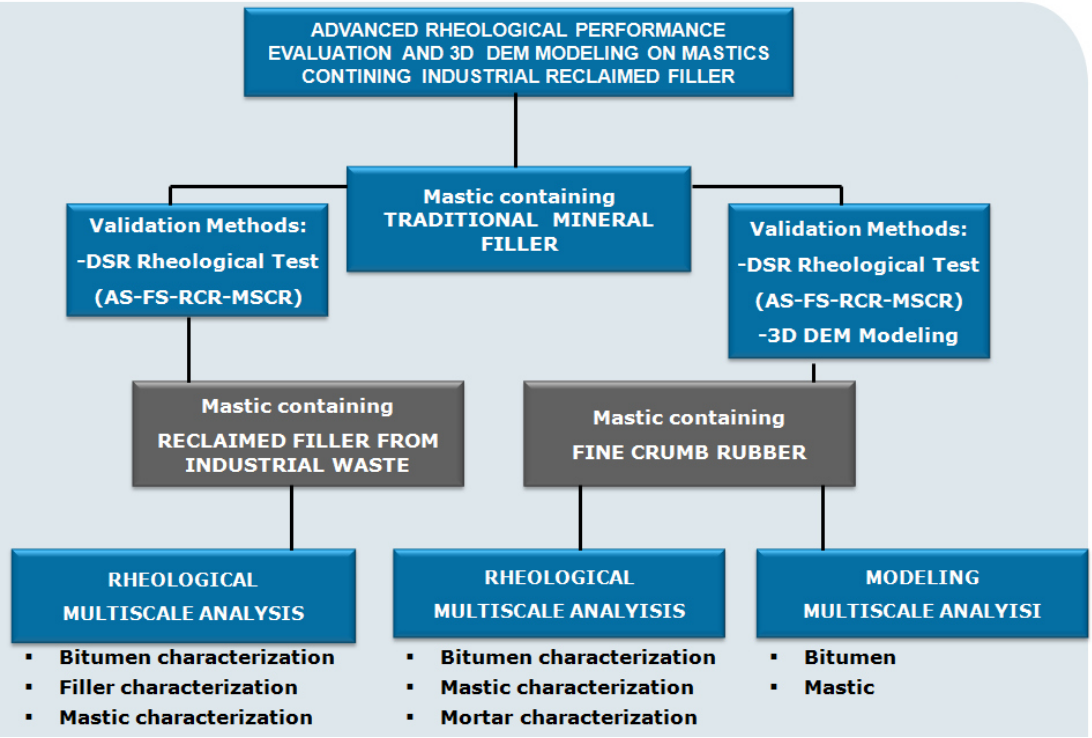

Figure I.2 Experimental program.

Samples production, modeling and test execution were carried out at the School of Engineering and Architecture Engineering of Bologna, in the laboratory of DICAM (Department of Civil, Chemical, Environmental and Materials Engineering), Road section.

In addition, the research related to the study of mastics and asphalt mortar modified with rubber powder from End of Life Tires (ELTs) was performed in collaboration with the laboratories of Nottingham Transport Engineering Centre of the University of Nottingham.

2. LITERATURE REVIEW: MATERIALS

2.1 Introduction

Asphalt mixtures are made of bitumen, filler, fine aggregates, coarse aggregates and air voids. Bitumen is the main element governing the mixture behavior and, with filler it constitutes the adhering agent mastic of the mixture. Incorporating fine aggregates with mastic constitutes the mortar scale; a material that exists between coarse aggregates (Elnasri M. 2014) and reflects the mechanical interactions between fine aggregates and mastic. In this chapter, therefore, the single components in the various scales of study are analyzed. Starting from the analysis of the bitumen and the mineral filler physical and chemical properties, a literature review of the bitumen-filler interaction within the bituminous mastics is needed. Nowadays, however, it is not possible to ignore the study of alternative materials instead of raw materials usually used in the production of asphalt mixtures. Therefore, detailed studies on the use of *non – common fillers* are presented, reviewing literature researches on nanoclays, fillers from C&D and industrial waste materials and fillers from ELTs crumb rubber being adopted within bituminous mortars.

2.2 Bitumen - Filler System: Mastic

2.2.1 Bitumen

2.2.1.1 Bitumen structure and constitution: SARA fractions

Bitumen is a byproduct of the distillation process of the crude oil in refineries. It is an oily, viscous and flammable material. Bitumen properties highly depend on crude oil type and production technology. Production technology is adjusted to the crude oil type: extra heavy, heavy, medium or light. Nowadays heavy oils are processed more frequently than 20–30 years ago, therefore due to the use of different types of crude oils, the distillation residue can differ significantly (Paliukaite M. *et al*. 2014). At room temperature, bitumen has solid texture, color from black to dark brown, and has a thermoplastic behavior, excellent adhesion and water resistance. The bitumen is comparable to a hydrocarbons compounds mixture, with a small amount of structurally analogous heterocyclic species and functional groups containing sulfur, nitrogen and oxygen atoms. Bitumen can be described as a colloidal system consisting of high molecular weight asphaltene micelles dispersed in a lower molecular weight maltenes (resins, aromatics and saturates). Fractional composition of bitumen (asphaltenes, resins, aromatics and saturates) has a large influence on the bitumen performance. Bitumen is widely used in the field of pavement construction due to its excellent mechanical properties, which also depends on bitumen fractional composition (Paliukaite M. *et al.* 2014). Asphaltenes, resins, aromatics and saturates, mostly called SARA, can be determined by various methods. All methods are based on the difference in solubility of the particular chemical groups of bitumen. The traditional method used to determine bitumen fractional composition is column chromatography, commonly known as SARA method. Fractional composition of bitumen are descibed below:

- *asphaltenes* are macromolecules of high molecular weight, responsible for the high viscosity of the bitumen, they represent the specific component. Microscopically are amorphous solids consisting of mixtures of hydrocarbons, have an aromatic structure, that is not cyclic saturated (Figure 2.1);

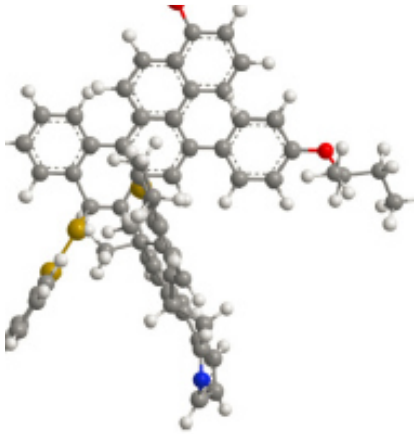

Figure 2.1 Molecular model of asphaltenes ("*Evaluation of bitumen fractional composition depending on the crude oil type and production technology"*).

They are black or brown and insoluble in n-heptane. They are distinguished because of their high polarity, which can be translated as the presence of molecules in which the individual polar bonds are not placed in a perfectly symmetrical manner and therefore not in balance. The molecular weights are very variable, ranging between 600 and 300,000 mol. The evaluation of the molecular weight of asphaltene particles is, indeed, one of the most controversial aspects of the studies on bituminous materials. Asphaltenes, generally, are present in a concentration range between 5% and 25% by weight, and they have a great effect on the bitumen characteristics: as consequence of the percentage increasing of these fraction within the bitumen, it can be noticed a penetration value decreasing, viscosity and softening point increasing (Mazzotta F. 2010). This fraction has a high molecular weight (800–3500 g/mol), and it is insoluble on n-heptane. Their elemental analysis is stable from one bitumen to the other with H/C ratio between 0.98 and 1.56. Their solubility parameter ranges between 17.6 and 21.7 MPa0.5 and their density at 20 °C is close to 1.15 g/cm^3 (Paliukaite M. *et al*. 2014);

- *resins* perform a dispersing action of asphaltenes in oily body of the bitumen and then give it stability and elastic properties. Compounds are soluble in n-heptane, have a structure very similar to that of the asphaltenes; submit to view a dark brown color with solid or semi-solid consistency, similar to that of the whole bitumen. The resins are polar in nature and have remarkable adhesive properties; perform the function of dispersing or peptizers for the asphaltic

macromolecular structures. They are of the co-solvents for oils and asphaltenes, mutually insoluble if not present in appropriate concentrations. Constitute a part of bitumen of between 10% and 25% by weight and have a molecular weight varying between 500 and 50000 (Figure 2.2) (Mazzotta F. 2010). Their solubility parameter ranges between 17.6 and 21.7 $MPa^{0.5}$ and their density at 20 °C is close to 1.15 g/cm3 (Paliukaite M. *et al.* 2014);

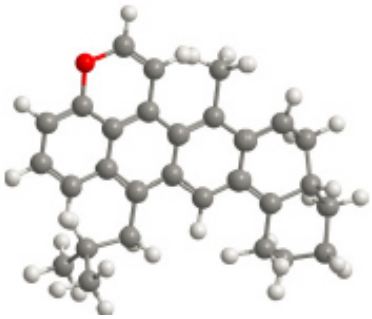

Figure 2.2 Molecular model of resins ("*Evaluation of bitumen fractional composition depending on the crude oil type and production technology"*).

- *maltenic oils* are divided into two classes: saturated and aromatic oils. The division is made according to the types of chemical bonds that prevail in the structure. The aromatic oils are representable as a viscous liquid, characterized by a dark brown color, containing many low molecular weight compounds with aromatic rings. They are made from non-polar carbon chains in which the unsaturated rings systems dominate (aromatic). They have a high solvent power towards the other high molecular weight hydrocarbons. The aromatic constitute is the main bitumen fraction, between 40% and 60% by weight. Their molecular weight is comprised between 300 and 2000 (Figure 2.3) (Mazzotta F. 2010). Their solubility parameter lies between 18.5 and 20 $MPa^{0.5}$ and their density at 20 °C is close to 1.07 g/cm^3 (Paliukaite M. *et al*. 2014);

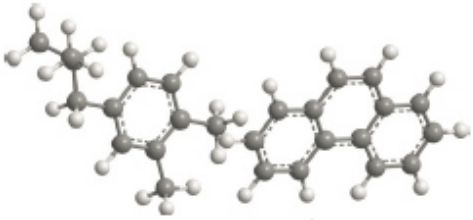

Figure 2.3 Molecular model of maltenic oils ("*Evaluation of bitumen fractional composition depending on the crude oil type and production technology"*))

- *saturated oils* are a viscous liquid, yellowish white in color, composed essentially saturated long chain hydrocarbons, some of which with ramifications, and naphthenes. They are non-polar compounds, of molecular weight similar to that of the aromatics, between 300 and 1500; constitute a percentage between 5% and 20% by weight of the bitumen (Paliukaite M. *et al.* 2014);

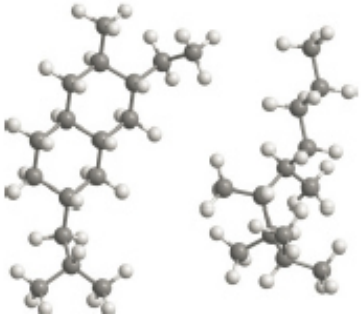

Figure 2.4 Molecular model of satured oils ("*Evaluation of bitumen fractional composition depending on the crude oil type and production technology"*).

Saturated contain the majority of the waxes present in the bitumen, which are in the form paraffin. The saturated and aromatic oils can be considered as elasticizing agents of the bitumen Their solubility parameter is between 15 and 17 $MPa^{0.5}$ and their density at 20 °C is around 0.9 g/cm^3 (Paliukaite M. *et al.* 2014).

2.2.1.2 Bitumen physical and chemical properties

From a physical point of view the bitumen has a typical density between 1.01 and 1.04 g/cm^3. This range is influenced from the crude oil characteristics and it is assumed that the bitumen density is directly proportional to the source oil density. The density depends on the amount and quality of the carbon atoms, and it influences both refining and extraction. The crude oil density is measured in API degrees (American Petroleum Institute) and it is possible to define heavy oils, those having API value smaller than 25 (specific gravity greater than 0.9) and light oils those with API value greater than 40 (lower specific weight of 0.83). Referring to a natural oil is generally called bitumen if its density exceeds $1g/cm^3$ at 15.6 °C. The bitumen has a glass transition around -20

°C, although it varies in a very wide range from +5 ° C to -40 ° C, as a function of the origin of the crude and the production process. Therefore, from a thermodynamic point of view the bitumen is defined as a very viscous liquid at room temperature (Leseur D. 2009). The chemistry of the bitumen study was conducted since the '80s, in the United States, within the Strategic Highway Research Program (SHRP). The chemical complexity of the bitumen analysis lies in its internal composition identified in a mixture of hydrocarbons. As mentioned in the previous paragraphs, the hydrocarbons are chemical compounds formed exclusively from carbon and hydrogen and, according to the proportions between these two elements and to their molecular structure, they are divided into several series:

- *paraffinic or alkanes* are hydrocarbons also called saturated because their molecules are incapable to incorporate other hydrogen atoms from the time that the nature of their links is of simple type. This type of hydrocarbon form linear chains, or branched. The simplest paraffin is methane (CH_4) which is the main natural gas, but there is also ethane (C_2H_6), propane (C_3H_8) and butane (C_4H_{10}). The propane and butane can be liquefied at low pressures and form what is called LPG (Low Pressure Gas) or LNG. The paraffins containing from 5 to 15 carbon atoms molecules are liquid at room temperature and pressure. Above 15 atoms they are extremely viscous or even solid (Leseur D. 2009);
- *naphthenic* are saturated hydrocarbons constituted by one or more rings of carbon atoms, to which may be joined paraffinic side chains. The general formula is C_nH_{2n+2}-$2R_n$ where R_n is the number of rings present in the molecule. The most stable rings are those in 5 (cyclopentane) or 6 (cyclohexane) atoms of C;
- *unsaturated* are hydrocarbons that have at least one double atom carbon bond;
- *aromatic* are hydrocarbons characterized by the presence of an aromatic ring;
- *resins* and asphaltenes are called NSO compounds because in the molecule are present one or more heteroatoms, i.e. atoms different from carbon and hydrogen, and usually are nitrogen (N), sulfur (S) or oxygen (O). This molecular classification of the oils is applied to the corresponding bitumen. For example, the Venezuelan bitumen are generally known as naphthenic. The foregoing shows that the elemental composition of a bitumen resulting from

the extraction source although it is very difficult to make a geographical generalization.

The most abundant element in the bitumen is carbon, typically present between 80-88% by weight, then the hydrogen present between 8-12% by weight. The presence of hydrocarbons is accordingly greater than 90% by weight with a H/C ratio equal to 1.5. The H/C ratio assumes intermediate values between those of the aromatic structures with a H/C equal to 1, and that of saturated alkanes with a H/C close 2. Inside the bitumen are also present, heteroatoms such as sulfur between 0-9% by weight, nitrogen between 0-2% by weight, and oxygen between 0-2% by weight. Generally there are also traces of metals, the most numerous are the vanadium, up to 2000 parts per million (ppm) and nickel up to 200 ppm. The sulfur is generally the more polar atom present, is in the form of sulfides, thiols and, to a lesser extent, sulfoxides. The oxygen is typically present in the form of ketones, phenols, and to a lesser extent, of carboxylic acids. Nitrogen typically shaped structures with pyrrole and pyridine rings and shape even amphoteric species such as 2-quinolones. The chemical bonds that link together the molecules are relatively weak and can easily broken by heating or applying tangential actions, this fact explains the viscoelastic and thermoplastic nature of the bitumen (Leseur 2009). All bitumen molecules can be classified into two functional categories:

- polar;
- non-polar.

The polar molecules form a network and provide to the bitumen elastic properties. Non-polar form a continuous body, arranged around the net, which gives the viscous characteristics to the material. From the relationship between these two molecular classes depends the binder properties. Bitumens having a large amount of non-polar molecules with high molecular weight, show a too brittle behavior at low temperatures. In order to have an accurate bitumen study, it is fractionated in homogeneous molecular groups, through methods that use, as basic principles for the separation the solubility in different solvents, the differences in molecular weight or the detection of particular chemical types. The quantitative relationships between the various components are then determined using these methods to split the bitumen in a few

groups of molecules that have similar properties and can be classified in colloidal schematic. The used methods can be classified into three main categories:

- selective solvent;
- chromatographic techniques of adsorption and desorption;
- chemical precipitation procedures.

The methods using selective solvents provide for the sequential treatment of the bitumen with increasing polarity solvents. Though these methods should avoid contact with the bitumen and supports that could alter, they are not frequently used because they do not allow to isolate those fractions not sufficiently different from each other. On the contrary, chromatographic techniques of selective adsorption and desorption instead have had a remarkable diffusion especially in the field of research (Mazzotta F. 2012). The principle used, common to these methods, is based on the separation of more polar and less soluble components, the asphaltenes, by precipitation in a non-polar paraffinic solvent. The solution obtained is then introduced into a chromatographic column in which the components are first adsorbed by a support alumina then desorbed mediated the use of solvents in greater polarity thus allowing the isolation of the fractions with a gradually increasing polarity. The different techniques can be distinguished depending on the kind of solvent used, depending on the type of porous support employed, and according to the method of which use is made for the quantization of each fraction. The chemical precipitation methods are substantially obtained as a variation of the analytical method developed by Rostler and Sternberg. Once obtained the separation of the asphaltenes by precipitation in n-pentane, the residual solution, composed by malthenes, is treated with increasing concentration solutions of sulfuric acid (H_2SO_4) and then with sulfuric acid fumes containing 30% of SO_3 (sulfur trioxide). The procedure described above allows and favors the precipitation thus allowing a quantitative evaluation of three other molecular classes, having gradually lower reactivity. These are called first acidaffine and second acidaffine. The remaining fractions of malthenes which do not react with sulfuric acid fumes are called paraffins. The Richardson method divides the bitumen into four classes based on solubility in certain solvents:

- *carboidi* are insoluble components in carbon disulfide (CS_2);
- *carbenes* are insoluble components in carbon tetrachloride (CCl_4);

- *asphaltenes* are insoluble elements in low-boiling alkane;
- *malthenes* are soluble elements in the low-boiling alkanes which may, in turn, be further subdivided by the use of chromatographic processes of adsorption and elution. The malthenes facts are first adsorbed on silica gel and then it proceeds to the step elution: respectively, eluting with hexane, toluene, chloride of methylene/methanol are separated saturated oils, aromatic oils and resins.

2.2.1.3 Bitumen colloidal model

The particular properties of the bitumen against mechanical stresses have led to attributing to this a colloidal structure, similar to a particular blend in which a substance is located in a state finely dispersed, intermediate between the homogeneous solution and, the heterogeneous dispersion. Within the bitumen there is a structure able to respond differently to deformation as a function of the load frequencies. Such behavior, as opposed to typical of the newtonian fluids, is only found in bitumen containing asphaltenes; it therefore has a direct association between the colloidal nature and the presence of asphaltene core surrounded by aromatic components with high molecular weight, the resins. Each asphaltene is in the center of a structure, called "micelle", which is surrounded by the resins (the polar character which is proportional to the asphaltene distance); resins interact with the aromatic oils that form the line of the structure and can interface with saturated oils (non-polar phase in which is immersed the micelles). If the amount of resin is high, the asphaltenes are completely solvated or peptizers, this allows the micelles to have good mobility in the bitumen achieving a non-newtonian fluid behavior at high temperatures elastic behavior at low temperatures. A bitumen having such features is called a sol type (Figure 2.5a). In the opposite case, in the absence of resins, asphaltenes are added between them to form a continuous network where the lighter components are limited to fill the voids. It has a fluid type non-newtonian behavior at high temperatures and an elastic solid at low temperatures, the bitumen is defined gel-type (figure 2.5b) (Leseur D. 2009).

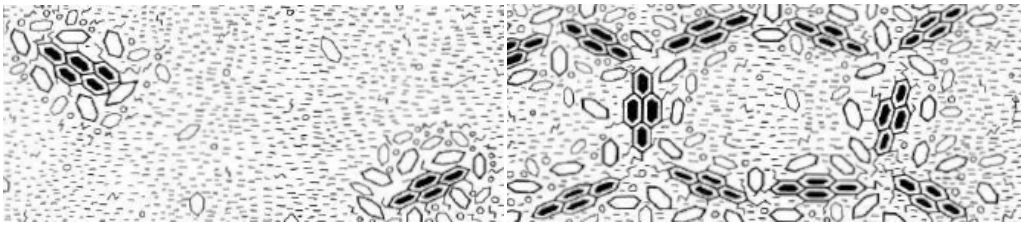

Figure 2.5 a) bitumen sol structure b) bitumen gel structure

In practice the most common bitumens have intermediate features between these two structures. The bitumen behavior depends on the temperature and on the micelles state of aggregations, i.e. from the ratio between asphaltenes, resins, saturated and aromatics. Table 2.1 associates the specific structure to the bitumen compound. The bitumen with "intermediate" behavior have elasticity and better mechanical properties then the sol, while the gel-type bitumens have improved mechanical strength improved, but worse elastic properties.

Table 2.1 Relationship between bitumen components and structure

Structure	**Asphaltenes [%]**	**Resins [%]**	**Malthenes [%]**
Gel	>25	<24	>50
Sol	<18	>36	<48
Intermediate	from 21 to 23	from 30 to 34	from 45 to 49

The bitumen behavior depends on the proportion of saturated oils in the mixture because of their capacity to decrease the solvent power of malthenes on the asphaltenes. As a direct result, high content of saturated can lead to flocculation of the asphaltenes, thereby transforming the structure into another, as similar to that of the gel. If asphaltenes are highly branched, their interaction with the resins is greater, and therefore are less affected by the destabilizing effect of the saturated. From the qualitative point of view the rheological properties of bitumens depend from the asphaltenes amount. It is therefore possible to observe that at constant temperature the viscosity of a bitumen tends to increase wit asphaltenes concentration increasing. At low and average temperatures the bitumen rheology is strongly influenced by the degree of asphaltene agglomerates association and by the presence of other species that favor such associations in the system. It then assumes that in the mixture, an equal asphaltenes content, increasing the percentage presence of aromatic and maintaining

constant the saturated/resins ratio are obtained negligible effects on the rheology and a minimum reduction of the deformability (Leseur 2009). Conversely keeping constant the ratio resin/aromatic and increasing saturated bitumen becomes "softer". In general it is assumed that the increase in the resin content increasing the hardness of the bitumen, in other words increase in viscosity, reducing penetration of the deformability and shear. At the macroscopic level, the behavior of the bitumen is determined by the compatibility and the interactions between the different components in the mixture. To simplify the problem two different synthetic parameters, directly related to the rheological behavior, are defined. Colloidal instability index Ic defined as:

$$I_c = \frac{As+Sa}{Ar+Re}; \quad (2.1)$$

and Rc compatibility ratio expressed by the formula:

$$R_c = \frac{\text{nuclelobases}}{\text{paraffins}}. \quad (2.2)$$

The numerator of the equation 2.1 shows the percentage of molecules that give body to the bitumen (asphaltenes) and the flocculating agents (saturated oils), while the denominator shows the sum of the percentages of solvents (aromatic oils) and of the peptizers (resins) agents. Ratio growing is followed by the transition from a dispersed sol type system to a flocculated gel-type. In equation 2.2 are instead related most reactive components with those less reactive: in general are considered acceptable values higher than 0.5 (Leseur 2009).

2.2.2 Mineral Filler

Mineral filler term refers to the fraction of the mineral aggregate, which mostly passes the 75 μm sieve. Filler can be defined as "*solid material capable of changing the physical and chemical properties of materials through surface interactions and their physical characteristics*". They may contain natural materials such as calcium carbonate, and materials obtained from industrial processes such as fly ash; other common fillers can included silica, kaolinite, mica and feldspar. The most widely used filler in bituminous mixtures is mainly composed of calcite (a form of calcium carbonate) generated from the micro-organisms solidification during the Earth's crust

formation. It may also contain magnesium carbonate, silica, clays, iron oxides and organic material. Also Portland cement is commonly used as filler in the asphalt increasing the mixture durability and its resistance to cracking and rutting failures.

Figure 2.6 a) Limestone Filler b) Portland Cement

The filler is important because of the surface area involved, and that properties of an asphalt pavement may be improved by the use of filler include strength, plasticity, amount of voids, resistance to water action and resistance to weathering; usually asphalt mixtures have been designed to include mineral filler (Liao 2007). Different filler types may be used interchangeably, and different quantities of one type may satisfy a single mixture design (Tunnicliff 1962). Kim *et al*. (2003) studied that the filler type affected the fatigue behavior of asphalt binders and mastics. Fillers stiffen the binders, providing to increase the resistance to micro cracking and, thus, increase fatigue life. Traxler and Miller (1936) classified filler characteristics as follows:

- primary characteristics of fundamental importance: particle size, size distribution, and shape;
- primary mineralogical characteristics of less importance: texture, hardness, strength, specific gravity and wettability;
- secondary characteristics dependent on one or more primary characteristics: void content, average void diameter and surface area.

2.2.2.1 Limestone Filler

The limestone filler is the product of limestone crushing and is configured as a fine aggregate whitish in color and characterized by an amorphous structure. Limestone filler is one of the most suitable materials for the mastics production because of the mineralogical and chemical nature of the origin rock (proportional to its specific surface area and, therefore, the presence of very fine elements); it is, in fact, able to give advantages to the asphalt mixture such as:

- selective absorption of the oils;
- improvement of the thermal susceptibility of the bitumen, due to a decrease in penetration and by a considerable increase in the softening point;
- improvement of binding action and adhesion to the aggregates;
- improvement of mixtures mechanical stability and resistance to the permanent deformations generated by the traffic action and, therefore, a increased strength and durability.

Specifically, the limestone filler should comply with the following requirements:

- calcium carbonate content $\geq 75\%$ by mass; typically $CaCO_3 \approx 95\%$;
- clay content (adsorption of methylene blue) ≤ 1.20g /100g;
- organic content (TOC) for the type L $\leq 0.20\%$ by mass; for the type LL $\leq 0.50\%$ by mass; typically $FeO_2 \approx 0.2\%$ to $\approx 0.4\%$ SiO_2;

2.2.2.2 Portland cement

Cement is a product from the milling and baking stones of various types that, mixed with water, returns with chemical and physical reactions, to its original solid state. It is used as a binder in mixture with inert materials (sand, gravel) to form the mortar and to produce concrete; in this case it is, therefore, used for the construction of buildings and structures in reinforced concrete. It, however, can be used as filler to produce bituminous mastics that, mixed with a suitable size and shape aggregates, improves asphalt mixture characteristics compared to the traditional ones. There are different types of cement, different to the composition, for the strength properties and durability and, therefore, for the use. From the chemical point of view it is in general a mixture of silicates and calcium aluminates, obtained by firing limestone, clay and sand. The material obtained, finely ground, once mixed with water hydrates and solidifies gradually over time. One of the most used cement is Portland cement, which is also configured as the most suitable type of cement to produce mastics. The raw materials for the production of Portland are minerals containing:

- calcium oxide (44%);
- silicon oxide (14.5%);
- aluminum oxide (3.5%);
- iron oxide (3%);

- magnesium oxide (1.6%).

The extraction takes place in the slots arranged near the factory (although this is generally constructed of the material where it is possible to provide, with little expense for transport), which generally have already the desired composition, while in some cases it is necessary to add clay or limestone, or iron ore, bauxite or other waste of foundry materials. The mixture is heated in a special furnace consists of a huge cylinder (called Kiln) horizontally arranged with slight inclination and rotating slowly. The temperature is grown along the cylinder up to about 1480 °C so that minerals are aggregated, but does not melt. At low temperatures calcium carbonate (limestone, stones) splits itself into oxide calcium and dioxide carbon (CO_2); at the high temperatures calcium oxide reacts with silicates to form calcium silicates (Ca_2Si and Ca_3Si). It also forms a small amount of tricalcium aluminate (Ca_3Al) and tricalcium aluminoferrite (Ca_3AlFe). The resulting material is generally referred to as clinker. The clinker may be stored for years before producing the cement, provided to avoid contact with the water. The theoretical energy needed to produce the clinker is about 1700 J/g. This entails a great energy requiring for the production of cement and, therefore, a significant release of carbon dioxide into the atmosphere, greenhouse gases. The powder thus obtained is the cement ready to use, which has obtained a composition of the type:

- 64% of calcium oxide;
- 21% silicon oxide;
- 5.5% of aluminum oxide;
- 4.5% of iron oxide;
- 2.4% magnesium oxide;
- 1.6% sulfates;
- 1% other materials, including especially water.

2.2.3 The role of mineral fillers in asphalt mastics

2.2.3.1Mastic characteristics depending on filler physical properties

Several studies have showed that the filler physical properties affects the bitumen-filler interaction and consequently the mastic stresses response. In particular, Anderson and Goetz (1973) examined the stiffening effect of a series of one-sized fillers ranging

from 0.6 to 75 mm (passing through no. 200 sieves). They concluded that both the size of the filler and bitumen binder composition had a significant influence on the stiffening effect and that a proportion of the bitumen could be replaced by fine filler (<10 μm), but the mixtures produced were very sensitive to changes in the filler type. Chen and Peng (1998) investigated the effect of mineral fillers on tensile strength of bitumen-filler mastics. They found a considerable effect of particle size on tensile strength of bitumen-filler mastics. The 5μm bitumen-filler mastic (size distribution was 100% passing 5μm) exhibited higher tensile strength than the 75 μm bitumen-filler mastic (size distribution was 100% passing 75 μm). At a given filler concentration, smaller particles with higher surface areas carried more tensile loads than bigger ones. If the distance between particles was smaller than the stress concentration area, there would be an overlap area between particles, whereas the strength of the particulate filled composite was deteriorate. In addition to particle size and surface area, filler voids content can affect the mastic stiffness, increasing the shear stress response. Faheem *et al.* (2012) have demonstrated that the Rigden fractional voids can demonstrate the potential of stiffening effect of fillers. Beside they have found that the modified binders could have significantly different interactions with fillers. In terms of mastic volumetrically analysis, several researchers have evaluated the filler-filler interaction and bitumen-filler in the two regions of diluted and concentrated suspensions, in order to assess the stiffening effect that the filler has on the mastic. In a diluted suspension filler particles are limited to hinder the flow of the bitumen because the interparticle distance is compared to the average size of the particles; in a concentrated suspension the interparticle distance is reduced: the stiffness increases so rapidly and the filler-filler interaction and filler-bitumen begins to dominate the rheological behavior of the mastic. Faheem and Bahia (2009) proposed a conceptual model able to determine quantitatively the stiffness influence of the filler on the mastic volume. The graph in Figure 2.7 shows the trend of the ratio between the rigidity of the mastic and stiffness of the bitumen in a simple function of the volume fraction of filler.

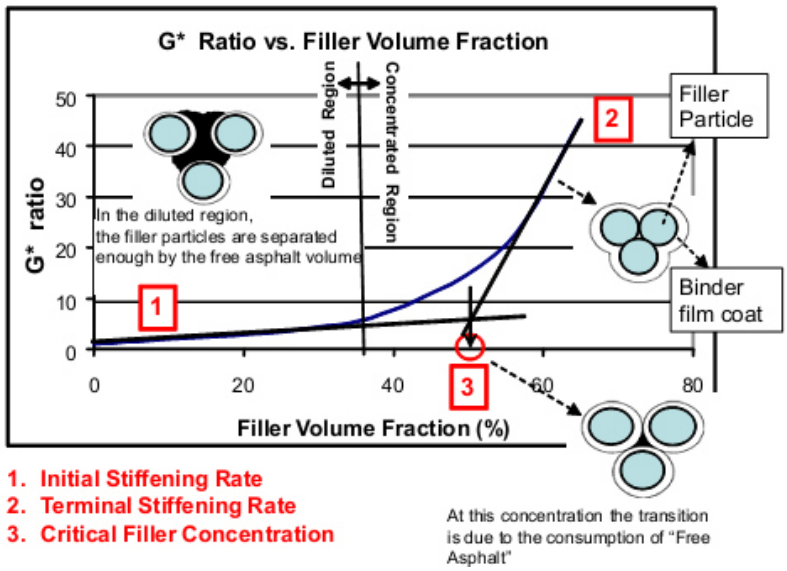

Figure 2.7 G* Ratio vs Filler volume fraction ("*Conceptual phenomenological model for interaction of asphalt binders with mineral fillers*").

The model introduces three definitions:

- *initial stiffening rate:* stiffness increase in the diluted region. The mastic stiffness increasing is low and exhibits a linear characteristic;
- terminal stiffening rate: stiffness increase within the concentrated region, due to the free bitumen and bitumen-filler interaction;
- critical filler concentration: the value of the volumetric concentration of filler in correspondence of the passage from dilute to concentrated phase to phase, obtained by the intersection between the two asymptotic lines.
- the evaluation of the critical volume of filler is needed because a too high amount would lead to an increase of the fatigue resistance but also a worse performance of the bituminous conglomerate in terms of rutting resistance.

The rheological behavior of mastic is influenced by the distribution, the size, the degree of dispersion and by the specific surface of the filler particles. Several studies showed that between bitumen and filler there is a chemical interaction; however, this reaction does not go to influence the linear viscoelastic behavior of the mastic: what matters most is the volume fraction of filler. The filler particles, at the time of mixing, are incorporated as a part of the bitumen and can absorb the fraction of light oils of the same leading, therefore, to stiffening. The amount of bitumen that coats the filler particles is called fixed bitumen

and represents the solid phase of the mixture, while the remaining quantity is called the free bitumen and represents the fluid phase (Figure 2.8).

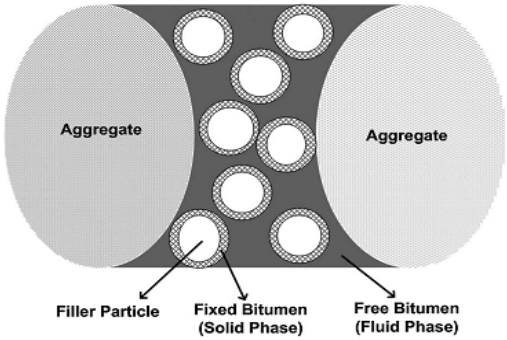

Figure 2.8 Schematic diagram of bitumen-filler system (*Fatigue Characteristics of Bitumen-Filler Mastics and Asphalt Mixtures*)

The actual volume of filler will thus be greater, as the actual solid phase is formed by the filler particles coated by the:

$$V_f = \frac{\frac{M_f}{S_f}}{\frac{M_b}{S_b}+\frac{M_f}{S_f}} \tag{2.3}$$

$$V_{fe} = \left(\frac{100}{V_{fR}}\right) \cdot V_f \tag{2.4}$$

Where:

- M_f = mass of filler in putty [GSF = filler density [g / cm3];
- M_b = mass of the bitumen in the sealing compound [g];
- S_b = bitumen density [g/cm3];
- V_{fR} = maximum volume fraction of filler granules in a dry sample compacted.

2.2.4 The role of mineral fillers in asphalt mixtures - The Stone Mastic Asphalt (SMA)

Mineral fillers serve a dual purpose when added to asphalt mixtures. The proportion of mineral filler that is finer than the thickness of the asphalt film blends with asphalt cement binder to form a mortar or mastic that contributes to improved stiffening of the mix. Particles larger than the thickness of the asphalt film behave as mineral aggregate and hence contribute to the contact points between individual aggregate particles (Puzinauskas 1969). Furthermore, they affect the workability, moisture sensitivity,

stiffness and ageing characteristics of Hot Mix Asphalt (HMA) (Mogawer *et al*. 1996). Also, fillers vary in gradation, particle shape, surface area, void content, mineral composition, and physico-chemical properties and, therefore, their influence on the properties of HMA mixtures also varies. The maximum allowable amount should be different for various types of filler. The filler also influences the optimum asphalt content (OAC) in bituminous mixtures increasing the surface area of mineral particles and, simultaneously, the surface properties of the filler particles modify significantly the rheological properties of asphalt such as penetration, ductility, and also those of the mixture, such as resistance to rutting. In order to improve the pavement performance, it is necessary to ensure that adequate behavior of the bituminous mixtures is achieved, which depends essentially on their composition (Muniandy *et al.* 2013). Therefore, selecting the proper type of filler in asphalt mixtures would improve the filler's properties and, thus, enhance the mixture's performance (Kandhal 1981). Several studies investigated the use of cement bypass dust (CBPD) as filler in asphalt concrete mixtures. Results indicated that the substitution of cement with limestone filler produces the same optimum asphalt binder content as the control mixture without any negative effect on the asphalt's concrete properties (stability, flow, and voids in total mix, mineral aggregate, and those filled with asphalt). Kandhal and Parker (1998) stated that the influence that mineral filler can have on the performance of HMA mixtures depended on the particle size, fines can act as a filler or an extender of asphalt cement binder. In the latter case, an over-rich HMA mix can lead to flushing and rutting. In many cases, the amount of asphalt cement used must be reduced to prevent a loss of stability or pavement bleeding. Some fines have a considerable effect on the asphalt cement, making it act as a much stiffer grade of asphalt cement as compared with the neat asphalt cement grade and, thus, affecting the HMA pavement performance, including its fracture behavior. Tayebali *et al*. (1998) investigated the possibility of increasing the amount of fines in asphalt mixtures based on a washed sieve analysis, from a maximum of about 8% as currently specified, without adversely affecting the performance of the mixture. At the same time, it was also desirable to investigate the influence of the mineral filler type (crushed versus natural river sands, or combinations thereof) on asphalt (Marshall) mix design and on the shear permanent deformation performance. They found out that by increasing the amount of mineral

filler, the Marshall stability and unit weight increased. This procedure led to a higher shear resilient modulus due to increased unit weight without adversely affecting its rutting during the repeated shear testing. Previous research by Superior Performing Asphalt Pavements (Superpave) Mix Design (1996) showed that the addition of mineral fillers such as LSD to asphalt could improve the rutting resistance performance of asphalt. The mineral powder improved the high-temperature thermal properties, presumably because of its small particle size which resulted in a large area of interface between mineral powder and asphalt. Kallas and Puzinauskas (1967) believed that filler performed a dual role in asphalt-aggregate mixtures. A portion of the filler with particles larger than the asphalt film will contribute in producing the contact points between aggregate particles, while the remaining filler is in colloidal suspension in the asphalt binder, resulting in a binder with a stiffer consistency. They also found that the stabilities of asphalt mixtures increased up to a certain filler concentration, then decrease with additional filler. Muniandy *et al.* (2013) found that filler type and particle size directly affect the engineering properties of the asphalt mixtures. In addition to filling the voids, the fillers' components interact with the binder present in the mix, potentially making it stiff and brittle. The change in mix properties is strongly related to the properties of the filler.

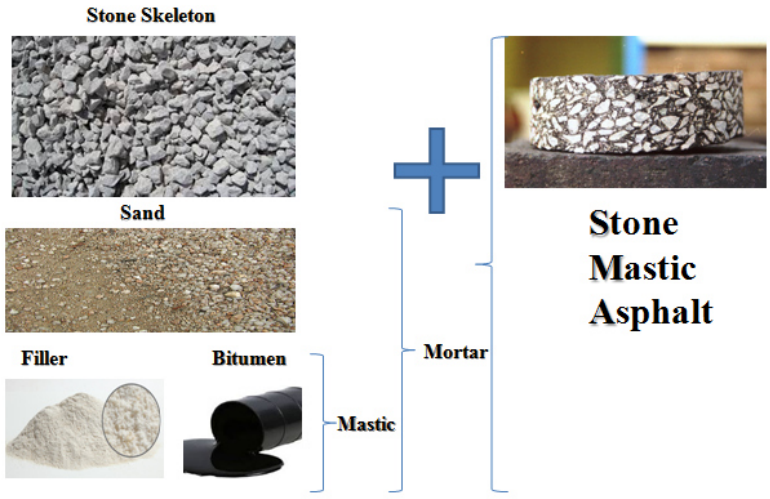

Figure 2.9 Stone Mastic Asphalt composition

The effect of mineral fillers is more prominent in gap graded asphalt mixtures such as the Stone Mastic Asphalt (SMA) mixture that contains large amounts of fines. The SMA (or "non-slip wear mixture") is a closed waterproof mixture, created by mixing

the lytic aggregate skeleton (crushed stone, gravel, sand, all by crushing) in hot-kneaded with a mastic obtained by mixing modified bitumen and filler (and sometimes fibers that reinforce the mixture) (Figure 2.9). Mixture voids, resulting from the granular composition, are filled by the bituminous mastic made from modified bitumen and filler characterizing the asphalt mixture by high consistency and cohesion.

2.4 Bitumen - Filler - Sand System: The Mortar

A simple recipe of a mortar mixture can be represented by idealized mixtures (Elnasri 2014). Idealized mixture that contains fine aggregates of one size has been studied to simplify the complexity provoked by including various aggregate sizes in one mixture. Deshpande *et al.* (2000) prepared idealized mixtures of particle size from 2.36 to 1.18 mm, 600 to 300 μm, and 300 to 150 μm with 50 pen bitumen grade. Cylindrical specimens were manufactured by casting in prepared moulds through compaction in three layers by a mechanical plunger. Uniaxial constant stress and strain rate tests were performed at temperatures ranging from 0 to 40°C. The temperature dependency of the mortar steady state deformation was seen to be governed by the bitumen unconstrained by the aggregates. The stiffening effect of single sized aggregates was measured by a stiffening factor 'S' included in the MCM. Also two types of idealized mixtures of 64% aggregate volume (300 to 600 μm size) and 75% aggregate volume (37.5% of 150 to 300 μm, and 37.5% of 1.18 to 2.36mm) were tested in triaxial by Deshpande *et al*. (1999) at 20°C. Again, the idealized mixes steady state had the same shape as the steady state of pure bitumen. The inclusion of fine aggregates increased the stiffness of the material and was found to increase with increasing the confinement pressure and the volume fraction of aggregates independent of the aggregate size. However, with larger fraction of aggregates the constitutive relationship may change from the pure bitumen as suggested. Khanzada (2000) followed the work of Deshpande and studied the deformation behaviour relationships of idealized mixtures with the same volumetrics, applied in uniaxial static compression, repeated load axial (RLA) and simulative wheel tracking tests. Specimens were manufactured through vibratory compaction with variation in density between specimens compacted in a single layer and compacted in three layers being less than 1%. The results from the uniaxial creep tests showed that above 500 kPa, the SSSR fitted a straight line with a slope of 2.4 indicating nonlinear behavior. Less than 70 kPa, the experimental points fitted a straight line with a slope of approximately 1 by means of linear behavior. The RLA standard test applied stresses ranging from 50 to 100 kPa and the plot of the SSSR against the stress level showed a power law relationship with a slope varying from 1.1 to 1.5. These relatively lower slope values compared to the static creep test were due to the lower operating stresses in the equipment. Therefore, it was pointed

out that the repeated loading technique could be utilized to rank rutting potential but with the inability to fully characterize the deformation behavior. Finally for laboratory scale wheel tracking tests on idealized mixtures over stresses ranging between 500 and 1500 kPa, the steady state rut rate after exceeding the linear region followed a nonlinear trend with a creep exponent that ranged from 1.9 to 2.4, similar to the creep exponent in the static creep test. It was therefore concluded that the static creep test proved to have the potential of characterizing materials in terms of rutting resistance (Elnasri 2014). Elnasri (2014) developed a new type of mortar that from mastics. The researcher found that the fine aggregates stiffening effect in shear, uniaxial compression, and triaxial testing. In particular in his research Elnasri asserts that the resistance to shear deformation was found to be controlled by the filler content more than fine aggregate, however, fine aggregate affects more the shear stress linearity limit. On the other hand, the sensitivity of the linearity stress limit to the bitumen content is only at high temperature. Moreover from the single shear creep recovery results, a trend similar to the binder was obtained between the recovered strain and total strain comprising a linear relationship followed by a constant recovered strain stage. Interestingly, the mortar attained higher recovery than mastic in the linear stage. Nevertheless, the constant recovered strain level was reached earlier in mortar than mastic in the constant stage (Elnasri 2014) (Figure 2.10).

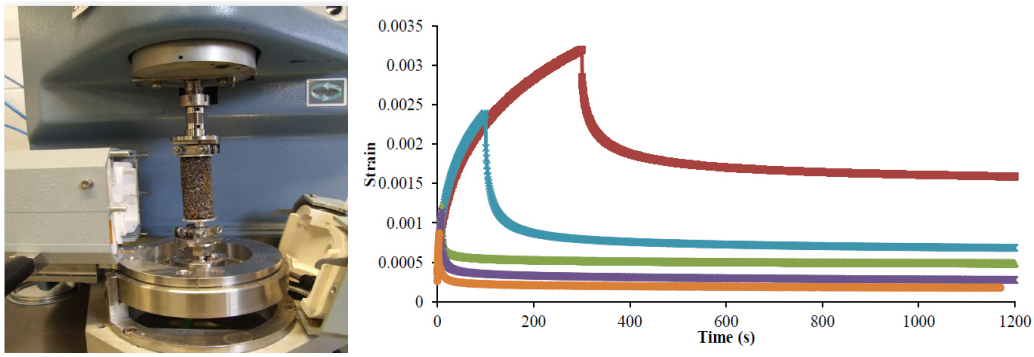

Figure 2.10 Mortar test device and Mortar creep test at 10kPa (*From binder to mixture; multiscale permanent deformation behavior*).

2.5 Bitumen modified with non-traditional filler

2.5.1 Nanoclay filler in bituminous mixtures

Nanoparticles used as fillers to modify binders and asphalt mixtures desired have receiving an increased interest for research and development. Various types of nanoparticles, including nanoclays, are currently used to modify the bitumen performances. Many studies have shown that nanoclays and montmorillonite change the behavior of bituminous materials, however, before to describe the rheological effect on bituminous materials it may be necessary to understand the properties of nanoclay filler. Common clays are the naturally occurring minerals and thus subjected to natural variation in their formation. The purity of the clay can affect the final nanocomposite properties. Clay mostly consist of alumina–silicates, which have a sheet-like (layered) structure, and consist of silica SiO_4 tetrahedron bonded to alumina AlO_6 octahedron in a various ways. A 2:1 ratio of the tetrahedron to the octahedron results in mineral clays; however, the most common one is montmorillonite (Figure 2.11) (Ghaffarpour Jahromi.and Khodaii 2009).

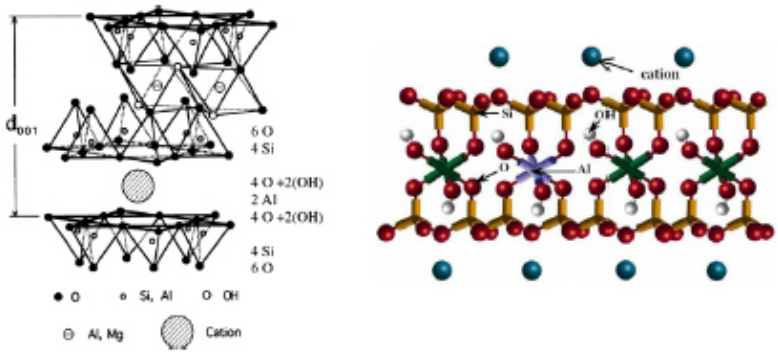

Figure 2.11 Montmorillonite structure (*"Effects of nanoclay on rheological properties of bitumen binder"*)

The thickness of the montmorillonite layers (platelets) is 1 nm with high aspect ratios, typically 100–1500 (Grim 1959). The expansion of montmorillonite is determined by their ion (e.g. cation) exchanging capacities, which can vary widely. One of the characteristics of these types of clay is the cation exchange capacity (CEC), which is a number for the amount of cations between the surfaces. The CEC of montmorillonite ranges from 80 to 120 meq/100 g (milli-equivalents per 100 g); whereas, kaolinite have CEC values ranging between 3 and 5. The expansion pressure of montmorillonite is

very high in which sodium ions constitute the majority of the adsorbed cations (called Na-montmorillonite), leading to exfoliation and dispersion of the crystal in the form of fine particles or even single layers. When Ca^{2+}, Mg^{2+} and ammonium are the dominant exchangeable cations, dispersion is low and the size of the particle is relatively large. Separation of clay discs from each other results in a nanoclay with a large active surface area (it can be as high as 700–800 m^2/g). This helps to have an intensive interaction between the nanoclay and its environment (bitumen in our case). In process, realizing the separation (surface treatment) depends upon the type of material mixed. A necessary prerequisite for successful formation of polymerclay nanocomposite is, therefore, alteration of the clay polarity to make it 'organophilic'. To achieve fine dispersion, mechanical forces alone are not sufficient; rather, there should be a thermodynamic driving force to separate the layers into the primary silicate sheets. This thermodynamic driving force is being introduced by inserting a certain coating of surfactants (an agent such as detergent, which reduces surface tension) on each individual layer (Ghaffarpour Jahromi and Khodaii 2009). These surfactant molecules increase the layer distance. They, moreover, improve the compatibility with the polymer and can give an increase in entropy because they can be mixed with the polymer. Organophilic clay can be produced normally from hydrophilic clay by ion exchange with an organic cation. The organic reagents are quaternary ammonium salt with alkyl chains such as 12-aminododecanoic acid (ADA), octadecanoic alkyl trimethyl quaternary ammonium salt. Addition of a positively loaded surface active material will in this case form an ADA layer around each clay disc, and consequently changes from a hydrophilic into a hydrophobic disc. These modified clay discs will be separated automatically in water and can be used as nano particles. The proper selection of modified clay is essential to ensure effective penetration of the polymer into the interlayer spacing of the clay and so resulting in the desired exfoliated or intercalated product. In intercalate structure, the organic component is inserted between the clay layers in a way that the interlayer spacing is expanded but the layers still bear a well-defined spatial relationship to each other. In an exfoliated structure (Fig. 4), the layers of the clay have been completely separated and the individual layers are distributed throughout the organic matrix (Ghaffarpour Jahromi and Khodaii 2009). Saeed Ghaffarpour Jahromi and Khodaii (2009) have performed rheological

dynamic test on bitumen samples modified with nanoclay. They have proved that the nanoclay modifications help to increase the stiffness and ageing resistances. The authors' proposed approach has shown that when bitumen was modified with small amount of nanoclay, its physical properties were successfully enhanced on the condition that the clay disperses at nanoscopic level. Nanoclay materials possess big aspect ratio and large surface area and their particles are also not niform in size and arrangement. The nanofil particles are curly and smaller in size, compare to the cloisite particles. The existing plastic limit of nanoclay shows that it is an expansive characteristics material. Therefore, a low percent of nanoclay in bitumen leads to the changes in rheological parameter, decreasing penetration and ductility as well as increasing softening point and ageing resistance. DSR results also show that the complex modulus (G*) increases by decreasing temperature and/or increasing frequency whereas the phase angle increases as temperature increases and/or frequency decreases. On the other hand, in modified bitumen temperature susceptibility is lower compare to unmodified bitumen. The results confirm that addition of the nanoclay had a significant effect on the internal structure of the blends and, therefore, on its rheological behavior. In polymer modified bitumen, the main differences appeared at low frequencies or high temperatures, for example, from the onset of the Newtonian behavior. Generally, the elasticity of the nanoclay modified bitumen is much higher and the dissipation of mechanical energy much lower than in the case of unmodified bitumen. Nanoclay and bitumen showed easy and higher compatibility compare to bitumen and polymer that need special method to blend. Therefore, a physical mix of the bitumen and nanoclay lead to nonocomposite, in which the intercalation in the nanoclay layers is mainly due to bitumen molecules, while the bitumen/polymer interactions are completely different. A different morphology was obtained in modified bitumen. Nanoclay that was present in a small quantity with respect to the total asphalt content, remained bonded with the bitumen macromolecules and may have significantly affected the overall properties. Finally, it can be concluded that nanoclay modification increases the stiffness of bitumen and decreases the phase angle compare to unmodified bitumen; hence, this can reduce ageing effect on bitumen too.

2.5.2 Filler from waste materials in bituminous mixtures

2.5.2.1 Filler from Construction & Demolition (C&D) waste materials

The increase of civil infrastructures has led to a fast decrease of available natural resources, and seeking for other alternative is crucial. Recycling aggregates or fillers from the construction and demolition (C&D) waste is one of the preferable and environmental friendly solutions. The effective utilization of waste cement concrete is to gain Recycled Concrete Aggregate (RCA), which can be reused in asphalt concrete. Chen *et al.* (2011) have studied the effects of waste cement concrete filler in asphalt mixture replacing conventional limestone powder. The authors to investigate the properties of the recycled filler on the asphalt mixtures, at high temperatures, have conducted creep tests in load axial configuration. From the results of dynamic creep tests, they have shown that the mixture with traditional limestone filler has a higher creep strain than that with reclaimed cement concrete. The waste cement powder increases the stiffness modulus at high temperatures improving asphalt mixtures permanent deformation resistance (Chen M-Z. 2011). In addition, several researches have investigated the effect of using waste cement dust as mineral filler on the mechanical properties of asphalt mixture, and the results indicated that cement dust can totally replace limestone powder in asphalt paving mixture. Also using waste lime as mineral filler can improve the permanent deformation characteristics, stiffness and fatigue endurance of asphalt mixture. Recycling waste bricks as filler for asphalt mixture may be an economic way in road and construction engineering, which can enlarge the application range and improve the utilization rate of C&D waste. Chen M-Z. *et al.* (2011) have investigated the mechanical properties of asphalt mixtures using brick powder as mineral filler, conducting indirect tensile strength and modulus, static and dynamic creep and fatigue tests to evaluate the properties of asphalt mixtures. They have shown that the mixture with recycled brick filler had higher indirect tensile modulus at 40°C, which indicated that the mixture with recycled brick filler exhibit better rutting resistance than the control mixture. As compared with the limestone filler in this study, the addition of recycled brick filler could improve the water sensitivity and the fatigue life of asphalt mixtures. The addition of recycled brick filler could also significantly decrease the permanent deformation at 60°C by both static and dynamic

creep tests, which result in better rutting resistance of asphalt mixture at high temperature.

Based on these researches above, the use of such waste powders as filler in asphalt mixture not only has no negative influence on asphalt mixture, but also can improve its engineering characteristics.

2.5.2.1 Filler from industrial waste materials

There are now many studies on scrap and/or waste materials used as fillers in addition or in substitution of raw materials in the production of asphalt concretes (Melotti R. *et al.* 2014). Melotti et al. (2014) on their paper *"A preliminary investigation into the physical and chemical properties of biomass ashes used as aggregate fillers for bituminous mixtures"* have evaluated morphological, physical and chemical characteristics of 21 different ashes and two traditional fillers (calcium carbonate and ''recovered'' plant filler). They found that the biomass ashes can be an alternative to natural filler in bituminous mixtures. In particular in this paper the main filler characteristics are analyzed through grading analysis (investigated by sieve analysis), water content (EN 1097-5), harmful fines (EN 933-9), particle density (EN 1097-7), voids of dry compacted filler (EN 1097-4), variation in ''Ring and Ball'' temperature (EN 13179-1) and water solubility (EN 1744-1). Beside the authors have investigated the main research on this topic, writing a completely literature review, extrapolated below: "European Directive 2009/28/CE defines biomass as the biodegradable fraction of products, waste and residues from biological origin from agriculture (including vegetal and animal substances), forestry and related industries including fisheries and aquaculture, as well as the biodegradable fraction of industrial and municipal waste. It is essentially any organic matter which contains stored solar energy and can, therefore, be used as an energy source. In this context, fossil fuels are not considered to be biomass. Fly and bottom ashes represent the main residues of a combustion process: they are composed of mineral materials (in their oxidized form) absorbed by the biomass during its lifecycle or incorporated during harvesting and of a small quantity (up to 20%) of unburned organic matter. The amount of ashes produced depends on combustion chamber conditions and biomass type, with values that vary between 2% (i.e. woodchips) and 20% (i.e. rice husk). Bottom ashes, which settle under the grate

of the combustion chamber, are the coarsest and heaviest constituent part of the combustion by-products, while fly ashes, which remain suspended in the flue gases, are the finest part. Fly ashes representnup to 40% of the total ashes produced and are usually removed through electrostatic precipitators and fabric-filter baghouses. The recycling of biomass ashes as construction materials meets the recommendations of the European Directive on waste 2008/98/ CE and has significant environmental benefits related to the decrease in the quantity of natural aggregates extracted from quarries and to the reduction of waste carried to landfills. In Italy, since the European Waste Catalogue (European Commission Decision 2000/532/CE) classifies waste from biomass combustion as a non-hazardous material, a simplified procedure (Regulation DM 05/02/98), requesting a communication of intent rather than a submission for formal authorisation for recycling these types of ashes, is sufficient. According to this regulation, biomass ashes can only be recycled in concrete, cement and brick production, in embankment construction and environmental re-use, but not other applications such as the production of bituminous mixtures. In this case, the usual authorisation procedure is required. In Italy, as a result of legal constraints, the majority of these ashes are taken to landfills, involving considerable transportation, processing and disposal costs. Their re-use in bituminous materials could make a significant contribution to a reduction in ash disposal costs when one considers that 34.9 million tons of bituminous mixtures were produced in Italy in 2009 (EAPA, 2009). Bituminous mixtures are basically composed of aggregates of different sizes, filler and bitumen. Fillers are mineral grains most of which pass at 63 lm sieve (EN 13043), and represent 5–10% of the aggregates by weight in the whole mixture. Filler can have a natural origin when derived from the crushing of rocks, or can be manufactured in industry as in the case of lime, cement, ash and slag. Although its main function is filling the voids in the aggregate skeleton to create a denser mixture, several studies have demonstrated that filler has other important roles. Depending on its particle size and structure, it stiffens and/or extends the binder (Kandhal and Parker, 1998; Grabowski and Wilanowicz, 2008), consequently affecting the occurrence of rutting and fatigue phenomena. Furthermore, filler also modifies the ageing processes (Gubler *et al.,* 1999; Recasens *et al*., 2005) and its finest part may act as an anti-stripping agent preventing moisture damage (Kandhal and Parker, 1998). Although its

importance is well recognised, most recent regulations on filler for bituminous mixtures (EN 13043, ASTM D242, AASHTO M17) establish limits for only a few characteristics such as grading, water content, plasticity index and organic content. In addition, the Superpave volumetric mix design system (Cominisky et al., 1994) defines a limit for the quantity of filler in the mixture (corresponding to a filler/binder ratio in the range 0.6–1.2 by weight). The above mentioned characteristics are necessary primarily for quality control, but are not sufficient to obtain information correlated with the expected performance of bituminous mixtures. This is even more evident for manufactured fillers, like biomass ashes, which often exhibit unique behaviours. The study described in this paper is part of RICCO, a 3-year research project financed by the Italian Ministry of Agricultural, Food and Forestry Policies which aims to investigate the possible re-use of biomass ash as filler in bituminous mixtures. In particular, the goal of the first part of the project is to characterise several ashes from biomass combustion by integrating the tests included in the technical standards on filler for bituminous mixtures EN 13043, with those tests that ongoing research has identified as reliable performance indicators. Furthermore, since it is important to substantiate the hazardous nature of ashes, their environmental impact can be assessed by the European regulation EN 12457-2 on the evaluation of leaching potential. Several studies have been carried out in recent years to assess the possible re-use of biomass ash and its recycling as a substitute for aggregates in concrete mixtures (Martin Morales *et al*., 2011), in cement production (Ajiwe *et al*., 2000), and also as a fertilizer (Insam and Knapp, 2011). In road applications, due to its cementing and pozzolanic properties, most of the researches focused on the recycling of biomass ash in soil stabilization (Basha *et al.*,2005; Nordmark *et al*., 2011). The recycling of biomass ashes as filler in bituminous mixtures has been studied in The Netherlands: an extensive study led by the Energy Research Centre of The Netherlands (Pels et al., 2006) showed that fly ashes from the gasification of solid biomass are a valuable alternative to natural fillers. Sarabèr and Haasnoot (2012) investigated the physical and chemical characteristics of several fly ashes derived from the combustion of different solid biomasses. Their experimental results indicated that most of the ashes do not meet the requirement for passing 125 and/or 63 lm, concluding that, due to their gradation, biomass fly ashes can compete more with Municipal Solid Waste

Incinerator fly ash and sewage sludge ash than coal fly ash when recycled as filler in bituminous mixtures. Unfortunately, the physical– mechanical properties of ash–bitumen mastics, slurries ormixtures were not investigated. Moreover, the investigation by Sarabèr and Haasnoot (2012) does not take into account the fact that characteristics like gradation, water solubility and soundness are insufficient for an assessment of the use of biomass ashes as filler in bituminous mixtures, as clearly indicated in the present paper. The majority of the studies concerning the possible re-use of ashes as filler in bituminous mixtures investigate the behavior of fly and bottom ash derived from coal combustion. A great quantity of ash (20–30% of the original matter) is produced from this combustible which still represents the most widespread energy source in many countries. In the European Union (EU 15) 61 million tons of coal combustion products were produced in 2006 (European Coal Combustion Products Association, 2006), while in the US 125 million tons were produced in 2009 (American Coal Ash Association, 2009). Kavussi and Hicks (1997) evaluated the properties of bituminous mixtures containing four different fillers (limestone, quartz, coal fly ash, kaolin): they found that mastics containing fly ash were more susceptible to brittle failure because of their high porosity, caused by the presence of very small air bubbles formed during the burning process. Sharma et al. (2010) demonstrated that coal fly ash having high calcium content exhibits anti-stripping properties. In order to avoid excessive stiffening of bituminous mixtures, they suggested a maximum value of 60% for the ratio between bulk volume of compacted filler and total filler– bitumen volume. This study also showed that high values for clay content in the ash, as revealed by the Methylene Blue (MB) test, were correlated to low tensile strength ratio and retained stability values, proving that this test can also provide a good estimate of moisture susceptibility. In recent years the National Cooperative Highway Research Program Project 9-45 (NCHRP, 2010) was developed in order to address the theme of filler role in bituminous mixtures. The study considered 32 different fillers for which the effect on bituminous mixture performance was thoroughly investigated. Out of the total set of analysed fillers, three were fly ashes collected from coal combustion plants. The research identified fractional voids, size distribution, content of calcium compound and active clay content as the most relevant properties for the characterisation of fillers. Compared to mineral fillers routinely used for paving

applications, the properties of fly ash encompassed a wider range of values. As a consequence, the prediction model developed to estimate mastic properties from filler characteristics was applicable only to natural fillers. The study concluded that manufactured fillers have a unique influence on mastics and mixtures, with this effect requiring a more detailed investigation. Although coal ash is the one most studied, many investigations deal with the possible re-use of other ashes in bituminous mixtures. Xue et al. (2009) investigated the effects of Municipal Solid Waste Incinerator (MSWI) ash on Stone Mix Asphalt (SMA). The use of 16% of MSWI ash meets the requirements of Marshall and Superpave mix design procedures. However, the ash lowers the water damage resistance of the mixtures due to its low CaO content causing poor adhesiveness between asphalt and ash. Hassan et al. (2007) studied the effect of replacing 0–3 mm natural aggregates with up to 40% of MSWI ash in bituminous mixtures: the Marshall mix design showed that optimum asphalt content increased significantly as more ash was introduced into the mix, owing to the high absorption properties of the ash. One solution to the problem of this increasing absorption of binder is represented by vitrification. Bassani et al. (2009) studied a bituminous mixture in which up to 32.5% of 0–2 mm natural sand was replaced with vitrified MSWI ash: they concluded that, due to the glassy surface of ash, a smaller percentage of bitumen can be used to reach given target values for mechanical and volumetric properties" (Melotti R. 2013).

Sangiorgi *et. al.* 2014 proposed waste bleaching clays from the food industry as an alternative to common limestone mineral filler for the production of Hot Mix Asphalts (HMA). The bleaching clays used in this study come from two consecutive stages in the industrial process for decolouring vegetable oils and producing biogas from waste clay, where the former is richer in residual organic fats (20–25% in weight against less than 1%). The authors have studied the performances of a common binder course asphalt mixture, in terms of physical and mechanical characteristics, when waste bleaching clays are used as an alternative. From the analysis of the dynamic creep test at 40°C (Figure 2.12), the authors concluded that the substitution of the limestone filler with the spent bentonite (first stage) filler determines a worsening of resistance to permanent deformations, which is, however, improved using the digested bentonite (second stage) filler. On the basis of the experimental results presented in this paper,

the conclusion is that it could be possible to substitute the traditional limestone filler in HMA mixtures for binder layers with bleaching clays. In this thesis, on Chapter 5, this study has been completed by the rheological analysis of the binders modified with the waste bleaching clays.

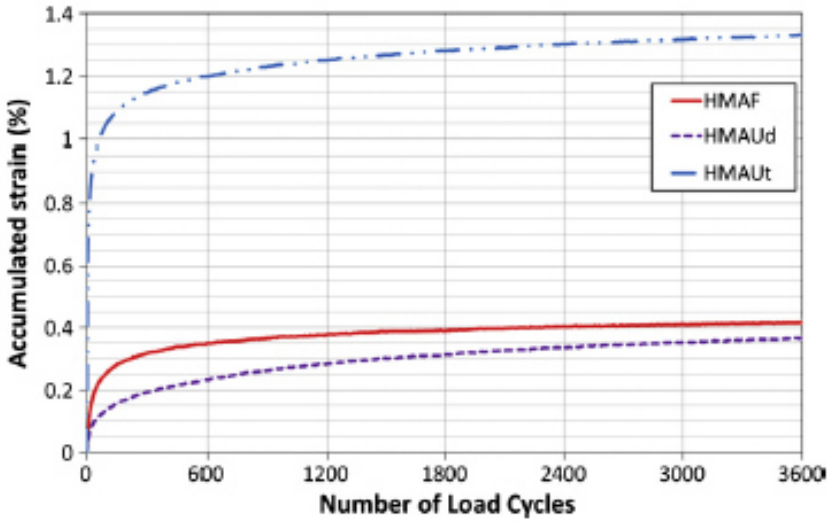

Figure 2.12 RLAT: accumulated strain vs. Number of load cycles (*Waste bleaching clays as fillers in hot bituminous mixture*).

2.6 Bitumen modified with Crumb Rubber

2.6.1 Tyre

Nowadays, because of the increasing of road transport in the global transport system, vehicles tires are creating a significant problem at the end of their useful life. The different tires types can be identified on two main categories: tires from passenger car and truck tires. These two type of tires differ in the composition of the materials from which they are made; these differences are not only expressed in terms of size, of steel or textile including in their structure, but also in the types and proportion of the ingredients used in the basic compound (Tataranni 2012). The composition, for the two sectors passenger cars and trucks, is determined mainly by natural and synthetic rubber, where the elastomeric component is made from the copolymer of Styrene-Butadiene-Rubber (SBR). Each components of the rubber composition (rubber elastomers, carbon black, metal, textile fiber, zinc oxide, sulfur and chemical additives) contributes to the specific characteristics of the tire, in order to favor a greater life. A rubber untreated is relatively weak, soft, very flexible and not soluble in water, alkalis and weak acids, while it is soluble in benzene, diesel oil, chlorinated hydrocarbons and in the carbon-sulfur compounds. In order to give to the crude rubber strength and elasticity characteristics it must necessary to give rise to bonds between the molecules that compose it: such processes are known as vulcanization. Once the vulcanized rubber becomes resistant to abrasion and impermeable to gases, to chemical action, heat and electricity. Both types mentioned above have good resistance during the driving of vehicles and are designed to have the great service life; it follows that one of their key features is to have a high resistance to the action of microorganisms, employing more than 100 years before being able to destroy them. Although these properties on the one hand allow the new tire to prolong the life cycle, on the other hand result in a negative feedback when it becomes waste (Viola 2013). In general, the tires are constituted by an elastic toroidal structure of natural or synthetic rubber and may be of two types:

- tube type: are tires with an air chamber that encloses the compressed air to obtain an adaptation effect and vehicle suspension from the road. The cover is

constituted by synthetic rubber, essential in transmitting the friction that is generated by the motion, and fiber canvas or metal;

- tubeless: are tires which possess the function of the air chamber and not requiring it, while the cover is identical to that of the tube type.

Currently all cars are produced with tubeless tires, while buses and trucks using both models. The structural composition of a tire is briefly consists of the following elements (Figure 2.13):

1. *synthetic rubber layer* to perfect air-tightness;
2. *the casing* is the structural part of the tire on which the tread is vulcanized. The carcass of a car tire is made up of thin textile fiber wires arranged in a straight arc and glued to the rubber that allow the tire to resist pressure; the textile component is not, however, present in tires for trucks, which incorporate a higher percentage of steel;
3. *the sidewall* is the lateral part of the carcass which serves two opposing objectives: flexible on vertical direction to minimize the transfer of irregularities of the ground on the vehicle, while it is relatively rigid horizontally on the ground to transfer the loads due to understeer , braking and acceleration;
4. *the heels* (ending in circles), which are used to fix the tire on the wheel; they are formed by wire rope rings that have the function of keeping the carcass well adherent to the hoop;
5. *the hips*, which protect the tires from shocks that could damage the casing;
6. *the belts*, which are as plans to put the material in a central position between the casing and the tread. They are generally armed with extremely resistant steel wires, obliquely crossed and glued one on the other and are joined together by vulcanization process that makes a unitary structure. These components are used to perfectly control the diameter of the tire and to overcome barriers;
7. *the tread* is the part of the tire designed to make contact with the road and essential to ensure adherence with the ground with which it is in contact. It consists of a compacted rubber ring that surrounds the housing and must be

able to withstand great forces, wear resistant and abrasion and must undergo a low heating. The first part of the tread, which comes in contact with the wet surface, serves to remove water and then allow the remaining part to provide friction on the drained surface. The channels, ranging from the center to the edge of the tread, are used to expel the water.

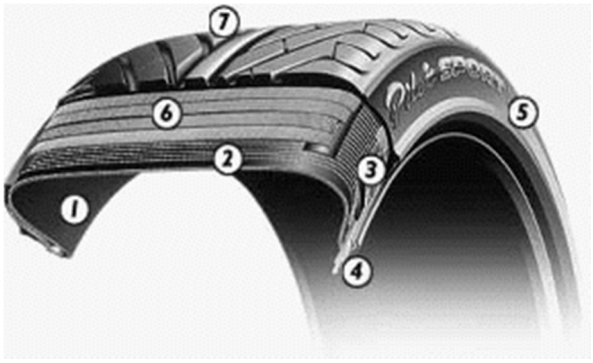

Figure 2.13 Tyre components.

In general, the rubber is distinguished in natural (product derived from the plant Hevea Brasiliensis in Brazil with 70% of elastomers) and synthetic (made from artificial polymers with amounts less than 50% of elastomers). The tire rubber is generally synthetic rubber, which is never used in the rough layer, not only for the poor mechanical and elastic properties but also for its vulnerability with respect to time and temperature. In order to stabilize these properties, the rubber is subjected to a curing process which causes the formation of a stable three-dimensional molecular structure. The elements that constitute the rubber composition are generally:

- vulcanizing agents and accelerators: allow the passage of the material from the plastic state to the elastic with a consequent increase in the mechanical strength and reduction of the solubility;
- fillers (carbon black and zinc oxide): increase the breaking load, the abrasion resistance to tearing and to solvents.

2.6.2 Management and procedures for recovery of ELTs

The disposal and recovery of waste rubber consists for the most part from the tires use deriving both from the periodic replacement of worn tires, from the rubber scraps and

from the retreading of tires. In recent years, he has aroused increasing interest, so much so that its flow has been included among the priority flows of waste within the Community. This interest is evident, since the disposal in landfill can give rise to harmful effects, contributing to the possibility of fire development and to mechanical instability, within the mass of stored waste, due to the cavity of the tire and elasticity. Furthermore constitutes loss of resources, being the rubber material is a recoverable form of matter is energy, in fact, although the quantity of discarded tires is not remarkable, the recoverable amount of energy, due to the high calorific value (7,500 - 8000 kcal/kg, between the coal and the fuel oil) is still worth noting. In 2009 the European Union has faced the challenge of managing, in compliance with ecological criteria, 3.2 million tons of used tires, of which 581,000 tons are started to reuse, remarketing or to export, while about 2.6 million tons remain in the market as "PFU" or discarded tires. In fact, the tire used, once detached from the vehicle, is not automatically identified as waste. The roads can still figuratively take are varied and depend on numerous factors such as the level of wear, susceptibility to reconstruction, the market demand and the holder's intent. The combination of these factors may, in fact, to decide the fate of the tire, which can then be reused, rebuilt or crushed and developed in various forms of recovery and recycling. There is a match almost mirror in the list of priorities identified by the Waste Directive 2008/98 / EC, which serves the well-known waste hierarchy (Viola 2013):

- prevention: reuse of used tires, in under-performing applications or reconstruction of those not become waste; this level you have to prefix to avoid creating waste wherever possible. The tires that still possess a depth of the upper tread to the legal limit and are not damaged in the structure can be used without any treatment in order to postpone in fact, production of a refusal;
- preparation for reuse: reconstruction of used tires become waste. This process allows the use of carcasses still structurally intact to produce tires, using only about 30% of new polymers and saving about 70% of process energy. The reconstruction takes place through numerous processing steps which include the buffing of the tread and replacing it with a new one;
- recycling: recovery of materials by ELTs, such as the production of rubber granules and powders. When the tires are worn out to be reused for their

original purpose, they are considered out of order and enter into a management system based on recycling. In this case, through the recovery of materials, other products are obtained as useful and, where this is not possible, an energy recovery (as described in the next point); this is because, unlike other types of waste, waste tires are difficult to recycle. The complete recycling, which is to process used tires to get the first, it is currently not possible because of the difficulties encountered in the full rubber devulcanization pretreatments materials

- other recovery: energy recovery by ELTs, such as incineration in cement factories;
- disposal: landfilling (mixed or dedicated) ELTs of large diameter (> 1.4 m). That level was until very recently the main destination of ELTs and still is in many geographical areas, not necessarily the most backward or developing; in Europe the landfilling ban was implemented in 2003 for the entire PFU and since 2006 for ELTs crushed. Since 2006, in fact, it prohibited landfilling of PFU, excluding tires used as engineering material, and those with outside diameter greater than 1400 mm. Data collected from ERTMA (European Tyre & Rubber Manufactorers' Association) show that the management of such a huge amount of material was possible only with the diffusion of management systems that enhance the materials through recycling (the problem is compounded by the presence of underground dumps ELTs, estimated at about 5.5 million tons).

Today in Europe there are three different ELTs management systems:

- a tax system (in force in Denmark and Slovakia): each country is responsible for the recovery and recycling ELTs. Manufacturers pay a fee to the state which is responsible for organizing and remunerates the operators in the recovery chain. The fee is then applied to the consumer;
- free market (in force in Austria, Bulgaria, Croatia, Germany, Ireland, United Kingdom and Switzerland), the law establishes the objectives to be achieved and the contact persons for the individual business segments, but does not provide for responsible supply chain. In this way, all players in the system enter

into contracts in accordance with free-market conditions and act in accordance with the local waste legislation;

- producer responsibility (exists in Belgium, Estonia, Finland, France, Greece, Italy, Norway, Poland, Netherlands, Portugal, Romania, Slovenia, Spain, Sweden, Turkey, Hungary): The law defines the legal framework and grants the responsibility to manufacturers to organize the management of ELTs. This system led to the establishment of non-profit companies to manage ELTs through the most cost-effective solutions. Producers are obliged to monitor and report to national authorities, which is a good example of transparency and traceability. The management costs are paid through a contribution clearly indicated at the time of purchase by the user, through the "polluter pays."

The common aim of these systems is the disposal of ELTs by the recovery of materials and energy, from which you derive environmental and economic benefits (Tataranni 2012) (Viola 2013):

- the re-use of a resource which, if not recovered, it would not biodegradable and would occupy deposits and dumps with serious damage to the environment and health;
- remediation of landfills or illegal deposits;
- use instead of precious raw materials, often imported;
- the reduction of the amount of waste and consequently lower costs to the community;
- improvement of the trade balance in relation to import of traditional fuels.

2.6.3 Crumb rubber in bituminous mixtures

The use of the modified bitumen with crumb rubber from recycled tires began in the United States, more than forty years ago, by the need to find an effective means to stop the propagation of cracks in flexible superstructures, mostly generated by particularly

high temperature gradients, which give rise to typical phenomena of thermal stress. Just need to find a product that would allow limiting the occurrence and spread of cracking conducted in the late '60s, the idea/patent *Asphalt Rubber* in Arizona by Charles McDonald. Later, the encouraging results made it possible to extend the scope of use in the field of surface treatment and, subsequently, of the asphalt. The practical applications of the results obtained over time made it possible to refine the production techniques and *Asphalt Rubber* performance, bringing the last decade to the definition of a specific rule that defines and identifies such material (ASTM D-6114) (Antunes *et al.*). Today the dust from ELTs can be included within the asphalt for road paving using two different production technologies:

- "WET" technology, by which the powder is added and dispersed in the bitumen, by modifying the viscoelastic characteristics, to obtain a bituminous mastic from the improved properties;
- "DRY" technology, in which the powder replaces a part of stone aggregates, modifying the characteristics of the resulting lytic skeleton and giving place to a limited interaction with the bituminous binder.

2.6.3.1 WET technology

WET technology consists in the dispersion of the rubber particles within the hot bitumen, through accurate mechanical mixing, at a temperature range between 170 and 225 °C for at least 1-2 hour. The aim is to obtain a modified binder in which the rheological properties are changed substantially same. The bitumen modification occurs in a separate operation from the asphalt mixing. The rubber grains are able to absorb bitumen oils, obtaining the same result as any polymer additive. The result is to improve bitumen ductility and fatigue resistance, reducing oxidation phenomena.

Depending on the type and dosage of powder used and the consequent interaction with the base bitumen, as well as the resulting product storage, rubber modify binders such technology can be divided into two categories (Ecopneus):

- high viscosity binders, or *Asphalt Rubber*; are binders with a high dosage of powder to and with marked elastic characteristics, which require to be maintained in a "stirring" prior to use;

- low viscosity binders, or *Terminal Blend*, with more reduced dosage but characterized by an increased storage stability.

Asphalt Rubber indicates a particular type of bitumen, with a specific rubber particle size, produced directly in work, close on the road construction site. These technologies and methods represent a solution to the problems related to the tire landfills due to the high application volume, fire risk and instability of the landfill and pollution due to their degradation. The *Asphalt Rubber* binders immediately after mixing are maintained in high temperature agitation (175-225 °C) for 45-60 minutes, necessary to activate the interaction between the two materials; the storage of these products must take place in tanks equipped with suitable stirring systems in order to ensure a homogeneous and stable dispersion of the powder particles. In particular, during the production phase, the particles of crumb rubber tend to absorb a part of the aromatic fractions of the bitumen, resulting in a significant bulge and the simultaneous formation of a gel which gives the binder its peculiar chemical-physical characteristics. The result is a composite material in which the individual particles of powder to maintain their integrity and are distinguishable, even visually, from the matrix in which they are included. From the physic-chemical point of view, the rubber powder mixed with a basic natural bitumen is able to absorb and fix the maltenic fraction own of aromatic volatile constituents of the bitumen. Just the fixing of maltenes allows to obtain a significant increase of the aging resistance of the bituminous mixtures, since this constituent of bitumen is, in general, destined to be lost over time to phenomena of oxidation and the action of UV rays. The introduction of the crumb rubber in bitumen at high temperatures (about 185 ºC) causes a physical-chemical reaction by which a three-component system is formed: bitumen, gels and powder. The gel is formed through the chemical reaction of dust with malthenes, consisting in the absorption of oily fractions; this process leads to swelling of the powder, altering the viscosity of the mastic, and to the formation of the same gel, which increases in percentage of the volume with the hot-curing time. Such are referred to as "high-viscosity" as to a given reference temperature (equal to 175 °C as indicated in ASTM standards) possess a viscosity of not less than 1500 cP. They generally contain a proportion of bitumen, expressed by weight relative to the weight of the total binder of at least 15% (with typical values comprised between 18 and 22%). The swelling

process determines the modification of the rheological properties of the binder, which also depend on the chemical constitution of the constituent materials, the dosing of the powder and the size and morphology of its particles; in particular:

- the viscosity proportionally increases as the percentage of powder added and the increase of the specific surface of the powder (in this sense are more reactive the powders of finer size particles consisting of rough and irregular in shape);
- the viscosity varies depending on the degree of maturation (ie the degree of swelling) of the binder and the temperature at which this occurs;
- the fatigue behavior of the binder tends to greatly improve: the properties of rubber are gradually transferred to the binder. These factors should be taken into account for the selection of the powder to be used in the editing process "wet". However, while the technical standards adopted by some departments of Transportation (DoT) US set of acceptance criteria based on their composition and grain size, ASTM D6114 merely requires a limit value to the maximum particle size (<2.36 mm), pointing out, however, that the particle size of dust must be agreed between the manufacturer and the buyer of the binder. This rule also establishes limits for density (1.15 ± 0.05 g / cm^3), the water content (≤ 0.75%) and the content of textile fibers (≤ 0.5%) and waste ferrous metals (≤ 0.01%) (Ecopneus). The use of high percentages of Asphalt Rubber bitumen allow to obtain asphalt concretes with excellent mechanical properties, such as high resistance to the propagation of cracks, high fatigue resistance and, in parallel, high resistance to permanent deformation, high stability to aging actions produced from UV rays and a sound absorbing significant contribution.

The binders named Terminal Blend do not reach the specified value of the viscosity threshold; this is partly because of the fact that finer powders are used (usually through a sieve 0.3 mm) and with a lower dosage (generally not exceeding 10%). Due to the high specific surface of the powder, its interaction with the bitumen occurs rather rapidly during mixing, with the consequent creation of a macroscopically homogeneous matrix in which are no longer distinguishable originating particles. As

there are no stability problems, the finished product can be recirculated into the normal storage tanks present in production plants of bituminous conglomerates, without the need to provide special stirring devices. Since the production of such binders normally takes place at the refinery, they are called Terminal Blend. However, with the appropriate technical devices, they can also be prepared directly from the manufacturing plants of bituminous conglomerates (something, in this case, the "field blend"). The characteristics of the modified bitumen products with both the WET technology variants may change significantly depending on the type and dosage of the powder, as well as by the temperature and the arrangements by which the mixing is carried out. In some cases, during production, other components can be added, such as aromatic oils and natural rubbers to impart to the finished product specific chemical-physical characteristics. The binders Asphalt Rubber and Terminal Blend can be used for the production of asphalt mixtures by following the same procedures as for the traditional mixtures. WET rubber modify binders must be used for the formation of asphalt concretes in which the aggregates grading curve is characterized by a certain discontinuity, necessary to be able to create an internal porosity which is sufficient to accommodate the particles of powder. This is the case of mixtures "gap-graded" and "open-graded", which fall respectively in the closed "semi type mixtures" (with residual voids in the work of the order of 5-8%), and "semi-open" (with 12-18% empty order). Both mixtures are characterized by a significant surface macrotexture, which leads to high tack values provided at the interface tire-pavement reeds in the presence of meteoric precipitation. While the mixtures "gap-graded" are actually waterproof, those "open-graded" have an internal porosity of morphology and size that allow rainwater to filter through them, resulting in a further increase in adhesion reason for the creation of a dry contact in all environmental conditions. To such effect, as in the case of the traditional draining mixtures (open), they are accompanied, in addition, certain advantages related to the elimination of the effects "splash" and "spray", sources of potential danger for the safety of road users. Discontinuity grading curve effects the internal structure of both types of mixture; the larger aggregates create indeed, in the case in which appropriate features of shape possess one lytic skeleton which stiffens the mixture and which opposes effectively the accumulation of permanent deformations under load. The carrier matrix is lytic, then, filled in part with

the finer fractions and in part with the bituminous binder, for which are adopted significantly higher dosages than those usually adopted for the ordinary type mixtures. This causes an increase of the ductility of such bituminous conglomerates, which have, compared to the traditional ones, a higher resistance to fatigue and to the propagation of cracks. Note, also, that due to the high viscosity of the binder does not determine, even with the use of high doses, "drain-off problems" during production and transportation, nor occurring phenomena of surface chin wastewater during the installation and during operation. The presence of elevated amount of binder in these mixtures has additional beneficial effects as regards the resistance to thermo-oxidative aging phenomena, the durability to water and the generation of noise from rolling on the part of the tires. In relation to the first two aspects, it is noted that the aggressive external agents (air and water) can penetrate only a modest portion of the heavy volume of binder surface therefore retains over time much of its original characteristics also performing the barrier function for access to the surfaces of stone aggregates. The reduction of the rolling noise is, however, due to the particular behavior of the bituminous binder matrix owing to its rheological characteristics and the high volume occupied determines attenuation of the vibrations that arise at the interface tire-pavement. Note, in this regard, that in the case of asphalt concretes "open-graded" can be added to these effects those due to surface porosity that provides an additional contribution of noise attenuation through the well-known sound absorption phenomena. According to literature, the identification of the optimal mixture of formula can be made with reference to the volumetric characteristics of the samples prepared in the laboratory by means of appropriate equipment. In particular, they are generally taken into account the percentage of residual voids, for which is set a target value, and the percentage of voids in the aggregate mixture (VMA), for which is often referred to a minimum admissible value. In some cases, also it verifies the compatibility of acceptance constraints related to the mechanical characteristics of the blends, usually measured with fairly simple techniques. The use of these conglomerates has been widely experienced so much in the construction of new infrastructure as in the maintenance and upgrading of existing ones, in particular for the realization of wear layers, the most superficial part of the road that has the purpose to ensure the functional characteristics of the pavement grip, smooth, quiet, etc. In

some cases it was also used, the combination of the two mixtures, with the laying of an "open-graded" conglomerate above of a connection layer "gap-graded. To effect the advantageous properties listed above, mixtures containing "Asphalt Rubber" have been adopted, in some contexts, such as the greater effectiveness solutions for maintenance and upgrading of the flooring already in operation. In this regard, it should be emphasized that the higher costs of production of mixtures appear to be largely offset by lower future maintenance costs, resulting in a decrease of the total cost if assessed throughout the entire life cycle of the pavement. These advantages are particularly marked in all those cases in which there is adequate diffusion of production technology, with the consequent creation of a real of the binder "Asphalt Rubber" market in which the content can be transposed costs and defining unit prices with a view to commercial competition. Further considerations related to the cost of the work with "Asphalt Rubber" descended from assessments that can be made for the thicknesses of the mixes to be laid; by virtue of their high mechanical performances and of their high durability. It was estimated that these mixtures can ensure performance similar to that of traditional type mixtures while using more content thicknesses. This aspect in some cases has been encoded with equivalence laws, which however must be properly calibrated for each application context to take account of the effects of all the factors that have an influence on the damage phenomena. The products that fall in the "Terminal Blend" category are, instead, used for the preparation of closed mixtures (with residual voids in work order of 4%) in continuous grain size of the aggregates, completely similar to those of the ordinary type; the most frequent applications still relate to wear layers, which are required particularly high durability characteristics. Such mixtures have a mechanical behavior that deviates from that of conventional mixtures to a degree, which depends on the degree of alteration made to the binder during the production process. In particular, the effect of the variation of the rheological characteristics of the binder itself, there is an increase of the elastic response of the component under load, with consequent improvement in the resistance to the accumulation of fatigue and permanent deformation. As pertains to the formulation, production, implementation and monitoring it may be introduced to the already validated procedures for traditional closed-mixtures, taking into account only the higher temperatures required in the mixing stages and compacting. In terms

of general all, it can, however, conclude that if properly proportioned and thickened, such asphalt have characteristics such that they can be employed in the construction and road maintenance to complement or replace those of ordinary type. The performance collected on the field were in line with the above, with a reduction of the phenomena of surface cracking and rutting compared to conventional mixtures; it was also found that the additional cost arising from the binder modification process is largely compensated by lower maintenance costs occurring during the useful life of pavements.

2.6.3.1 DRY technology

Traditionally, in the dry process it is normally assumed that the rubber is part of the aggregate. Reaction between bitumen and CR is considered negligible because the mixtures are fabricated without any significant interaction time between bitumen and rubber. In this process, some fractions of the aggregate blend are generally substituted by rubber particles of similar size. Several studies indicate that with "DRY" technology is possible to produce "gap-graded" and "open-graded" mixtures. For their formulation may be introduced the same grading curve employed for mixtures containing binder product with "WET" method. Bitumen proportion must be determined taking into account that the rubber powder tends to absorb bitumen oils during the phases of transport and installation of the mixture. In the case of "gap graded" mixtures, in continuous grain size, best performances are obtained using fine crumb rubber. In the case of "open-graded concretes", the possible presence of dust coarse (larger than 4.75 mm) could reduce the aggregates cohesion. For the application of the "dry" technology, it can be use two different modes of production of asphalt:

- dry-hot technology;
- dry-cold technology;

On dry-hot technology, aggregates and bitumen (equal to about 5% of the weight of aggregates) mixture is produced on range temperature between 160-180°C in places relatively close to the construction site. In addition to bitumen and aggregates, in this case also it is added a proportion of rubber powder, which must always be less than 5% of the weight of the aggregates which are, in part, to be replaced by the dust particles. Dry-cold technology allows to obtain asphalt mixture, mixing aggregates and

rubber with bituminous emulsion and cement. The bitumen emulsion is composed of two liquids, emulsion and water-immiscible; the liquids are dispersed in one another using a colloidal mill. Often for the construction of base layers with this technique, the cement is added to improve the mechanical properties and to increase the moisture resistance; it also acts as catalyst, controlling the breaking of the emulsion, and increasing the initial resistance of the pavement properties. The rupture emulsion condition is important to achieve mixture desired performances. Obtained the stabilized mixture with emulsion, it must dissipate the excess water, ie mature, so that its resistance increases; the duration of this period is influenced by the moisture content of the material, by the interactions between emulsion and aggregates, from the local climate and the void percentage of the mixture. For both WET and DRY production technologies several studies, research, technical standards and test data related to the performance observed in operation, which are characterized mainly by:

- longer life of the pavement;
- less noise generated by passing vehicles;
- increased resistance to staining;
- increased resistance to weathering;
- optimal water drainage, and increased visibility with rain;
- better grip, especially in wet weather.

Dondi G. *et al.* 2014 have evaluated the physical and mechanical characteristics induced by the shared use of two different types of Crumb Rubber in the Cold Recycled Mixes. They have found that the replacement of fine RAP with Crumb Rubber improved the self-compaction of the mixtures while influenced their volumetric characteristics after compaction. Moreover, the authors have shown that from failure fatigue results the adoption of crumb rubber increase the failure resistance at low strain levels.

3 LITERATURE REVIEW: METHODS

3.1 Introduction

The linear viscoelastic theory is the necessary base to understand the rheological behavior of bituminous materials. The viscoelastic material has properties between solid and fluid. The interaction of the two phases, elastic-solid and the viscous-liquid, means that there is internal energy dissipation and hence a deviation of the stress-strain response compared to perfectly elastic state. In fact, a perfectly elastic response requires that the potential energy gained during the deformation had been returned totally in order to respect the perfect reversible transformation from the thermodynamic point of view. The greater or lesser influence of the solid matrix of the liquid determines an infinite amount of viscoelastic responses, whose extreme limits are represented by the ideal states corresponding to the pure elastic solid and perfectly viscous fluid. On bituminous binders these limit situations can be achieved by varying the temperature or charging the load time. In the following chapter, clarifying the basics principles of elasticity and viscosity, the viscoelastic relations used on the rheological analysis are introduced. In order to represent the viscoelastic phenomena is essential to identify the real material as model continuous, homogeneous and isotropic. In fact all the materials, and in particular polyphase systems such as bitumens, are composed of a large number of discrete elements, the individual molecules, and their overall properties are the average of the elements of groups behavior. The aggregation of the various particles gives rise to a specific type of group from which the same group is characterized, and in respect of the overall response assume importance constitutive laws of connection between the individual particles rather than the intrinsic properties to the particles themselves. The concepts viscoelasticity theory, presented on this chapter, represent the theoretical basis to understand the rheological tests performed on bitumen. The set of problems related to the execution of those tests, the definition of operational protocols, treatment, processing and interpretation of experimental results, is a subject of rheometry. This can be defined as the branch of the rheology that concerns the measurement of the rheological quantities. The study and understanding of these variables assumes considerable importance to analyze bitumens and mastics performances; a binder,

which under the application of a load manifests high deformation, could generate rutting phenomena, on the contrary, a very hard bitumen, at low temperatures, could increases mixture sensitivity to fatigue flooring. For this reason is essential to investigate the mate*r*ial in the most varied conditions, which can be combined giving rise to a potentially unlimited number of test types. To date, the rheological properties of the binders are usually determined using equipment operating in oscillatory regime, including the DSR (Dyanamic Shear Rheometer), thanks to which it is possible to study the elastic, viscous and viscoelastic properties of the bitumen in a wide range of temperatures and loading frequencies. It also describes the torsional actions on cylindrical mortar specimens, highlighting the analytical complexity of the extracts results from this type of test. Finally, like the rheological tests will be analyzed in detail the Discrete Element Method (DEM) approach, studying the main researches that have led the micro - particles study of binders and asphalt concretes.

3.2 Rheology

3.2.1 Elastic solid

The elastic solid is deformed by force effect, and at the end of the solicitation, summarizes the initial shape. At the microscopic level, the elastic deformation is a coordinated and reversible distortion of the various atoms constituting the material. Considering a sample of dimension l (height) and d (diameter) after the vertical force application it is experimentally observed that the relative shortening, or deformation, is equal to:

$$\frac{\Delta l}{l} = \frac{N}{S} \cdot \frac{1}{E} \tag{3.1}$$

where:

E = Young's modulus [N/mm^2];

Δl = vertical shortening;

N = vertical force;

S = specimen surface.

If E is independent from the strain level there is direct proportionality between tension (N/S) and unitary deformation (Δl/l), in this case, there is linear elasticity, and the (3.1) takes the name of Hooke law. Contextually to the vertical deflection, the elastic body has a radial deformation equal to:

$$\frac{\Delta d}{d} = \nu \cdot \frac{\Delta l}{l} \tag{3.2}$$

where:

ν: Poisson's ratio;

Δd: the diameter variation;

d: diameter.

In elastic bodies, the work spent in the deformation process is fully recovered when the stress is removed and returns in the initial non-deformed conditions (Mazzotta 2012).

3.2.2 Viscous flow

It defines viscous fluid a deformation process in which the mechanical energy applied to a material is, completely or in part, dissipated irreversibly on heat form; when the mechanical energy is fully converted into heat this is purely viscous flow. The quantity characterizing the viscous flow is the viscosity, which can be defined as material sliding resistance opposite under the action of the effort. The viscous behavior is believed to have originated from a laminar motion of the components of the medium, said flow, which can take generically four different configurations of which are summarized below (Mazzotta 2012):

- flow between two parallel planes, takes place between two planes, one fixed and one moving. The thickness of the two plates is not influential on the motion and the flow that is generated is for parallel planes to the two moving surfaces (Figure 3.1) (Mazzotta 2012);

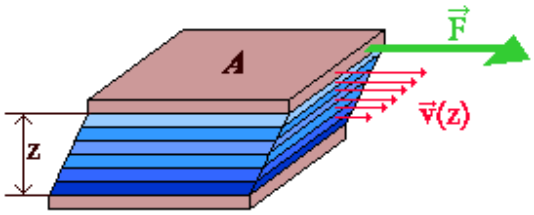

Figure 3.1 Viscous flow between two parallel planes at distance Z ("*Studio reologico avanzato di bitumi modificati ed additivati: proposta di una nuova procedura di aging"*).

- rotational flow between coaxial cylinders, takes place by a fluid contained in the cavity formed by two coaxial cylinders. One of the two cylinders is fixed and the other rotates dragging with it in relative motion successive layers of fluid (Figure 3.2) (Mazzotta 2012);

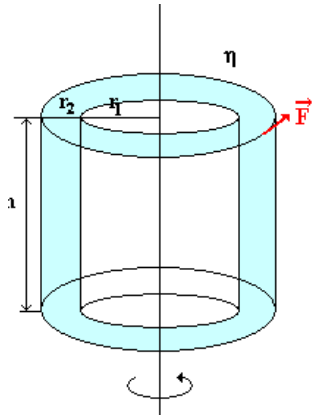

Figure 3.2 Rotational flow between coaxial cylinders ("*Studio reologico avanzato di bitumi modificati ed additivati: proposta di una nuova procedura di aging"*).

- capillary flow, it is realized in the fluid flowing in a pipe or in a thin element, subject to a pressure difference between the inlet and the outlet; in the capillary motion of the speed profile takes on a parabolic curve (Mazzotta 2012);
- flow between a plate and a cone, in this case the plate constituting the fixed element while the wheel cone. The fluid present between the two elements assumes a motorcycle of the type circular that takes place on parallel layers (Mazzotta 2012).

The viscous flow and viscosity concept is related by Newton's law:

$$\eta = \frac{\tau}{\frac{d\gamma}{dt}} \tag{3.3}$$

where:

τ = shear stress;

$d\gamma/dt$ = shear rate;

η = dinamic viscosity [Pa·s].

If η is constant, the fluid is Newtonian and the viscosity varies only with changing temperature. In addition to the dynamic viscosity exists the kinematic viscosity ν; it is measured trough special tools called capillary viscometers and is defined dimensionally on the basis of kinematic quantities such as the length and the time, in contrast to the dynamic viscosity for which also necessary to evaluate the intensity of the force which determines it. The relationship between the kinematic and dynamic viscosity is the following:

$$\nu = \frac{\eta}{\rho} \tag{3.4}$$

where:

ν: kinematic viscosity [mm^2/s];

η: dinamic viscosity [Pa·s];

ρ: density.

For a Newtonian fluid the shear stress diagram as function of shear rate is represented by a straight line whose angular coefficient defines precisely the viscosity (Figure 3.3) (Mazzotta 2012).

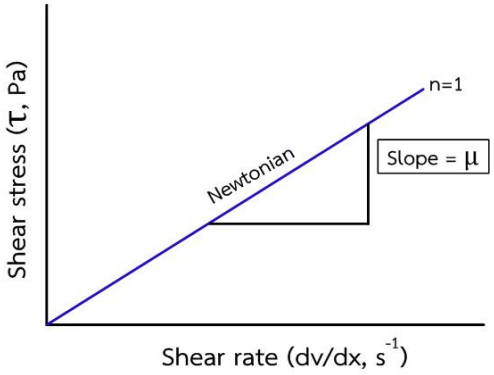

Figure 3.3 Newtonian flow curve.

Those fluids for which does not apply the law of proportionality between stress and strain gradient are generically called non-Newtonian; for such materials viscosity it depends not only on the temperature but is also a function of the sliding speed. In these cases, Newton's law becomes:

$$\tau = \eta(\dot{\gamma}) \cdot \dot{\gamma} \tag{3.5}$$

As shown in Figure 3.4, the non-linearity behavior can manifest itself in many forms, depending on the variation law η = f(dγ/dt).

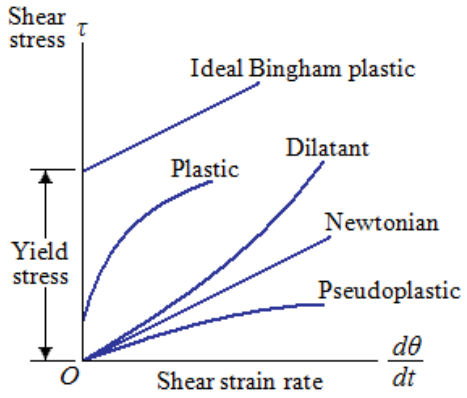

Figure 3.4 Non-Newtonian flow curves.

3.2.3 Viscoelastic models

Related both ideal elastic materials (solid Hooke) and ideal viscous fluids (Newton fluid) apply linear relationships between stress and deformation or between the strain and the strain rate: the proportionality coefficients (moduli and viscosity) are independent by stress conditions. This concept applies to the viscoelastic material is the linear viscoelasticity. The mechanical behavior of a viscoelastic body can be represented by models composed of elements in simple mechanical behavior, such as springs, dampers and shoes. Every real behavior can be described by a particular model, obtained combining the basic elements. The most known models are those of Maxwell and the Kelvin-Voigt, which describe, classically, the two phenomena of delayed and the viscous flow elasticity. In general these two aspects are simultaneously present in the bitumen, to which the complete viscoelastic behavior can be achieved by the superimposition of the effects (Mazzotta 2012).

3.2.3.1 Hooke model

The Hooke model, is constituted by a spring, that describes the behavior of a perfect elastic element, capable instantly to reach the deformed configuration under load action and to instantly take back the non-deformed configuration after the ending of the action.

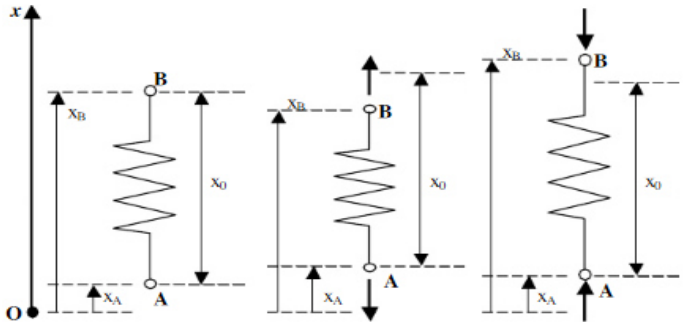

Figure 3.5 Hooke model configuration.

In energy terms, the hysteretic area is nil. The characterization of the material can be made by two parameters: the elastic modulus or Young modulus (E) and Poisson's ratio (ν). In the case of homogeneous and isotropic materials Hooke's law assumes the following formulation on three cardinal directions x, y, z:

$$\varepsilon_x = \frac{1}{E}[\sigma_x - \nu(\sigma_y + \sigma_z)]$$
$$\varepsilon_y = \frac{1}{E}[\sigma_y - \nu(\sigma_x + \sigma_z)]$$
$$\varepsilon_z = \frac{1}{E}[\sigma_z - \nu(\sigma_x + \sigma_y)$$
$$\gamma_{xy} = \frac{\tau_{xy}}{G} \qquad (3.6)$$
$$\gamma_{yz} = \frac{\tau_{yz}}{G}$$
$$\gamma_{zx} = \frac{\tau_{zx}}{G}$$

Where G is the shear modulus, which can be expressed as a function of the two independent constants in the following way:

$$G = \frac{E}{2(1+\nu)} \qquad (3.7)$$

In the case of harmonic stress, the Hooke's model can be represented by a spring connected to a crank, which is driven by a rotating element with angular velocity ω. Knowing the equation of the imposed deformation is obtained the tension trend:

$$\gamma = \gamma_0 \text{sen}(\omega \cdot t)$$

$$\frac{\tau}{\gamma} = G \tag{3.8}$$

$$\gamma = G \cdot \gamma_0 \text{sen}(\omega \cdot t)$$

The spring gives a deformation perfectly in phase with the stress response, the phase angle between stress and strain is $\delta = 0\ °$ (Mazzotta 2012).

3.2.3.2 Linear viscosity model (Newton viscous dasphot)

In a perfect viscous body deformation is directly proportional to the tension application time according to a coefficient η, said dynamic viscosity. If the tension is removed the deformation not be returned, the energy used in the deformation process is completely dissipated. The viscous dashpot (Figure 3.6) obeys the law of Newton:

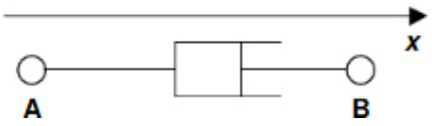

Figure 3.6 Viscous Newton dasphot.

$$\tau = \eta \cdot \dot{\gamma} \tag{3.9}$$

$$\sigma = \lambda \cdot \dot{\varepsilon} \tag{3.10}$$

where:
η: dinamic viscosity;
λ: elongational viscosity.

In the oscillatory test schematization, it can be made a damper connected to a crank, which is driven by a rotating element with angular velocity ω. The tension equation can be derived from that of deformation:

$$\gamma = \gamma_0 \text{sen}(\omega \cdot t) \tag{3.11}$$

$$\frac{\tau}{\dot{\gamma}} = \eta \tag{3.12}$$

$$\dot{\gamma} = \omega \cdot \gamma_0 \cos(\omega \cdot t) \tag{3.13}$$

$$\tau = \eta \cdot \omega \cdot \gamma_0 \cos(\omega \cdot t) \tag{3.14}$$

This demonstrates that the damper gives a deformation response in phase quadrature with the stress, ie there is a phase angle δ = 90 ° (Mazzotta F. 2012).

3.2.3.3 Maxwell model

It is the most simple viscoelastic model, consisting of the series combination of spring (stiffness G) and dashpot containing an ideal fluid viscosity η (Figure 3.7). As already specified earlier, the Maxwell model describes the behavior of a viscoelastic liquid. The strain rate of the system is given by the sum of the spring and dashpot strain rate:

$$\left(\frac{d\gamma}{dt}\right)_{tot} = \left(\frac{d\gamma}{dt}\right)_{spring} + \left(\frac{d\gamma}{dt}\right)_{dashpot} \tag{3.15}$$

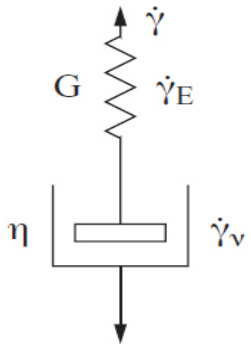

Figure 3.7 Maxwell linear viscoelastic model.

By the laws of Hooke and Newton are derived as follows:

$$\left(\frac{d\gamma}{dt}\right)_{spring} = \frac{1}{G}\frac{d\tau}{dt} \tag{3.16}$$

$$\left(\frac{d\gamma}{dt}\right)_{damper} = \frac{\tau}{\eta} \tag{3.17}$$

from which the differential equation that adjusts the model:

$$\left(\frac{d\gamma}{dt}\right)_{tot} = \frac{1}{G}\frac{d\tau}{dt} + \frac{\tau}{\eta} \tag{3.18}$$

The relationship between the damper viscosity η and the spring stiffness G is defined relaxation time λ. Applying τ_0 at time t=0 with constant deformation γ that occurs instantaneously, is measured the stress decreasing with time. Since dγ/dt =0 for t> 0:

$$\frac{\tau(t)}{\tau_0} = e^{-(t/\lambda)} \tag{3.19}$$

The (3.19) shows that the strain is zero at a sufficiently long time, after which deformation imposed remains in an irreversible way. In addition, if the deformation is kept constant, according to Hooke's law we have:

$$\frac{\tau(t)}{\tau_0} = \frac{G(t)}{G} \tag{3.20}$$

There where the elastic constant of the spring and G (t) is the form of the deformed system, said relaxation modulus:

$$\frac{G(t)}{G} = e^{-(t/\lambda)} \tag{3.21}$$

However applying to the Maxwell model a stress τ_0 at time t=0 there is an instantaneous deformation $\gamma_0 = \tau_0/G$ due to elongation of the Hook element; maintaining constant in time τ_0, elongation of the elastic element is added to the viscous deformation. Integrating (3.18) is obtained:

$$\gamma(t) = \left(\frac{1}{G} + \frac{t}{\eta}\right) \cdot \tau_0 \tag{3.22}$$

In the case in which it applies a periodic deformation to the Maxwell model equation it is obtained explaining the state equation and solving the differential equation (Mazzotta 2012):

$$\dot{\gamma} = \dot{\gamma}e + \dot{\gamma}\,v \tag{3.23}$$

$$\omega \cdot \gamma_0 \cdot \cos(\omega t) = \frac{1}{G}\frac{\partial \tau}{\partial t} + \frac{\tau}{\eta} \tag{3.24}$$

$$\tau = \frac{G \cdot \eta^2 \cdot \omega^2}{1+\eta^2 \cdot \omega^2} \operatorname{sen}(\omega t) + \cos(\omega t) \tag{3.25}$$

3.2.3.3 Kelvin-Voigt model

It consists of a spring with stiffness G = 1/J and by a damper with constant η placed in parallel (Figure 3.8). The Kelvin-Voigt model describes the behavior of a viscoelastic solid. In this case the overall effort that emphasizes system is divided between spring and dashpot:

$$\tau_{tot} = \tau_{spring} + \tau_{dasphot} \tag{3.26}$$

where:

$$\tau_{spring} = G \cdot \gamma = \frac{\gamma}{J} \tag{3.27}$$

$$\tau_{damper} = \eta \frac{d\gamma}{dt} \tag{3.28}$$

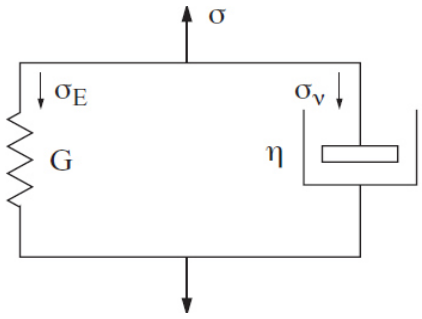

Figure 3.8 Kelvin- Voigt linear viscoelastic model.

The differential relationship between stress and strain is therefore given by:

$$\tau = \frac{\gamma}{J} + \eta \frac{d\gamma}{dt} \tag{3.29}$$

In the Kelvin-Voigt model the magnitude ηJ = λ is called the delay time. Assuming you perform a creep test, ie imposing at time t=0 a stress τ_0 which is kept constant over time:

$$\gamma = J \cdot \tau_0 [1 - e^{-\left(\frac{t}{\lambda}\right)}] \tag{3.30}$$

This result highlights that the Kelvin-Voigt model behaves as an elastic solid ideal only in infinitely long times. From the comparison with the Hooke's law we can deduce the following:

$$J(t) = J[1 - e^{-\left(\frac{t}{\lambda}\right)}] \tag{3.31}$$

where λ is a measure of the delay with which the compliance becomes independent of time. Removing the stress τ_0 at time t_0, when the deformation has reached the value γ_0, you are obtained:

$$\gamma = \gamma_0 \cdot e^{\left(\frac{-t-t_0}{\lambda}\right)} \tag{3.32}$$

The 2.29 shows that, for a sufficiently long time, the deformation is canceled; the Kelvin-Voigt model therefore does not give rise to permanent deformations and represents a delayed elasticity body. In the case in which the stress various periodically according to the law $\tau = \tau_0 \sin(\omega t)$, obtaining the following expressions for the real and imaginary components of the complex deformability J* (Mazzotta 2102):

$$J'(\omega) = \frac{J_0}{1+\omega^2\lambda^2} \tag{3.33}$$

$$J''(\omega) = \frac{J_0\omega\lambda}{1+\omega^2\lambda^2} \tag{3.34}$$

3.2.3.4 Burger model

As mentioned previously, the Maxwell and Kelvin-Voigt models are inadequate to describe the actual behavior of viscoelastic materials, except in special boundary conditions. In the specific case of bituminous binders that may be considered realized for very short load times and/or low temperatures (viscoelastic solid), or for very long load times and/or high temperatures (liquid-viscoelastic). To describe, however, the trends of G (t) in stress relaxation tests, and J (t) in the creep tests conducted on a large scale of the times and temperatures, it is appropriate to use more complex models. The simplest model that is traditionally considered is to Burger; it consists of two springs with G_0 and G_1 moduli and two dampers with coefficients η_0 and η_1. Using the principle effects superposition, for the elements connected in series, it is possible to write the system of equation in the form:

$$\gamma(t) = \frac{\tau_0}{\eta_0}t + \frac{\tau_0}{G_0} + \frac{\tau_0}{G_1}(1 - e^{-\frac{t}{\lambda_1}}) \quad (3.35)$$

Understanding the model passes through the step by step analysis of its behavior under load. From the applied load occurs an instantaneous elastic deformation (τ0/G0) and simultaneously the creepy begins to manifest; immediately after delayed elastic deformation follows (with continuity of the tangent) which, once died out, gives way to the viscous phase (always with continuity of the tangent). At the stop of the load, has a first elastic recovery, then an elastic recovery delayed until the degree of irreversible deformation that represents the stability condition (figure 3.9) (Mazzotta 2012).

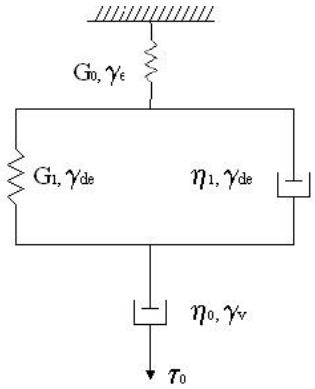

Figure 3.9 Burger viscoelastic model.

3.2.3.4 Generalized model

The materials such as bitumen have a viscoelastic behavior that is much more complex than that defined by the model of Burger. The behavior can't be simply described with reference to a relaxation time or to a delay time, but it is necessary to consider the spectrum of these magnitudes. In case it is sufficient not only to refer to a relaxation time, or a single system with spring and damper in parallel, multiple delay times are considered: born the extension of the Kelvin-Voigt model (Figure 3.10). In the case in which it is observed that the elastic deformation and viscose are not characterizable with a single elastic constant and only a viscous damper, reference is made to multiple systems of the type of Maxwell's interacting with each other, and then connected in parallel: born the extension of Maxwell model (figure 3.11). In the case, for example, of a generalized model with n elements Kelvin-Voigt in series, the resulting

deformation of the application of a constant shear stress τ_0 varies with the following law:

$$\gamma = \frac{\tau_0}{G_0}\left(1 + \frac{t}{\lambda_0}\right) + \sum_{i=1}^{n} \frac{\tau_0}{G_i}\left[1 - \exp\left(-\frac{t}{\lambda_i}\right)\right] \tag{3.36}$$

where G_0 and λ_0, represent the constants of the first element Maxwell (more sink spring in series) (Mazzotta 2012).

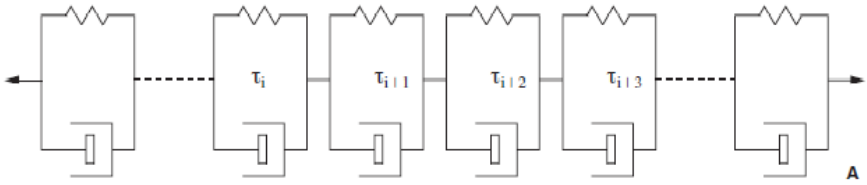

Figure 3.10 Kelvin-Voigt generalized model.

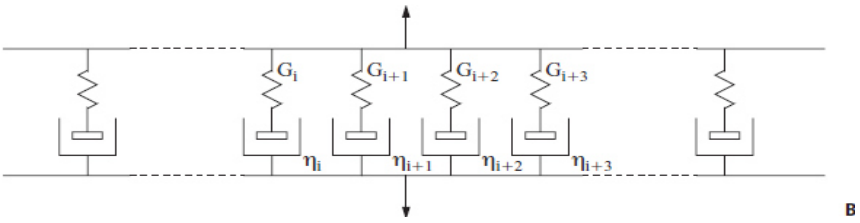

Figure 3.11 Maxwell generalized model.

3.3 Rheological parameters of bituminous binder

3.3.1 Oscillatory rheological bitumen parameters

The oscillatory tests consist to subject the sample to a stress or a deformation, which varies in time according to a harmonic law. Referring to the stress, this can be described according to the formula:

$$\tau = \tau_0 \cdot \text{sen}(\omega t) \tag{3.37}$$

where

τ_0: stress oscillation amplitude;

ω: pulse (equal to the frequency to less than 2π factor).

The corresponding deformation is measured:

$$\gamma = \gamma_0 \cdot \text{sen}(\omega t - \delta) \tag{3.38}$$

where:

γ_0: strain amplitude;

δ: phase angle.

The bitumen viscoelastic nature causes that the deformation oscillates with the same stress frequency, but on delay than this. The delay amount is represented by the phase angle δ; it can assume values on the range between 0 and $\pi/2$ and measures the ratio between the reversible and viscous components: value 0 corresponds to a condition of perfect elasticity while in correspondence of $\delta = \pi/2$ the material behaves like ideal viscous fluid (figure 2.12) (Mazzotta 2012).

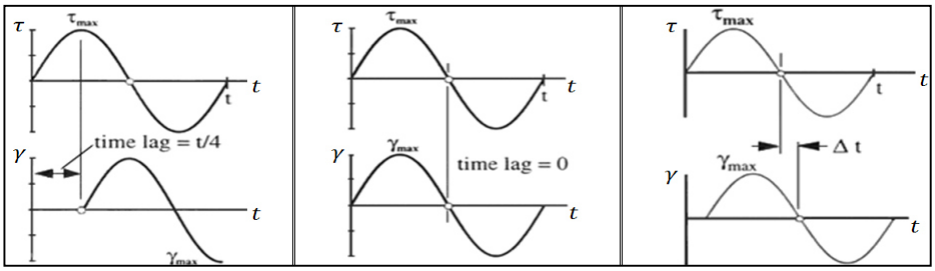

Figure 3.12 Materials behavior on phase angle function.

Note the applied stress and measured the deformation (controlled stress) it is possible to determine the complex modulus G:

$$G^* = \frac{\tau_0}{\gamma_0} \tag{3.39}$$

The complex modulus G* is represented as a complex number:

$$G^* = G' + iG'' \tag{3.40}$$

G' is the elastic modulus (storage modulus) and constitutes the complex modulus in-phase component to the load application; G'' is said viscous dissipation modulus and is the component in phase opposition (loss modulus). In Figure 3.13 are reproduced the two components in the complex plane.

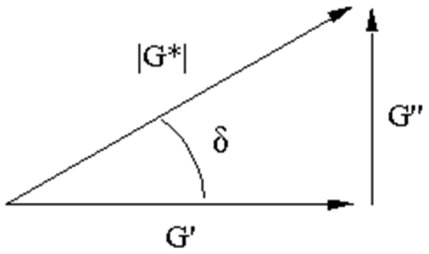

Figure 3.13 Complex plane.

So:

$$G' = G^*\cos\delta$$

$$G'' = G^*\text{sen} \tag{3.41}$$

$$G^* = \sqrt{G'^2 + G''^2}$$

The same considerations can be made in strain control. One of the main advantages to use oscillatory regime consists to perform a dynamic analysis of the behavior of bitumen, in order to simulate traffic load.

3.3.2 Data representation on sinusoidal oscillatory test

3.3.2.1 Black Diagram

One possible representation of the data from sinusoidal oscillatory test, alternative to viscoelastic functions representation in the frequency domain, is made from Black Diagram (Figure 3.14), in which each pair δ-G* is representative of one frequency and one temperature.

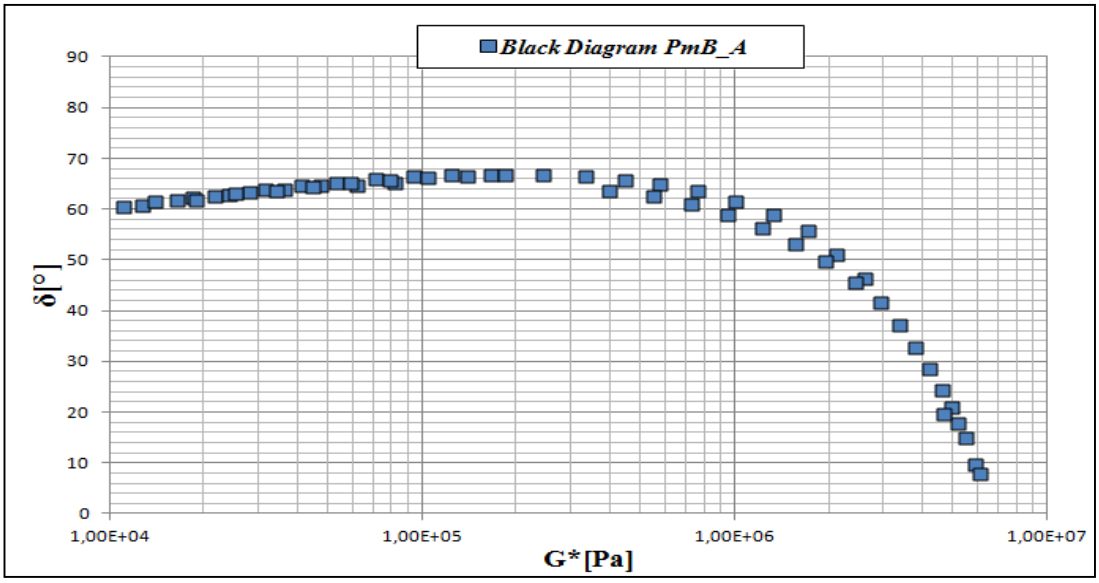

Figure 3.14 Black Diagram.

3.3.2.2 Cole-Cole Diagram

A different data representation of the sinusoidal oscillatory test is possible on Cole-Cole plane (Figure 3.15), where the origin functions are the storage modulus G' and the loss modulus G''. Referring to the equivalent mechanical models is possible to represent the behavior through Cole-Cole plane curves (Figure 3.16).

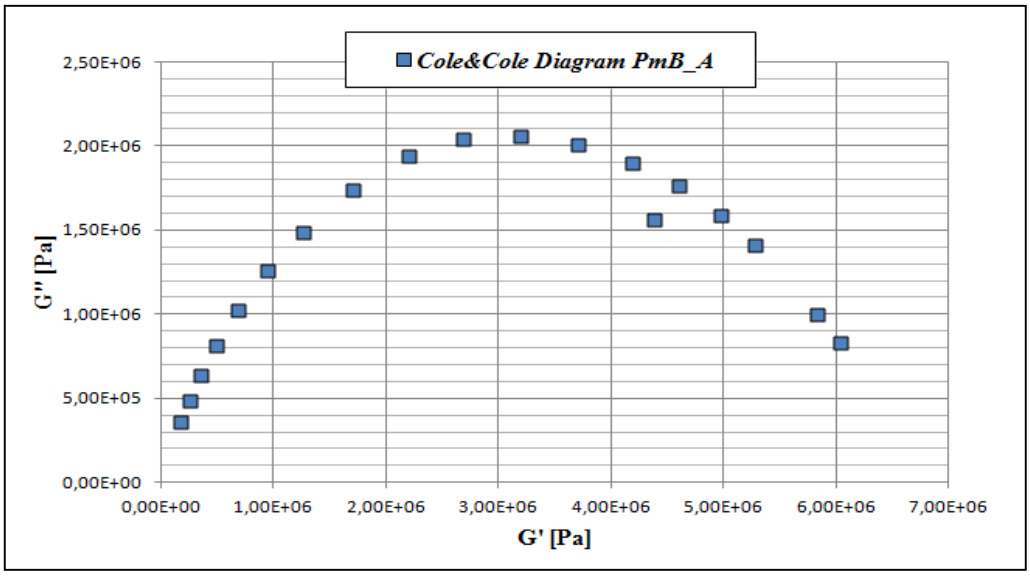

Figure 3.15 Cole-Cole diagram.

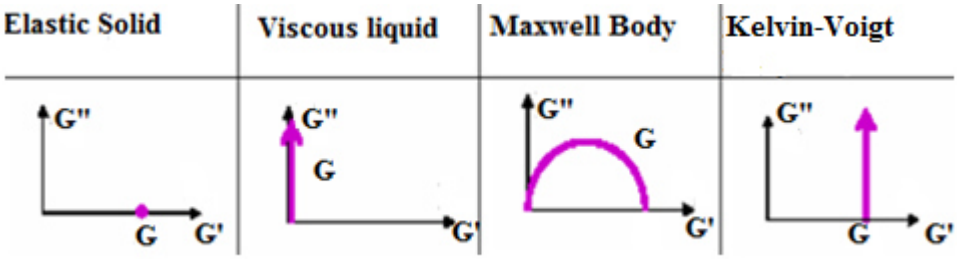

Figure 3.16 Rheological model on Cole-Cole diagram.

Complex modulus and phase angle variations are represented, varying the load frequencies, through the variation of storage and loss modulus. At high frequencies the loss modulus is 0, the opposite happens for low frequency. On the elementary models, special situations are obtained. The spring behavior is independent by the frequency and the Cole-Cole plot is identified by a single point in correspondence of the spring elastic modulus G. For the dashpot the curve coincides with the axis of ordinates, and the module tends to infinity for high values of the frequency, while it is zero for zero frequency (Mazzotta 2012).

3.2.2.3 Time-temperature superposition principle (TTS)

The viscoelastic properties are often heavily dependent on temperature. Several studies have shown that the G' and G'' moduli at different temperatures can be gathered together into a single curve, called master curve, through the time-temperature

equivalence principle, also known as the principle of time-temperature superposition (TTS). The principle implies that the same variation of a mechanical quantity, which the complex modulus G*, obtained by varying the frequency at fixed temperature can be obtained by varying the frequency and keeping the temperature fixed (Figure 3.17). Immediate consequence is the possible display on a single curve of the viscoelastic behavior of the test material in a frequency range far wider than that accessible experimental apparatus at fixed temperature. The materials whose behavior you can see in this way are said thermo-rheological simple. The principle of time-temperature superposition is therefore expected that a change of temperature variation across the relaxation times of a same factor said shift factor (Figure 3.17). If that is, τ_1 (T_0), τ_2 (T_0), τ_3 (T_0), ... are the relaxation times at a reference temperature T_0, then the effect of varying the temperature to a different value T will be to change these times in: τ_1 (a_T), τ_2 (a_T), τ_3 (a_T) where a_T is the shift factor, function of T. This factor is 1 for T = T_0. Then:

$$\tau_1(T) = a_T \cdot \tau_1 (T_o) \tag{3.42}$$

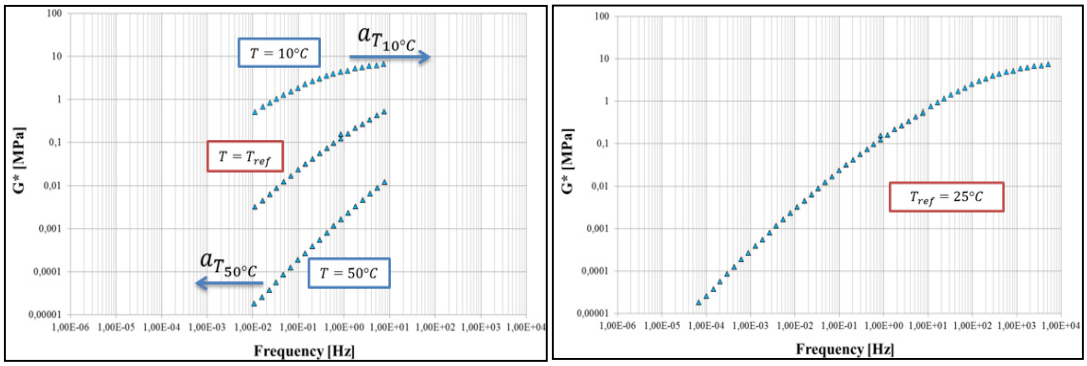

Figure 3.17 Master curve construction with TTS principle.

P.E. Rouse proposed a theory that can explain the origins and deduce the implications of the principle of time-temperature superposition (Merusi F. 2009). It examines the motion of a polymer chain summarized as a masses connected by springs necklace (Figure 2.17). The masses then undergo the effect of viscous forces. The problem is studied searching the normal modes of oscillation. The results include the principle of time-temperature superposition (Merusi F. 2009).

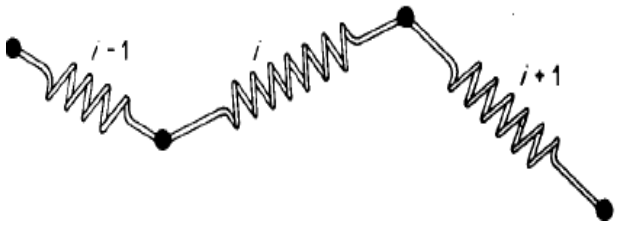

Figure 3.18 Rouse model.

It is shown that the stiffness of all of the individual spring elements G_i vary by an identical factor determined according to the following equation where ρ is the density of the material:

$$G_i(T) = G_i(T_o)\frac{T\cdot\rho}{T_o\cdot\rho_0} \tag{3.43}$$

The temperature dependence can then be made explicit in the formulation of the relaxation modulus of the generalized Maxwell model:

$$G_i(t,T) = \frac{T\cdot\rho}{T_o\cdot\rho_0}\cdot\sum_{i=1}^{n} G_i(T_0)\, e^{\frac{t}{a_T\cdot\lambda_i(T_0)}} \tag{3.44}$$

Defined the reduced relaxation modulus:

$$G_r(t) = G_i(t,T)\frac{T_0\cdot\rho_0}{T\cdot\rho} \tag{3.45}$$

and the limited time:

$$t_r = \frac{t}{a_T} \tag{3.46}$$

The equation that describes the evolution of the module reduced in the domain of the reduced time, that contains in its interior both relating to the dependency information by time and temperature:

$$G_r(t_r) = \sum_{i=1}^{n} G_i(T_0)\, e^{\frac{t_r}{\cdot\lambda_i(T_0)}} \tag{3.47}$$

It follows that G (t, T), as well as other viscoelastic magnitudes, directly dependent on both time and temperature, can be expressed as functions of a single variable, the reduced time. The law of variation of a_T shift factors with temperature is constructed through the analysis of experimental data and is generally described by the Willimas-Landel-Ferry (WLF):

$$\log(a_T) = -\frac{C_1(T_1-T_0)}{C_2+T-T_0} \quad (3.48)$$

where C1 and C2 are two constants which depend on the material of the fitting, or the law of Arrehnius::

$$\log(a_T) = \frac{E_f}{R}\left(\frac{1}{T}-\frac{1}{T_0}\right) \quad (3.49)$$

The use of the law WLF or that of Arrhenius depends in general on external conditions and in particular, for bituminous and polymeric materials, on the location of the test temperature than the glass transition and the material. For T <Tg is generally has the domain of validity of the Arrhenius law while the WLF equation is applicable in the region T> Tg (Mazzotta 2012).

3.3.3 Master curve and empirical model

The TTS principle is realized in the development of master curves, the curves obtained by the translation of the data measured for several test temperatures that determine the trend of the viscoelastic function in question, in a new domain, more extensive than that of the individual initial curves, and in which effects of time and temperature coexist. The master curves can be used to represent the behavior of the material in a wide time or load frequency range where the experimental way determined by the only curve encloses both the effects of time and temperature. The extent of the transfer of individual curves defines the offset factors. For some thermo-theologically simple materials overlap Trends are requiring only horizontal translations. In this case, the offset factors coincide with the only horizontal shift factors a_T, defined in the previous paragraph. In the case of data derived from analysis in sinusoidal oscillatory regime, the data translation, according to the determination of the reduced frequencies, are obtained:

$$\omega_r(T_0) = a_T\omega(T) \quad (3.50)$$

$$a_T = \frac{\omega_r(T_0)}{\omega(T)}$$

In more complex cases use it should be made also with vertical offsets (vertical shift factors, b_T) attributable to non-negligible variation of the density ρ of the material with

temperature and defined in accordance with the assumptions set out in the preceding paragraph.

$$b_T = \frac{T_0 \rho_0}{T \rho} \tag{3.51}$$

The complex modulus and phase angle master curves have employees trends from the material but the general shape of the curve can however be described through some parameters and general considerations valid and commonly also applied in the case of road bitumens.

- glassy asymptote, defines the limit behavior of the material T at low and high frequencies. The value of G * tending to glassy asymptote is shown with Gg;
- viscous asymptote defines the limit behavior of the material at high T and low frequencies. Viscous asymptote defines the viscosity of the stationary state $\eta_{ss} = \lim_{\omega \to 0} \frac{G^*}{\omega}$ for small oscillation amplitudes can then place $\eta_{ss} = \eta_0$;
- crossover frequency ω_c: in correspondence of the oscillation frequency of which at a given temperature it has tan δ = 1, ie δ = π / 4 and G '= G".
- rheological index R: difference between the glassy form and the complex form the crossover frequency,, $R = G_{gg} - G^*(\omega_c)$. R indicates the "speed" at which the curve reaches the asymptote glassy (Dalmazzo 2008)

Hereinafter will be described a number of models derived empirically. All described models estimate the rheological properties of bitumen inside dl linear viscoelastic range (LVE). These properties are normally represented in terms of master curves and trend of 'phase angle δ to a specific reference temperature. In general, all the exhibited models are able to predict the rheological properties of bitumen (LVE) and will be processed in the following chapters in order to provide analytical support to the data collected empirically.

3.3.3.1 Christensen and Anderson (CA) Model

The linear viscoelastic model, developed at Pennsylvania State University (PSU), is a mathematical model which reproduces, for all temperatures and frequencies of interest of a road pavement, the behavior of the bitumen subjected to creep tests and tests in

oscillatory regime. The pattern consists of two sets of reports produced by Christensen and Anderson: one for the viscous zone, the other for the rest of the frequencies of the field. In Figure 3.19 the characterization of a master curve parameters are indicated:

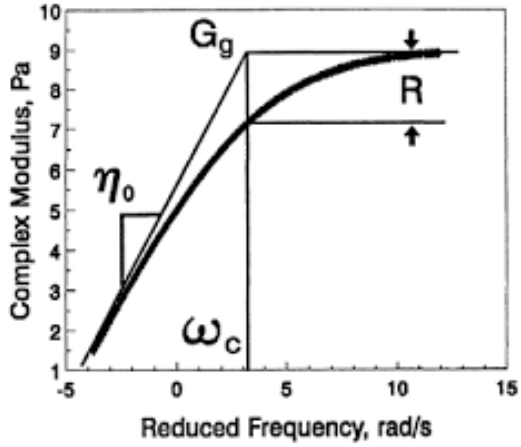

Figure 3.19 Characteristic master curve parameters on CA model.

Linear viscoelastic limit definition, it is in the field of linear-viscoelastic (LVE) if the stress-strain relationship, τ / γ, is constant at any point. The model determines the linear limit on the curve-frequency elastic modulus defining the limit at the point at which the module drops to 95% of the maximum value obtained. It is also suggested to carry out the tests with voltage more than 75% of that of the linear limit.

- the glassy form (glassy modulus) - horizontal asymptote value at which the complex modulus tends to low temperatures and high load frequency. It is a constant value for each type of bitumen and is approximately equal to 1 GPa. The phase angle, when the bitumen approaches the glassy form, tends to $\delta=0°$.
- the viscosity of the stationary zone - the zone Newtonian viscosity achieved at high temperatures and at low load frequencies; is also called the asymptote viscous and is represented by a straight line with angular coefficient equal to 1. The phase angle is close to $\delta = 90°$.
- the "crossover" rate - defined as the frequency that the master curve of the diagram corresponds to the intersection between the asymptote glassy and viscous asymptote. Its inverse is called "crossover time". This value indicates the transition from the viscous zone at viscoelastic region, so it is an indicator of the consistency and hardness of the material.

- the rheological index - defined as the difference between the glassy form and the dynamic complex modulus obtained at the crossover frequency. It is a very important parameter because it is directly proportional to the amplitude of the relaxation spectrum, which gives it the property of being an excellent indicator of the rheological type of material; in practice, it characterizes the performance of the rheological curves. It is independent from the reference temperature but not the type of bitumen.

The equations that describe the complex modulus |G*| and the phase angle δ, as a function of the previously described parameters, are followed below (Dalmazzo 2008):

$$|G^*| = G_g \left[1 + \left(\frac{\omega_c}{\omega}\right)^{\frac{(\log 2)}{R}}\right]^{-\frac{R}{\log 2}} \tag{3.52}$$

$$\delta = \frac{90}{\left[1+\frac{\omega}{\omega_c}\right]^{\frac{(\log 2)}{R}}} \tag{3.53}$$

$$R = \frac{\log 2 \times \log\left(\frac{|G^*|}{G_g}\right)}{\log\left(1-\frac{\delta}{90}\right)} \tag{3.54}$$

with:

G_g: glassy modulus;

η_{ss}: stationary state viscosity ;

ω_c: crossover frequency [rad/s];

R: rheological index.

3.3.3.2 Christensen, Anderson and Marasteanu (CAM) Model

The CAM model was found by the rheological study performed on modified bitumen, and with respect to the CA model describes more accurately the behavior of such binders to low and high frequencies. Below the equations proposed by the researchers:

$$|G^*| = G_g \left[1 + \left(\frac{\omega_c}{\omega}\right)^{v}\right]^{-\frac{w}{v}} \tag{3.55}$$

with v = log 2 / R, and R the rheological index previously described. The phase angle δ is described as follows:

$$\delta = \frac{90}{\left[1+\frac{\omega_c}{\omega}\right]^v} \tag{3.56}$$

The parameter w describes the speed with which the module |G*|. It tends to the two horizontal asymptotes (asymptote viscous at 45° and glassy asymptote Gg). During their studies Christensen, Anderson and Marasteanu, analyzing 35 modified bitumen and additives, and comparing the two models (CA-CAM) they found the form values that differed by about 10-35%. This finding can be explained by the more or less high presence of waxes and asphaltenes, which influence the simple thermo-rheological behavior of the binders. While making significant improvements compared to the CA model, the model has shown some gaps especially at high temperatures (Yusoff *et al.* 2011).

3.3.3.3Modified Christensen, Anderson and Marasteanu Model

The model described below was proposed by Zeng, and was developed as a result of dynamic tests in oscillatory regime executed on 9 modified bitumen. All were tested with the Dynamic Shear Rheometer simulating a wide range of load frequencies, and temperatures. The model is valid for both ligands that for bituminous conglomerates. In particular models the behavior of the bitumen as a viscoelastic fluid, that of the mixture as a viscoelastic solid (Anderson and Marasteanu 2010) (Yusoff *et al.* 2011). Generalizing the CAM model, the complex module is described by the following formula:

$$|G^*| = G_e + \frac{G_g - G_e}{\left[1+\left(\frac{f_c}{f'_c}\right)^k\right]^{\frac{m_e}{k}}} \tag{3.57}$$

where:

G_e = |G*| per $f \rightarrow 0$, equilibrium moduls;

G_g = |G*| per $f \rightarrow \infty$, glassy modulus;

f_c = position parameter;

f'_c = reduced frequency.

The reduced frequency is a function of both the temperature that the deformation, and is equal to:

$$f_c' = f_c \left(\frac{G_e}{G_g}\right)^{\frac{1}{m_e}} \tag{3.58}$$

K with me and shape parameters, dimensionless and estimable during calibration of the model through a linear regression. The term fc, is comparable to the crossover frequency of the AC and CAM models. Figure 19.2 reproduces the model parameters, and through the course of the master curve is immediate notice how G_g and G_e are the two horizontal asymptotes when the frequency tends to infinity and zero, respectively. The third asymptote visible in the figure has slope m, and its intersection with the asymptotes G_g and G_e, on the horizontal axis identifies the crossover frequency fc and the reduced frequency f'c. Whereas a log decade as a unit, the distance between G_g (fc) and G_g is given by:

$$R = \log \frac{2^{\frac{m_e}{k}}}{1+\left(2^{\frac{m_e}{k}}-1\right)\frac{G_e}{G_g}} \tag{3.59}$$

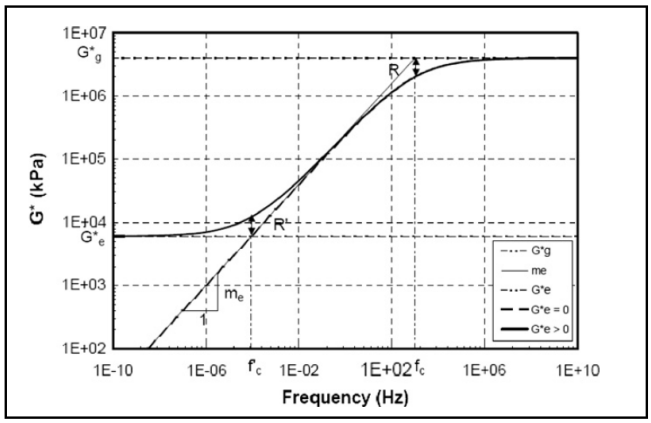

Figure 3.20 Characteristic master curve parameters on CAM model.

The phase angle:

$$\delta = 90I - (90I - \delta_m)\left\{1 + \left[\frac{\log(\frac{f_d}{f'_c})}{R_d}\right]^2\right\}^{\frac{m_d}{2}} \tag{3.60}$$

con:

δ_m : phase angle at f_d ;

f_d : frequency of bitumen inflection;

R_d e m_d: shape parameters.

Zeng has no I explicit parameter however, has shown that I = 0 if f > fd and I = 1 if f <fd. Furthermore, the δ phase angle function satisfies the interval between 90° and 0°. Like other seekers the same Zeng used the WLF equation (described in the previous section) to detect the shift factor or alternatively the formulation of Arrheenius to translate the frequencies at low test temperatures. In the course of the study the author has found that the modulus | G * | derived from the model followed the trend of modules derived empirically. For what concerns the phase angle, on the contrary, it is not respected such two-way nature, probably due to some errors in measurement and analysis (Yusoff *et al.* 2011).

3.3.3.4 Sigmoidal model (CAM)

The function of the dynamic module obtained from the sigmoidal model, was introduced in the Mechanistic-Empirical Pavement Design Guide (ME PDG), developed in the course of the National Cooperative Highway Research Program (NCHRP), Project A-37A. Mathematically, the model takes the following form (Figure 3.21):

$$\log|G^*| = v + \frac{\alpha}{1+e^{\beta+\gamma\{\log(\omega)\}}} \quad (3.61)$$

with:

log(ω) : logaritmic reduced frequency;

v : lowest asymptote;

β e γ : shape factors between the asymptotes and the local inflection points (points corresponding to a frequency $\omega = 10^{-\beta/\gamma}$);

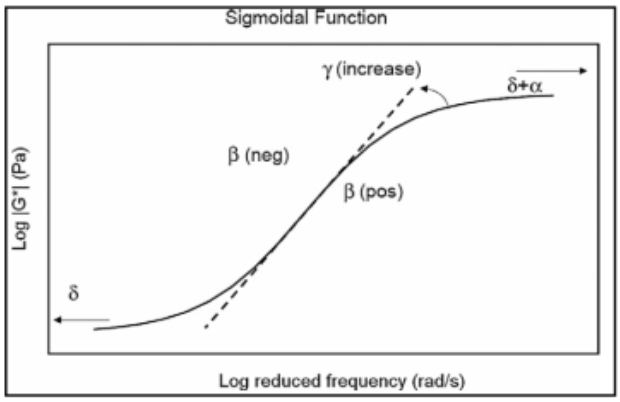

Figure 3.21 Sigmoidal model master curve.

In sigmoidal model the shift factor a_T is calculated as a function of the viscosity of the bitumen, in order to have a correlation with the pavement aging. In this model the master curve construction refers to the modulus cannot regardless the phase angle. Normally in polymer modified bitumen assume values G_g = 1GPa (Yusoff N.I. *et al.* 2011). Bonaquist and Christensen have proposed an amendment to the sigmoidal model in this report:

$$\log|G^*| = v + \frac{Max-v}{1+e^{\beta+\gamma\{\log(\omega)\}}} \tag{3.62}$$

with

Max : limit value complex modulus.

3.4 Dynamic Oscillatory Test using DSR

3.4.1 Dynamic Shear Rheometer

DSR is the acronym for Dynamic Shear Rheometer and is used to measure the dynamic shear modulus and phase angle of bituminous binders at intermediate and high pavement temperatures. In the DSR dynamic oscillatory testing, the shear stresses and shear strains vary with time from positive to negative in a sinusoidal fashion. The DSR provides stress-strain moduli at different rate of loading expressed in terms of frequency at different test temperatures (Anderson *et al.* 1994). The DSR equipment used in bituminous binders characterisation can be divided into two categories:

- controlled stress, when the rheometer applies a stress to the specimen and measures the resulting strain;
- controlled strain, when the rheometer applies a strain to the specimen and measures the resulting stress.

A 1-mm by 25-mm or 2-mm by 8-mm, hockey puck-shaped, sample of bituminous binder squeezed between two parallel metal plates is placed in a temperature controlled chamber, as shown in Figure 2.12. The chamber for controlling the test specimen temperature by heating or cooling maintains a constant specimen environment. The medium in the environment chamber can be liquid or gas. Due to the extreme temperature dependency of bituminous binders, it is necessary to control the temperature for the rheological testing of bituminous binders to a much finer degree than for most other viscoelastic materials. A change in temperature of 1°C can result in a modulus change of up to 25 percent for some binders (Anderson et al., 1994). Two types of spindles (upper plate) used in the DSR testing are 25-mm diameter parallel plate geometry, and 8-mm diameter parallel geometry. It is essential to select spindle geometry due to the effect of compliance of parallel plate geometry on rheological measurements for the extremely high stiffness binders under dynamic loading at low temperatures. Anderson et al. (1994) suggested that 25-mm parallel plates should be used when the complex modulus ranges from 103 to 105 Pa; 8-mm parallel plates should be used when the complex modulus ranges from 105 to 107 Pa; torsion bar or bending beam rheometer should be used when the complex modulus is greater than 107 Pa. During the test, the sample of bituminous binder is sheared between two parallel plates. One of the parallel plates is oscillated with respect to the other at

selected frequencies and rotational deformation amplitude (or torque amplitude). As shown in Figure 2.13, the spindle (upper plate) is caused to oscillate sinusoidally while the base plate is fixed during testing. The testing is carried out by oscillating the spindle about its own axis such that a radial line through point A moves to point B, then reverses direction and moves through point A to point C, followed by moving back from point C to point A (Figure 2.1) (Airey G.,1997) .

3.4.2 Plate – Plate configuration

The measurement system consists of a lower plate which is generally fixed, and a top plate connected to the motor shaft of the instrument through which the rotation is applied (Figure 3.22).

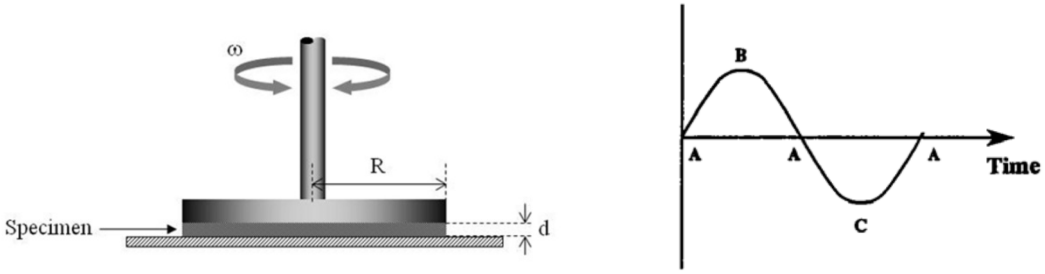

Figure 3.22 Configuration plate - plate

The geometric quantities that define the system are the radius R and the so-called gap which is the distance between the plates, upper and lower measurement position (Figure 3.22). The gap must be appropriately determined based on the type of material to be tested. In general it can be said that it should be at least 5 times larger than the maximum size of the particles contained in the specimen, in order not to result in interference with the system and, therefore, errors in measurement. It is noted the torque T, the rotation angle Θ and the angular velocity Ω, the quantities of interest are obtained with the following equations (Figure 3.22) :

$$\tau = \frac{2T}{\pi r^3} \ ;$$

$$\gamma = \frac{\Theta r}{h} \ ;$$

$$\dot{\gamma} = \frac{\Omega r}{h}.$$

The value of the complex modulus G* is calculated from the ratio between the maximum applied shear stress and the maximum deformation obtained and expressed, as mentioned above, the measurement of the total resistance to the deformation of a material. Conversely, the phase angle δ is calculated by evaluating the delay of the wave of deformation respect to that of the load and represents the delay or the phase difference which occurs between the application of stress and the setting up of deformation. The following expressions show what was said: $G^*=\tau_{max}/\gamma_{max}$ and $\delta= \Delta t/t *360$.

3.5 Mortar configuration test

3.5.1 Viscoelastic stress analysis of torsional circular bars

Figure 3.23 simply illustrates a sand asphalt sample installed in the DMA. The solid circular sand asphalt sample of length *L* and constant radius *R* is subjected to a twisting moment (torque) *T* , so as to produce a prescribed angle of twist φ . For a viscoelastic material, this problem can be treated by an approximate method to solve for the torque and stress distribution as a function of time resulting from the prescribed angle of twist. Equilibrium equations governing the problem are automatically satisfied because the problem is statically determinate (Kim Y-R. and Little D.N. 2005).

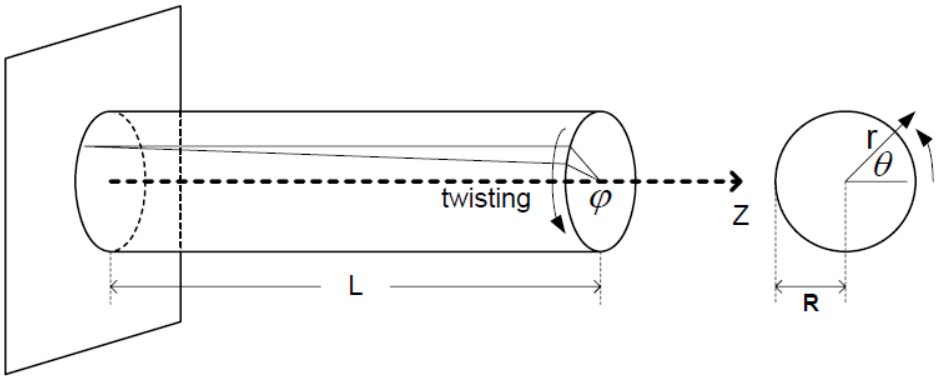

Figure 3.23 Simple Illustration of the Cylindrical Bar under Torsion.

Displacement of a general point can be reasonably expressed as a tangential direction displacement, u_θ , in cylindrical coordinates r,θ,z :

$$u_\theta = \Theta(t) r z \tag{3.63}$$

Where $\Theta(t) = \frac{\varphi(t)}{L}$ angle twist per unit length. The only valid strain-displacement relationship considering the tangential displacement, u_θ, is given by:

$$\gamma(t) = \frac{\partial u_\theta(t)}{\partial z} + \frac{1}{r}\frac{\partial u_z(t)}{\partial \theta} \tag{3.64}$$

It should be noted that the second term in equation 3.64 is negligible, because vertical displacement $u_z(t)$ is assumed to be zero. If the material is isothermal linear viscoelastic, the constitutive equation in terms of a convolution integral is given as follows:

$$\tau(t) = \int_0^t G(t-\xi)\frac{\partial \gamma}{\partial \xi} d\xi \tag{3.65}$$

$$\gamma(t) = \int_0^t J(t-\xi)\frac{\partial \tau}{\partial \xi} d\xi \tag{3.66}$$

Where τ (t) = time-dependent shear stress,

γ (t)= time-dependent shear strain,

G(t) = shear relaxation modulus,

J (t)= shear creep compliance,

t = time of interest, and

ξ = time-history integration variable.

The torque T(t) required to maintain a constant angle of twist Θ(t) can be calculated as follows by summing the moment of tangential force increments over the cross-sectional area:

$$T(t) = \int_0^{2\pi} \int_0^r r\,\tau(t) r dr d\theta \tag{3.67}$$

It should be noted that the shear stress in equation 3.67 is not necessarily linear viscoelastic. Equation 3.67 can be expressed in the following simple form:

$$\tau(t) = \frac{T(t)}{J} r \tag{3.68}$$

$$J = \int_0^{2\pi} \int_0^r r^3\, dr d\theta \tag{3.69}$$

$$\gamma(t) = \frac{\varphi(t)}{L} r \tag{3.70}$$

With the displacement function ϕ(t) , linear viscoelastic material property G(t), and sample geometry, corresponding shear stress and shear strain as a function of time can be calculated by equations 3.65 and 3.70. Alternatively, the shear stress can also be determined by equation 3.68, when the resisting torque is measured (Kim Y-R. and Little D.N. 2005). Given measurements of the displacement and torque, the linear viscoelastic material property is identified based on the constitutive relation, and viscoelastic stress analyses can be conducted analytically and/or numerically. The DMA instrument typically requires an oscillatory twisting displacement as input and provides resisting transducer torque responses. Under dynamic loading conditions, viscoelastic materials normally produce frequency domain dynamic properties such as storage modulus, loss modulus, and the phase angle between stress and strain due to

time-dependency. The combined form of the storage and loss properties reduces to a complex modulus and a dynamic modulus (Kim Y-R. and Little D.N. 2005):

$$|G^*(\omega)| = \sqrt{|G'(\omega)|^2 + |G''(\omega)|^2} \quad (3.71)$$

$$G^*(\omega) = G'(\omega) + iG''(\omega)^2 \quad (3.72)$$

$$\phi = \tan^{-1}\left[\frac{G''(\omega)}{G'(\omega)}\right] \quad (3.73)$$

Where G* (ω) = dynamic shear modulus,
G* (ω) = complex shear modulus,
G' (ω) = storage shear modulus,
G" (ω) = loss shear modulus,
φ (ω) = phase angle,
ω = angular frequency, and
$i = -1$.

The shear stress-shear strain relation under the sinusoidal harmonic dynamic loading condition can be represented by:

$$\tau(t) = G^*(\omega)\gamma(t) \quad (3.74)$$

The relaxation modulus as a function of time can be determined by static creep, static relaxation, and/or dynamic frequency sweep tests within the linear viscoelastic region. Because torsional device usually employs dynamic loading, such as oscillatory vibration, the dynamic frequency sweep tests are performed to determine the linear viscoelastic relaxation behavior of materials. This is based on the theory of linear viscoelasticity inferring correspondence between frequency-domain and time-domain (Kim Y-R. and Little D.N. 2005).

3.5.1 Dynamic Mechanical Analyzer

The Dynamic Mechanical Analyzer DMA was originally intended to be used as a mechanical test system for evaluating viscoelastic properties of materials, especially polymers. The materials can be in solid, melt, or liquid state. The DMA system consists

of three main components: a test station, a system controller, and control computers. An environmental controller is optionally used for temperature control. The environmental controller provides low temperatures down to – 150°C using liquid nitrogen and high temperatures up to 600°C using a controlled electric heater. The impetus for the DMA testing of asphalt was originally from work performed by Goodrich (1988, 1991), Christensen and Anderson (1992), and Smith and Hesp (2000). Specifically, Smith and Hesp demonstrated that controlled-strain testing of mastics in a DMA leads to a controlled rate of microcrack development and growth, whereas controlled-stress testing would lead to rapid and uncontrolled crack growth (2000). Differences between the current study and those studies include the sample geometry used, the sample composition, and the loading sequence (including rest periods). A cylindrical rather than a rectangular sample was adopted in an attempt to avoid complex stress distribution in the samples and to make calculation easier. Rectangular samples have been the typical testing geometry for DMA (Kim Y-R. and Little D.N. 2005). Sand asphalt mixtures were employed so that samples could be tested at an intermediate temperature to minimize unstable plastic flow. A sample holder capable of properly securing the cylindrical sample was developed. Epoxy glue was used to secure the sand asphalt sample to the holder. In the gluing process, care was taken not to cause any undesirable stress concentrations. Figure 3.24 shows a schematic diagram of the cylindrical DMA sample with holders. Each sample was mounted in the DMA instrument, and the chamber was closed and allowed to equilibrate to the desired testing temperature. All tests were started after at least a 20-minute equilibration period at the test temperature. Figure 3.24 shows the cylindrical sand asphalt sample configuration installed in the DMA The DMA machine measures resisting torque of a sample due to sinusoidal displacement-controlled rotational input. According to a study by Reese, torsional loading is a better simulation of damage than bending loads when considering traffic movements(1997). Test data (applied displacement and corresponding torque response) were collected by a data acquisition (DAQ) system with a 16-bit multichannel board (Kim Y-R. and Little D.N. 2005)..

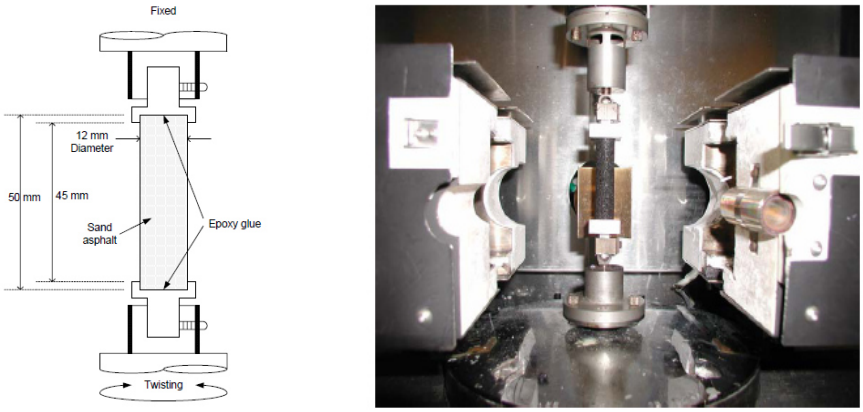

Figure 3.24 Schematic Diagram of the Cylindrical DMA Sample with Holders *("Development of specification-type tests to assess the impact of fine aggregate and mineral filler on fatigue damage").*

3.6 Permanent Deformation Behavior and testing of bituminous binders

3.6.1 Introduction of Rutting Phenomena

Asphalt concrete is among the materials which are widely used for roads and airports pavement. About 95% of all of the world pavements is of asphalt type (Huang, 1993) (Shafabakhsh G.H. and Sadeghnejad Y.S. 2014). These pavements over time suffer failure due to passing traffic loads and exposure to different environmental conditions. Among the most important of these failures, we can mention rutting which is considered as the main concern of transportation agencies in the field of pavement. Annually, millions of dollars have been spending to compensate rutting failures in the pavement. The temperature and stress-induced by loading can be named as two main parameters that lead to permanent deformation in asphalt pavements. When the traffic loading increases and temperatures are high, rutting failure are more likely to occurring. Rutting is a surface depression in the wheel path where pavement uplift occurs along the side of the rut. Rutting may lead to pavement failure and potential of hydroplaning. Due to this, the design process has to be taken into consideration. The asphalt design mix must involve a proper proportioning. Compaction factor and the pavement thickness need to bear in mind. Rutting potential also can be minimized by limiting the stress inducting by moving wheel load besides maximizing its fatigue life. The influence of each of the properties of the mixture in the performance of asphalt pavement must be determined to balance all the properties of the specific application embedded in mixtures of hot mix asphalt compacted asphalt can be evaluated through their properties mixture. This is particularly the density, stability, flow and stiffness. Numerous test methods are being used to evaluate the performance of Hot Mix Asphalt (HMA). Permanent deformation (Rutting), fatigue cracking, thermal cracking, loss of surface friction, and stripping are the five main distress types of (HMA) pavements. All of these distresses can result in loss performance, but rutting is the one distress that is the most likely to be a sudden failure as a result of unsatisfactory HMA. Other distresses are typically long term and show up after a few years of traffic. Permanent deformation or rutting is a primary failure mode of HMA pavements (Esmail M. *et al.* 2014). Rutting usually occur in the linear with wheel path. Rutting also known as permanent deformation can be defined as the accumulation of small amounts of unrecoverable strain as a result of applied loading to pavement (Esmail

M. *et al.* 2014). It is seen as longitudinal depression which follows the line of the wheelpaths (Esmail M. *et al.* 2014). The phenomena of rutting are an accumulation of permanent deformations and it is confined to the top layers of the pavement. These permanent deformations in the wearing course layer could be developed due to densification and plastic flow of this layer. They also recommend that rutting progress in two stages. Initial stage is that of densification of the bituminous concrete under moving trafficwhile the second stage is resulted due to plastic flow of bituminous concrete. Excessive binder, inadequate compaction, substandard materials, excessive loading or high moisture content can also create this problem (Esmail M. *et al.* 2014). Besides that, rutting can also manifest because of a poor pavement subgrade. Two of the causes of a weak subgrade are moisture and poor compaction during construction work. A weakened subgrade is susceptible to higher stress attributable to traffic loading; thus there is an increased probability of rutting in the pavement. Research in the field of improving the constituent materials of hot mix asphalt (HMA), mix designs and methods of analysis and pavements design, including laboratory and field tests are needed to cause providing more serves life for pavements and as a result, the loss of costs which are set to be spent to repair pavement failures is prevented. Researchers and engineers are continuously trying to improve asphalt pavement performance (Huang 1993) (Shafabakhsh G.H. and Sadeghnejad Y.S. 2014).

Figure 3.25 Rutting phenomena on surface layer.

Once two rheological values of G* and δ derived, it is possible to determine the "Performance Grade" to evaluate the rutting sensitivity at high temperatures. In fact,

each bituminous binder can be classified attributing to a class performance (Performance Grade PG), characterized by a number that defines a representative temperature range of the road paving project in which it is guaranteed satisfactory performance. This is the interval in which the binder is able to withstand, in operation, the dynamic stresses that simulate the behavior on the road. The standard identifies seven classes each in turn divided into subclasses. All classes are equivalent from the performance point of view; this means the level of required performance is equal in all cases but what distinguishes each class is the severity of the conditions at which this level should be guaranteed, and this makes a material more "practical (performance able)" than the other. A bitumen, for example, classified as PG 64 -28, may be used, without incurring deteriorations due to shortcomings in the performance of the binder, for a range of design temperatures between 64°C and -28°C. The logic that is the basis of this criterion is to provide the user with different territorial maps, divided into climatic areas, within each of them prescribes specific Performance Grade of the binder, always subordinate to the importance of the road. Related to environmental conditions, the territory is divided into climatic zones based on the minimum and maximum temperatures of the paving project, which is determined in accordance with appropriate models developed just under SHRP. On the basis of all the information available, the user can identify which type of binder must be used: in hot climates are suggested binders that meet the specifications in a wide range of temperatures, for example between 70°C and -22°C (PG 70 -22). In the cold areas are suggested binders with interval performance more shifted towards low temperatures, for example between 46°C and -34°C (PG 46 -34) Through G* and δ, we can calculate the PGs corresponding to the test material through the following two expressions:

- PGmax = G* / sin δ, (representing the upper limit of performance that is the one referring to the phenomenon of deterioration at high temperatures, identified the rutting);
- PGmin = G* · sin δ, (representing the lower limit of performance that is what refers to the phenomenon of deterioration at low temperatures, identified by fatigue failure).

3.6.2 Creep characterization of bituminous binder

It is widely recognised that the permanent deformation behavior of asphalt mixtures is dependent on the flow of bituminous binders. Theoretical considerations show that the binder contribution to rutting is a permanent deformation described by a viscosity (Philips and Robertus, 1995). In a long time creep test for the bituminous binder, the effect of delayed elasticity decreases with time and after a sufficient long time period, the rheological behavior of the bituminous binder is dominated by viscous flow. Under low stress creep, structures within the bituminous binder deform so slowly that they can continuously adapt thereby maintaining a situation close to equilibrium without building up any significant structural change in the material. Three regions of behavior are included: linear elastic, delay elastic and viscous. The viscous component is operative whenever the bitumen is loaded and is solely responsible for the non-recoverable deformation. The elastic and delay elastic strain are totally recoverable upon the release of an applied load. The elastic response dominates at short loading times or low temperatures, while the viscous response dominates at long loading times or high temperatures. At intermediate loading times and temperatures the delay elastic response dominates (Anderson et al., 1991). Collop et al. (2002) performed creep tests using a DSR on 50 and 100 penetration grade bitumens at 20°C over a range of shear stress levels. Creep curve can be divided into three regions. In the first region, namely primary creep, the shear strain rate (shear strain divided by time) decreases with time and the bitumen behavior is dominated by elastic and delay elastic effects. In the second region, namely steady-state creep region, the shear strain rate remains approximately constant with time and viscous effects dominate the bitumen behavior. In the third region, namely tertiary creep, the shear strain rate increases with time and the bitumen is progressively damaged (Liao M.C., 2007).

3.6.3 Creep test using DSR

3.6.3.1 Elastic Recovery Test

Clopotel C.S. and Bahia H.U. (2012) have proposed a novel test procedure using the Dynamic Shear Rheometer (DSR) to measure elastic recovery of asphalt binders and mastics. They developed a simple protocol for measuring the elastic recovery in the DSR (ER-DSR) :

- RTFO aged binder sample is heated in the oven until is fluid enough to be poured into a silicon mold. The procedure follows the ASTM D7175 "Standard Test Method for Determining the Rheological Properties of Asphalt Binder Using a Dynamic Shear Rheometer" [9].
- The binder sample is transferred from the silicon mold to the DSR plate. The gap is set to 2.10 mm to allow for trimming the excess binder from the sample. The gap is then set to 2 mm.
- The temperature of the sample is kept at the required temperature (25^0C) for 20 minutes. This step is required to reach thermal equilibrium.
- A constant strain rate of 0.023 1/s is applied for 2 minutes. This step is run in strain controlled mode.
- A constant zero shear stress is applied for a period of 1 hour. This step is run in stress controlled mode and corresponds to the relaxation part of the test.

The elastic recovery at the end of the relaxation step is calculated as follows:

$$ER=\frac{revored\ strain\ at\ the\ end\ of\ relaxation\ step\ (\varepsilon_2)}{strain\ at\ the\ end\ of\ loading\ step\ (\varepsilon_2)}\cdot 100$$

A typical plot for the shear strain versus time in the DSR is presented in Figure 3.26.

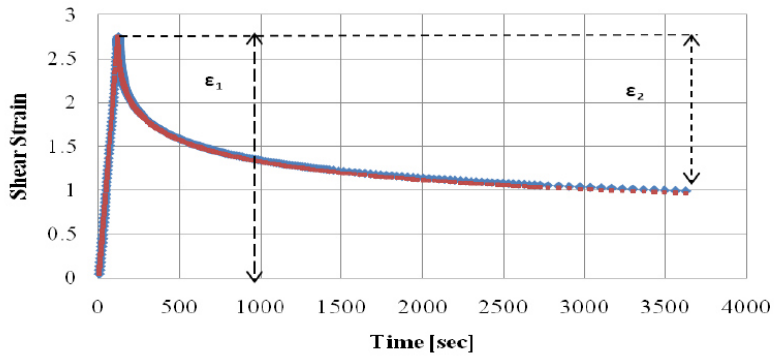

Figure 3.26 Typical shear strain curve for the elastic recovery test in the DSR. (*"Importance of Elastic Recovery in the DSR for Binders and Mastics"*).

In this study, a new procedure for measuring elastic recovery in the DSR was developed by the authors and used to measure the response for polymer modified binders and mastics. The DSR-ER results were first correlated to the standard ductility bath test for elastic recovery. The elastic recovery measured in the ductility bath can be replaced by elastic recovery measured in the DSR. A very good correlation between

these tests was obtained for both asphalt binder and mastics (R2 =0.97 and R2 =0.96 respectively).

3.6.3.2 Repeated Creep Recovery Test

Suggested specification parameters and test protocols were developed on NCHRP 459 (2001). In order to study permanent deformation, the viscous component of the binder creep stiffness, G_V, measured by a repeated creep test in the dynamic shear rheometer (DSR) was extracted. To establish a better rating of the role of binders in mixture rutting, the parameter Gv, defined as the viscous component of the creep stiffness, is recommended to replace the current binder parameter $G^*/\sin\delta$. This parameter is measured with a newly developed repeated creep test conducted with the dynamic shear rheometer (DSR). The protocol test consist to 100 creep cycles applying a shear stress of 1 kPa for 1 second and a shear stress of 0 kPa for 9 second in arrange temperarue between 46 and 64°C. The non recoverable compliance J_{nr}, the accumulated strain and the average recovery percentage can be extrapolated in order to study the permanent deformation response of bituminous materials.

3.6.3.3 Multiple Stress Creep Recovery Test

The Multiple Stress Creep Recovery (MSCR) test is the latest improvement to the Superpave Performance Graded (PG) Asphalt Binder specification. This new test and specification – listed as AASHTO TP70 *''Standard Method of Test for Multiple Stress Creep and Recovery (MSCR) of Asphalt Binders using a Dynamic Shear Rheometer''*, AASHTO MP19, and AASHTO M320 – provide the user with a new high temperature binder specification that more accurately indicates the rutting performance of the asphalt binder and is blind to modification. The main benefit of the MSCR test is that it eliminates the need to run tests such as elastic recovery, toughness and tenacity, and force ductility, procedures designed specifically to indicate polymer modification of asphalt binders. A single MSCR test can provide information on both performance and formulation of the asphalt binder (Vignali *et al.* 2014). The MSCR test uses the well–established creep and recovery test concept to evaluate the binder's potential permanent deformation. Using the Dynamic Shear Rheometer (DSR), the same piece of equipment used today in the existing PG specification, according to AASHTO

TP70, a constant one–second creep stress load is applied to the asphalt binder sample. After the 1–second load is removed, the sample is allowed to recover for 9 seconds (zero stress recovery). The test is started with the application of a low stress (0.1 kPa) for 10 creep/recovery cycles then the stress in increased to 3.2 kPa and repeated for an additional 10 cycles (Figure 3.27) (Vignali *et al.* 2014) (FHWA-HIF-11-038 2011) .

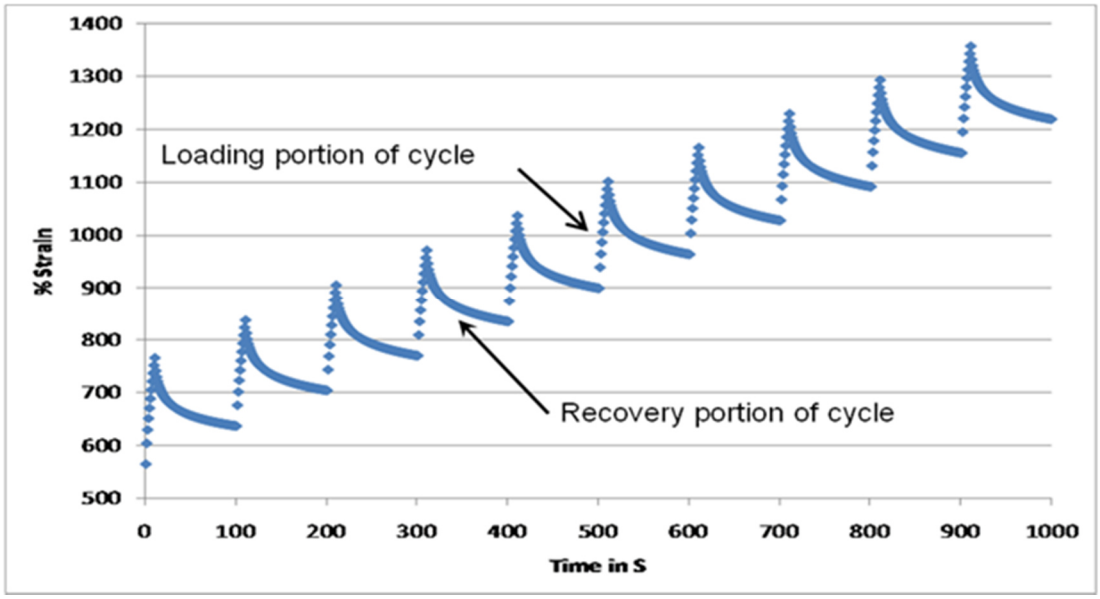

Figure 3.27 Typical data of MSCR test for a polymer modified Binder (*The Multiple Stress Creep Recovery (MSCR) Procedure*).

The non-recoverable compliance (J_{nr}) and the percent recovery after ten cycles at 0.1 kPa and 3.2 kPa will be studied (Figure 3.28). The J_{nr} value was calculated as the ratio between the average non recoverable strain for 10 creep and recovery cycles, and the applied stress for those cycles. The testing temperatures is selected 58℃ and 64℃ in agreement with AASHTO M320 (FHWA-HIF-11-038 2011). The main MSCR parameters are described in Table 3.1.

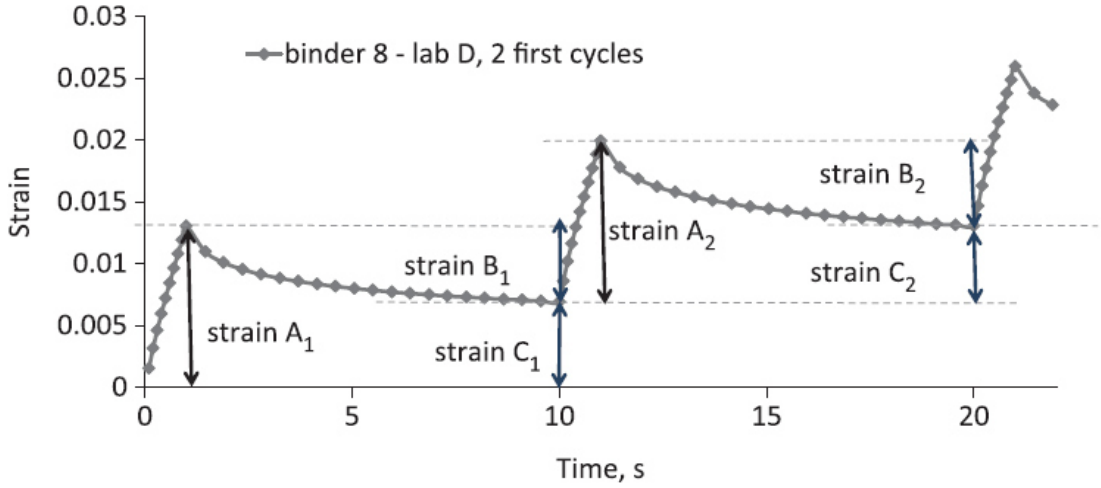

Figure 3.28 First two MSCR cycles, strain values to obtain results parameters.

Table 3.1 Main bitumen characteristics

Multiple Stress Creep Recovery Parameters		
R100%	Average recovery of the 10 cycles tested at 100 Pa	$R100\% = \frac{1}{10}\left\{\sum_{n=1}^{10}\frac{\text{strain B}}{\text{strain A}}\right\}100$
R3200%	Average recovery of the 10 cycles tested at 3200 Pa	$R3200\% = \frac{1}{10}\left\{\sum_{n=1}^{10}\frac{\text{strain B}}{\text{strain A}}\right\}100$
J_{nr100}(1/kPa)	Average non – recoverable part of cycles tested at 100 Pa	$J_{nr}100 = \frac{1}{10}\left\{\sum_{n=1}^{10}\frac{\text{strain C}}{0.1}\right\}$
J_{nr3200}(1/kPa)	Average non – recoverable part of cycles tested at 3200 Pa	$J_{nr}3200 = \frac{1}{10}\left\{\sum_{n=1}^{10}\frac{\text{strain C}}{3.2}\right\}100$
R_{diff}(%)	Difference in recovery	$(R100 - R3200)100/R100$
J_{nrdiff}(%)	Difference in non-recoverable complience	$(J_{nr}3200 - J_{nr}100)100/J_{nr}100$

The material response in the MSCR test is significantly different than the response in the existing PG tests. In the PG system, the high temperature parameter, G*/sinδ, is measured by applying an oscillating load to the binder at very low strain. Due to the low strain level, the PG high temperature parameter doesn't accurately represent the ability of polymer modified binders to resist rutting (FHWA-HIF-11-038 2011). Under the very low levels of stress and strain present in dynamic modulus testing, the polymer network is never really activated. In the existing PG specification the polymer is really

only measured as a filler that stiffens the asphalt. In the MSCR test, higher levels of stress and strain are applied to the binder, better representing what occurs in an actual pavement. By using the higher levels of stress and strain in the MSCR test, the response of the asphalt binder captures not only the stiffening effects of the polymer, but also the delayed elastic effects (where the binder behaves like a rubber band) (FHWA-HIF-11-038 2011). The MSCR test does a better job of identifying the rut resistance of both neat and polymer modified binders, but some highway agencies still want to make sure polymer is in the binder for other purposes such as crack resistance and durability. Here the MSCR test provides great improvements over the existing tests like the elastic recovery and toughness and tenacity. Data from the exact same sample from the MSCR test that was used to do high temperature grading provides information on the polymer modification as well. The one test provides the high temperature grade and quality of polymer modification eliminating the need to run additional tests like elastic recovery on additional samples. The compliance value Jnr from the MSCR test provides the rut resistance and the amount of recovered strain from the test identifies the presence of polymer and also the quality of the blending of the polymer in the binder (FHWA-HIF-11-038 2011).

3.7 3D Discrete Element Method (DEM)

3.7.1 Introduction of Discrete Element Method

The mechanical response of asphalt composites is frequently modeled by computational methods. The traditional approach treats them at the macro-scale using continuum-based methods that usually involve undertaking careful experiments over a range of conditions, measuring the macroscopic materials response and fitting continuum-based constitutive models to the measured performance. Numerous research works, however, show that the mechanical performance of asphalt mixture is largely dependent on the material properties of its individual components and on the way they interact (contacting) at the microscale. A fundamental understanding of the contact mechanisms of a particulate system through a well-calibrated micromechanical model provides insight into the material behavior at macroscale, and guide material design and performance prediction. In this way, moreover, the effects of individual components on the performance of the mixture can also be captured by the calibrated micromechanical model. As Discrete particle Element Method (DEM) considers particles as distinct interacting bodies, it is an excellent tool to investigate the micromechanical behavior of binders. Interactions between particles are considered to be a dynamic process with states of equilibrium developing whenever the internal forces are in balance. Contact forces and displacements of an assembly are found by tracing the movements of individual particles. The calculations in the DEM procedure involve first applying Newton's second law to the particles and then a force-displacement law to the contact points between particles.

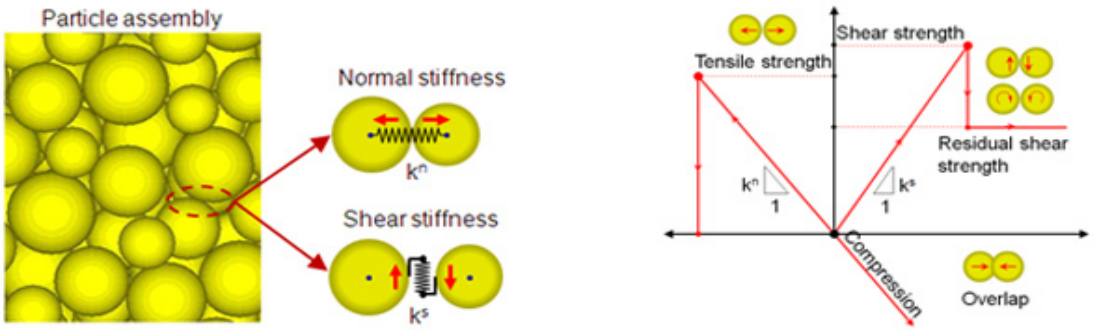

Figure 3.27 Schematic Diagram of the Cylindrical DMA Sample with Holders

3.7.1.1 DEM Fundamental Principles

In recent years the traditional numerical methods to continuously have been progressively complemented by innovative methods based on the division of the problem domain into discrete elements. The fundamental difference between the continuous and discontinuous methods ones is that in the first contact between elementary units remain unchanged regardless of the response of the model, in seconds are updated at each iteration, based on the position and the relative movement of the individual elements. In the method of discrete elements defining the mesh and constitutive models of materials it is replaced by the determination of the distribution and size of the elements that make up the system and from the description of the contact behavior (Calvetti F. 2003). In addition, the stress state of departure cannot be specified independently of the initial distribution of the individual units. Using the DEM modeling is possible to investigate the evolution of the system response in stable equilibrium conditions, and limit at break, beyond which, as previously mentioned, it admits the domain separation into blocks that continue to feel the stress agents. This allows taking advantage of numerical modeling to outline the interaction between discrete objects and subject to large deformation or fracture processes. Discrete methods in the system is modeled as a set of independent bodies that interact with each other through mutual contact points, which are responsible for the transmission of forces inside the vehicle. The interaction between the elements is considered as a dynamic process that reaches equilibrium when the system internal stresses are balanced. The forces and means of the displacements are obtained by tracing the movements of individual bodies which compose it, which are the result of propagation within the soil of causes of disturbance that originate at the edge of the model. In particular, it applies the Newton's second law to the elements and the law force-displacement to the contact points. The first is used to determine the motion of the individual units caused by stresses acting on them; the second is used to update the contact forces resulting (Jing L. 2003). To get an outcome consistent with the DEM model to simulate reality, there are five basic steps to follow:

- the problem domain subdivision and the type identification of items with which divide the system;

- representation of the deformation of the individual blocks (which may be rigid or deformable);
- development of an algorithm for the identification of the contacts;
- formulation of the equations of motion of the system;
- integration of the equations of motion and updating of contacts between the blocks, which vary as a result of the movements and deformations which apply to the system.

3.7.1.2 Particles DEM

The method of distinct particulate elements, proposed by Cundall and Strack in 1979, is based on principles similar to those of the traditional DEM, unlike which summarizes the blocks forming the system as rigid particles of circular or spherical shape. The calculation algorithm requires at each cycle the update of contacts based on the position and the relative movement of the particles. The Newton's second law to determine the speed and the position on the basis of the forces and moments applied to every contact is applied the force-displacement law in order to assess the magnitude of the forces, while in each element is applied. To illustrate how are certain forces and displacements during a calculation cycle, it is possible to consider the case shown in Figure 3.30 used by Cundall and Strack to explain the basic principles of the method. Consider two disks, devoid of weight, indicated with x and y, squeezed between two rigid walls moving toward each other with constant velocity v.

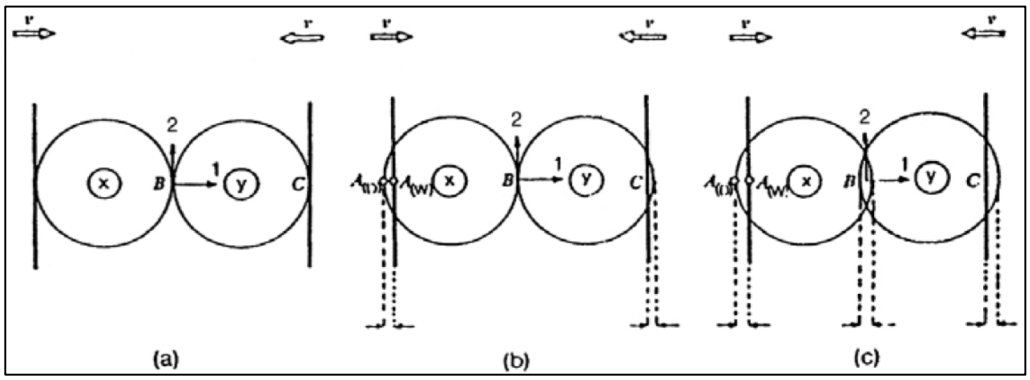

Figure 3.30 Disk compressed between rigid walls.

Initially, at time $t = t_0$, the walls and the discs are in contact, but no force was born. After a time interval Δt, the walls are moved inward by an amount equal to $v\Delta t$. Assuming that the disturbances cannot propagate over a single disk during each time

interval, it is assumed that both disks maintain their initial position during the time interval between $t = t_0$ and $t = t_0 + \Delta t$. The overlap is then instantly verify $t_1 = t_0 + \Delta t$ at the contact points A and C and its entities will amount to $\Delta n = v\Delta t$. The points $A_{(D)}$ and $A_{(W)}$ are respectively the points of the disc and the wall that lie on the same line perpendicular to and passing through the center of the wall; the contact A is defined as the midpoint between $A_{(D)}$ and $A_{(W)}$. With it indicates the relative displacement of $A_{(D)}$ with respect to point $A_{(W)}$ that occurs in a single time increment. The relative displacements which have at the contact points A and C at time $t_1 = t_0 + \Delta t$ are inserted in the force-displacement law for the calculation of the contact forces:

$$\Delta F_n = k_n \cdot (\Delta n)_{t1} = k_n \cdot v \cdot \Delta t \tag{3.75}$$

where:

k_n = normal stiffness;

ΔF_n = increasing normal force.

positive defining the direction 1 that goes from x to y disk (Figure 3.28), the resultant of the forces $F_{(x)}$ and $F_{(x)1}$ for the disks x and y at time $t_1 = t_0 + \Delta t$ will be:

$$F_{(x)1} = k_n \cdot (\Delta_n)_{t1} \tag{3.76}$$

$$F_{(y)1} = -k_n \cdot (\Delta_n)_{t1} \tag{3.77}$$

These forces are used to determine the new acceleration by resorting to Newton's second law:

$$\ddot{x}_1 = \frac{F_{(x)1}}{m_{(x)}} \tag{3.78}$$

$$\ddot{y}_1 = \frac{F_{(y)1}}{m_{(y)}} \tag{3.79}$$

where:

$\ddot{x}_1$ = x disk acceleration towards 1;

$\ddot{y}_1$ = y disk acceleration towards 1;

$m_{(x)}$ = mass disk *x*;

$m_{(y)}$ = massa disk *y*.

The accelerations thus found are assumed constant in the time interval from $t_1 = t_0 + \Delta t$, $t_2 = t_0 + 2\Delta t$ and can be integrated to derive the speed:

$$\left[\dot{x}_1\right] = \left[\frac{F_{(x)1}}{m_{(x)}}\right] \cdot \Delta t \tag{3.80}$$

$$\left[\dot{y}_1\right] = \left[\frac{F_{(y)1}}{m_{(y)}}\right] \cdot \Delta t \tag{3.81}$$

The displacement increases its contacts A, B and C at time $t_2 = t_0 + 2\Delta t$ are determined through the following reports:

$$\left(\Delta n_{(A)}\right)_{t2} = \left\{v - \left[\frac{F_{(x)1}}{m_{(x)}}\right] \cdot \Delta t\right\} \cdot \Delta t \tag{3.82}$$

$$\left(\Delta n_{(B)}\right)_{t2} = \left\{\left[\frac{F_{(x)1}}{m_{(x)}}\right] \cdot \Delta t - \left[\frac{F_{(y)1}}{m_{(y)}}\right] \cdot \Delta t\right\} \cdot \Delta t \tag{3.83}$$

$$\left(\Delta n_{(C)}\right)_{t2} = \left\{\left[\frac{F_{(y)1}}{m_{(y)}}\right] \cdot \Delta t - \left[-v\right]\right\} \cdot \Delta t \tag{3.84}$$

Where $\Delta n_{(A)}$, $\Delta n_{(B)}$ e $\Delta n_{(C)}$ are considered positive if there is compression stress. The first calculation cycle provides for the application of the force-displacement law to all contacts of each element, in order to determine the resultant force. In this way through the second law of Newton are calculated before the new acceleration, then again the individual discs move.

3.7.1.3 Force - Displacement law

The force-displacement law is applied to the contact points in order to determine the contact forces resulting from the respective movements. Consider the two disks x and y of Figure 3.31 in mutual contact. The coordinates of the centers are indicated with $x_i = (x_1, x_2)$ and $y_i = (y_1, y_2)$, where the indices 1 and 2 refer to the axes of the cartesian reference system represented in Figure 3.31. The components of the velocity vectors of the two disks are respectively $\dot{x}_i = (\dot{x}_1, \dot{x}_2)$ and $\dot{y}_i = (\dot{y}_1, \dot{y}_2)$, while the angular velocities are $\dot{\theta}_{(x)}$ and $\dot{\theta}_{(y)}$, if considered positive counterclockwise. The points $P_{(x)}$ and $P_{(y)}$ are defined as the points for intersection of the line connecting the centers of the disks x_i and y_i which have a radius equal to $R_{(x)}$ and $R_{(y)}$ and the masses equal to $m_{(x)}$ and $m_{(y)}$.

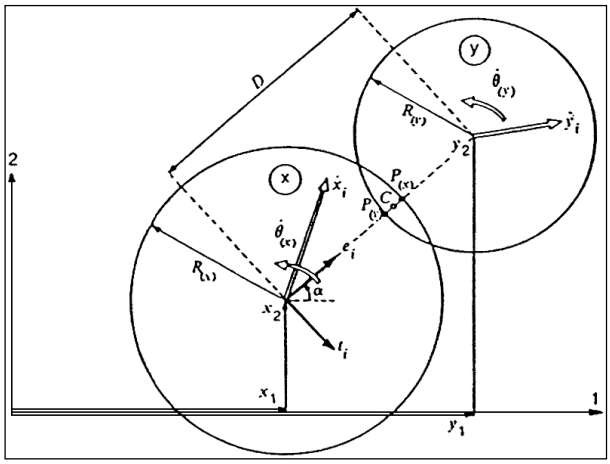

Figure 3.31 Force – displacement law

.

Two disks are considered in contact only if the distance D between their centers appears to be less than the sum of their radii:

$$D < R_{(x)} + R_{(y)} \tag{3.85}$$

If this condition occurs, the relative displacement of the contact point C is determined by integrating the relative velocity, defined as the speed of the point P (x) with respect to point P (y). They introduce the normal unit vector with the direction from the disk center x to y of the center of the disc, such that:

$$e_i = \frac{y_i - x_i}{D} = (\cos\alpha, \sin\alpha) \tag{3.86}$$

and the unit vector tangential obtained through 90° rotation of e_i:

$$t_i = (e_2 - e_1) \tag{3.87}$$

The relative velocity of the point P (x) with respect to point P (y) can be expressed as:

$$\dot{X}_i = (\dot{x}_i - \dot{y}_i) - (\dot{\theta}_{(x)} R_{(x)} + \dot{\theta}_{(y)} R_{(y)}) \cdot t_i \tag{3.88}$$

The normal $(\dot{n})$ and tangential $(\dot{s})$ components of the relative velocities are calculated as the $\dot{X}_i$ projections respectively long e_i and t_i :

$$\dot{n} = \dot{X}_i \cdot e_i = (\dot{x}_i - \dot{y}_i) \cdot e_i - (\dot{\theta}_{(x)} \cdot R_{(x)} + \dot{\theta}_{(y)} \cdot R_{(y)}) \cdot t_i \cdot e_i = (\dot{x}_i - \dot{y}_i) \cdot e_i \tag{3.89}$$

$$\dot{s} = \dot{X}_i \cdot t_i = (\dot{x}_i - \dot{y}_i) \cdot t_i - (\dot{\theta}_{(x)} \cdot R_{(x)} + \dot{\theta}_{(y)} \cdot R_{(y)}) \cdot t_i \cdot t_i = (\dot{x}_i - \dot{y}_i) \cdot t_i - (\dot{\theta}_{(x)} \cdot R_{(x)} + \dot{\theta}_{(y)} \cdot R_{(y)}) \tag{3.90}$$

The integration with respect to time of the component of the relative speed provides the Δn and Δs components of the increase of the relative displacement.

$$\Delta n = (\dot{n}) \cdot \Delta t = \{(\dot{x}_i - \dot{y}_i) \cdot e_i\} \cdot \Delta t \tag{3.91}$$

$$\Delta s = (\dot{s}) \cdot \Delta t = (\dot{x}_i - \dot{y}_i) \cdot t_i - (\dot{\theta}_{(x)} \cdot R_{(x)} + \dot{\theta}_{(y)} \cdot R_{(y)}) \cdot \Delta t \tag{3.92}$$

These shift increments are used in the law on force-displacement with the purpose of calculating the increments of the normal and tangential forces ΔF_n and ΔF_s:

$$\Delta F_n = k_n \cdot (\Delta n) = (\dot{x}_i - \dot{y}_i) \cdot e_i \cdot k_n \cdot \Delta t \tag{3.93}$$

$$\Delta F_s = k_s \cdot \Delta s = k_s \cdot \{(\dot{x}_i - \dot{y}_i) \cdot t_i - (\dot{\theta}_{(x)} \cdot R_{(x)} + \dot{\theta}_{(y)} \cdot R_{(y)})\} \cdot \Delta t \tag{3.94}$$

where kn and ks respectively represent the normal and tangential stiffness. ΔF_n and ΔF_s are added at each time interval to the sum of all increments of certain forces in previous intervals:

$$(F_n)_N = (F_n)_{N-1} + \Delta F_n \tag{3.95}$$

$$(F_s)_N = (F_s)_{N-1} + \Delta F_s \tag{3.96}$$

where the indices N and N-1 refer to the Rates and t_N t_N-1, so that. F_n and F_s are considered positive if oppositely directed to the unit vectors and and you (Figure 3.32).

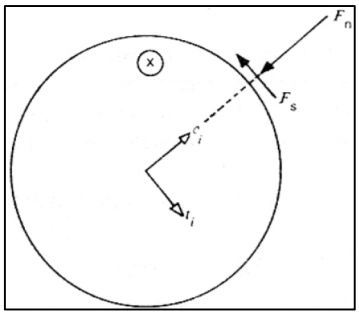

Figure 3.32 Sign convention Fn - Fs

As regards the sliding between the two disks, the extent of the tangential force F_s calculated above is compared with the maximum permissible value, defined as:

$$(F_s)_{\max} = F_n \cdot \tan\phi_\mu + c \tag{3.97}$$

where ϕ_μ is the smallest angle of friction of the disks in contact and c cohesion After determining the normal and tangential forces to each contact of a disc, for example, that x, they are broken down into two components along the directions 1 and 2. The sum of these components and provides the resultant forces $\sum F_{(x)1}$ e $\sum F_{(x)2}$. The resulting moment acting on the disk x $\sum M_{(x)}$, is considered positive if it acts counterclockwise and is given by:

$$\sum M_{(x)} = \sum F_s \cdot R_{(x)} \tag{3.98}$$

where the sum is extended to all of the hard contacts. The resulting forces and moments acting on the disk x are subsequently inserted in the Newton's second law for the purpose of determining the new and accelerations $\ddot{x}_i$ and $\ddot{\theta}_{(x)}$.

3.7.1.3 Equations of motions

The velocities $\dot{x}_i$ and $\dot{\theta}_{(x)}$ are evaluated, as indicated by Cundall and Strack, assuming that the resulting force and moment to time t_N acts on the disk x in the range from Δt tN-1/2 to t_N + 1/2. The Newton's second law applied to the dick x becomes:

$$m_{(x)} \cdot \ddot{x}_i = \sum F_{(x)i} \tag{3.99}$$

$$I_{(x)} \cdot \ddot{\theta}_{(x)} = \sum M_{(x)} \tag{3.100}$$

where Y (x) represents the moment of inertia of the disk x. Considering the range and time constants Δt, from the previous equations the following expressions of the velocities are obtained:

$$\left(\dot{x}_i\right)_{N+1/2} = \left(\dot{x}_i\right)_{N-1/2} + \left[\sum \frac{F_{(x)i}}{m_{(x)}}\right] \cdot \Delta t \tag{3.101}$$

$$\left(\dot{\theta}_{(x)}\right)_{N+1/2} = \left(\dot{\theta}_{(x)}\right)_{N-1/2} + \left[\sum \frac{M_{(x)i}}{I_{(x)}}\right] \cdot \Delta t \tag{3.102}$$

These equations are applied to the rotation to each disk; the values of the speeds thus obtained can be inserted in the force-displacement law, and the cycle can be repeated for a new time increment. The new speed values are also used to update the positions and rotations of the discs by means of a further numerical integration:

$$\left(x_i\right)_{N+1} = \left(x_i\right)_N + \left(\dot{x}_i\right)_{N+1/2} \cdot \Delta t \tag{3.103}$$

$$\left(\theta_{(x)}\right)_{N+1} = \left(\theta_{(x)}\right)_N + \left(\theta_{(x)}\right)_{N+1/2} \cdot \Delta t \tag{3.104}$$

In the model you can also be incorporated mass forces, such as gravitational ones. In this case we add the term to the sum of the forces that appears in the equation of the speed, it is where the two components of the acceleration vector due to the mass force.

3.7.1.3 Damping law

The damping comes into play during the slip between two discs when the value of the tangential force at each contact is equal to (F_s) max. Taking into account the effect of damping the equations of speed turn:

$$\left(\dot{x}_i\right)_{N+1/2} = \left(\dot{x}_i\right)_{N-1/2} + \left\{\sum \frac{\left[F_{(x)i} + D_{(x)i}\right]}{m_{(x)}}\right\}_N \cdot \Delta t \tag{3.105}$$

$$\left(\dot{\theta}_{(x)}\right)_{N+1/2} = \left(\dot{\theta}_{(x)}\right)_{N-1/2} + \left\{\sum \frac{M_{(x)}}{I_{(x)}}\right\}_N \cdot \Delta t \tag{3.106}$$

where it represents the sum of the components of the damping forces. To evaluate it considering the normal components (D_n) and tangential (D_s) as follows:

$$\left(D_n\right)_N = c_n \cdot \dot{n} = c_n \cdot \left[\dot{x}_i - \dot{y}_i\right]_{N-1/2} \cdot e_i \tag{3.107}$$

$$\left(D_s\right)_N = c_s \cdot \dot{s} = c_s \cdot \left[\left(\dot{x}_i - \dot{y}_i\right)_{N-1/2} \cdot t_i - \left(\dot{\theta}_{(x)} \cdot R_{(x)} + \dot{\theta}_{(y)} \cdot R_{(y)}\right)_{N-1/2}\right] \tag{3.108}$$

where the damping coefficients in the normal direction (c_n) and tangential (c_s) are assumed proportional to the stiffness k_n and k_s with β constant:

$$c_n = \beta \cdot k_n \tag{3.109}$$

$$c_s = \beta \cdot k_s \tag{3.110}$$

3.7.1.4 Time critical range

Distinct Element Method Particle integrates the equations of motion using a scheme of finite difference; the solution thus calculated is stable only if the time interval Δt does not exceed the critical value. For its determination is considered a system to a dimension it consists of a mass (m) and by a spring of stiffness k (Figure 3.33).

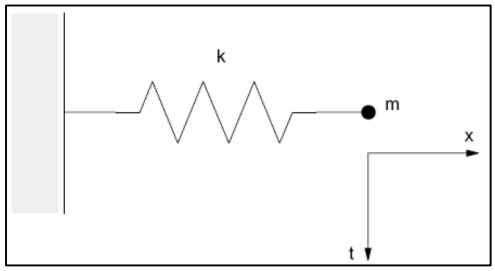

Figure 3.33 Mass and spring system.

The motion of the point in which is concentrated the mass is governed by the following differential equation:

$$-kx = m\ddot{x} \tag{3.111}$$

Denoting by T the period of the system, the critical time interval becomes:

$$t_{crit} = \frac{T}{\pi} = \frac{2 \cdot \pi \cdot \sqrt{\frac{m}{k}}}{\pi} \tag{3.112}$$

The discretization of a circular particle system adopted in Distinct Element Method Particle may seem a simplistic schematic than in irregularly shaped blocks provided by traditional DEM. In fact this characteristic is the greater potential of this technique compared to other DEM proceedings, since making it particularly suitable for the modeling of granular materials, whose behavior is strongly influenced by the nature of individual particles that compose it. It is therefore possible to consider its discreet character through a microscopic approach, so as to understand the basic physical processes that determine the macroscopic stress-strain response (Manganelli 2013).

3.7.2The use of DEM to study rheological behavior of bitumen

Dondi *et al.* 2014 through three-dimensional discrete element approach have captured the time-dependent behavior usually studied with the Dynamic Shear Rheometer analysis. In their research study Dondi *et al*. generated model geometry using an arrangement of spherical particles, contained inside walls which simulated the dynamic shear rheometer device. Only spherical particles were used because they can provide a close coupling between DEM simulations and laboratory tests. More information about the micro-mechanics of a real material could be achieved by incorporating more realistic particle geometries into the DEM model contact (Dondi *et al.* 2012).

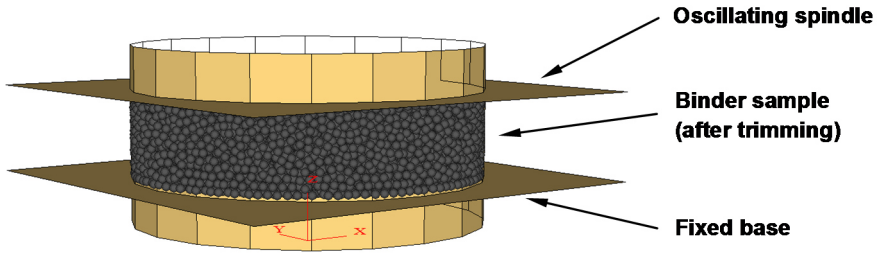

Figure 3.34 - DEM model of the DSR sample ("*Modeling the DSR complex shear modulus of asphalt binder using 3d discrete element approach*")

In this study the authors have applied the linear contact model, where the normal and shear stiffness of a discrete element (the linear contact model parameters) change with loading time, based on the Burger's constitutive relations (Collop et al. 2004-2006-2007). It evaluates, in particular, the normal and shear stiffness of a discrete element by the following formulas (Abbas et al. 2004):

$$k_n = \left[\frac{1}{K_{mn}} + \frac{t}{C_{mn}} + \frac{1}{K_{kn}} \cdot \left(1 - e^{\frac{-t}{\tau_n}} \right) \right]^{-1} \tag{3.113}$$

$$k_s = \left[\frac{1}{K_{ms}} + \frac{t}{C_{ms}} + \frac{1}{K_{ks}} \cdot \left(1 - e^{\frac{-t}{\tau_s}} \right) \right]^{-1} \tag{3.114}$$

where:

t is the loading time;

K_{mn} is the normal stiffness for Maxwell section;

K_{ms} is the shear stiffness for Maxwell section;

C_{mn} is the normal viscosity for Maxwell section;

C_{ms} is the shear viscosity for Maxwell section;

K_{kn} is the normal stiffness for Kelvin section;

K_{ks} is the shear stiffness for Kelvin section;

C_{kn} is the normal viscosity for Kelvin section;

C_{ks} is the shear viscosity for Kelvin section.

τ_n and τ_s are the normal and shear components of the relaxation time:

$$\tau_n = \frac{C_{kn}}{K_{kn}} \tag{3.115}$$

$$\tau_s = \frac{C_{ks}}{K_{ks}} \tag{3.116}$$

It has been chosen to equate the normal and shear direction parameters:

$$K_{mn} = K_{ms} = K_m \tag{3.117}$$

$$C_{mn} = C_{ms} = C_m \tag{3.118}$$

$$K_{kn} = K_{ks} = K_k \tag{3.119}$$

$$C_{kn} = C_{ks} = C_k \tag{3.120}$$

The response of the Burger model to a constant shear stress is characterized using the dynamic shear compliance ($\left|J^*(\omega)\right|$) and the dynamic shear modulus ($\left|G^*(\omega)\right|$). These relationships are presented in following equations:

$$\left|J^*(\omega)\right| = \sqrt{J'(\omega)^2 + J''(\omega)^2} \tag{3.121}$$

$$\left|G^*(\omega)\right| = \frac{1}{\left|J*(\omega)\right|} = \frac{1}{\sqrt{J'(\omega)^2 + J''(\omega)^2}} \tag{3.122}$$

$$G'(\omega) = \left|G*(\omega)\right| \cdot \cos\delta \tag{3.123}$$

$$G''(\omega) = \left|G*(\omega)\right| \cdot \sin\delta \tag{3.124}$$

$$G'(\omega) = \frac{1}{\left|J*(\omega)\right|} \times \frac{J'(\omega)}{\left|J*(\omega)\right|} = \frac{J'(\omega)}{[J'(\omega)]^2 + [J''(\omega)]^2} \tag{3.125}$$

$$G''(\omega) = \frac{1}{\left|J*(\omega)\right|} \times \frac{J''(\omega)}{\left|J*(\omega)\right|} = \frac{J''(\omega)}{[J'(\omega)]^2 + [J''(\omega)]^2} \tag{3.126}$$

$$J'(\omega) = \left(\frac{1}{K_m} + \frac{K_k}{K^2{}_k + \omega^2 \cdot C^2{}_k}\right) \tag{3.127}$$

$$J''(\omega) = \left(\frac{1}{\omega \cdot C_m} + \frac{\omega \cdot C_k}{K^2{}_k + \omega^2 \cdot C^2{}_k}\right) \tag{3.128}$$

$$\left|G^*(\omega)\right| = \frac{1}{\sqrt{\left(\frac{1}{K_m} + \frac{K_k}{K^2{}_k + \omega^2 \cdot C^2{}_k}\right)^2 + \left(\frac{1}{\omega \cdot C_m} + \frac{\omega \cdot C_k}{K^2{}_k + \omega^2 \cdot C^2{}_k}\right)^2}} \tag{3.129}$$

where:

$G'(\omega)$ = is the real part referred to as the storage shear modulus;

$G''(\omega)$ = is the imaginary part referred to as the loss shear modulus;

$J'(\omega)$ = is the real part referred to as the storage shear compliance;

$J''(\omega)$ = is the imaginary part referred to as the loss shear compliance.

Burger's model parameters, in particular, were obtained following the methodology developed by Baumgaertel and Winter, whereby the viscoelastic behavior of bitumen was determined by fitting the Burger model to DSR measurements. Two rheological measurements were fitted simultaneously, namely the storage and the loss shear moduli respectively. The fitting procedure was based on minimizing an objective function that is equal to the sum of square of errors in predicting the storage and loss shear moduli over the available range of testing frequencies (Abbas A. 2004):

$$objective\_function = \sum_{j=1}^{m}\left[\left(\frac{G'(\omega_j)}{G'_J{}^0} - 1\right)^2 + \left(\frac{G''(\omega_j)}{G''_J{}^0} - 1\right)^2\right] \tag{3.130}$$

where:

G'^0_j and G''^0_j are respectively the storage and loss shear moduli measured at the j^{th} frequency w_j; G'j and G''j are respectively the predicted storage and shear moduli from equations (3.125) and (3.126); m is the number of data points. After the extraction of Burgers' parameter the authors have and imposed the boundary condition test. In particular boundary and loading conditions were defined in order to select a combination of parameters that best matched the stress-strain response observed in laboratory tests. An oscillatory shear load of constant amplitude was applied on the upper parallel wall, at nineteen loading frequencies ranging between 0.01 and 10 Hz and several different temperatures (10, 20, 30, 40 and 50°C). Since in PFC forces can be applied only to balls and not to walls, an oscillatory shear angular velocity was used for each temperature. Laboratory test results and numerical ones, have been evaluated and compared in terms of complex modulus (|G*|) and phase angle (δ). In according

to equation (3.131) and (3.132) the numerical results have been calculated using the following equations:

$$|G^*| = \frac{|F_{S_{MAX}}|}{|S_{S_{MAX}}|} \tag{3.131}$$

$$\delta = \frac{\Delta t}{t} \cdot 360 \tag{3.132}$$

where:

$F_{S\,MAX}$ = is the maximum amplitude of the particles shear contact forces;

$S_{S\,MAX}$ = is the maximum amplitude of the particles shear displacements;

Δt = is the time lag between the peak shear contact force and the peak shear displacement;

t = is the loading time of one cycle.

The DEM approach used in this study is potentially good to predict the bitumen response in the frequency sweep configuration as shown on Figure 3.35. From the obtained master curves Dondi *et al.* confirm that the TTS principle is valid also for DEM simulations results, using the horizontal shifting obtained with WLF theory.

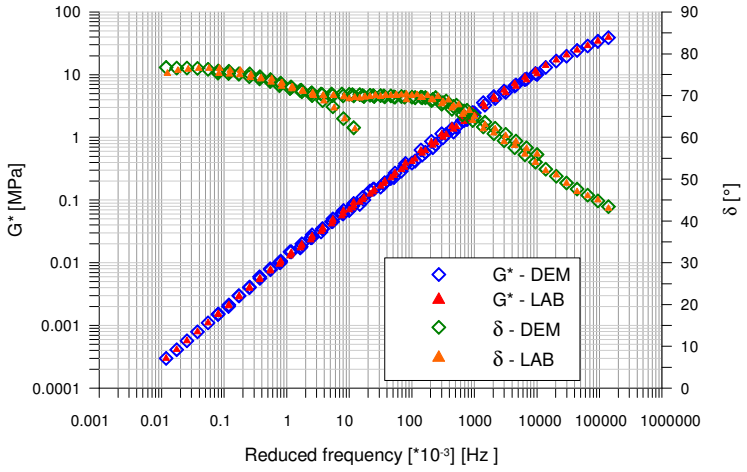

Figure 3.35 – Master curves of experimental (LAB) and numerical (DEM) results for complex modulus (G*) and phase angle δ (“*Modeling the dsr complex shear modulus of asphalt binder using 3D discrete element approach*”)

Based on the obtained macro-scale results, that validates the DEM approach, the micro-scale response was analyzed by the authors considering both the total number of contacts inside the specimen and the contact forces with their internal distribution. These are plotted as lines with thickness proportional to the contact force magnitude. During the frequency sweep test three significant conditions, representatives of the

PBM time-dependent behavior, were considered (Figure 3.36). Using the principle of time – temperature superposition, in fact, point A is representative of low temperatures and high frequencies, at which the bitumen behaves as elastic solid, while point C is characteristic of high temperatures and low frequencies, at which the bitumen behaves as viscous liquid. The intermediate range of temperature and frequency results in visco-elastic behavior (point B).

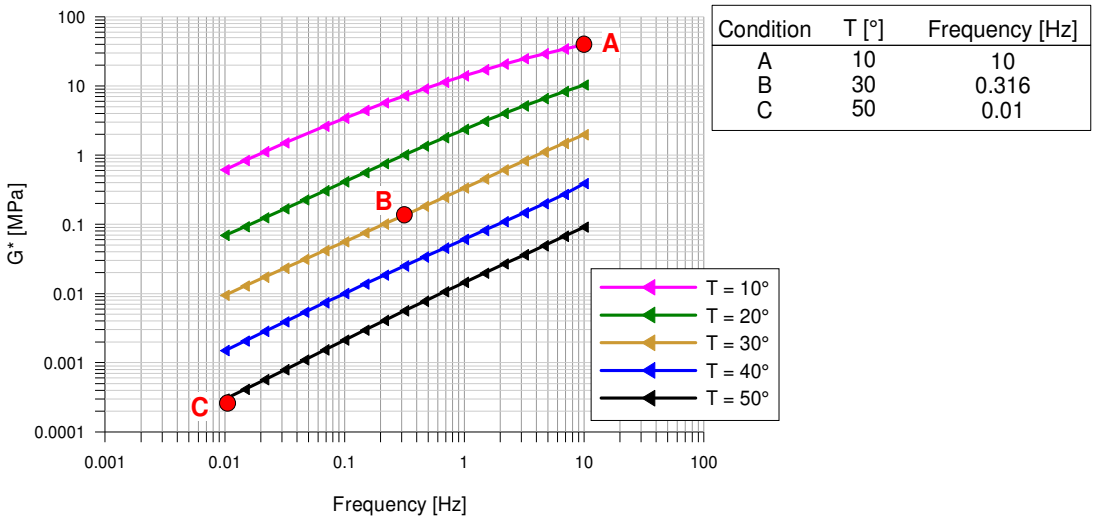

Figure 3.36 – Conditions for evaluating the contact forces (“*Modeling the dsr complex shear modulus of asphalt binder using 3d discrete element approach*”)

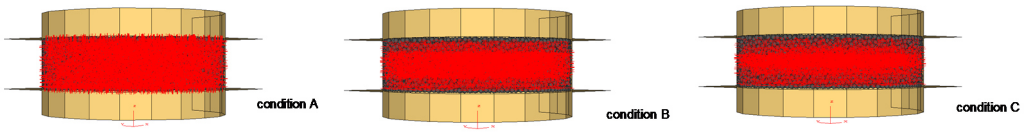

Figure 3.37 – Contact forces evaluated on the vertical plane of simmetry (“*Modeling the dsr complex shear modulus of asphalt binder using 3d discrete element approach*”)

The results obtained, comparing the numerical simulation of a frequency sweep test with a laboratory one, show that the authors’ adopted approach is found to be successful in predicting, both quantitatively and qualitatively, the complex modulus and the phase angle of the studied polymer modified bitumen, over a wide range of temperatures and frequencies. In addition the microstructural analysis has permitted to evaluate the internal forces configuration induced by shear stress in the specimen (Figure 3.37).

3.7.3 The use of DEM to study rheological behavior of Asphalt Mixtures

Over the past 10 years, the use of micromechanics to predict properties of asphalt mixtures has drawn increasing attention. A number of researchers have developed micromechanical models with the discrete particle element method (DEM). Among these, asphalt binders were usually simulated with elastic models. Buttlar and You (2001), for example, presented a 2D microfabric discrete element approach to simulate the behavior of asphalt mixture in indirect tension testing. They described the internal structure of the mix using clusters of circular particles, adopting elastic contact model with bonding and sliding capabilities to define the particles' interaction. Further they extended this approach to model compression tests and hollow cylinder tensile tests on asphalt mixtures, in order to estimate theirs stiffness, and the complex material behavior was always simulated by combining the elastic contact constitutive model with complex geometrical features. Also Kim et al. (2005-2006-2008) implemented the microfabric discrete element approach to investigate fracture mechanisms in asphalt concrete, and they described the material contact behavior by using an elastic contact-stiffness model. In the same years Collop *et al.* (2004-2006-2007) investigated the use of distinct element modelling to simulate the behavior of a highly idealized bituminous mixture in a uniaxial and triaxial compressive creep test. The effect of bitumen was represented as shear and normal contact stiffness. Elastic contact properties have been used to investigate the effect of sample size and of the values of the shear and normal contact stiffness on bulk material properties. Abbas *et al.* (2005) simulated the mechanical behavior of asphalt mastics with the discrete element method, in order to evaluate the effect of binder stiffness and mineral filler volume fraction on the overall mix stiffness. They used a combination of stiff and soft particles, representing the aggregate filler and the binder phases respectively, and bonding together by the linear elastic contact model. Dai and You (2007) presented micromechanical finite-element and discrete-element models for the prediction of viscoelastic creep stiffness of asphalt mixture, simulated by graded aggregates bound with mastic (asphalt mixed with fines and fine aggregates) through an elastic contact model. In 2008 You *et al.* focused their research work on the development of 3D microstructure-based discrete element model of asphalt mixtures, studying the dynamic modulus from the stress-strain response under compressive loads. The

geometry of aggregates and mastic was simulated with the captured aggregate and mastic images, bonding by an elastic contact-stiffness model. Masad *et al.* 2009 introduced a numerical approach that account for aggregate strength, gradation and shape to model the HMA performance. The simulation, adopting an elastic contact-stiffness model of the particle interaction, showed that these factors were of significant influence on the HMA performance in terms of resistance to fatigue and rutting. Mahmoud et al. (2010) introduced an approach that combines the discrete element method and image processing techniques to analyze the combined effects of aggregate gradation, shape, stiffness and strength on HMA resistance to fracture. The DEM input parameters were determined based on measuring aggregate and HMA properties, adopting the elastic model at contact points. Consequently, the model was used to quantify the internal forces in asphalt mixtures and determine their relationship to aggregate fracture which cannot be accomplished by conventional experimental methods. The analyzed research studies shows that elastic models are found to be a useful tool to predict only some time-independent properties of asphalt binders, such as stiffness at a specified frequency or time, and not theirs real time-dependent behaviors. To overcome this limitation, therefore, the adoption of viscoelastic models is necessary. In this way, in fact, some real time-dependent behavior of asphalt binders, such as dynamic modulus and phase angle, can be predicted. The simplest option is to use a Burger's model, which comprises a spring (K_k) and dashpot (C_k) in parallel (delayed elastic component) connected in series to a spring (K_m, elastic component) and a dashpot (C_k, viscous component). Wu et al. (2011), starting from obtained results in DEM modeling of a creep test of a highly idealized bituminous mixture bonding linear elastic contact model, introduced a Burger's model to give a time dependent shear and normal contact stiffness. It can be seen that the predicted and measured curves are similar in magnitude and shape, demonstrating the applicability of this type of approach. Its reliability was confirmed by Dondi et al. (2005-2007) by simulation of the behavior of an asphalt mixture under Marshall test, and of the fatigue performance of an asphalt pavement under traffic loading. Abbas et al. (2007) simulated with DEM the viscoelastic behavior of nine asphalt mixtures, containing unmodified and modified asphalt binders, in simple performance tests. Aggregates were modeled as rigid objects and the viscoelastic interaction among the mix

constituents was defined using a time-dependent viscoelastic model (Burger's model). The predicted dynamic moduli compared well with the experimentally measured values for all mixes. Liu et al. presented a viscoelastic model of asphalt mixtures with the discrete element method, where the viscoelastic behaviors of asphalt mastics (fine aggregates, fines, and asphalt binder) were represented by a Burger's model. Aggregates were simulated with irregular shape particles, consisting of balls bonded together by elastic contact models, and the interspaces between aggregates were filled with balls bonded with viscoelastic Burger's model to represent asphalt mastic. The favorable agreement between the DEM prediction and the lab results on dynamic moduli and phase angles, from uniaxial compressive tests, indicates that the viscoelastic DEM model approach adopted in this study is very capable of simulating constitutive behavior of asphalt mixtures. According to the model developed by Liu et al. (2007-2008-2009), Chen et al. (2011) established a user-defined micromechanical model using DEM to investigate the cracking behavior of asphalt concrete. The comparison between numerical and laboratory results, obtained from uniaxial complex modulus tests and indirect tensile strength tests, showed that the 3D DEM model is able to predict accurately the fracture pattern of different asphalt mixtures. Adhikari and You (2010) used the discrete element model to predict the asphalt mixture dynamic modulus in a hollow cylindrical specimen across a range of test temperatures and load frequencies. The microstructure of the asphalt concrete specimen was captured by X-ray tomography techniques. The linear contact-stiffness model and Burger's contact model, respectively for the aggregate and for the interactions within the sand mastics, were used to calculate this strain response. You et al. (2011) presented a method for the simulation of asphalt mixture creep compliance tests, with a 3D microstructural-based DE viscoelastic model (Burger's model), on the basis of the time-temperature superposition principle to reduce the computation time. It was observed that the DE viscoelastic model and the experimental measurements yielded similar results. The background reported shows that the DEM method has been extensively adopted to reproduce the behavior of asphalt mixtures, while a very small number of research studies model asphalt binder. Moreover these cases confirmed that DEM elastic model is not efficient for modeling the time and temperature dependent behavior of binders, and the viscoleastic model is necessary.

4 RHEOLOGICAL AND 3D DEM CHARACTERIZATION OF TRADITIONAL BITUMINOUS MASTIC: METHODS VALIDATION

4.1 Introduction

Asphalt mastics are defined as dispersions of fillers within a medium of asphalt binder. The fillers refer to the fraction of mineral aggregate passing the 200-mesh sieve (i.e. smaller than 75 μm), as described on Chapter 2. All the test procedures described on Chapter 3 were implemented on cold mastics made with traditional filler. The objective of this study is to evaluate the effects of limestone filler and Portland cement on cold mastics properties. Two different fillers volumetric percentages were investigated. The mastics response to permanent deformation was investigated with two approaches:

- a rheology-based approach, which includes temperature sweep and Multiple Stress Creep Recovery tests, implemented according to AASHTO TP 70-07 (Dondi G., Mazzotta F., *et al.* 2014);
- a micromechanical approach, to capture the real time-dependent behavior of asphalt mastic and to predict its performance through the better understanding of its internal interaction (Vignali V., Mazzotta F., *et al.* 2014).

Numerous research works, in fact, show that the mechanical performance of asphalt mastic is largely dependent on the material properties of its individual components and on the way they interact (contacting) at the microscale. A fundamental understanding of the contact mechanisms of a particulate system through a well-calibrated micromechanical model provides insight into the material behavior at macroscale, and guide material design and performance prediction. As Discrete particle Element Method (DEM) considers particles as distinct interacting bodies, it is an excellent tool to investigate the micromechanical behavior of mastics. Interactions between particles are considered to be a dynamic process with states of equilibrium developing whenever the internal forces are in balance. Contact forces and displacements of an assembly are found by tracing the movements of individual particles. The calculations in the DEM procedure involve first applying Newton's second law to the particles and then a force-displacement law to the contact points between particles. A commercially available

three-dimensional DEM code called Particle Flow Code (PFC), developed by Itasca Consulting Group, was used in this study.

4.2 Materials

4.2.1 Bitumen

A SBS modified bitumen, typically used to make bituminous emulsion, was used to produce the mastics. The bitumen main characteristics from traditional test are shown in Table 4.1:

Table 4.1 Main bitumen characteristics

Penetration [dmm] (UNI EN 1426)	**Softening point [°C] (UNI EN 1427)**	**Fraass breaking point [°C] (UNI EN 12593)**
55	62	-16

From Frequency Sweep Test (10-50°C) the master curve for base bitumen has been found by applying the appropriate shift-factor for all the bitumen (WLF theory Chapter 3). Amplitude sweep test was performed to find the Linear Viscoelastic Elastic (LVE) range for the material 1.8% in this case. The test was controlled on shear strain and with the frequency of 1.59 Hz..

Figure 4.1 – Bitumen Master Curves

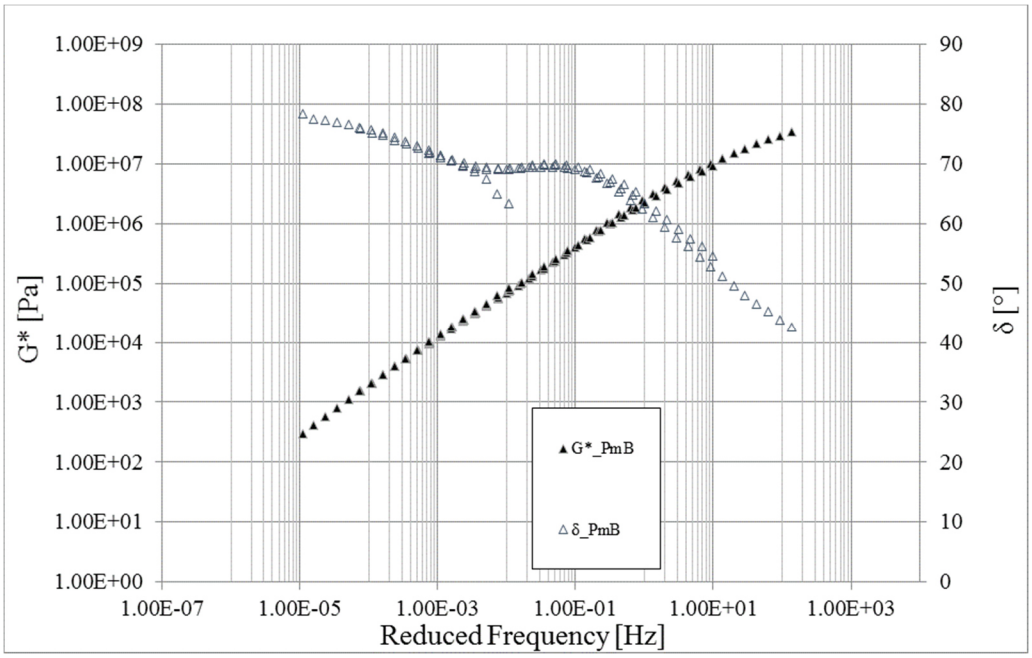

4.2.2 Limestone Filler

The filler used in this study is a product obtained from the fine grinding of limestone composed primarily of calcium carbonate ($CaCO_3$). The limestone filler is referring to the particles passing 0.063 mm sieve. In this research natural limestone filler has been

choose to add in to the bitumen due to its good behavior with bitumen in the stiffness index. The limestone filler was characterized geometrically through a gradation analysis (EN 933-10) and volumetrically, determining their volumetric mass (EN 1097-7). Rigden Voids (EN 1097-4) and Delta Ring & Ball (EN 13179-1) were also performed according to EN 13179-1. Table 4.2 shows the limestone filler characteristics.

Table 4.2 Limestone filler main characteristics

Test Name	Standard	Limestone filler
Gradation analysis (mm)	EN933-10	0.063
Particle density (Mg/m^3)	EN 1097- 7	2.73
Rigden voids (%)	EN 1097- 4	33.82
Δ Ring & Ball [°C]	EN 13179-1	8

4.2.3 Cement

The cement used in this research is a Cement Portland 32.5R made by heating (calcium carbonate) with other materials (such as clay) to 1450 °C in a kiln, in a process known as calcination. The cement is referring to the particles passing 0.063 mm sieve. The cement was characterized geometrically through a gradation analysis (EN 933-10) and volumetrically, determining their volumetric mass (EN 1097-7). Rigden Voids (EN 1097-4) and Delta Ring & Ball (EN 13179-1) were also performed according to EN 13179-1. Table 4.3 shows the limestone filler characteristics

Table 4.3 Cement main characteristics

Test Name	Standard	Limestone filler
Gradation analysis (mm)	EN933-10	0.063
Particle density (Mg/m^3)	EN 1097- 7	3
Rigden voids (%)	EN 1097- 4	25
Δ Ring & Ball [°C]	EN 13179-1	12

4.3 Mastics

4.3.1 Mastics Design

The volumetric analysis has been conducted on the two studied mastics. The calculation of the compositional volume of cement and limestone filler particles (V_f, V_c) has been obtained through the following equations:

$$V_f = \frac{\frac{M_c}{S_c}}{\frac{M_b}{S_b}+\frac{M_c}{S_c}} \tag{4.1}$$

$$V_r = \frac{\frac{M_r}{S_r}}{\frac{M_b}{S_b}+\frac{M_f}{S_f}+\frac{M_c}{S_c}} \tag{4.2}$$

where M_c = mass of cement in the mastic; S_c = specific gravity of cement M_f = mass of filler in the mastic; S_f = specific gravity of filler; M_b = mass of bitumen in the mastic; and S_b = specific gravity of bitumen. The results of equations applied on studied mastic are reported on Table 4.4.

Table 4.4 Mastics volumetric composition

Mastic Name Code	**V_f [%]**	**V_c [%]**	**V_b [%]**
MC	0	25	75
MCF	12.5	12.5	75

4.3.2 Mastics Preparation

Cement end filler were manually mixed with the bituminous emulsion and the obtained mastics were stored in a shallow container. The choice to produce small size test specimens has permitted to avoid separation between the materials with different densities, obtaining homogenous DSR samples. Moreover, curing of specimens of small size can be performed at room temperature and takes place in a relatively short time.

4.4 Test Programme

4.4.1. Test Equipment and Sample Preparation

Dynamic Shear Rheometers (DSR) **Anton Paar - MCR 302,** using peltier system temperature control with peltier hood (APPENDIX A), have been used to obtain the mastic rheological properties). Prior to mounting a bituminous sample between a parallel plate geometry, two plates should be sufficiently warm (approximately 90°C for modified bitumen) that a good adhesion between a sample and plates can be achieved. The procedure of bituminous sample preparation is listed as follows:

- remove the bituminous sample from shallow container, being careful that the filler is homogeneous in the mix;
- pour directly the mastic sample onto the upper plate until it nearly covered the plate.
- close the plates to the target gap of 2.025mm or 1.025mm for the bulge.
- trim the extra specimen by moving a heating trimming tool around the upper and lower plates.
- adjust the gap to the desired testing gap after trimming.
- the procedure causes a hockey puck-shaped specimen and a desired bulge at the periphery of specimen. It is noted that the periphery of a specimen retains a convex shape as the temperature is changed. The sample should not shrink to the point where the edge becomes concave (Liao 2007).

4.4.2 Amplitude Sweep Test

Amplitude Sweep (AS) tests were preliminary carried out, to investigate the viscoelastic region at 10°C, applying a constant frequency of 10 rad/s (1.59 Hz). The investigated strains level come from 0.01% to 100% of mastic deformation. It was chosen the strain amplitude at which the complex modulus not differ by more 10% of its initial value.

4.4.3 Frequency Sweep Test

The Frequency Sweep (FS) test was performed in strain control configuration, where the strain amplitude was limited within the linear viscoelastic (LVE) response.

Amplitude Sweep (AS) tests were preliminary carried out to investigate the viscoelasticity region at 10°C, applying a constant frequency of 10 rad/s (1.59 Hz). It was then chosen the strain amplitude at which the complex modulus does not differ more than 10% from its initial value, in this case 1% for both mastics. FS test was conducted in a range of frequencies between 0.01 and 10 Hz, at the temperatures of 0, 10, 20, 30, 40, 50 and 60°C. The 8 mm plate with a 2 mm gap was adopted below 30°C and above this temperature 25 mm plate and 1 mm gap was used (Fig 4.2).

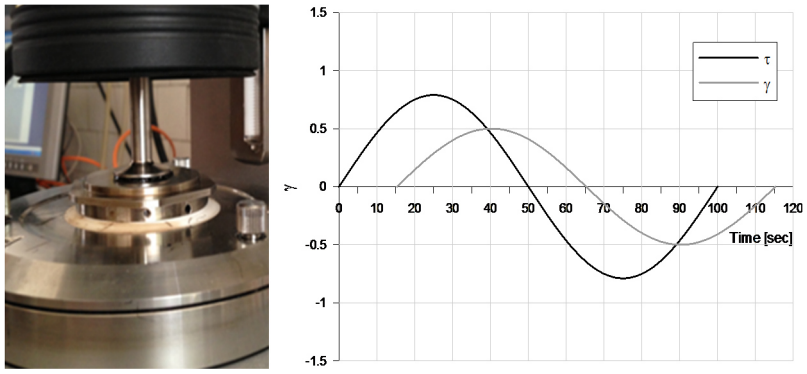

Figure 4.2 – DSR 25mm configuration and shear tendion/deformation curves for a load frequency of 0.01Hz @30°C.

4.4.4 Repeated Creep Recovery Test

Repeated Creep Recovery tests (RCR) were conducted with 25 mm parallel plates (PP) and a 1 mm gap under two different temperature conditions. MC and MCF were tested with a 100 cycles RCR test at a stress level of 1 kPa. RCR tests were conducted at two different temperatures: 46°, 58°C. Each loading cycle consisted of 1 s creep and 9 s recovery (NCHRP report 459). Following AASHTO TP70-07 standard, J_{nr} was calculated as the ratio between the unrecovered shear strain and the applied shear stress. The percentages of recovery were obtained as the ratio between recovered strain and peak strain.

4.4.5 Multiple Stress Creep Recovery Test

The Multiple Stress Creep and Recovery test (MSCR) was run according to the ASSHTO TP 70-07 *"Standard Method of Test for Multiple Stress Creep and Recovery (MSCR) of Asphalt Binders using a Dynamic Shear Rheometer"*. According to this standard, mastic sample is loaded at a constant creep stress for 1 second, followed by

a zero stress recovery of 9 seconds. Ten cycles of creep and recovery are run at 0.1 kPa creep stress, followed by ten at 3.2 kPa creep stress. The non-recoverable compliance (J_{nr}) and the percent recovery after ten cycles at 0.1 kPa and 3.2 kPa were studied. The J_{nr} value was calculated as the ratio between the average non recoverable strain for 10 creep and recovery cycles, and the applied stress for those cycles (Chapter 3). The testing temperatures were selected in agreement with AASHTO M320 table, in particular 48°C and 56°C were chosen.

4.5 Discrete Element Test Simulation

The three-dimensional discrete element modeling approach has been used in order to capture, both quantitatively and qualitatively, the behavior of MC and MCF mastics during the frequency sweep test. Since many research works show that the mechanical performance of mastics is largely dependent on the material properties of its individual components and on the way they interact (contacting) at the microscale, an understanding of the contacts mechanisms of the system through a 3D micromechanical model provides insight into the macroscale material behavior and guides its design and performance prediction. Therefore, for MC and MCF samples, the discrete element simulation includes three main steps:

- definition of the model geometry;
- description of the contact material properties;
- simulation of the frequency sweep test.

These aspects are here discussed in detail. A commercially available three-dimensional DEM code called Particle flow code (PFC), developed by Itasca Consulting Group, was used in this study. In PFC3D, particles are spheres that move independently and interact at the contact points.

4.5.1 Model geometry

According to Dondi *et al.* (2014) the model geometry was generated in PFC3D using an arrangement of spherical particles, contained inside walls which simulated the dynamic shear rheometer device. The bitumen spheres diameter was set to 200 μm according to the magnitude of the bitumen film coating aggregates in bituminous mixes (Kose *et al.* 2000) (Hammoum *et al.* 2012) and (Abbas et *al.* 2004). The spheres diameter of Portland cement and limestone filler was set to 100 μm according to their grading curves. The selection of these particle sizes was also motivated by the need of reducing the computational time. In fact it should be noted that in the DEM simulation it is almost impossible to take the fine particles fully into consideration because not only this significantly increase computational time, but it also affects the system's capability to reach equilibrium. The spheres material density was set as measured by the manufacturer (Table 4.5). Density scaling technique was not used, despite it reducing computation time.

Table 4.5 Properties of the DEM models

Mastic	Material	Density [kg/m^3]	Spheres diameter [µm]
MC	Bitumen	1000	200
	Portland cement	3000	100
MCF	Bitumen	1000	200
	Portland cement	3000	100
	Limestone filler	2700	100

Three walls were adopted in order to simulate the dynamic shear rheometer, in which the samples of mastics, represented by 49,200 spheres, were generated (Figures 4.3 – 4.4). The test device was modeled by a cylindrical wall closed at the top and bottom by planes simulating the parallel plates. The lower plane is fixed, while the upper one oscillates back and forth to create a shearing action. The samples of mastics, 2 mm thick and 8 mm in diameter, were sandwiched between walls. The contact stiffness of the cylindrical wall has been obtained by a calibration analysis and it is equal to 10^2 N/m (Dondi *et al.* 2014).

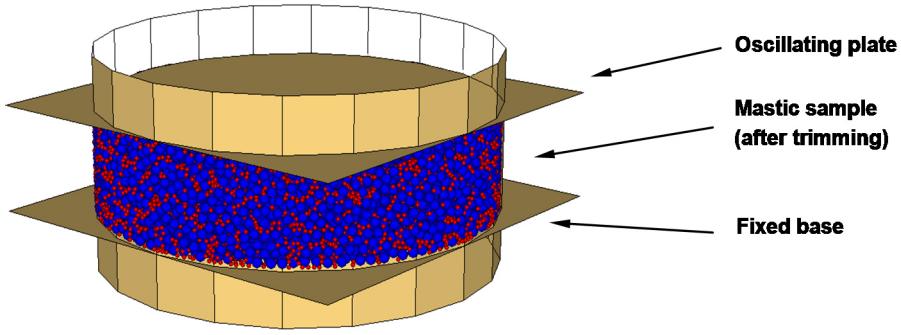

Figure 4.3 – MC, DEM model of the DSR sample (in blue the bitumen spheres, in red the Portland cement spheres)

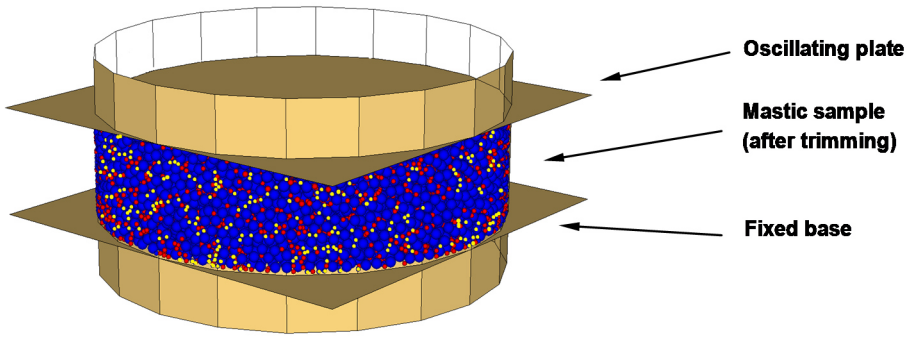

Figure 4.4 – MCF, DEM model of the DSR sample (in blue the bitumen spheres, in red the Portland cement spheres, in yellow the limestone filler spheres)

4.5.2 Contact material properties

According to Dondi *et al.* (2014), in this study, the linear contact model, based on the Burger's constitutive relations was applied the first approach was adopted. It evaluates, in particular, the normal and shear stiffness of the contact of a discrete element by the following formulas:

$$k_n = \left[\frac{1}{K_{mn}} + \frac{t}{C_{mn}} + \frac{1}{K_{kn}} \cdot \left(1 - e^{\frac{-t}{\tau_n}} \right) \right]^{-1} \tag{4.2}$$

$$k_s = \left[\frac{1}{K_{ms}} + \frac{t}{C_{ms}} + \frac{1}{K_{ks}} \cdot \left(1 - e^{\frac{-t}{\tau_s}} \right) \right]^{-1} \tag{4.3}$$

where:

t is the loading time;

K_{mn} is the normal stiffness for Maxwell section;

K_{ms} is the shear stiffness for Maxwell section;

C_{mn} is the normal viscosity for Maxwell section;

C_{ms} is the shear viscosity for Maxwell section;

K_{kn} is the normal stiffness for Kelvin section;

K_{ks} is the shear stiffness for Kelvin section;

C_{kn} is the normal viscosity for Kelvin section;

C_{ks} is the shear viscosity for Kelvin section.

τ_n and τ_s are the normal and shear components of the relaxation time:

$$\tau_n = \frac{C_{kn}}{K_{kn}} \tag{4.4}$$

$$\tau_s = \frac{C_{ks}}{K_{ks}} \tag{4.5}$$

It has been chosen to equate the normal and shear direction parameters:

$$K_{mn} = K_{ms} = K_m \tag{4.6}$$

$$C_{mn} = C_{ms} = C_m \tag{4.7}$$

$$K_{kn} = K_{ks} = K_k \tag{4.8}$$

$$C_{kn} = C_{ks} = C_k \tag{4.9}$$

Burger's model parameters, in particular, were obtained following the methodology developed by Baumgaertel and Winter (1989), whereby the viscoelastic behavior of the studied mastics was determined by fitting the Burger model to DSR test results. Two rheological measurements were fitted simultaneously, namely the storage and the loss shear moduli respectively. The fitting procedure was based on minimizing an objective function (Equation 3.130):

$$objective\_function = \sum_{j=1}^{m}\left[\left(\frac{G'(\omega_j)}{G'^{0}_{J}}-1\right)^2+\left(\frac{G''(\omega_j)}{G''^{0}_{J}}-1\right)^2\right] \tag{4.10}$$

The "Solver" option in Microsoft Excel was utilized for the purpose of minimizing the objective function and results were highly dependent on initial values inserted for the model parameters (Table 4.6).

Table 4.6 Mastics Burger Parameters.

Burger Parameter	**Initial Value**	**"Solver" Value**	
		MC	**MCF**
K_k [MPa]	3	0.03	0.26
K_m [MPa]	2	56.09	24.36
C_k [MPa·s]	4	1.10	3.61
C_m [MPa·s]	5	8.18	13.11

4.5.3 Simulation of Frequency Sweep Test

The micro-scale contact parameters of each mastic has been validate through a comparison between DEM results and laboratory ones obtained in a frequency sweep test (FS), which is normally adopted to establish the response of mastic to different loading frequencies, in term of |G*| and δ master curves. The Frequency Sweep (FS) test was performed in strain control configuration, where the strain amplitude was limited within the linear viscoelastic (LVE) response. Since in PFC forces can be applied only to spheres and not to walls, an oscillatory shear angular velocity was used for each temperature as shown on Figure 4.4b. In laboratory, according to Dondi *et al*. (2014), FS test was conducted in a range of frequencies between 0.01 and 10 Hz, at the temperatures of 10°C, 20°C, 30°C, 40°C, 50°C and 60°C. The 8 mm plate with 2 mm gap set-up was adopted in all the range of temperatures.

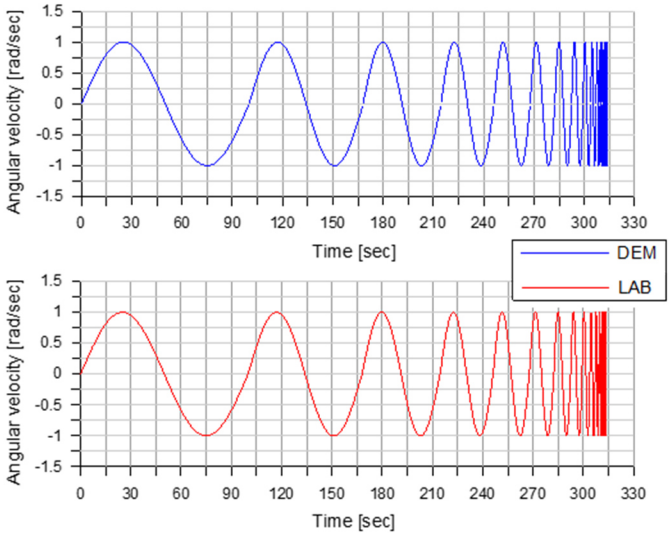

Figure 4.4b – Frequency sweep test loading wave.

The complex shear modulus (G*) and the phase angle (δ) were measured. G* is an indicator of the stiffness or resistance to deformation under load of bitumen and is defined by the following equation:

$$|G^*| = \left| \frac{F_{MAX}}{S_{SMAX}} \right| \tag{4.11}$$

where F_{MAX} is the maximum amplitude of the particles shear contact forces and the S_{Smax} is the maximum amplitude of the particles shear displacements.

The phase angle is defined by:

$$\delta = \frac{\Delta t}{t} \cdot 360 \tag{4.12}$$

where t is the loading time and Δt is the time lag between the peak shear contact force and the peak shear displacement. Using the principle of Time – Temperature Superposition (TTS) (Equation 3.48) the master curve of G* and δ were constructed at the reference temperature of 20°C.

4.6 Test Results and Discussion

4.6.1 Master Curves

4.6.2.1 Frequency Sweep Test Results

The rheological parameters complex modulus G* and phase angle δ of mastics MC and MCF are represented in terms of master curves in Figure 4.6. As in Figure 4.5 the Black Diagram curves of mastics are continuous, it can be stated that the TTS principle is also valid for the studied mastics in the entire temperature domain (Tan and Guo 2013).

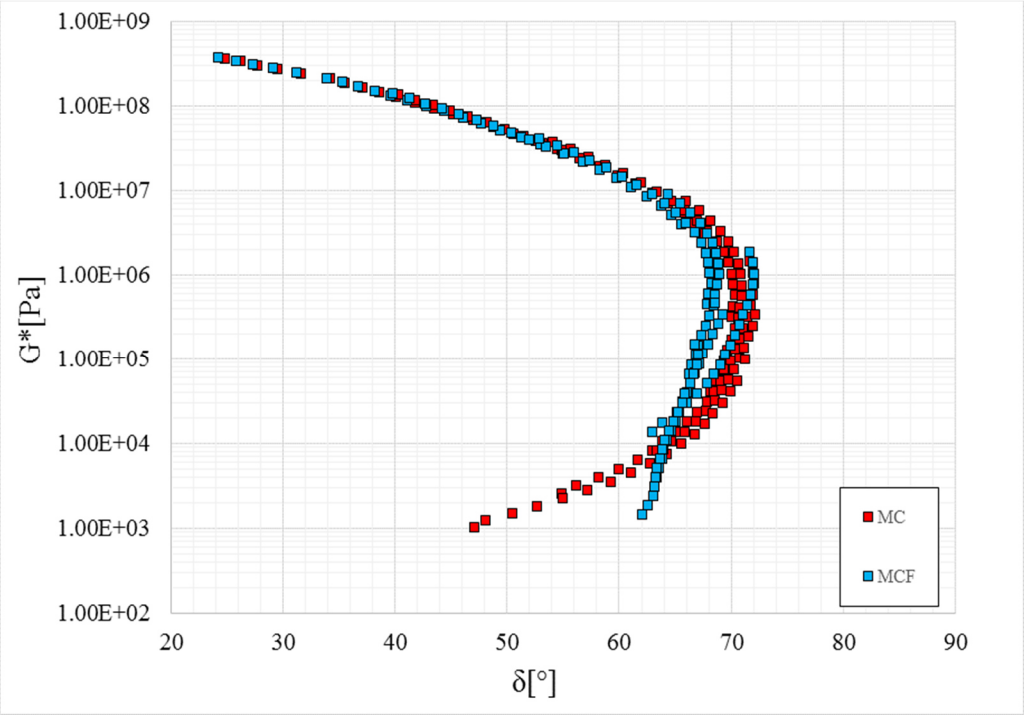

Figure 4.5 – MC and MCF Black Diagram.

At medium and high frequencies, G* tends to the same value for both mastics (1.32E+08 Pa at 176 Hz). Differences can be observed at low frequencies, where the MCF mastic shows slightly higher moduli. In particular the G* values of MCF at the frequencies of 0.002 Hz and 2.5E-06 Hz are equal to 144.0 kPa and 1.4 kPa; G* values of MC are equal to 95.6 kPa and 1.0 kPa at the same frequencies. The presence of limestone filler increases the sample stiffness at high temperature: that means resistance to the permanent deformation is increased (Saeed *et al.* 2010). The frequency dependence of MC phase angle shows a significant reduction of δ at low

frequencies. The mastic obtained by adding only cement exhibits lower phase angles than the mastic with both cement and limestone filler. This suggests that the cement preserves the elastic properties of the modified bitumen of the emulsion: for shear stresses applied at low frequencies MC shows reversible deformation greater than MCF's ones and the phase angle curve appears similar in trend to that one of a Polymer modified Bitumen (PmB). At intermediate and high frequencies, phase angle values are about the same for both mastics, in particular at high frequencies/low temperatures the mechanical response of mastics is almost elastic (25°) (Figure 4.6).

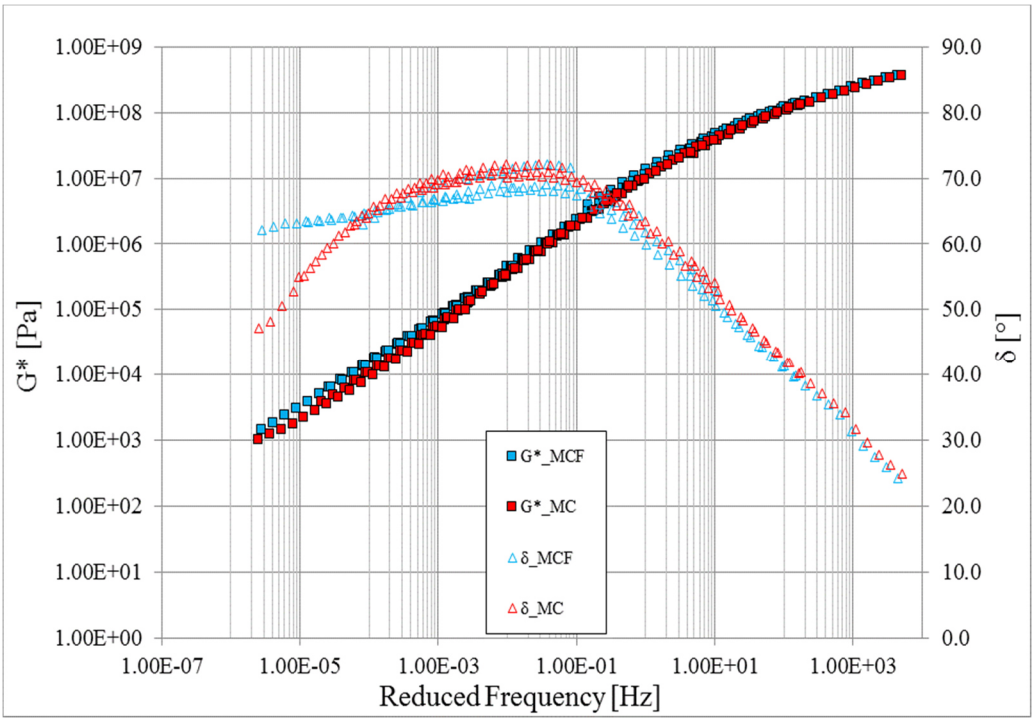

Figure 4.6 – MC and MCF Master Curves.

4.6.2 Creep Test Results

4.6.2.1 Repeated Creep Recovery Test

In order to evaluate the mastics response to permanent deformations, RCR tests in plate-plate (PP) configuration were performed at the temperatures of 46 and 58°C. A shear stress of 1 kPa was chosen to test the mastics in the LVE range, preventing both MC and MCF from reaching the tertiary flow behavior at the end of the 100 loading cycles (Motamed and Bahia 2011).

As shown in Figures 4.7- 4.8, the MC mastic has accumulated greater deformations at 46 and 58°C. However, the temperature increase has produced a 87% increase of the accumulated strain value for both MC and MCF. As it is shown in Table 5, the average creep non-recoverable compliance was calculated during 100 cycles of loading and J_{nr} values referred to MCF were lower than the J_{nr} values of MC at both test temperatures.

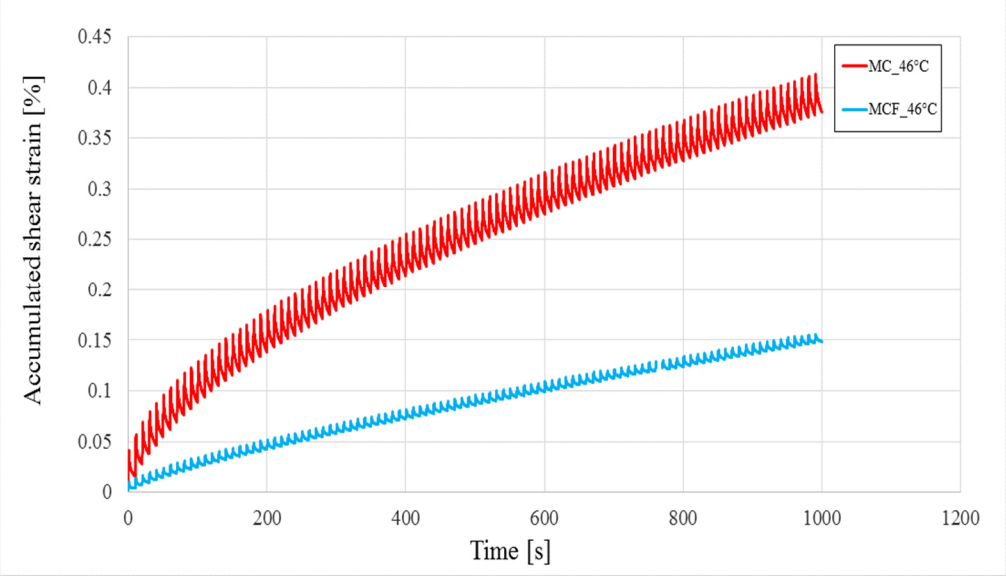

Figure 4.7 – MC and MCF Master Curves.

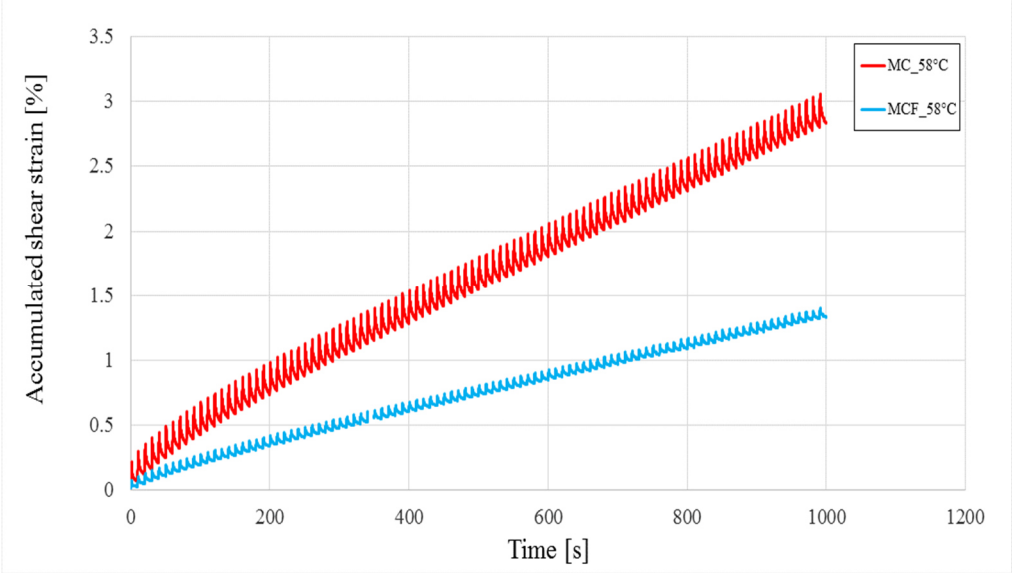

Figure 4.8 – MC and MCF Master Curves.

Moreover, the non recoverable creep compliance, J_{nr}, was estimated also at different loading cycles in order to evaluate its variation as a function of the percentage of recovery (Fig 4.9). At the same Jnr and temperature, MC shows higher% recovery than MCF. From a different perspective, for the same% recovery the mastic with filler shows lower values of Jnr: hence it has accumulated less permanent deformation by applying the same shear stress. Table 6 shows strain levels attained by the two mastics at the first and 100th load cycle at both test temperatures. It can be noted how, at 46°C, are no evident differences of strain level between the first and the 100th cycle for the MC mastic. As opposed, at the temperature of 58°C, the same mastic has shown a greater deformation at the end of 100 load cycles. This difference was not found between the two test temperatures on MCF: the strain at the end of 100 loading cycle is not changing with accumulated strain. The MCF has shown greater resistance to deformation at both test temperatures (i.e. lower values of J_{nr}) and its behavior is not affected by the accumulated strain.

Table 4.6 RCR results at 46 and 58°C.

Mastic Name Code	**Temperature [°C]**	**Accumulated Strain 100th cycle [%]**	**Shear Stress [Pa]**	**Average J_{nr} [Pa^{-1}]**
MC	46	0.41	1000	0.006
MCF	58	3.00	1000	0.030
MC	46	0.15	1000	0.002
MCF	58	1.40	1000	0.016

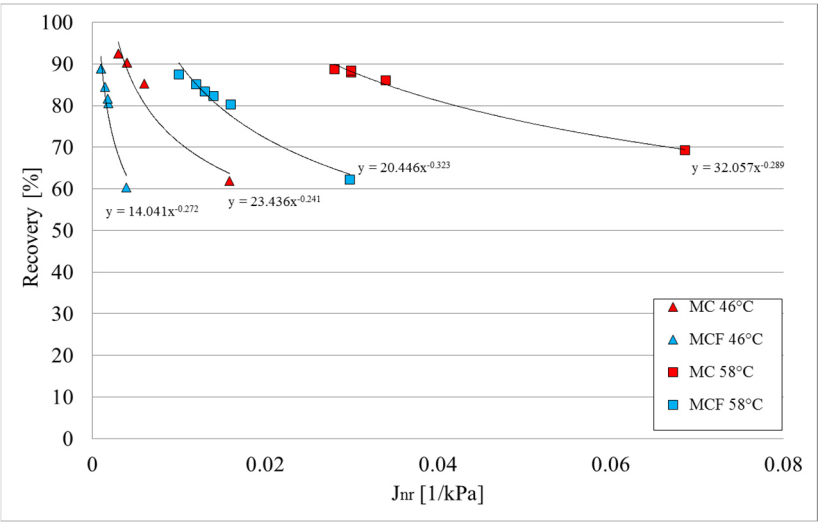

Figure 4.9 – Comparison of RCR J_{nr} and Recovery @46 and 58°C.

4.6.2.3 Multiple Stress Creep Recovery Test

In this study temperature sweep tests at 1.59 Hz were implemented and small deformations were employed. However pavement deformations in the top layers of pavements may be attributed to the accumulation of irreversible strains. For this reason it was chosen to study the potential rutting of the cold mastics through Multiple Stress Creep Recovery (MSCR) tests run at 0.1 and 3.2 kPa. For both stress levels the average percentage of recovery of ten cycles was determinate according to AASHTO TP 70-07.

Figures 4.10 – 4.11 shows the MSCR results at both test temperatures (46°C and 58°C). The MC shows considerable larger creep strains than MCF for both test conditions. The rate of strain value increases and significantly changes when the 3.2 kPa stress level starts.

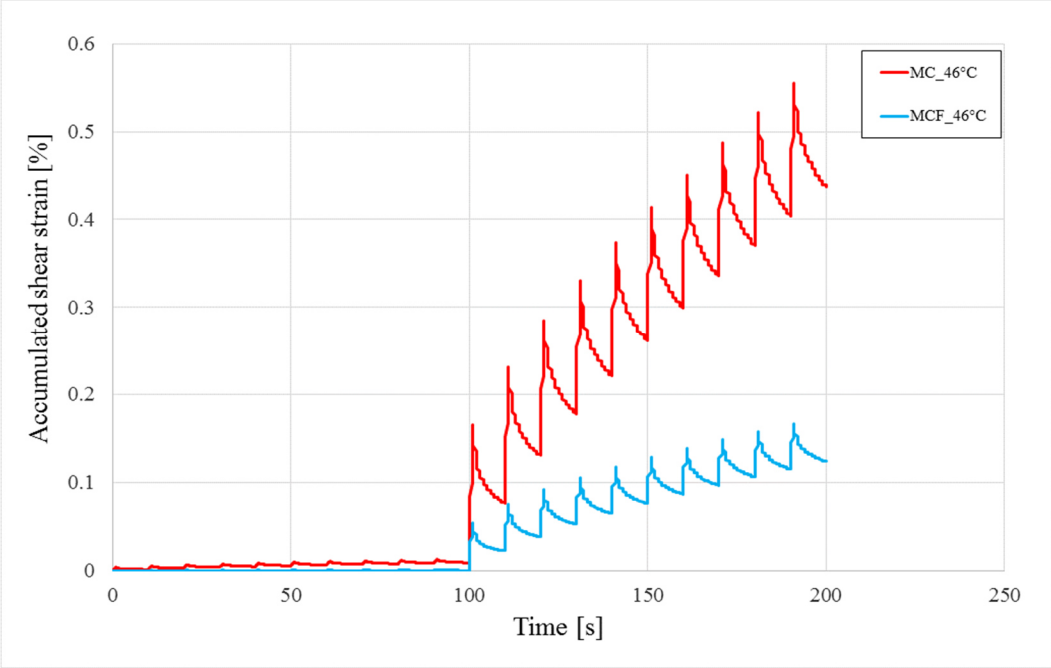

Figure 4.10 – MC and MCF MSCR results.

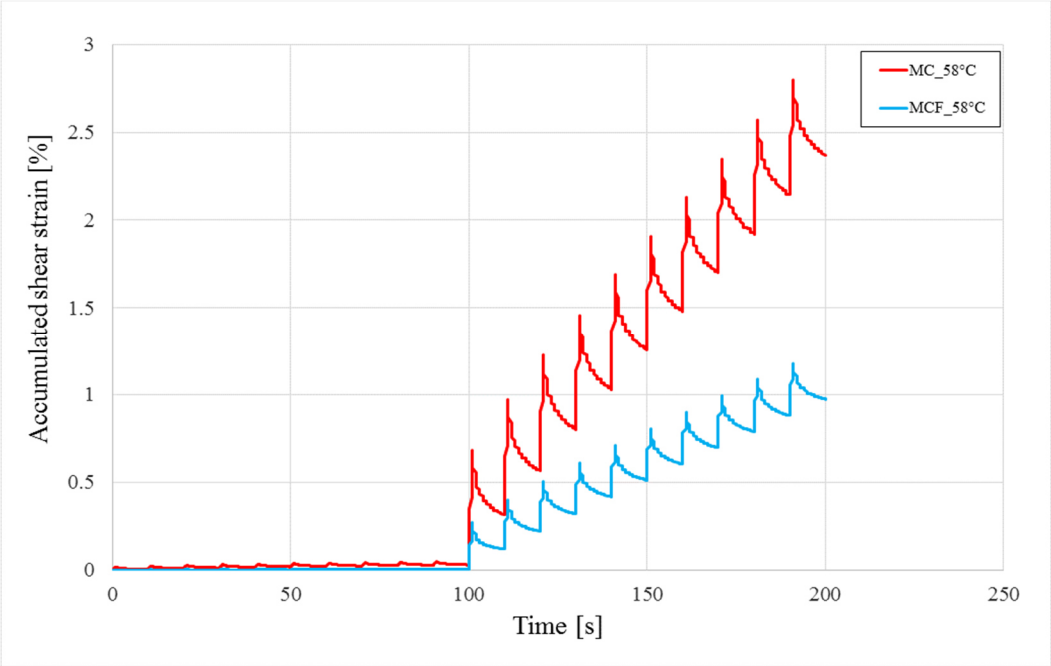

Figure 4.11 – MC and MCF MSCR results.

The non recoverable compliance represented in Figure 4.12 clearly shows the sensitivity of mastic MC to permanent deformations under repeated loads. On the other hand MCF have lower values of non recoverable compliance. In particular, at 3.2 kPa and 58°C the mastic containing limestone filler shows a J_{nr} value of 0.17 1/kPa; this value is 2.5 times lower than the J_{nr} obtained for the mastic containing only cement at the same shear stress and temperature. For the MC the temperature rise from 46°C to 58°C increases of 5 times the J_{nr} values at both stress levels. For the MCF the temperature stress increases of 8 times the J_{nr} values. The mastic with limestone filler is potentially less expose to the phenomenon of permanent deformations, while being more sensitive to temperature variations. Figure 4.13 shows the close relationship between average recoverable strain and average non recoverable compliance for the stress level of 3.2 kPa. The regression equations of the empirical points is well identified by power functions. For the same percentage recovery the mastic with filler shows lower values of J_{nr}, it has accumulated less permanent deformation by applying the same shear stress.

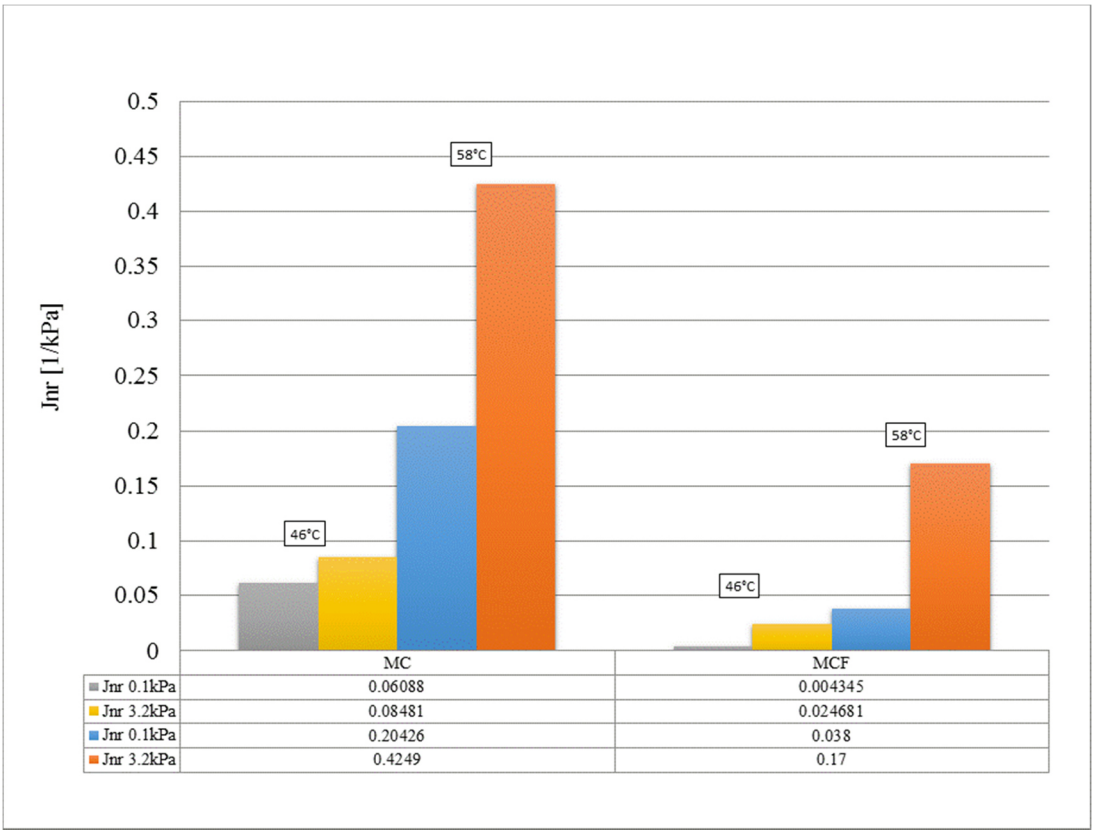

	MC	MCF
Jnr 0.1kPa	0.06088	0.004345
Jnr 3.2kPa	0.08481	0.024681
Jnr 0.1kPa	0.20426	0.038
Jnr 3.2kPa	0.4249	0.17

Figure 4.12 – MC and MCF non recoverable compliance.

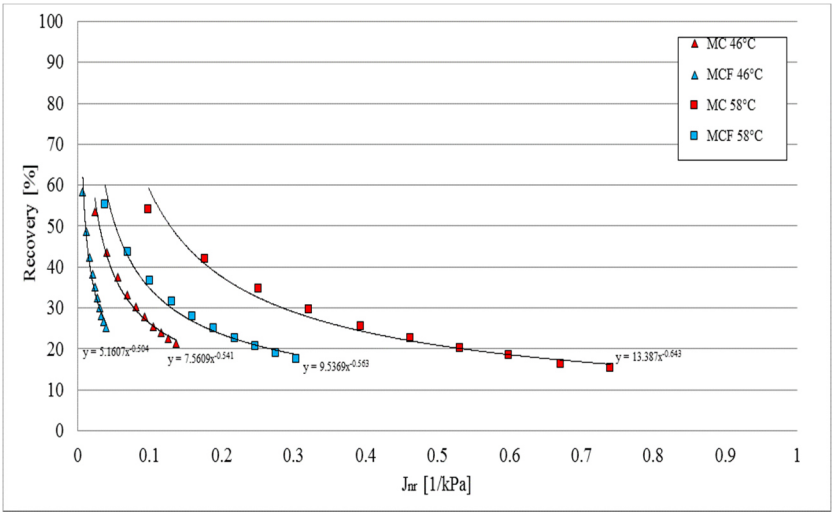

Figure 4.13 – MC and MCF MSCR results.

4.6.3 DEM simulation results

4.6.3.1 Frequency Sweep Test

Figures 4.14 and 4.15 compare the G* and δ master curves from the DEM simulation with the results obtained from the DSR test, for each type of mastic. Both for MC and

for MCF mastic the measured data and the simulated ones have the same trend, confirming that the selected micro-scale contact parameters best matched the response observed in laboratory tests.

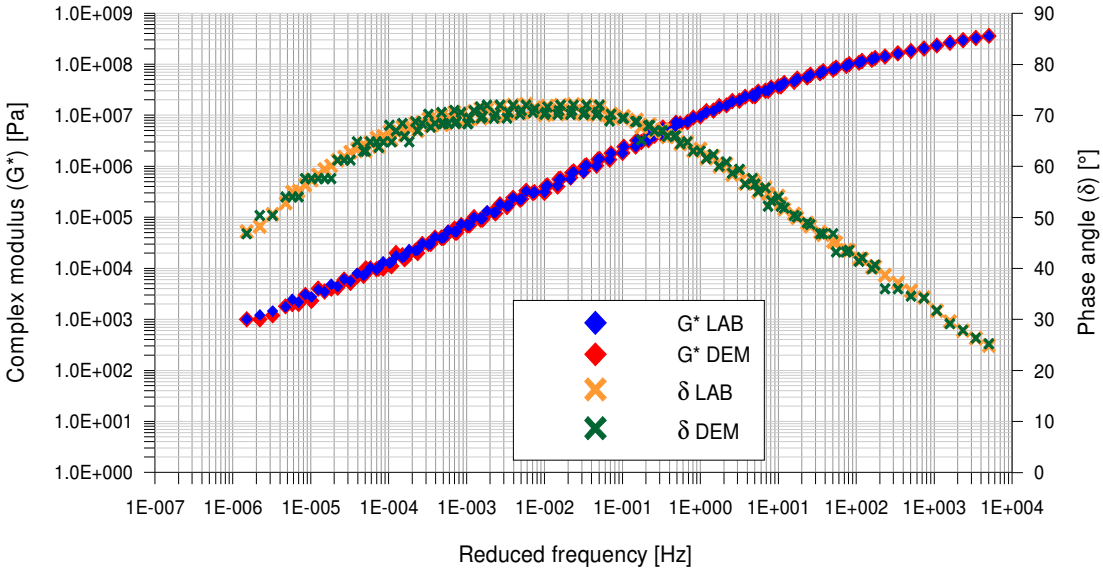

Figure 4.14 - MCF, master curves of experimental (LAB) and numerical (DEM) results for complex modulus (G*) and phase angle (δ).

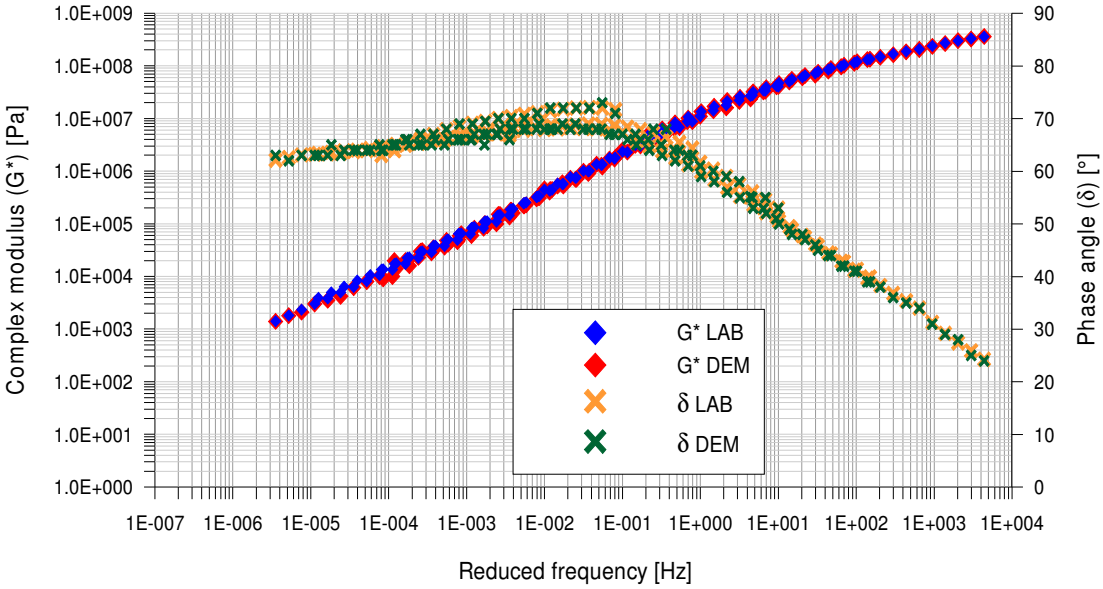

Figure 4.15 - MCF, master curves of experimental (LAB) and numerical (DEM) results for complex modulus (G*) and phase angle (δ).

For each temperature Figures 4.16 and 4.17 show the mean error (Δ) between DEM and laboratory data, for complex modulus and phase angle. The obtained values are

small, confirming that the DEM approach used in this study has a good potential in predicting the mastic response in the frequency sweep configuration.

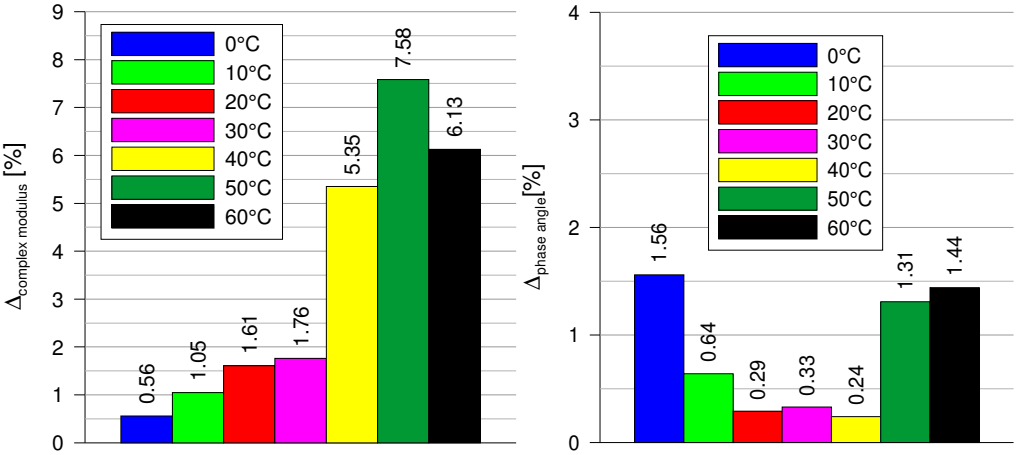

Figure 4.16 - MC, mean error (Δ) between DEM and laboratory data for each temperature, for complex modulus and phase angle.

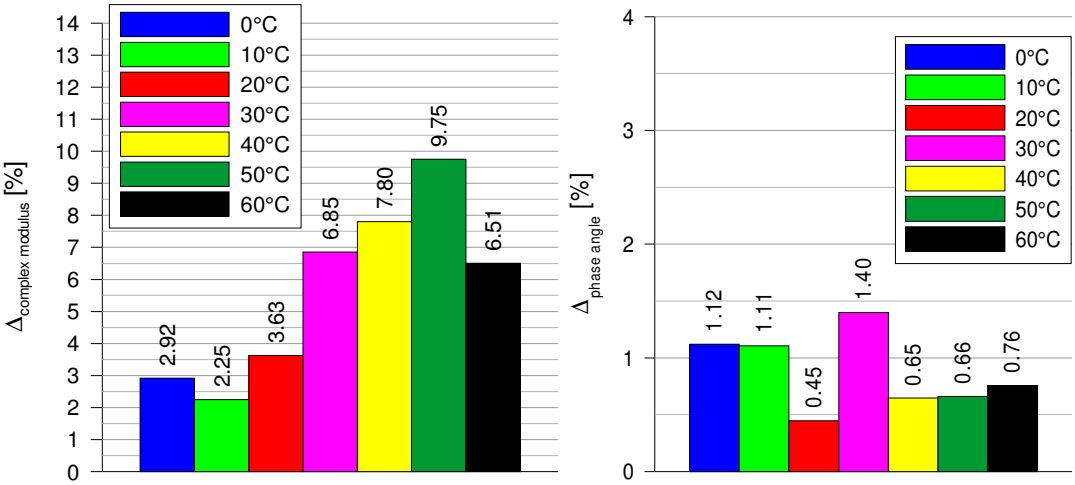

Figure 4.17- MCF, mean error (Δ) between DEM and laboratory data for each temperature, for complex modulus and phase angle.

Based on the obtained macro-scale results, that validates the DEM approach, the micro-scale response was analyzed by considering both the contact forces inside the specimens and the corresponding spheres displacements. For both cases three significant conditions, representative of the MC and MCF mastics time-dependent behavior, were considered during the frequency sweep tests: 0°C and 30°C are representative of low temperatures, at which the mastics do not show significant differences on the complex modulus and phase angle. 60°C is representative of high

temperatures, at which the limestone filler have larger effects on the mastic in terms of increase of the complex modulus.

Contact forces have been evaluated inside the MC and MCF modeled samples at the end of the sweep test at different temperatures (0°C, 30°C, and 60°C). For each mastic the contact forces network is mainly horizontally oriented, reflecting the orientation of the shear stresses. Shear contact forces have a uniform distribution inside the specimen and they are significantly larger than normal ones. As shown in Table 4.7, as the temperature increases, the maximum shear contact force inside the sample increases. While at 0°C and 30°C the maximum shear contact force inside the MC and MCF specimens are very similar, increasing the temperature the difference between the MCF and the MC behavior increases. The maximum shear contact force of the MCF sample, in particular, are always higher than the MC one, and the relative difference (Δ) increases passing from 60°C to 90°C. This trend confirms the ability of the limestone filler to improve the sample stiffness and the mastic resistance to permanent deformation, at high temperatures.

Table 4.7 - Maximum shear contact force inside the mastic sample [$*10^{-3}$ N/m]

Temperature [°C]	**0**	**30**	**60**
MC	2.544	5.696	21.250
MCF	2.840	5.731	28.470
Δ	-0.296	-0.035	-7.220

For each mastic, as the temperature increases, the total number of spheres displacements inside the sample increases. From 0°C to 60°C, the 3D contacts network in the MC and MCF mastics is characterized by a better interconnection between particles. The spheres displacements, in particular, are evaluated in a Cartesian coordinate system, with:

- the origin in the centre of the upper horizontal plane of the model, which simulates the oscillating plate;
- the z direction is coincident to the vertical axis of symmetry of the sample, pointing to the lower plate.

They are calculated at the end of the sweep test at different temperatures (0°C, 30°C, 60°C). As shown in Table 4.8, for the same mastic, as the temperature increases, the maximum and minimum displacements of the particles in x, y and z directions

increase. The increase is lower for the x and y components and it is larger for the z direction.

Comparing the MC and MCF specimens, for each temperature, the MC shows larger spheres displacements than the MCF one. Inside the MC sample, without limestone filler, the particles move more independently of each other. The difference between the MC displacements and the MCF ones increases as the temperature increases. At 0°C and 30°C, in fact, the displacements are similar, while at 60°C the first ones are larger than the seconds. So the master curve trend, which shows that MCF is stiffer than MC, is confirmed by the displacements of the spheres of the two models.

Table 4.8 - Particles displacements of MC and MCF models in x (xdisp), y (ydisp) and z (zdisp) direction [mm]

Temperature [°C]	**Mastic**	**xdisp min**	**xdisp max**	**ydisp min**	**ydisp max**	**zdisp min**	**zdisp max**
0	MC	0.000050	1.09	0.00004	1.10	0	0.28
	MCF	0.000049	1.03	0.00004	1.01	0	0.26
30	MC	0.000060	1.20	0.00005	1.20	0	0.50
	MCF	0.000058	1.11	0.00005	1.10	0	0.45
60	MC	0.000100	2.00	0.00015	1.90	0	1.03
	MCF	0.000090	1.80	0.00011	1.60	0	0.60

4.7 Summary

The main objective of this study was to evaluate the rheological and micro-structural properties of cold mastics containing traditional filler in order to validate laboratory and model methods that will be applied, in the follow chapters, on mastics containing industrial reclaimed fillers. Based upon the developed research work, the following concluding remarks can be made; in terms of method validation:

- there is a reproducibility of the rheological tests with the DSR in the study of cold bituminous mastics; the principles behind the linear analysis of hot bitumen have been validated also for that type of material;
- the obtained results confirmed that the DEM is a useful and promising tool to model the rheological behavior of asphalt mastics. The adopted approach is successful in predicting, both quantitatively and qualitatively, the complex modulus and the phase angle in a temperature sweep test. On the micro-scale it is suitable to capture the real time-dependent behavior of asphalt binder and to predict its performance through the study of its internal interaction.

In terms of limestone and cement fillers action on mastics:

- it was found that at medium and low temperatures no substantial differences can be observed in terms of rheological properties between the two mastics. The complex modulus G* and phase angle δ values are similar as to the results of ER performed at 25°C;
- the main differences between the MC and the MCF are found at high temperatures. At low frequencies, the mastic with only cement exhibits a perfectly viscoelastic response as opposed to the mastic with filler which shows a predominantly viscous response. The cement has increased the elastic component of the mastic, but the presence of the filler has increased the stiffness of the mixture. The MCF showed higher moduli than the MC's;
- the mastics behavior differences at high temperatures were investigated through ER and RCR test. The results of the recovery test show that the MC has higher values of elastic recovery than MCF. However, in repeated stress condition, the MCF has accumulated less deformation at the end of loading phase showing a better response in terms of resistant to permanent deformation.

- the Multiple Stress Creep and Recovery test has confirmed the temperature sweep test results. The mastic with limestone filler has accumulated less deformation at both test temperatures (46°C and 58°C) and at both stress levels (0.1 kPa and 3.2 kPa). The presence of limestone filler has reduced the J_{nr} values, showing a better response of mastic to permanent deformations;
- the DEM approach confirms the rheological data. The sample with limestone filler particles has lower displacement and higher shear contact force than the one with only cement, highlighting the stiffer behavior of the first.

5 RHEOLOGICAL CHARACTERIZATION OF BITUMINOUS MASTICS CONTAINING WASTE BLEACHING CLAYS

5.1 Introduction

As described on chapter 2 the analysis of the response to load and temperature stresses of the asphalt pavement cannot be separated from the rheological study of the asphalt mastic. Usually asphalt-filler mastic consists of bitumen and mineral filler that is defined as the portion of aggregates passing the 63 μm sieve (EN 13043) and that is generally added to the aggregate mixture during the asphalt mixing process. Numerous research works show that the mechanical performance of asphalt mastics is largely dependent on fillers properties and on the way they interact with the bitumen (Vignali V. *et al.* 2014). This also happens when alternative materials are used instead of common fillers. Sangiorgi *et al.* (2014) have examined two different types of bentonite clays as replacement of limestone filler for the production of binders course HMAs. The bentonites come from two consecutive industrial processes: spent bentonite (Ut) obtained from a vegetable oil bleaching process (stage 1), and digested spent bentonite (Ud) the result of the anaerobic digestion of spent bentonite within a reactor producing biogas (stage 2). From the analysis of Indirect Tensile Strength and Indirect Tensile Stiffness Modulus data, it was found that the presence of Ut or Ud fillers has a totally different effect on the bituminous mixture's mechanical properties. While digested spent bentonite clay determines an increase in indirect tensile strength and stiffness compared to the mixture with limestone filler, the presence of Ut filler results in an evident reduction of these properties. Besides from the analysis of the dynamic creep test, it was concluded that the substitution of the limestone filler with the Ut filler determines a reduction of resistance to permanent deformations, which is, however, improved using the Ud filler. Based on these findings, the main objective of the research analyzed on this chapter is to investigate the rheological properties of bituminous mastics containing Ut and Ud fillers, to compare with a traditional mastic containing limestone filler (Mazzotta F. *et al.* 2015). The mastic stress-strain response is studied through Frequency Sweep (FS), Repeated Creep Recovery (RCR) and

Multiple Stress Creep Recovery (MSCR) tests, validated for cold mastic response on the previous paragraph.

5.2 Materials

5.2.1 Bitumen

In this study three different mastics were produced with a hot mixing process using a 50/70 penetration grade bitumen. The characteristics of the bitumen are shown in Table 5.1.

Table 5.1 Properties of the 50/70 pen bitumen

	Unit	Characteristic value	Standard
Penetration @ 25°C	dmm	50-70	EN 1426
Soft.Point	°C	50	EN 1427
Dynamic Visc. @60 °C	Pa s	≥145	EN 12596
Fraass	°C	-8	EN 12593

From Frequency Sweep Test (0-60°C) the master curve for base bitumen has been found by applying the appropriate shift-factor for all the bitumen (WLF theory Chapter 3). Amplitude sweep test was performed on all the bitumens to find the Linear Viscoelastic Elastic (LVE) range for the material (2.6%). The test was controlled on shear strain and with the frequency of 1.59 Hz.

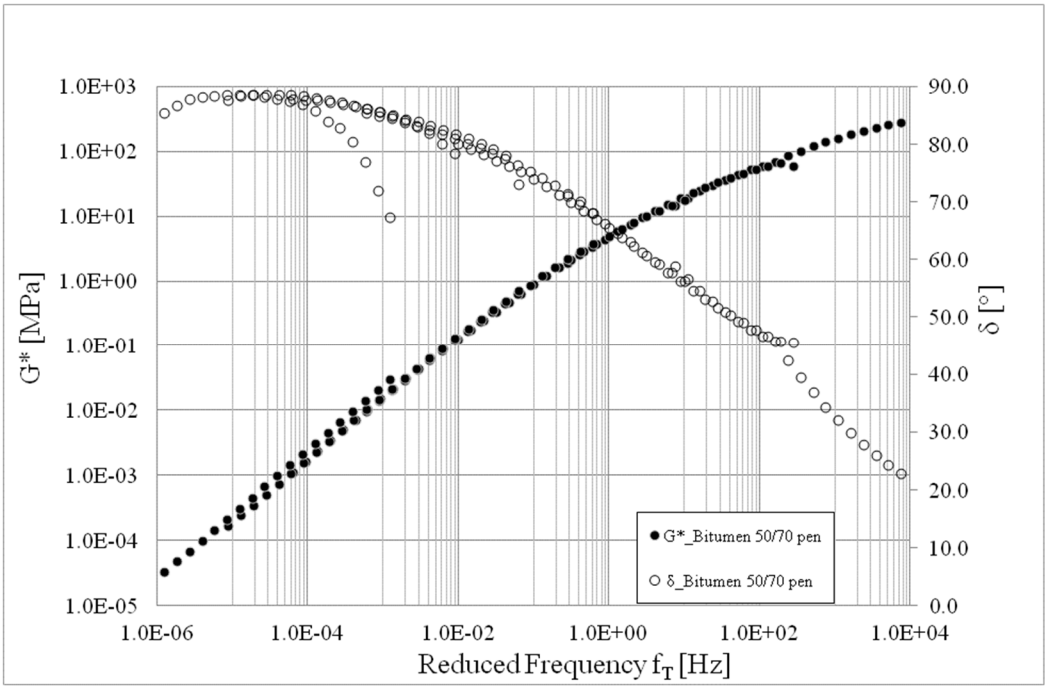

Figure 5.1 – Bitumen 50/70 pen Master Curve.

5.2.2 Fillers from bleaching clay

5.2.2.1Bentonite

The fillers used in this study come from bentonitic origin. Bentonite is the commercial name of a series of natural clays characterized by the capacity to absorb water inflating. The main component of bentonite is montmorillonite (described in details on Chapeter 2). In the bentonite, montmorillonite is always combined with other clay minerals (such as kaolin, mica, illite, etc.) and no clay (such as quartz, feldspar, calcite and gypsum). The presence or absence of these minerals can affect the bentonite quality and make it more or less suitable for certain applications. In its natural state the raw bentonite is a soft rock crumbly and variable color greasy. The specific dry density varies from 2.2 to 2.8 g/cm^3. The specific density of bentonite dug and crowded at the natural moisture state is between 1.5 and 1.8 g/cm^3. The various bentonites can be traced to a common basic structure, however, there are considerable differences between the various types, both as to chemical constitution, both to the physical state of the constituents which accentuate or not the properties toward a particular Lighting Technologies. Bentonite is a raw material common in many countries of the world that is mined in open sky quarries. The deposits are generally lenticular of considerable size and the thickness is usually limited to a few meters. The production of bentonite provides for the mining, the eventual exchange of base treatment, drying and grinding. The exchange treatment is effective to transform the calcium bentonite in sodium bentonite in through the activation process which consists in cation exchange with sodium carbonate. The drying process allows to reduce the natural moisture of bentonite normally between 25 and 35%. Because of the hygroscopic nature of bentonite water it is released slowly. It must be carried out at a controlled temperature to avoid the risk of ruining the structure molecular. Starting from temperatures above 500 °C in fact the bentonite away so irreversible water of crystallization, in these conditions permanently loses its features becoming an inert powder. A fundamental property of the bentonite is to absorb water by re-inflating, the absorption capacity depends on bentonite type. The degree of hydration and the power swelling depend on the types of exchangeable

cations present, each of them possessing a different hydrophilic and solvating power. The swelling is due to two main causes: the absorption of water to the surface of the crystalline lamellae and repulsive forces of type osmotic, for which the unitary strip are forced to come off each other, opening up to "accordion". The sodium bentonite, with a prevalence of sodium cation (Na^+), allows water to enter deeply between the slats, separating them until elementary unit and thus giving rise to characteristic swelling. On the contrary, the calcium bentonite, with a prevalence of calcium cation (Ca^{2+}), is hydrated in a similar way, but has absorbent properties minors being characterized by a strong positive charge which does not allow water molecules to penetrate between the lamellae; the particles then fall apart in packets rather than swell. The bentonite dispersed in water gives rise to very stable colloidal suspensions characterized by viscosity and thixotropy: these suspensions to the right concentrations are real gel. The formation of the suspension is due to penetration of water molecules in the interspaces present among the crystalline lamellae: between these layers of the bridges are established in which the water is bound by hydrogen bonds. When the system is subjected to a mechanical stress mechanics there is a partial braking of the ties that allows greater mobility of individual lamellae causing the system purchases a lower viscosity as its state rest. This sol-gel-sol transformation is reversible and is known as thixotropy. The property of aqueous bentonite suspensions are used mainly in the excavation fluid. A micelle of montmorillonite can be considered consists of a thin pack of layers elementary negatively charged. Because of this charge each micelle is able to repel another giving rise to the penetration and absorption of water molecules drawn around the grid elementary; for this reason, while the package expands, giving rise to swelling, around each particle it will form a stable casing which, reached its saturation limit, It rejects other water even when it is subjected to pressure. Thanks to these characteristics bentonite is used to stop water infiltration and waterproof land landfills, ponds and reservoirs. The absorption and adsorption properties of bentonite are determined by considerable specific surface area and the free charges present on each micelle. This particular configuration of fillers results in a considerable filtering capacity for the bentonite.

5.2.2.2 Use of Bentonite

Thanks to its special properties uses of bentonite are numerous and diversified. Today the main areas of use include the following:

- foundry: the bentonite is used as a binder in the green molding for the production of high quality castings in iron foundries, steel, and nonferrous. The use of bentonite as agglomerating sand gives it the necessary cohesion ensuring sufficient plasticity and refractoriness;
- engineering: thanks to rheological properties and to the thixotropic suspension aqueous, the bentonite is employed for preparing the excavation sludge used in drilling. The role of the excavation fluid is mainly to stabilize the hole, seal up the wall and transport the excavated material. The bentonite are so used in oil drilling, in drilling water wells and drilling of tunnels and mini-tunnel. Execution of special foundations are used bentonite for the excavation of diaphragms and for the perforation of the poles. In the geotechnical Bentonite is used in the self-hardening mixtures used for plastic diaphragms, for the clogging of mortars and for the injections. Finally, the waterproofing properties of the bentonite are exploited in environmental engineering to seal the landfill and waterproof the soil. Water treatment: due to its ion exchange capacity, flocculation and sedimentation, the bentonite is used in water treatment as an auxiliary of polyelectrolyte and inorganic flocculants;
- agriculture: having regard to the ion exchange capacity, the bentonite is used in the conditioning of land. It is also used to absorb moisture in soils for gardening and as a support for pesticides and herbicides.
- ceramic industry: the bentonite is used as a plasticizer in the ceramic bodies and how anti-sedimentation in glazes.
- paper industry: the bentonite is used to improve the efficiency of the conversion from pulp to paper and to improve its quality by preventing the agglomeration of the particles chewy. Thanks to the adsorbent capacity is also useful in the recycling process for the ink elimination.

- food industry (wine, oil and edible fats): thanks to its absorbent properties, the bentonite is used in the purification of the oil and edible fats and in the clarification of alimentary drinks.

From an ecological point of view and the preservation of health, the bentonite is neither dangerous for the environment or to humans according to the EC Regulation 1272/2008 and Directive 67/548 / EC.

5.2.2.3 Production Process of bleaching clays

Two different bentonite fillers were used in the experimental study obtained from two consecutive phases in the process of bleaching vegetable oils and producing energy from biogas:

- the filler named Ut (Fig. 5.2) was derived directly from the bleaching phase (stage 1) and, for this reason, its oil content ranges between 20% and 25% of its dry weight;

Figure 5.2 – Spent Bentonite: Ut

- the other filler, Ud (Fig. 5.3), i.e. the digested spent bentonite, is the result of the anaerobic digestion of the Ut filler during the process to produce biogas (stage 2). This phase of biochemical conversion determines a reduction of the content of residual oils, to below 1%.

Figure 5.3 – Digested Bentonite: Ud

The following sections describes the production processes of bentonite filler exhausted; in particular, describes the oil refining process with specific reference to discoloration and the process of anaerobic digestion.

5.2.2.3 Ut Production - oils and grease refining and bleaching process.

Refining term covers all the manufacturing processes to eliminate from product all the unwanted substances in order to obtain a better oil quality. During this process is important, however, that no structural changes occur in the fat. The refining process aims to the satisfaction of three basic aspects:

- qualitative: obtaining a better oil quality;
- quantitative: get a yield as high as possible;
- finalization of the product.

As regards the qualitative aspect, the refining must not make changes in composition and structure of the fat. The second aspect concerns the quantitative yields of the refining process and it is linked to the quality of the raw material, the suitability of facilities, to consumption needed to reach the end of the refining. The purpose of bleaching is to remove substances that cause anomalous coloring of the oils. It can be done either by physical methods and chemical: in oil technology and fats the physical method is resorted using absorbent materials. The adsorbent materials are of two types, namely bleaching clays and activated carbon; the bleaching clays, can be the source natural such as montmorillonite, or artificial. The natural clays have a less adsorbent capacity of those activated despite the washings, are slightly acidic, while the former are neutral. So the advantage of using natural clays is that these reacts to a lesser degree than those activated artificially; also having a higher density retains less oil.The ground apparent density is given by the unit of volume weight and is one of the most important land characteristics. It depends on the volume of the empty spaces: more empty spaces there are, the less the apparent density. The bleaching clays contain moisture close to 20-18% In the specific case of montmorillonite, the molecules are arranged in parallel layers and the water molecules lie between these layers and serve as a backing to keep them separate. This explains the decrease of their activity that occurs when the lands are dried before their use; the operation, in fact, causes the collapse of the structure by preventing the pigments of reaching the active centers. It is therefore necessary to

operate the dehydration under vacuum at a suitable temperature for a certain time, thus allowing that water is removed in the same moment in which the earth is in contact with the material to decolorize. Another important feature of bleaching clays is the particle size distribution, represented by very small particles (<5 μm) up to the relatively large (80). The smaller the particle size and the greater the activity of the earth, but at the same time increases the amount of retained oil and is more difficult filtration. It is still important that the distribution of the particles remains in a narrow range between 5 and 80 microns. The retained oil can be an average of 20 and 70% of the weight of the land, whether natural or activated respectively artificially. Regardless of how it is made up of the bleaching plant, the operating steps are the following:

- oil drying under vacuum at a temperature of about 60 °C;
- mixing oil / land;
- heating for 15-30 minutes at 90-110 ° C;
- cooling to a suitable temperature (30-60 ° C);
- filtration;
- oil recovery held land.

In conventional plants the land is separated from the oil by means of the press-bleached filters discontinuous operation, which require a considerable labor and also do not allow the recovering oil from the clay which remains on the filter cloths; another drawback is constituted by the short shelf life of filter cloths, which are often damaged during manual cleaning operations. On discontinuous rotating filters generally closed in a metal chamber and equipped with accessories that allow both the washing of the panels with solvents, either remove the residue and download it mechanically.

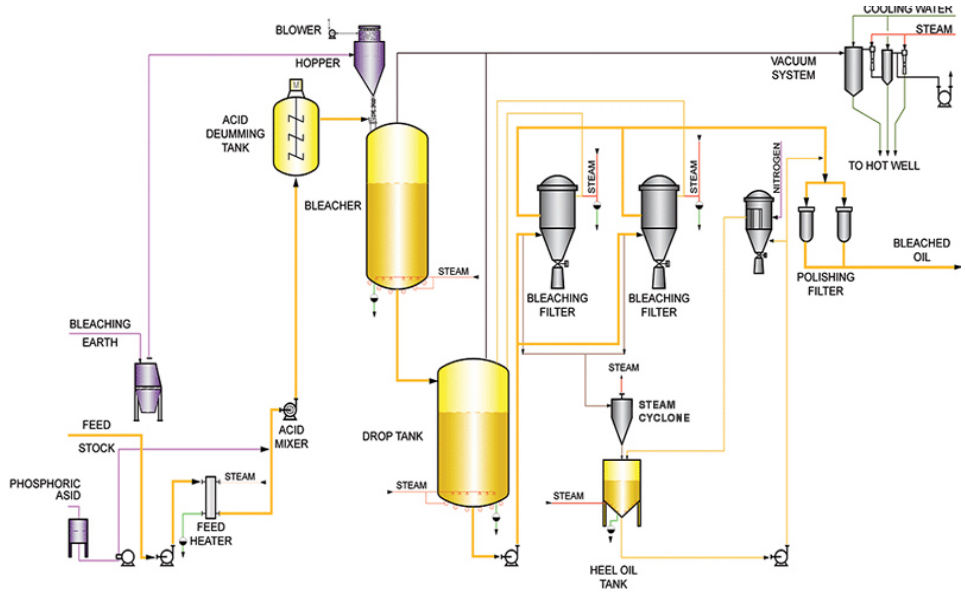

Figure 5.4– Bleaching clays plant.

5.2.2.4 Ud Production - Anaerobic digestion for biogas

Anaerobic digestion is a biochemical conversion process that takes place in the oxygen absence and consists of the demolition, by micro-organisms, of complex organic substances (lipids, proteins, carbohydrates) contained in plants and animal by-products, which produces a gas (biogas) made from 50-70% methane and the rest is mainly CO_2 and having an average calorific value of 23,000 kJ per cubic meter. The produced biogas is collected, dried, and compressed and stored and can be used as a fuel to power gas boilers to produce heat (perhaps coupled to turbines for the production of electricity), or combined cycle power plants or internal combustion engines. The plants anaerobic digestion can be fed by means of residues with a high moisture content, such as animal manure, the civil waste, food waste and the organic fraction of solid waste urban. In the factory where Ud filler is produced there is an anaerobic digestion plant with group of cogeneration constituted by an internal engine combustion able to use biogas as fuel in order to produce electricity and thermal energy. The entire production process of electrical energy from biomass waste is divided into the following phases:

- power plant and mixing;
- dosage of chemical agents;

- digestion step;
- processing of gas;
- cogeneration;
- digestate treatment.

5.2.2.5 Ut and Ud preliminary investigation

In order to be used as fillers, both spent bleaching clays were geometrically characterized through a gradation analysis (EN 933-10) and volumetrically, determining their volumetric mass (EN 1097-7) and Rigden Voids (EN 1097-4) (Sangiorgi *et al.* 2014). Delta Ring & Ball test was also performed according to EN 13179-1. Table 5.2 shows the fillers characteristics.

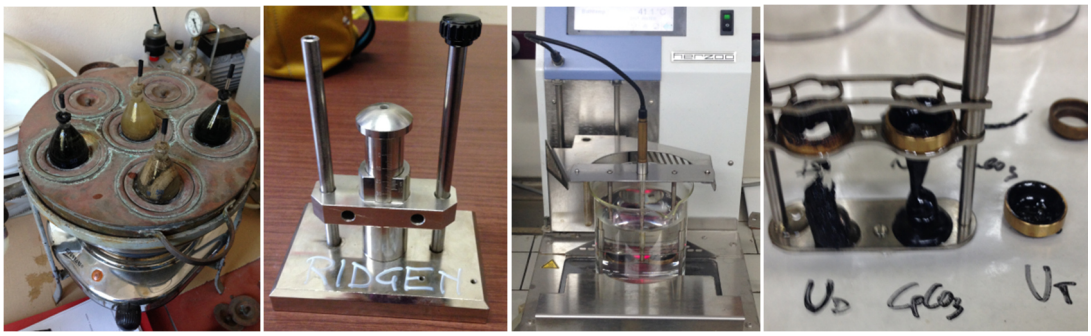

Figure 5.5– Fillers Ut and Ud characterization devices. a)volumetric mass (EN 1097-7); b)Rigden voids (EN 1097-4); c) d) Delta Ring & Ball (EN 13179-1).

Table 5.2 Main fillers characteristics

	Standard	**Limestone filler**	**Ut filler**	**Ud filler**
Particle density (Mg/m^3)	EN 1097- 7	2.73	1.59	1.84
Rigden voids (%)	EN 1097- 4	33.82	31.69	53.75
Δ Ring & Ball [°C]	EN 13179-1	8	-22	32

5.3 Mastics

5.3.1 Mastics Design

The following mastics were produced according to the proportions of a typical binder layer mixture. All the filler percentages has been considered in weight of bitumen. mixtures studied and summarized in Table 5.3.

- mastic Mff: 50/70 bitumen with limestone filler;
- mastic MUt: 50/70 bitumen with spent bentonite Ut and limestone filler;
- mastic MUd: 50/70 bitumen with digested bentonite Ud and limestone filler;

Table 5.3 Weights percentages of fillers on bitumen

Mastic	Limestone filler	Ut	Ud
Mff	70.6%	-	-
MUt	41.8%	28.8%	-
MUd	41.8%	-	28.8%

5.3.2 Mastics Preparation

The bitumen-filler mastics were produced by adding the correct mass of filler to heated bitumen at a temperature of 160°C while mixing the two components together with the Silverson L4RT high shear mixer until a homogeneous mastic was obtained. The mixing time was restricted to a maximum of 15 minutes. The mixing procedures are detailed as follows:

- both U_t and U_d fillers were put into a 160°C oven for 24 hours to ensure moisture-free particle surfaces.
- the 50/70 penetration grade bitumen stored in a 5 litre tin needed 5 hours to preheat in a 160°C oven and to make bitumen liquid and ready to mix.
- the accurate quantity of the bitumen was poured into a 1 litre tin. The tin with the bitumen was left on a hot plate maintained at 160°C.
- the bitumen was mechanically stirred for 30 seconds.
- the designed mass of Ut and Ud fillers was added slowly while the mechanical stirring was continued for 4.5 minutes.

- the mastic was continuously stirred as it cooled to prevent settling and was then transferred to several vials to make samples for further testing.
- the mixing process was carefully followed so that the mineral filler was homogeneously dispersed in the bitumen.

5.4 Test Programme

Amplitude Sweep tests (AS), Frequency Sweep Test (FS), Repeated Creep Test (RCR) and Multiple Stress Creep Recovery (MSCR) tests have been performed as shown previously on validation methods (Chapter 4). The tests procedures are described on the following paragraphs.

Test Equipment and sample preparation

Dynamic Shear Rheometers (DSR) **Anton Paar - MCR 302,** using peltier system temperature control with peltier hood (APPENDIX A), have been used to obtain the mastic rheological properties). Prior to mounting a bituminous sample between a parallel plate geometry, two plates should be sufficiently warm (approximately 70°C) that a good adhesion between a sample and plates can be achieved. The procedure of bituminous sample preparation is listed as follows:

- preheat the bituminous mastic in a 160°C oven to make the sample liquid and ready to pour.
- remove the bituminous sample from an oven and then stir it manually for 20 seconds to ensure the mineral filler were not settled.
- pour directly the sufficient quantity of the bituminous sample onto the lower plate until it nearly covered the plate.
- close the plates to the target gap of 2.025mm or 1.025mm for the bulge.
- trim the extra specimen by moving a heating trimming tool around the upper and lower plates.

5.4.2 Amplitude Sweep Test

Amplitude Sweep (AS) tests were preliminary carried out, to investigate the viscoelastic region at 10°C, applying a constant frequency of 10 rad/s (1.59 Hz). The investigated strains level come from 0.01% to 100% of mastic deformation. It was chosen the strain amplitude at which the complex modulus not differ by more 10% of its initial value. Linear visco-elastic deformations, γ_{LVE}, found for the three mastic were: 1.5% for Mff, 2.5% for MUt and 1.0% for MUd.

5.4.3 Frequency Sweep Test

Rheological measurements were performed using a stress/strain controlled Dynamic Shear Rheometer equipped with a parallel plate and plate geometry. The frequency sweep (FS) test was performed in strain control configuration, where the strain amplitude was limited within the linear viscoelastic (LVE) range. FS test was conducted in a range of frequencies between 0.01 and 10 Hz, at the temperatures of 0, 10, 20, 30, 40, 50 and 60°C. The 8 mm plate with a 2 mm gap was adopted in all the range of temperatures (Dondi *et al.* 2014). With the FS test the complex shear modulus (G*) and the phase angle (δ) were measured.

5.4.4 Repeated Creep Recovery Test

Repeated Creep Recovery tests (RCR) were conducted with 25 mm parallel plates (PP) and a 1 mm gap under three different temperature conditions 46°C, 58°C and 64°C. The testing temperatures were selected in agreement with AASHTO M-320. Mff, MUt and MUd were tested with 100 cycles at a stress level of 1 kPa. Each loading cycle consisted of 1 s creep and 9 s recovery (NCHRP Report 459). The accumulated strain was calculated for each test at the end of 100 cycles.

5.4.5 Multiple Stress Creep Recovery Test

The Multiple Stress Creep and Recovery test (MSCR) was run according to the AASHTO TP 70-07 ‘‘*Standard Method of Test for Multiple Stress Creep and Recovery (MSCR) of Asphalt Binders using a Dynamic Shear Rheometer*’’. According to this standard, mastic sample is loaded at a constant creep stress for 1 s, followed by a zero stress recovery of 9 s. Ten cycles of creep and recovery are run at 0.1 kPa creep stress, followed by ten at 3.2 kPa creep stress. The non-recoverable compliance (J_{nr}) and the percent recovery after ten cycles at 0.1 kPa and 3.2 kPa were studied. The J_{nr} value was calculated as the ratio between the average non recoverable strain for 10 creep and recovery cycles, and the applied stress for those cycles. The testing temperatures of 46°C, 58°C and 64°C were adopted.

5.5 Test Results and Discussion

5.5.1 Master Curves

The complex modulus G* and phase angle δ of mastics MUt, Mff and MUd are represented in terms of master curves in Figure 5.6. Using the principle of time-temperature superposition (TTS) the master curves of G* and δ were plotted at the reference temperature of 20°C. The Williams-Landel-Ferry model was used to obtain the temperatures shift factors.

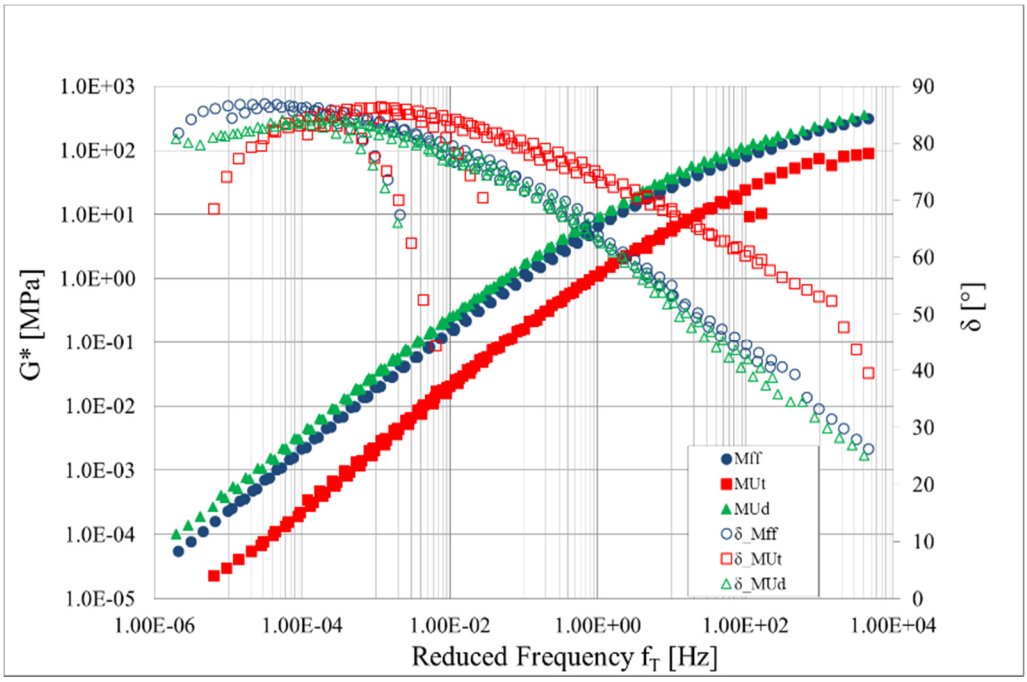

Figure 5.6 Master Curves for Mff, MUt, and MUd mastics at 20°C

Results show that in all range of frequencies the mastic containing the spent bentonite Ut attains G* values lower than the Mff and MUd mastics ones. Given the nature of the two recycled fillers it can be stated that this difference is mainly due to the different content in residual oil. This is evident at low temperatures or high frequencies where the behavior of the Ut mastic should be dominated by the properties of the base bitumen, but which, in this case, does not tend to the glassy modulus as the Mff and MUd mastics do. Consistent differences between Mff and MUd mastic can be seen at low frequencies, where the MUd mastic shows higher moduli. It can be inferred that if the presence of filler Ud increases the mastic stiffness at low frequencies it will potentially increase also the resistance to permanent deformations. This can be traced

back to the high level of Rigden voids that can demonstrate the stiffening power of the Ud filler (Faheem *et al.* 2012). The mastic containing Ut filler exhibits higher phase angles at medium and high temperatures than Mff and MUd phase angles. At the high temperatures the MUt phase angle decreases, but this effect is significantly far from the one of polymers in polymer modified bitumens. The Mff and MUd δ values are approximately equivalent at medium and high frequencies, and in particular at high frequencies/low temperatures the mastics response is almost elastic (30°). At high temperatures, on the contrary, the MUd phase angle shows a significant reduction compared to Mff phase angle. The presence of digested bentonite Ud shifts the rutting parameter G*/senδ to higher values. This could be seen in Table 5.4, in which G*/senδ values are reported for the three mastics at 60°C.

Table 5.4 Rutting parameters of Mff, MUt and MUd

Mastic	Temperature [°C]	G*/senδ [kPa]
Mff	60	7.0
MUt	60	2.5
MUd	60	9.5

5.5.2 Creep Test Results

5.5.2.1 Repeated Creep Recovery Test

In order to investigate the materials response to permanent deformations RCR test in plate-plate (PP) configuration were performed at the temperatures of 46°C, 58°C and 64°C. Figure 5.7 shows, as an example, the test results at the temperature of 46°C. In this case, the mastic containing the digested bentonite Ud has accumulated less deformations compared to Mff and MUt that has reached shear strain values close to 100.

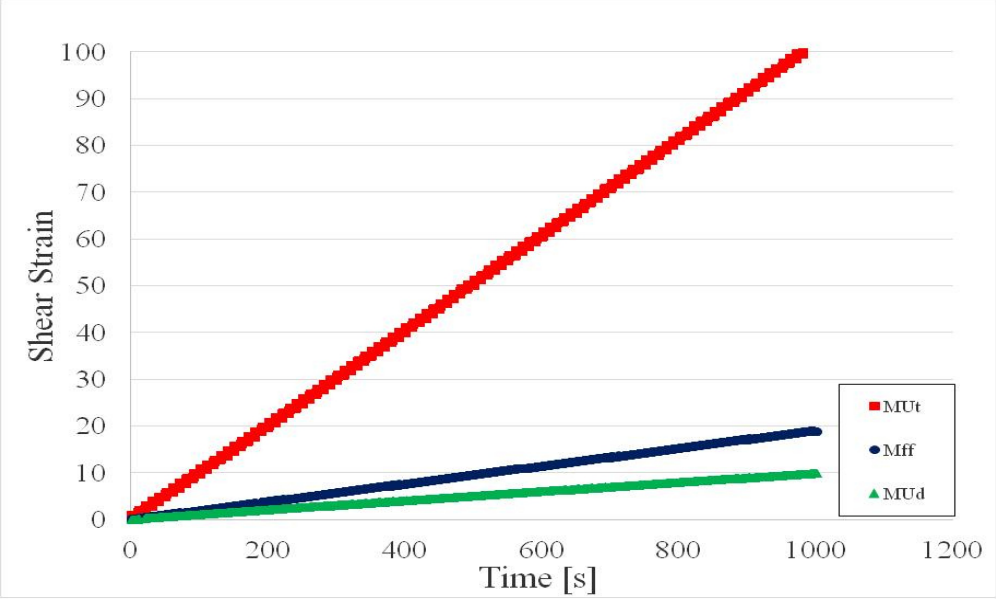

Figure 5.7 Results of the accumulated strain under repeated creep testing @ 46°C.

Figure 5.8 shows the test results of the first cycle at 1 kPa at the three test temperatures. The MUt shows considerable higher creep strain at all test conditions. In particular, at 58°C the mastic containing the spent bentonite reaches a peak of deformation even higher than the Mff and MUd peaks strain at 64°C. The MUd mastic shows less sensitivity to deformation in all test conditions.

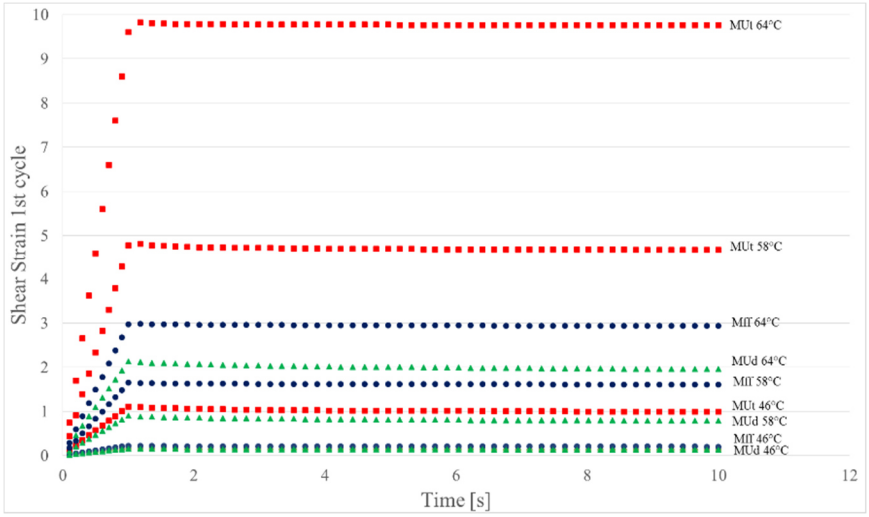

Figure 5.8 Strain/time for the first cycle of RCR test at 1 kPa at 46°C, 58°C and 64°C

As shown in Figure 5.9 this mastics relative behavior is enhanced at the end of the 100th cycle. In fact, MUt has accumulated 461 and 961 strain at 58°C and 64°C respectively, while Mff and MUd that have reached 75 and 158 strain at 58°C and 197

and 295 strain at 64°C. The accumulated strain difference between the Mff and MUd mastics is close to 10 at 46°C and undergoes a significant increase to 96 at the temperature of 58°C, remaining constant up to 64°C.

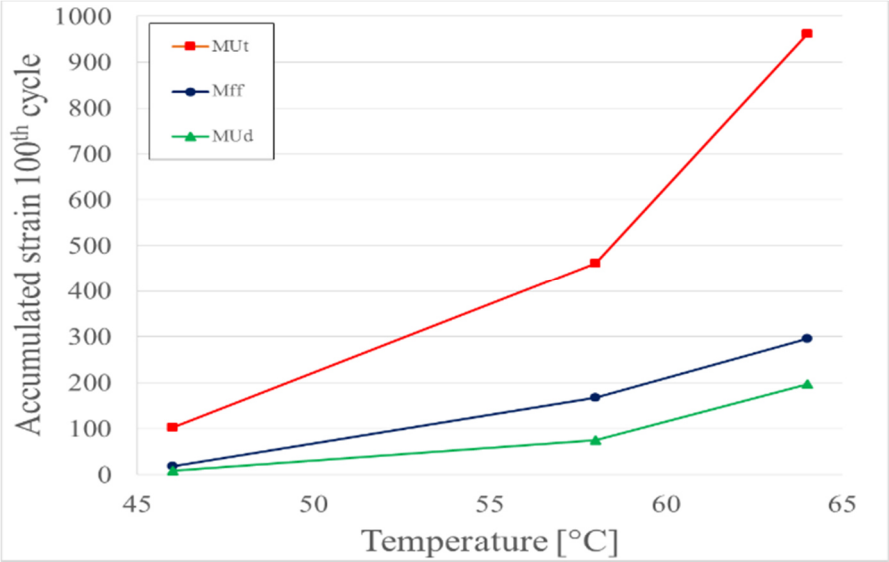

Figure 5.9 Accumulated strain values at the end of 100th cycle at @46°C, 58°C and 64°C.

From this analysis, it is possible to confirm the repeated load axial test results on binder course mixtures presented by Sangiorgi *et al.* (2014) where the presence of Ud filler used in substitution of the traditional limestone filler decreases the accumulated strain compared to the adopted control mixture. The percentage of recovery from RCR tests was also obtained and calculated as the ratio between recovered strain and peak strain at the 1st cycle and at the 100th cycle. In Figure 5.10, the MUd mastic has higher recovery than Mff and MUt at the three test temperatures. Mff and MUt have the same recovery for each test configuration. For MUd there is a constant decrease of 25% of recovery with increasing temperature than Mff and MUt mastics for which there is a decrease of 80% of recovery from 46 °C to 58 °C. At the last load cycle for MUt and Mff mastics the percentage of recovery is 0 at all temperatures. The MUd is the only mastic that shows a small percentage of recovery of 0.3% at 46°C and 0.13% at 58°C.

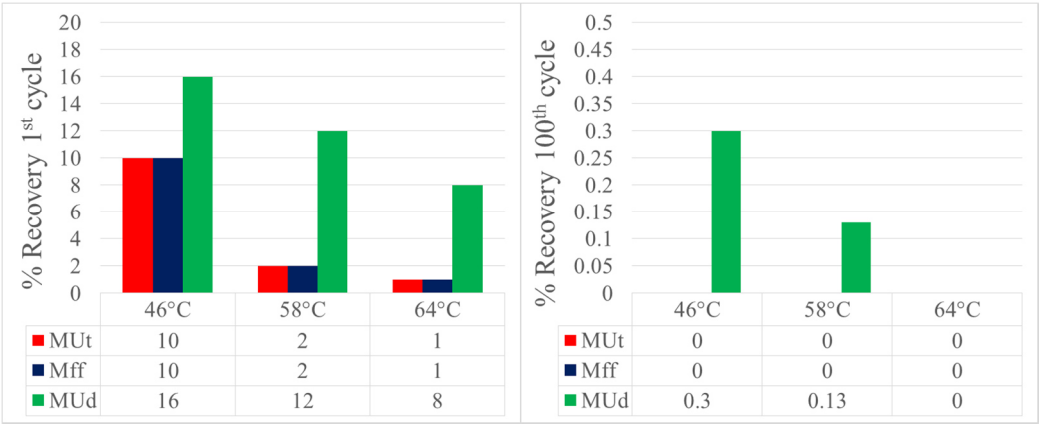

Figure 5.10 Comparison of RCR % recovery at the 1st and 100th cycle @46°C, 58°C and 64°C.

5.5.2.2 Multiple Stress Creep Recovery Test

The multiple stress creep-recovery (MSCR) test was developed based on creep studies conduct during the NCHRP 9-10 research program (Bahia & Hanson 2001). According to the literature (D'Angelo *et al.* 2007; D'Angelo, 2009b; Wasage *et al.* 2010), this test can predict the deformation behavior of binders. By applying different stress levels, it can identify binders that are overly stress sensitive in the nonlinear region (Soenen *et al.* 2013). For this reason it was chosen to investigate further the potential rutting of the three mastics Mff, MUt and MUd through MSCR test run at 0.1 and 3.2 kPa. Figure 5.11 shows the test results at the temperature of 46°C. Also in this test configuration the mastic containing the digested bentonite Ud always exhibits the stiffer behavior, accumulating less deformation at the end of the 10 cycles at 3.2 kPa.

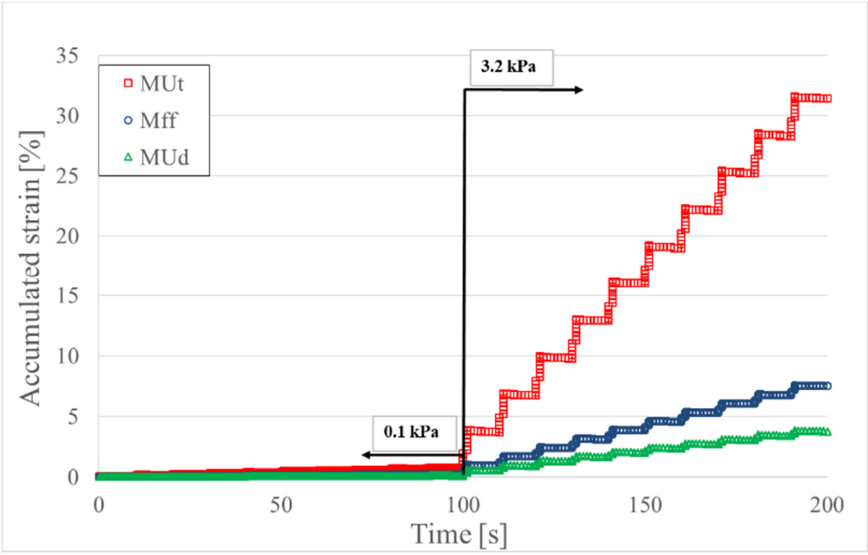

Figure 5.11 MSCR test results at @46°C.

As shown in Figure 5.12 the mastic MUt has accumulated the largest deformation under the two stress conditions, while the MUd mastic shows the lower values of deformation, even when the temperature increases. For the MUt mastic most part of the strains was developed at the higher stress level.

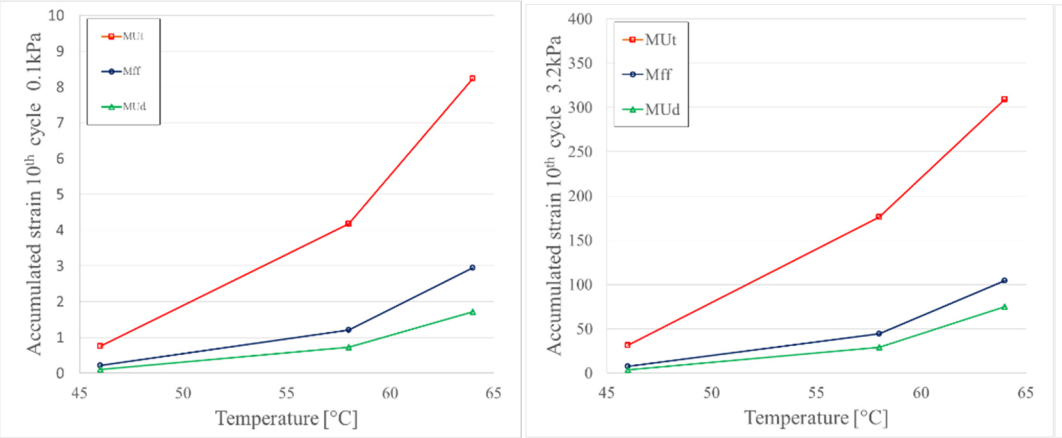

Figure 5.12 Accumulated strain values at the end of 10th cycle at 0.1kPa and 3.2kPa.

Table 5.5 shows the average percentage of recovery of the three mastics under 3.2 kPa shear load at the three test temperatures of 46°C, 58°C and 64°C. At the temperature of 46°C the MUd mastic attains an average recovery % value higher than Mff and MUt; in particular, the average recovery % of mastic containing digested bentonite reaches 3%. At 58°C Mff and MUt do not recover and MUd recovers only the 0.25% of deformation. At the highest test temperature of 64°C all the mastics have no recovery.

Table 5.5 Mff, MUt and MUd average percentage of recovery at 3.2 kPa

Mastic	**Temperature [°C]**		
	46	**58**	**64**
	Average % recovery	**Average % recovery**	**Average % recovery**
Mff	1.00	0	0
MUt	0.42	0	0
MUd	3.07	0.25	0

The creep compliance J_{nr} parameter is a measure of the non-recoverable behavior of a binder caused by creep-recovery cycles, and it is therefore suggested to describe the binder contribution to asphalt mixture permanent deformations (D'Angelo *et al.* 2006). The J_{nr} values were calculated for the three mastics under 0.1kPa (Figure 5.13 a) and

3.2 kPa (Figure 5.13 b) shear stresses at the three test temperatures of 46°C, 58°C and 64°C. The MUd mastic has lower values of non recoverable compliance at both shear stresses, showing a less sensitivity of the mastic to permanent deformations. In particular, at 3.2 kPa the mastic containing the Ud filler shows a J_{nr} value of 13.0 1/kPa at 64°C while the J_{nr} value of mastic containing only limestone filler that is of 18.3 1/kPa at the same shear stress and temperature. The MUt mastic has the higher values of J_{nr} under all test conditions, it is once again proven that the 25% of oil in the Ut filler acts on the base bitumen and makes the mastic softer and more susceptible to permanent deformations.

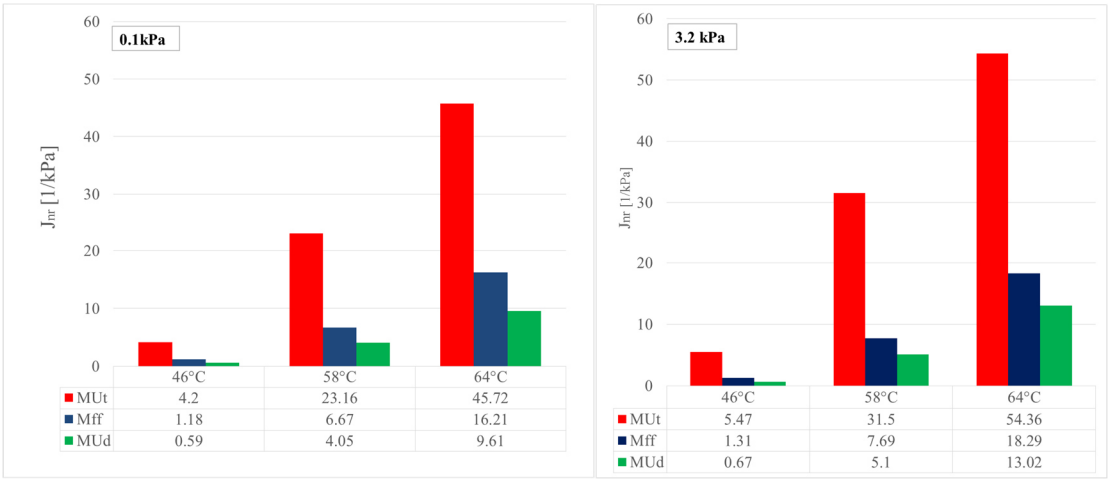

Figure 5.13 Mff, MUt andMUd non recoverable compliance at 0.1 kPa and 3.2 kPa.

5.6 Summary

In this chapter the rheological analysis of mastics containing waste bleaching clay was conducted, based on the methods validate on Chapter 4. On the basis of the experimental data the following conclusions can be drawn:

- the comparison of the mastics master curves from FS and AS tests show that the substitution of part of the filler in the mixture with the proposed bleaching clays fillers is significantly effective on altering their rheological behavior. Substitutions were made so as to replicate the actual binding mastics of the HMAs tested in previous research. In particular, the study at the mastic scale confirmed that the Ud filler stiffens the base bitumen, while the Ut filler softens the mastic by a considerable amount.
- the RCR and MSCR tests results corroborate the repeated load axial test results from previous research on HMAs. The Ut filler reduces the resistance to permanent deformations, while the Ud filler increases it at the different testing temperatures. Also the J_{nr} analysis confirms that the non recovered deformations are reduced in the MUd mastic. Again the rheological effect of the Ut filler is more evident in comparison with the traditional mastics containing only limestone filler. The residual oil in the Ut filler is evidently interacting with the bituminous phase more than the mineral particles, thus reversing the effects of the Ud filler;

6 RHEOLOGICAL CHARACTERIZATION OF BITUMEN, MASTICS AND MORTARS CONTAINING FINE CRUMB RUBBER

6.1 Introduction

The fields of use of crumb rubber in the road construction are various and the studies that validate the use are numerous as well as the quality of the results achieved by research in reuse of this recycled material. Traditionally, studies in Italy have followed the US research and have been catered embedding the crumb rubber within the hot mix asphalt with Wet and Dry techniques. Recently, many studies have been developed also as part of the warm and cold asphalt (low energy or WMA). In the latter, bituminous mixtures for base layers have been successfully studied, containing high percentages of Reclaimed Asphalt Pavement, cement and crumb rubber from dismissed tires. In this context, in which the rubber acquires the characteristics of the raw material inside the mixtures, more environmentally friendly, cheap and durable, the research proposal aims to optimize the crumb rubber content in the asphalt mixtures through advanced laboratory studies. The innovative proposal involves the use of rubber powder with dry technique within the bituminous mix, to reduce costs and externalities produced by bituminous binders traditionally produced with recycled rubber solutions. The aim is to improve both mechanical and mix workability characteristics. The obtained product is a modified bituminous binder (Binder Polymer Modified) in which the rubber powder is added mechanically to the mixer, without significant alterations of the production process of a modified asphalt mixtures. The embedding to the mixer constitutes a continuity with the dry technique, which preserves the advantages (absence of odors) and those related to the enhancement of the rheological properties of PmB modified binder content in the mixture. The rubber operates as active filler capable of increasing the workability of the modified binder inside of bituminous mixtures whose volumetric proportioning of the components plays a key role in terms of asphalt mixture elastic recovery increasing, acoustic emissions containing (wheel-tire contact) and sound absorption. The compatibility between powder and bituminous binder can be an advantage in the production of rich bitumen asphalt (SMA type) for which the rubber can act as a stabilizer to equal the

traditional fiber. In order to study the fine rubber effects on the asphalt mixtures, Frequency Sweep Test and creep tests were implemented on the obtained mastics, following the methods described and validated on Chapter 4. This analysis was improved by the micromechanical model with Discrete Element Approach (validated for mastic on Chpater 4). Furthermore, based on multiscale approach, fine crumb rubber and filler interaction with the fine coarse aggregates was studied through Frequency Sweep Test on bituminous mortar.

The rheological tests on bituminous mastics and mortar, described on this chapter, has been realized in collaboration with the laboratories of Nottingham Transport Engineering Centre of the University of Nottingham (UK).

6.2 Materials

6.2.1 Bitumen

Three different bitumens have been selected in this research to make the mastic combination:

- Traditional *Unmodified Bitumen* to compare the result with the other two modified binders.
- *Zero_Bitumen* and *A_Bitumen* which are polymer and wax modified binders (PWmB).

The differences between *Zero_Bitumen* and *A_Bitumen* come from the differences of the two base binders used before the modification. For the base bitumen of the first PWmB the internal composition has shown an asphaltenic fraction higher than the second one, and an aromatic fraction less than the base bitumen of *A* binder. The characteristics of bitumens are shown in Tables 6.1-6.2-6.3.

Table 6.1 Properties of the Unmodified Bitumen

Unmodified Bitumen	Unit	Characteristic value	Standard
Penetration @ 25°C	dmm	40	EN 1426
Soft.Point	°C	50	EN 1427
Dynamic Visc. @160 °C	Pa·s	0.16	EN 12596
Dynamic Visc. @150 °C	Pa·s	0.24	EN 12596
Dynamic Visc. @135 °C	Pa·s	0.48	EN 12596

Table 6.2 Properties of Zero - Bitumen

Zero_Bitumen	Unit	Characteristic value	Standard
Penetration @ 25°C	dmm	50	EN 1426
Soft.Point	°C	87.3	EN 1427
Dynamic Visc. @160 °C	Pa·s	0.58	EN 12596
Dynamic Visc. @150 °C	Pa·s	0.81	EN 12596
Dynamic Visc. @135 °C	Pa·s	1.37	EN 12596

Table 6.3 Properties of A - Bitumen

A_Bitumen	Unit	Characteristic value	Standard
Penetration @ 25°C	dmm	48	EN 1426
Soft.Point	°C	78.4	EN 1427
Dynamic Visc. @160 °C	Pa·s	0.29	EN 12596
Dynamic Visc. @150 °C	Pa·s	0.39	EN 12596
Dynamic Visc. @135 °C	Pa·s	0.63	EN 12596

Figure 6.1 Setematic penetrometer – figure 1 (EN1426); RB365G Ring and Ball (EN1427); Brookfield Rotational Viscosimeter (EN 12596).

Oscillating, sinusoidal shear stresses and strains have been applied on samples of bitumen using the DSR devices to find the complex modulus and the phase angle of the bitumen with respect to the different frequencies. Master curves for each bitumen have been found by applying the appropriate shift-factor for all the bitumen. Amplitude sweep test was performed on all the bitumens to find the Linear Viscoelastic Elastic (LVE) range for the material. The test was controlled on shear strain and with the frequency of 1.59 Hz. The LVE range for the three bitumen is shown in the following table.

Table 6.4 Bitumen Linear Visco-Elastic range

Bitumen	γ LVE [%]
Unmodified Bitumen	1.5
Zero_Bitumen	2.0
A_Bitumen	2.0

For the Frequency Sweep the LVE ranges of the tables above were used testing the bitumen from 0.01Hz to 10Hz with temperature varying from 10°C to 60°C. 6 points

of observation were carried out between each decade with the total number of 19 for each temperature (Figure 6.2).

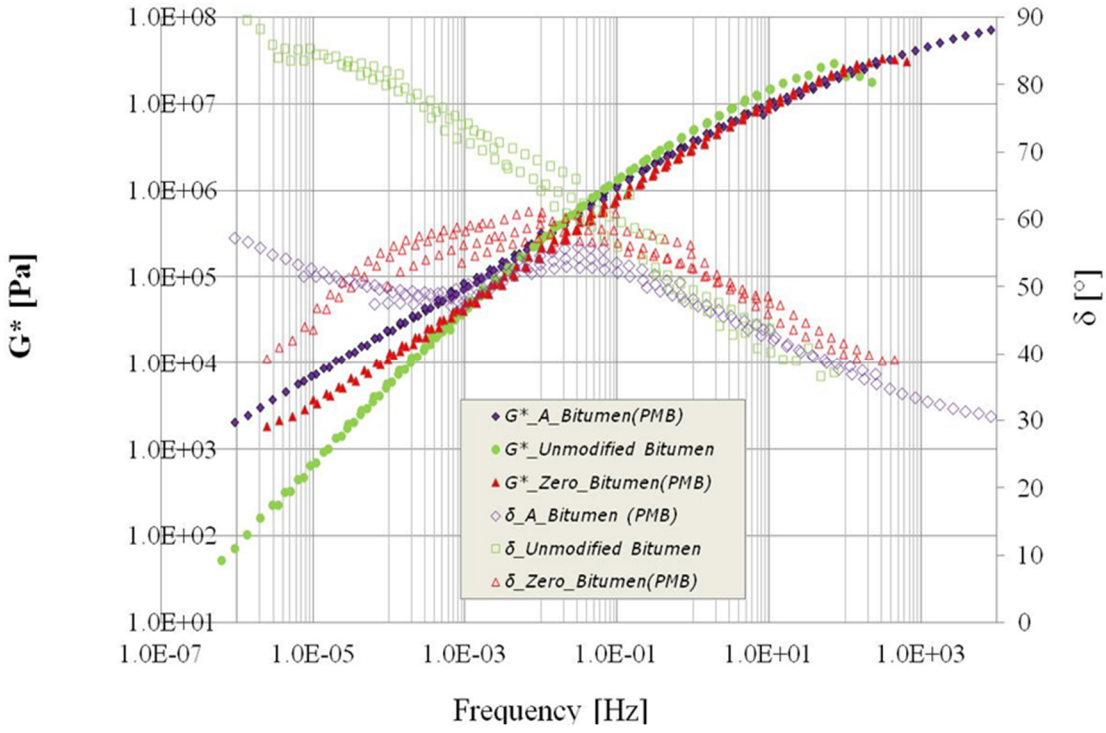

Figure 6.2 Base Bitumens Master Curves

The test result shows that A_bitumen and Zero_bitumen have complex modulus (G*) values higher than the unmodified bitumen G* values. The polymer increases the shear responses at high temperature and therefore reduces the bitumen thermos-sensitivity. The phase angle for the two modified bitumens is considerably lower than the unmodified bitumen, however the A_bitumen shows less elastic behaviour with high phase angle at high temperatures. These results combined to the traditional tests confirm that the A_bitumen is more aromatic than the ZERO_Bitumen. The linear SBS polymer reacts with the oils inside the A_bitumen and the stirenic part increase, in this way the elastic response given by the butadienic part is reduced and the stiffness at high temperature increases. All the bitumens are showing the same behaviour for the complex modulus at low temperature.

6.2.2 Limestone Filler

The filler used in this study is a product obtained from the fine grinding of limestone composed primarily of calcium carbonate ($CaCO_3$). The limestone filler is referring to

the particles passing 0.063 mm sieve. In this research natural limestone filler was choosen due to its good interaction with bitumen. The limestone filler was geometrically characterized through a gradation analysis (EN 933-10) and volumetrically, determining their volumetric mass (EN 1097-7). Rigden Voids (EN 1097-4) and Delta Ring & Ball (EN 13179-1) were also performed according to EN 13179-1. Table 6.5 shows the limestone filler characteristics.

Table 6.5 Limestone filler main characteristics

Test Name	Standard	Limestone filler
Gradation analysis (mm)	EN933-10	0.063
Particle density (Mg/m^3)	EN 1097- 7	2.73
Rigden voids (%)	EN 1097- 4	33.82
Δ Ring & Ball [°C]	EN 13179-1	8

6.2.3 Fine Crumb Rubber

The recycled powder rubber used in this study comes from scrap tires and it was produced in ambient mechanical grinding process at room temperature. Ambient grinding is a multi-step technology and uses whole or pre-treated car or truck tires in the form of shred or chips, or sidewalls or treads.

6.2.3.1 Fine Crumb Rubber production

The crumb rubber powder is one of the main products derived from ETLs; approximately the 25% of ETLs recovered in Italy start to a treatment and recovery process that allows reducing the ELTs into fragments less than a millimeter size. It to set up as the result of processing rubber to achieve finely dispersed particles with sizes less than 1 mm (Figure 6.3a).

Figure 6.3 a) Fine Crumb Rubber b) Granulate Rubber

Rubber granule differ from crumb rubber (Figure 6.3b) because particles dimensions, in the range 1-10 mm. Both crumb and granulate rubber can be used as bitumen additive and modifier; the granulate costs are inevitably less than fine crumb rubber. and if it can use more but the final product, or the modified bitumen, will have inferior characteristics compared to that obtained with powder, which has superior characteristics. More precisely, the shredded material is referred to as:

- CRB (Crumb Rubber Modifier): size between 0.24 and 5 mm;
- PRM (Powdered Rubber Modifier): smaller size of 0.24 mm;
- poor ultrafine: size less than 0.074 mm.

All the materials mentioned above are characterized by the grinding of the tires, in particular by crushing only the upper part of the carcass fibers and excluded. These materials are also recognized as Secondary Raw Materials by Italian law; In fact, since 1998, the national legislation provides for the exclusion from the legislation on waste for the powder used for the production of modified bitumen. In order to reduce the generic waste rubber in a particle size suitable to allow the re-use in the rubber composition used for the production of artifacts, it may be used three different production processes: the traditional, cryogenic and electrothermic.

6.2.3.2 The traditional granulation: Traditional Crumb Rubber

The traditional granulation commonly called mechanical grinding. Mechanical grinding is a process that takes place in stages, performed by means of rotating knives and blades. It can be treated in different tires of trucks, cars and waste of rubber materials. The process is normally aimed at the production of granules and powder with a different treatment, depending on whether mentioned products are obtained from tires of a car or truck. For the latter is necessary a preliminary operation of removal of the bead, with which are separated, without breaking, the two rings on the tire to limit significantly the wear of the fragmentation machines. In this technology, all the phases of grinding and granulation are carried out in room temperature. The manufacturing process begins with the removal of the tire bead in order to separate the two rings without breaking the tire itself. This phase is done only for truck tires as they are equipped with two metal rings of variable section from 12 to 20 mm with the

purpose of supporting the bead. At this point is performed a real phase of coarse crushing of the tire. With this second phase, all the tires of passenger cars and light vehicles, as well as truck tires (individuals of the metal rings), are introduced in the different shredders who then reduce them into pieces ranging from 70 x70 mm to 100 x100 mm (Charamia *et al*. 1991). During this phase the speed of shredding can not be high to avoid the heating of the mills and so that the different rubber parts may adhere to the blades. The obtained fragments, through a system of conveyor belts operating in weight, they are conducted in other grinding chambers in which are cut in order to obtain increasingly smaller remains; this phase takes the name of granulation, as the building debris coming from the shredding increasingly smaller is reduced in the "grains". During the various phases of grinding, with the progress of the reduction of the size of the product, provision is made to separate and to remove in one or more subsequent moments the metal and the textile fiber. The absence of chemical or thermal treatment, maintains unchanged the molecular structure of the polymeric material. The cutting operations with metal blades are predominant and are carried out in successive phases, reducing the size rubber in stage to stage. The roughness of the surface obtained is predominantly related to the state of wear of the blades during the manufacturing process. new and sharp blades allow to reduce the roughness of the granulate, when compared to that obtained with worn blades. In the case of a prolonged use of the blades of the granulating unit life it is greatly reduced. It has, now, the step of micronization, thanks to which, through the use of magnetic tapes of a different nature, the rubber coming from the granulation step, is cleaned by the various impurities present, and thereafter, divided by grain size through the use of sifting machines, where the materials are divided according to particle size to be obtained. The final product is packaged or stored in silos. And possible to further reduce the particle size by adding to the system a few sprayers mills. Subsequently the material is stocked in different big-bag.

6.2.3.3 Main characteristics of Crumb Rubber

The rubber powder used in this research is fine crumb rubber with 0.4 mm size, and it was characterized geometrically (Fig. 6.4) through a gradation analysis (EN 933-10) and volumetrically, determining their volumetric mass (EN 1097-7).

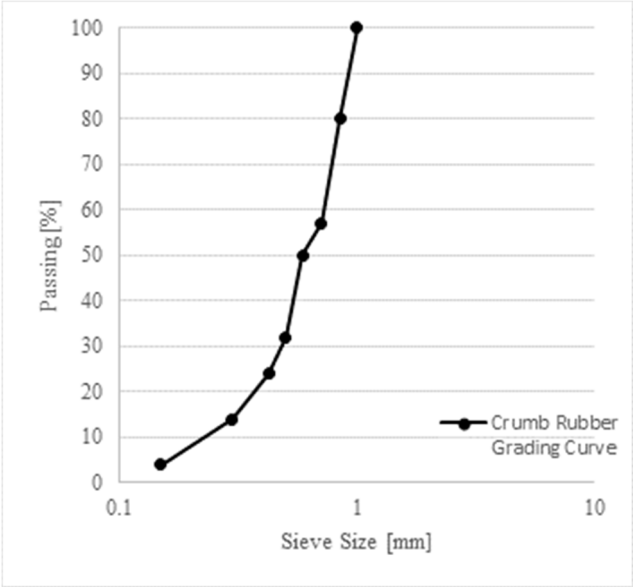

Figure 6.4 Crumb Rubber grading curve.

Table 6.6 shows the crumb rubber main characteristics.

Table 6.6 Crumb rubber main characteristics

Test Name	Standard	Crumb Rubber
Gradation analysis (mm)	EN933-10	0.4
Particle density (Mg/m^3)	EN 1097- 7	1.01

6.3 Bitumen – Limestone Filler – Fine Crumb Rubber Mastic System

6.3.1 Mastics Design

Three binders (two modified with polymer and wax, one unmodified 40/60 pen.), limestone filler and fine crumb rubber, were mixed to obtain five mastics combinations for each bitumen type. Filler and rubber concentration was calculated by mass in order to easily compare with the proportions in asphalt mixture design in which the filler proportion is shown by mass content. The reference asphalt mixture is a Stone Mastic Asphalt (SMA) surface layer, therefore starting from a traditional SMA mixture, the mastics were produced according to the proportions of three different SMA surface layers. The mastics were designed by mixing the components with proportions linked to the weight of the aggregate mixture as reported in Tables 6.5-6.6-6.7.

Table 6.5 Mastics percentages on weight of aggregates for the UNMODIFIED BITUMEN

UNMODIFIED BITUMEN			
Mastic Name Code	**Bitumen/Aggregates [%]**	**Rubber/Aggregates [%]**	**Filler/Aggregates [%]**
UN_7_1_5	7.0	1.00	5
UN_8.5_1.2_5	8.5	1.20	5
UN_8_1_6	8.0	1.00	6
UN_7.5_0.75_5	7.5	0.75	3
UN_SMA	6.6	0.00	9

Table 6.6 Mastics percentages on weight of aggregates for the ZERO BITUMEN

ZERO BITUMEN			
Mastic Name Code	**Bitumen/Aggregates [%]**	**Rubber/Aggregates [%]**	**Filler/Aggregates [%]**
Z_7_1_5	7.0	1.00	5
Z_8.5_1.2_5	8.5	1.20	5
Z_8_1_6	8.0	1.00	6
Z_7.5_0.75_5	7.5	0.75	3
Z_SMA	6.6	0.00	9

Table 6.6 Mastics percentages on weight of aggregates for the A BITUMEN

A BITUMEN			
Mastic Name Code	**Bitumen/Aggregates [%]**	**Rubber/Aggregates [%]**	**Filler/Aggregates [%]**
A_7_1_5	7.0	1.00	5
A_8.5_1.2_5	8.5	1.20	5
A_8_1_6	8.0	1.00	6
A_7.5_0.75_5	7.5	0.75	3
A_SMA	6.6	0.00	9

The determination of filler and rubber concentration in a bitumen-filler mastic is given by:

$$Filler\ concentration\ by\ mass = \frac{M_f}{M_b+M_f+M_r} \cdot 100 \quad (6.1)$$

$$Rubber\ concentration\ by\ mass = \frac{M_R}{M_b+M_f+M_r} \cdot 100 \quad (6.2)$$

The determination of ratio of filler to bitumen based on mass is given by:

$$Ratio\ of\ filler\ on\ bituminous\ mass\ = \frac{M_F}{M_B} \quad (6.3)$$

$$Ratio\ of\ rubber\ on\ bituminous\ mass\ = \frac{M_R}{M_B} \quad (6.4)$$

The comparison of filler to bitumen (by mass) and rubber to bitumen (by mass) ratios for each mastic is shown in Tables 6.7-6.8-6.9. The requirement within Superpave system is a filler-to-bitumen ratios ranging between 0.6 and 1.2 based on mass. In this investigation, the sum of filler-to-bitumen and rubber to bitumen ratios is between 0.73 and 0.87, the filler and rubber particles are suspended in bitumen, excluding the mastic containing only filler for which the ratio of 1.36 exceeds the Superpave upper limit. For the SMA mastics the physical contact between filler particles is present in bitumen. The rubber presence has allowed to reduce the amount of filler inside the mastic. For this reason in this study the physical properties such as particle size distribution, Rigden voids, particle shape and specific surface must be associated with physical and chemical action induced by the rubber.

Table 6.7 Mastics composition for the UNMODIFIED BITUMEN

UNMODIFIED BITUMEN				
Mastic Name Code	**Filler Concentration by mass [%]**	**Rubber Concentration by mass [%]**	**M_F/M_B**	**M_R/M_B**
UN_7_1_5	38.46	7.69	0.71	0.14
UN_8.5_1.2_5	34.01	8.16	0.59	0.14
UN_8_1_6	40.00	6.67	0.75	0.12
UN_7.5_0.75_5	37.74	5.66	0.67	0.10
UN_SMA	57.69	0.00	1.36	0.00

Table 6.8 Mastics composition for the ZERO BITUMEN

ZERO BITUMEN				
Mastic Name Code	**Filler Concentration by mass [%]**	**Rubber Concentration by mass [%]**	**M_F/M_B**	**M_R/M_B**
Z_7_1_5	38.46	7.69	0.71	0.14
Z_8.5_1.2_5	34.01	8.16	0.59	0.14
Z_8_1_6	40.00	6.67	0.75	0.12
Z_7.5_0.75_5	37.74	5.66	0.67	0.10
Z_SMA	57.69	0.00	1.36	0.00

Table 6.9 Mastics composition for the A BITUMEN

A BITUMEN				
Mastic Name Code	**Filler Concentration by mass [%]**	**Rubber Concentration by mass [%]**	**M_F/M_B**	**M_R/M_B**
A_7_1_5	38.46	7.69	0.71	0.14
A_8.5_1.2_5	34.01	8.16	0.59	0.14
A_8_1_6	40.00	6.67	0.75	0.12
A_7.5_0.75_5	37.74	5.66	0.67	0.10
A_SMA	57.69	0.00	1.36	0.00

The volumetric analysis has been conducted on the three studied mastic. The calculation of the compositional volume of bitumen, filler and rubber particle (V_b,V_f, V_r) has been obtained through the following equations:

$$V_f = \frac{\frac{M_f}{S_f}}{\frac{M_b}{S_b}+\frac{M_f}{S_f}+\frac{M_r}{S_r}} \cdot 100 \tag{6.6}$$

$$V_r = \frac{\frac{M_r}{S_r}}{\frac{M_b}{S_b}+\frac{M_f}{S_f}+\frac{M_r}{S_r}} \cdot 100 \tag{6.7}$$

$$V_b = \frac{\frac{M_b}{S_b}}{\frac{M_b}{S_b}+\frac{M_f}{S_f}+\frac{M_r}{S_r}} \cdot 100 \quad (6.8)$$

where M_f = mass of filler in the mastic; S_f = specific gravity of filler; M_r = mass of rubber in the mastic; S_r = specific gravity of rubber; M_b = mass of bitumen in the mastic; and S_b = specific gravity of bitumen. The results of the equations applied to the studied mastics are reported in Tables 6.10-6.11-6.12.

Table 6.10 Mastics volumetric composition for the UNMODIFIED BITUMEN

UNMODIFIED BITUMEN			
Mastic Name Code	**V_f [%]**	**V_r [%]**	**V_b [%]**
UN_7_1_5	19	10	71
UN_8.5_1.2_5	16	11	73
UN_8_1_6	20	9	70
UN_7.5_0.75_5	19	7	74
UN_SMA	33	0	67

Table 6.11 Mastics volumetric composition for the ZERO BITUMEN

ZERO BITUMEN			
Mastic Name Code	**V_f [%]**	**V_r [%]**	**V_b [%]**
Z_7_1_5	19	10	71
Z_8.5_1.2_5	16	11	73
Z_8_1_6	20	9	70
Z_7.5_0.75_5	19	7	74
Z_SMA	33	0	67

Table 6.12 Mastics volumetric composition for the UNMODIFIED BITUMEN

A BITUMEN			
Mastic Name Code	**V_f [%]**	**V_r [%]**	**V_b [%]**
A_7_1_5	19	10	71
A_8.5_1.2_5	16	11	73
A_8_1_6	20	9	70
A_7.5_0.75_5	19	7	74
A_SMA	33	0	67

In Table 6.13-6.14-6.15 the mastic compositions and the ratios between each components inside the mastics are reported. It can be noted that the studied mastics represent a wide panorama of design choice for asphalt mixtures. The mastics called SMA, containing only filler, represent the comparison parameter to understand better the fine crumb rubber action. The 8.5_1.2_5 mastic was studied to understand the action of the bitumen associated with the presence of rubber; in this mastic in fact the sum of volumetric part of filler and rubber is less than the others mastics and the presence of rubber is the highest. The 8_1_6 and 7_1_5 mastics have been designed to extrapolate the action of the filler within the mixture. Finally, the 7.5_0.75_5 mastics combines bitumen and fine crumb rubber percentages reduction. The rheological study is therefore connected with a parametric study of the individual components within the mastic.

Table 6.13 Mastics composition for the UNMODIFIED BITUMEN

UNMODIFIED BITUMEN									
Mastic Name Code	**%B**	**%R**	**%F**	**%B/ %R**	**%B/ %F**	**%R/ %F**	**%R/ %B**	**%F/ %R**	**%F/ %B**
UN_7_1_5	53.85	7.70	38.45	6.99	1.40	0.20	0.14	4.99	0.71
UN_8.5_1.2_5	57.80	8.09	34.10	7.14	1.69	0.24	0.14	4.21	0.59
UN_8_1_6	53.33	6.67	40.00	8.00	1.33	0.17	0.13	6.00	0.75
UN_7.5_0.75_5	56.50	5.65	37.85	10.00	1.49	0.15	0.10	6.70	0.67
UN_SMA	42.37	0.00	57.63	0.00	0.74	0.00	0.00	0.00	1.36

Table 6.14 Mastics composition for the ZERO BITUMEN

ZERO BITUMEN									
Mastic Name Code	**%B**	**%R**	**%F**	**%B/ %R**	**%B/ %F**	**%R/ %F**	**%R/ %B**	**%F/ %R**	**%F/ %B**
Z_7_1_5	53.85	7.70	38.45	6.99	1.40	0.20	0.14	4.99	0.71
Z_8.5_1.2_5	57.80	8.09	34.10	7.14	1.69	0.24	0.14	4.21	0.59
Z_8_1_6	53.33	6.67	40.00	8.00	1.33	0.17	0.13	6.00	0.75
Z_7.5_0.75_5	56.50	5.65	37.85	10.00	1.49	0.15	0.10	6.70	0.67
Z_SMA	42.37	0.00	57.63	0.00	0.74	0.00	0.00	0.00	1.36

Table 6.15 Mastics composition for the A BITUMEN

A BITUMEN									
Mastic Name Code	**%B**	**%R**	**%F**	**%B/ %R**	**%B/ %F**	**%R/ %F**	**%R/ %B**	**%F/ %R**	**%F/ %B**
A_7_1_5	53.85	7.70	38.45	6.99	1.40	0.20	0.14	4.99	0.71
A_8.5_1.2_5	57.80	8.09	34.10	7.14	1.69	0.24	0.14	4.21	0.59
A_8_1_6	53.33	6.67	40.00	8.00	1.33	0.17	0.13	6.00	0.75
A_7.5_0.75_5	56.50	5.65	37.85	10.00	1.49	0.15	0.10	6.70	0.67
A_SMA	42.37	0.00	57.63	0.00	0.74	0.00	0.00	0.00	1.36

6.3.2 Mastics Preparation

The bitumen-filler mastics were produced by adding the mass of Limestone Filler and Fine Crumb Rubber to heated bitumen at a temperature of 160°C while mixing the three components together with an high shear mixer (shown in Figure 6.5) for one minute until a homogeneous mastic was obtained. This procedure simulates what happens in the production phase of the mixture in plant. The mixing procedures are detailed as follows:

- limestone filler was put into a 160◦C oven for 24 hours to ensure moisture free particle surfaces;
- the unmodified bitumen was stored in a 5 litre tin needed 5 hours preheat into a 160°C oven to make bitumen homogeneous and ready to mix;
- the two modified bitumen was stored in a 5 litre tin needed 7 hours preheat into a 160◦C oven to make bitumen homogeneous and ready to mix;
- the accurate amount of the bitumen was poured into a 1 litre tin. The tin with the bitumen was placed on a hot plate and kept at 160◦C;
- the bitumen was mechanically stirred for 30 seconds;
- the accurate mass of the limestone filler and crumb rubber was added slowly and the mixing process was followed so that the limestone filler and the fine crumb rubber were homogeneously dispersed in the bitumen.

Fig. 6.5 Mastic mixing process.

6.4 Mastics Testing Programme

The general principle of the dynamic oscillatory shear load test is to determine the dynamic rheological properties of bituminous binders in a wide range of angular frequencies and test temperatures by means of an oscillatory rheometer with a parallel plate test geometry. A bituminous sample is squeezed between two concentric, circular, and parallel plates. The sample is subjected to either a sinusoidal torque or a sinusoidal angular displacement of constant angular frequency during the test. The DSR and dynamic mechanical analysis have been described in Chapter 3.

6.4.1 Test Equipment and Sample Preparation

Three different types of Dynamic Shear Rheometers (DSR) have been used to obtain the mastic rheological properties:

- **Bohlin - Gemini 200** (Figure 6.6a) using water (fluid) bath system controlling temperature (APPENDIX A).
- **Anton Paar - Smart Pave 102** (Figure 6.6b) using Peltier system temperature control with Peltier hood (APPENDIX A).
- **Anton Paar - MCR 302** (Figure 6.6c) using Peltier system temperature control with peltier hood (APPENDIX A).

Figure 6.6 DSR used: a) Bohlin - Gemini 200 b) Anton Paar – Smart Pave 102 c) Anton Paar – Smart Paar – MCR 302

Using parallel plate geometry for the DSR, the set up machine steps described below were followed:

- starting up the rheometer and the connected temperature/water control unit;
- choosing and installing the correct geometry [8mm or 25mm parallel plate].

- setting the Zero Gap;
- sample loading, gap setting (inc. trimming if needed);
- starting the test and data collection;
- saving data, removing sample and the geometry;

6.4.2 Amplitude Sweep Test

Amplitude Sweep (AS) tests were preliminary carried out, to investigate the viscoelastic region at 10°C, applying a constant frequency of 10 rad/s (1.59 Hz). The investigated strain level range is between 0.01% and 100% of mastic deformation. It was chosen the strain amplitude at which the complex modulus not differ by more 10% of its initial value.

6.4.3 Frequency Sweep Test

Dynamic mechanical analysis, using oscillatory tests, was performed on the four bitumens to determine their rheological properties using a Dynamic Shear Rheometer (DSR). The tests were performed under controlled strain, and the strain amplitude was limited within the linear viscoelastic (LVE) response of the samples. Data were obtained from frequency sweep tests between 0.01 and 10 Hz, conducted between 10°C and 60°C. The 8 mm measurement system with 2 mm gap was adopted in all the temperature range. The rheological parameters obtained from frequency sweep tests were the complex shear modulus G*and phase angle δ. Using the principle of time – temperature superposition (TTS) the master curve of G*and δ were constructed at the reference temperature.

6.4.4 Multiple Stress Creep Recovery Test

The MSCR test was operated in rotational mode at 58 and 64°C using 1 s creep load followed by 9 s recovery for each cycle according to ASTM D7405. Ten creep and recovery cycles were run at 0.1 kPa creep stress followed by ten at 3.2 kPa creep stress. For each cycle, two parameters, the percent recovery (%R) and non-recoverable creep compliance (J_{nr}) are calculated.

6.5 Mastic Discrete Element Simulation

The three-dimensional discrete element modeling approach has been used in order to capture, both quantitatively and qualitatively, the behavior of Z_8.5_1.2_5 and Z_SMA mastics, following the methods validated and described on Chapter 4. Also in this study for Z_8.5_1.2_5 and Z_SMA samples, the discrete element simulation includes three main steps:

- definition of the model geometry;
- description of the contact material properties;
- simulation of the frequency sweep test.

6.5.1 Model Geometry

According to Dondi *et al.* (2014) the model geometry was generated in PFC3D using an arrangement of spherical particles, contained inside walls which simulated the dynamic shear rheometer device. The bitumen spheres diameter was set to 200 µm, the spheres diameter of crumb rubber and limestone filler was set to 100 µm. The bitumen, limestone filler and crumb rubber density and thermal properties were set as measured by the manufacturer (Table6.16).

Table 6.16 Properties of the DEM models

Mastic	Material	Density [kg/m^3]	Spheres diameter [µm]
Z_8.5_1.2_5	Bitumen	1000	200
	Limestone Filler	2700	100
	Crumb Rubber	1010	100
Z_SMA	Bitumen	1000	200
	Limestone filler	2700	100

Three walls were adopted in order to simulate the dynamic shear rheometer, in which the samples of mastics, represented by 74400 spheres on Z_8.5_1.2_5 and 79440 spheres on Z_SMA, were generated (Figures 6.7 – 6.8). The test device was modeled by a cylindrical wall closed at the top and bottom by planes simulating the parallel plates. The lower plane is fixed, while the upper one oscillates back and forth to create a shearing action. The samples of mastics, 2 mm thick and 8 mm in diameter, were

sandwiched between walls. The contact stiffness of the cylindrical wall has been obtained by a calibration analysis and it is equal to 10^2 N/m (Dondi *et al.* 2014).

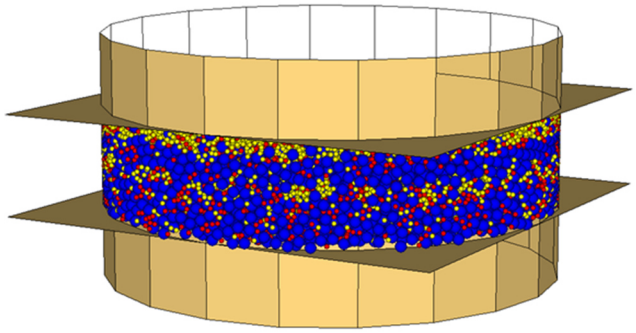

Figure 6.7 – Z_8.5_1.2_5, DEM model of the DSR sample (in blue the bitumen spheres, in red the Crumb Rubber Spheres, in yellow the limestone filler spheres)

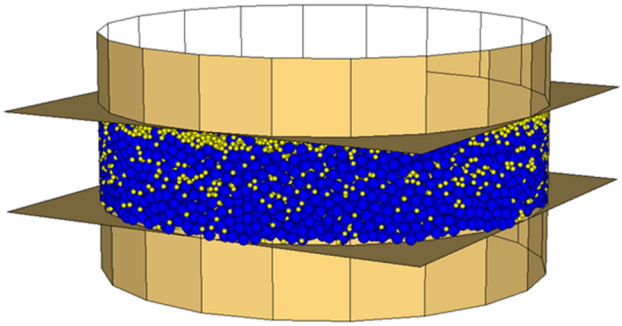

Figure 6.8 – Z_SMA, DEM model of the DSR sample (in blue the bitumen spheres, in yellow the limestone filler spheres)

6.5.2 Contact Materials Properties

According to Dondi *et al.* (2014), in this study in, the linear contact model was applied, where the normal and shear stiffness of a discrete element (the linear contact model parameters) change with loading time, based on the Burger's constitutive relations (Collop *et al.* 2004 – 2006 - 2007). Burger's model parameters were obtained, as validated for mastics on chapter 4, fitting the Burger model to DSR measurements. The fitting procedure was based on minimizing an objective function reported on equation (3.130). The "Solver" option in Microsoft Excel was utilized to minimize the objective function. The obtained Burgers' parameters are reported in (Table 6.17).

Table 6.17 Mastics Burger Parameters.

Burger Parameter	Initial Value	"Solver" Value	
		Z_8.5_1.2_5	**Z_SMA**
K_k [MPa]	3	0.05	0.45
K_m [MPa]	2	26.05	47.32
C_k [MPa·s]	4	3.90	7.65
C_m [MPa·s]	5	37.16	45.97

6.5.3 Simulation of Frequency Sweep Test

According to Dondi *et al.* 2014 in the DEM simulation of the Frequency Sweep test an oscillatory shear load of constant amplitude was applied on the upper parallel wall, at nineteen loading frequencies ranging between 0.01 and 10 Hz and several different temperatures (10, 20, 30, 40, 50 and 60°C). An oscillatory shear angular velocity applied to the walls was used for each temperature. Numerical results have been evaluated and compared in terms of complex modulus (|G*|) and phase angle (δ) as reported in equations (4.11 and 4.12). The sinusoidal load, applied at low strain levels and transferred through the wall to the sample, allows for the adoption of a linear analysis. Using the TTS principle, the simulated master curves of complex modulus and phase angle were shifted at the reference temperature of 20°C.

6.6 Mastic Test Results and Discussion

6.6.1 Linear Viscoelastic Limit

The LVE range for each of the 15 studied mastics is shown in the following tables.

Table 6.18 UNMODIFIED BITUMEN Linear Visco-Elastic range

UNMODIFIED BITUMEN		
Mastic	**γ LVE [%]**	**Temperature [°C]**
UN_7_1_5	0.5	10
UN_8.5_1.2_5	0.6	10
UN_8_1_6	0.5	10
UN_7.5_0.75_5	0.5	10
UN_SMA	0.4	10

Table 6.19 ZERO BITUMEN Linear Visco-Elastic range

ZERO BITUMEN		
Mastic	**γ LVE [%]**	**Temperature [°C]**
Z_7_1_5	0.8	10
Z_8.5_1.2_5	0.9	10
Z_8_1_6	0.8	10
Z_7.5_0.75_5	0.8	10
Z_SMA	0.5	10

Table 6.20 A BITUMEN Linear Visco-Elastic range

A BITUMEN		
Mastic	**γ LVE [%]**	**Temperature [°C]**
A_7_1_5	0.4	10
A_8.5_1.2_5	0.5	10
A_8_1_6	0.4	10
A_7.5_0.75_5	0.4	10
A_SMA	0.2	10

The Linear Visco-Elastic range reflects for each mastics the rheological properties of the base bitumen. Comparing Zero and A bitumen mastics, the linear LVE range is lower for mastics made with the A bitumen, demonstrating how the A bitumen is less sensitive to polymer modification, and stiffer than the Zero one.

6.6.2 Master Curves

6.6.2.1 Mastic made with the UNMODIFIED BITUMEN

Results in Figure 6.9 show that in all the range of frequencies the mastics containing both limestone filler and crumb rubber attains G* values lower than the SMA mastic at high frequencies (low temperatures) and G* values higher than the SMA mastic at low frequencies (high temperatures).

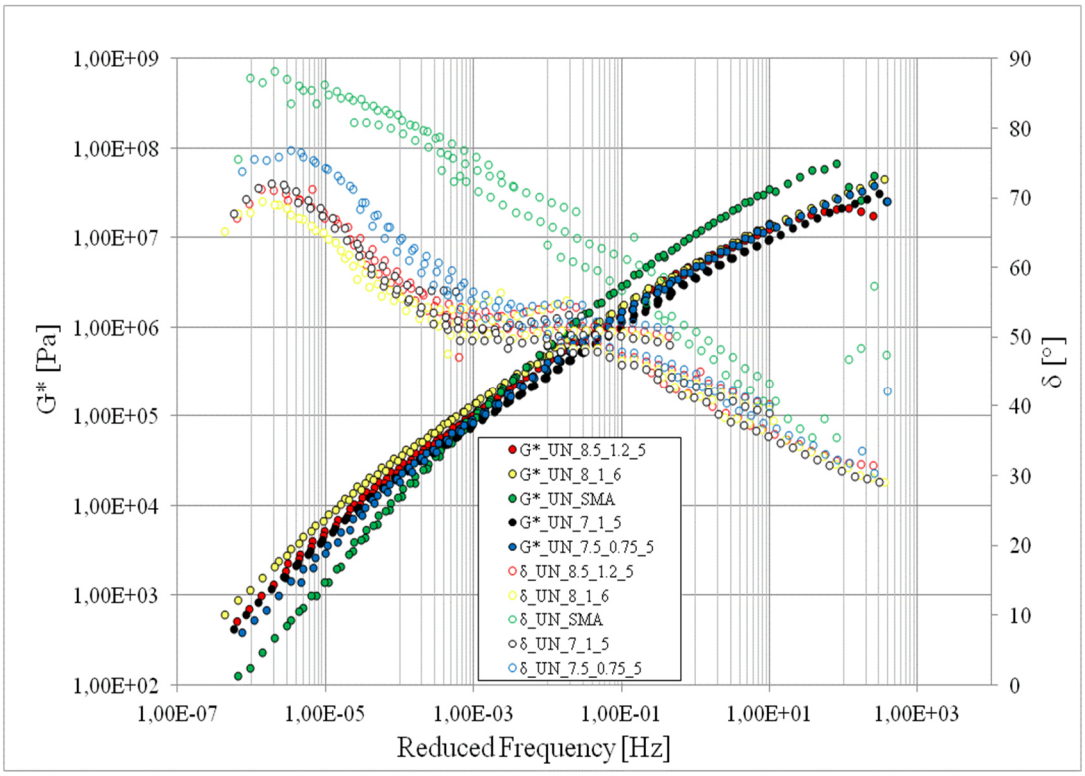

Figure 6.9 Master Curves of mastics made with Unmodified Bitumen

It can be stated that the rubber effect on the rheological behavior of mastic is to reduce the bitumen thermo-sensitivity, giving high performances in terms of shear response at high temperatures and reducing the rigid behavior at low temperatures. The UN_8_1_6 mastic shows the highest complex modulus values at high temperature. The higher amount of limestone filler than the other mastics combined with the rubber increase the mastic resistance to permanent deformations. The rheological behavior of UN_8.5_1.2_5 and UN_7_1_5 mastics is equivalent, despite their internal differences in terms of single components percentages. The 1% addition of rubber in UN_8.5_1.2_5 mastic compensates the 4% less limestone filler comparing UN_7_1_5 mastic. The UN_7.5_0.75_5 mastic shows an intermediate rheological behavior

between the UN_SMA mastic (57% limestone filler and 0% rubber by mass) and the other three mentioned above. Although within UN_7.5_0.75_5 mastic containing the 37.74% by mass of limestone filler, reducing the proportion of rubber to 5.66% by mass leads to decrease complex modulus values at high frequencies. At medium and high frequencies the G* values of mastic containing crumb rubber are the same. It may noted that the SMA mastic has a behavior similar to the base bitumen one (*Unmodified Bitumen*), tending at high frequencies to values close to those the glassy modulus.
The UN_8_1_6 mastic exhibits lower phase angles values at high temperatures than UN_8.5_1.2_5 and UN_7_1_5. The phase angle of mastics UN_8.5_1.2_5 and UN_7_1_5 tends towards the same phase angle versus frequency relationship at high frequencies. Figure 6.9 shows that phase angle values for the UN_7.5_0.75_5 tend to diverge at high frequencies compared to those for the mastic containing more than 6% by mass of rubber. At high temperatures, the phase angle values of mastic containing only limestone filler have the same trend of those of the base bitumen. The elastic response of the mastic containing rubber increase, however the rheological response of the mastic made with the unmodified bitumen is significantly far from the polymer-modified bitumen. At medium frequencies, the visco-elastic response of mastics containing both rubber and filler is the same, in the other side the UN_SMA mastic shows higher phase angle values at medium frequencies than the other four mastics. At low temperatures the elastic response of the all mastics is the same, this may indicates that the base bitumen controls the behavior at the high frequencies.

6.6.2.2 Mastic made with the ZERO BITUMEN

Figure 6.10 shows the complex modulus and phase-angle master curves of mastics made with the modified bitumen named *Zero*.

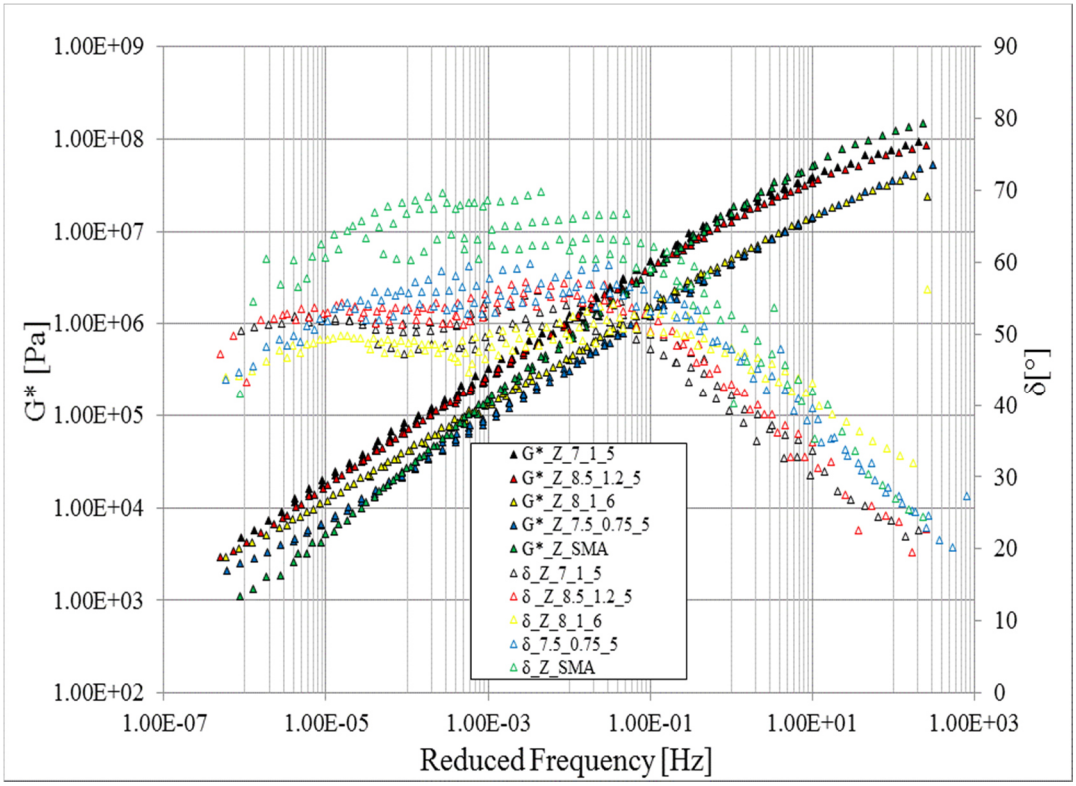

Figure 6.10 Master Curves of mastics made with Zero Bitumen

The master curves show greater complex modulus values and lower phase angle values than mastics made with the unmodified bitumen at all frequencies. The polymeric modification within the binder is evident particularly at high temperatures. The complex modulus tends to the horizontal asymptote and the phase angle, in the neighborhood of 45°, shows the perfect visco-elastic behavior. However even in this case there are clear differences between the mastics containing the fine crumb rubber and the Z_SMA mastic containing only limestone filler. This is the mastic that have lowest values of G* at high frequencies and highest values at high frequencies. The combined action of rubber and limestone filler increases the characteristics given by the SBS polymer to the bitumen, reducing the thermo-sensitivity and increasing the visco-elasticity range. The Z_8_1_6 mastic containing the greater percentage of limestone filler tends to have less thermo-sensitive behavior, showing a reduced difference between the complex modulus at high temperatures and the complex modulus at low temperatures. In terms of response to shear stress at high temperatures, the mastics with the rubber content higher than 6% by mass show the best shear stress response. The complex modulus values are higher than those of Z_7.5_0.75_5 and

Z_SMA mastics. Also with the *Zero_Bitumen* the rheological behavior of Z_8.5_1.2_5 and Z_7_1_5 is the same at medium and low temperatures. Despite in the second mastic the filler-powder skeleton covers a wider surface than the first one, it is the bitumen-matrix itself that bears the shear stresses induced by the DSR. The phase angle values of mastic containing only limestone filler have the same trend of those of *Zero_Bitumen* but shifted to higher modulus values. At the high temperatures, the elastic response of the mastic containing rubber increases, exalting significantly the elastic behavior given by the polymer. At medium frequencies, the visco-elastic response of mastics containing both rubber and filler is the same. At low temperatures the mastic containing less filler and more rubber shows phase angles values lower than the δ values of mastics containing more filler.

6.6.2.3 Mastic made with A BITUMEN

The rheological behavior of mastics made with the *A* bitumen is affected by the interaction between the bitumen matrix, containing high aromatic fraction, with limestone filler and crumb rubber. Also in this case the A_SMA mastic with only limestone filler shows the highest complex modulus values at high frequencies and low stiffness at low frequencies. However, at high temperatures, the difference between the values of complex modulus G* between the A_SMA mastic and mastics with rubber powder is smaller than the two mastics described previously. On *A* bitumen, limestone filler exerts greater action to high temperatures in terms of response to shear stress. This is evident from the rheological behavior of all the studied mastics since the value of the complex modulus at high temperatures shows the same orders of magnitude. The main differences between the mastics are visible at low temperatures. The mastic A_8.5_1.2_5 containing more rubber and a prevailing bitumen matrix has the complex modulus values lower than the other mastics. Compared to the limestone filler, the action of the rubber powder is evident at low temperatures. The highest phase angle values of mastic containing only limestone filler confirms the previous analysis. Also in this case, at high temperatures, the elastic response of the mastic containing rubber has improved, exalting the elastic behavior given by the polymer. At medium frequencies, the visco-elastic response of mastics containing both rubber and limestone filler is the At low temperatures the mastic

containing less filler and more rubber shows phase angles values lower than the values of δ mastics containing filler.

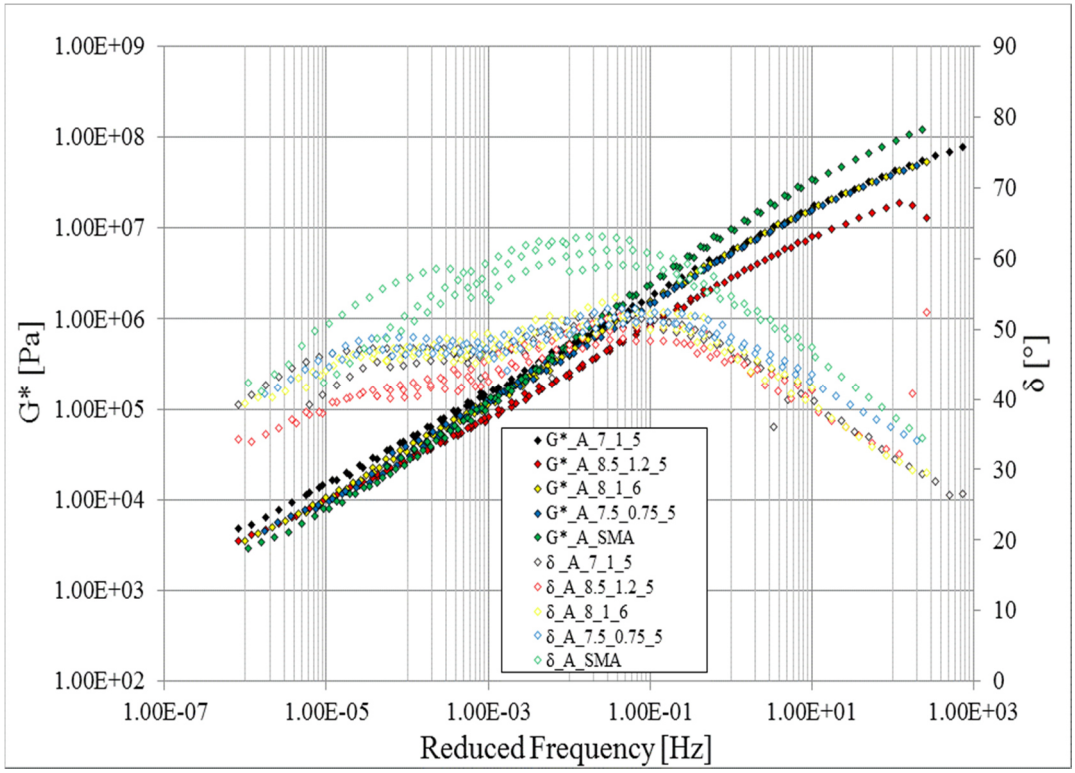

Figure 6.11 Master Curves of mastics made with A Bitumen

6.6.3 Black Diagram

Black diagram is also a common way to present and comment on the rheological characteristics of bituminous binders. The complex modulus and phase angle measurement obtained from a dynamic test are plotted in the graph. The effects of temperature and loading time are eliminated from the plot, which allow the dynamic data to be presented in a plot without requiring the shifting of raw data. The Black diagrams for the mastics made with the unmodified bitumen are presented in Figures 6.12. The curves are not smooth and continuous compared to Black diagram curves typical of neat bitumen. In all mastic the high rubber and filler concentrations implies that the studied mastics has not a simple rheological behavior, and the particles are not suspended in the bitumen. However, as with the master curves, the Black diagram curves for the mastic made with only limestone filler mastics are distinctive. The Black diagram curves of the SMA mastics tend to a viscous behavior from high complex modulus values (low temperatures) to low complex modulus values (high

temperature). The mastic containing crumb rubber shows an increasing of the elastic behavior. For the mastic made with the unmodified bitumen at medium G* values it is evident the elastic recovery typical of the polymer modified bitumen. This behavior is enhanced for the mastics made with the PWmB, the elastic recovery covers the modulus range from medium to low values. Limestone filler and rubber act when combined to the SBS polymer increasing the materials stiffness at high temperatures and consequently their elastic response. As shown in the previous paragraph, the rubber elastic effects are enhanced on mastic made with the A bitumen (Figures 6.13-6.14).

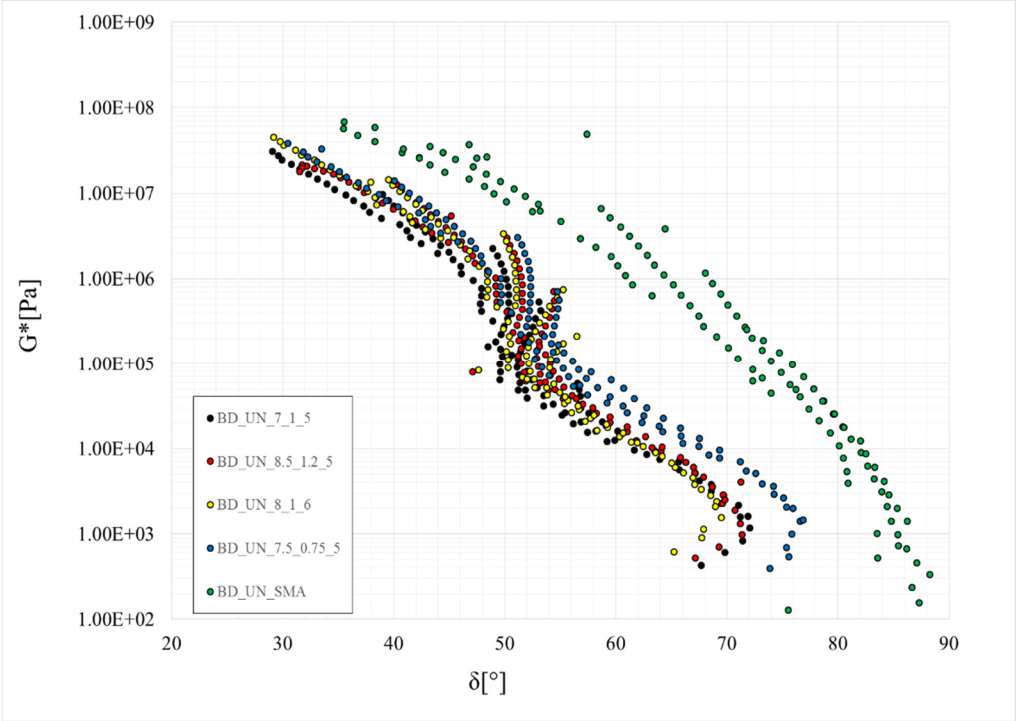

Figure 6.12 Black diagram of mastics made with Unmodified Bitumen

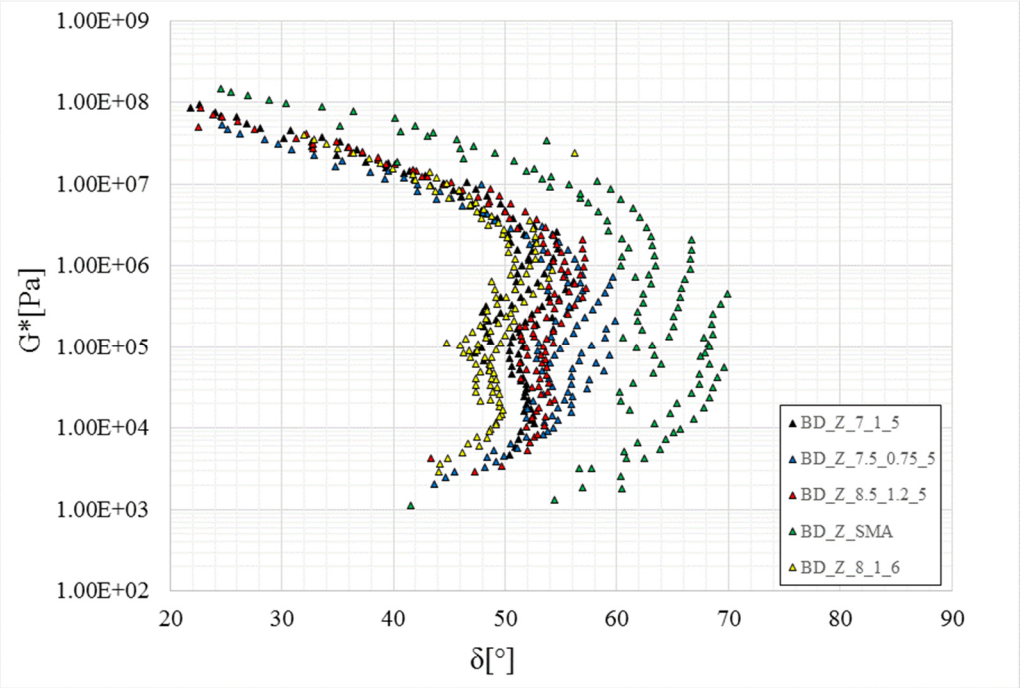

Figure 6.13 Black diagram of mastics made with Zero Bitumen

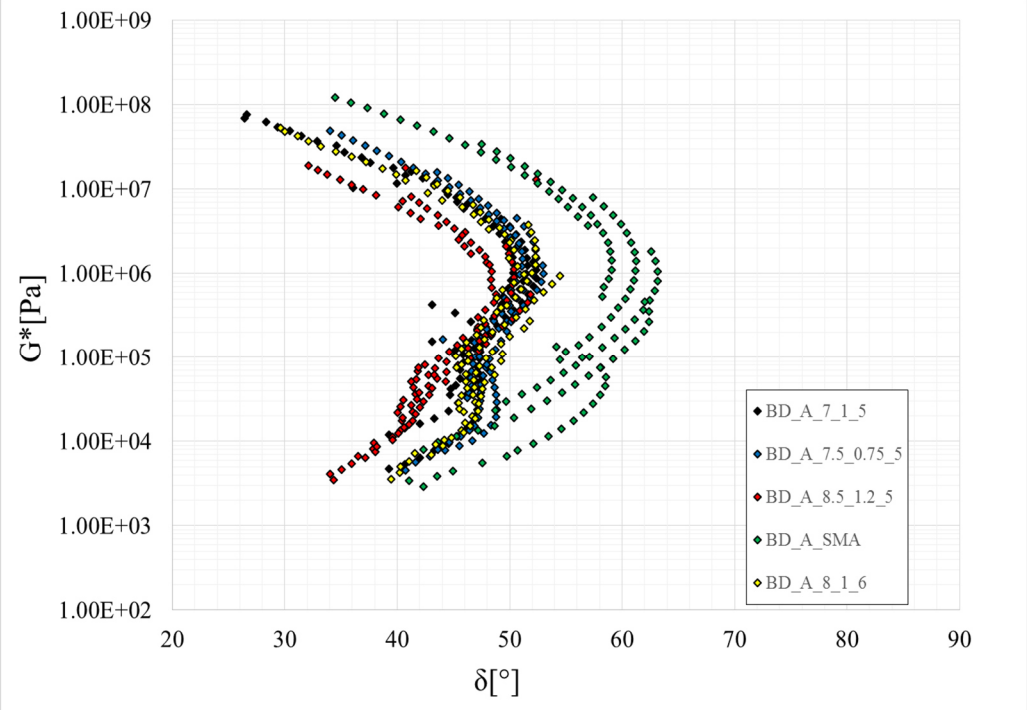

Figure 6.14 Black diagram of mastics made with A Bitumen

6.6.4 MSCR and J_{nr} Results

6.6.4.1 Mastic made with UNMODIFIED BITUMEN

The mastics potential rutting was evaluated through MSCR tests run at 0.1 and 3.2 kPa. Figure 7.10 shows the test results at the temperature of 58°C related to the mastics made with the unmodified bitumen. In this test configuration, the UN_8_1_6 and UN_7_1_5 mastics have accumulated less deformation at the end of the 10 cycles at 3.2 kPa. For the mastics containing both limestone filler and crumb rubber, the mastics that have the highest concentration of limestone filler (40% and 38.5% by mass respectively) exhibit the stiffer behavior. The crumb rubber action in terms of recovery is also evident comparing the accumulated strains of the UN_SMA mastic with the other four mastics blended with the rubberized filler. As shown in Figure 6.13 the UN_SMA (58% of limestone filler by mass, 0% rubber) accumulated the highest strain percentage and, among the mastics containing both limestone filler and crumb rubber, the mastic UN_7.5_0.75_5 containing less crumb rubber (5.5% by mass) reaches the greatest accumulated strain. These results confirm the analysis made in the visco-elastic range through the Frequency sweep test and commented in the previous paragraph.

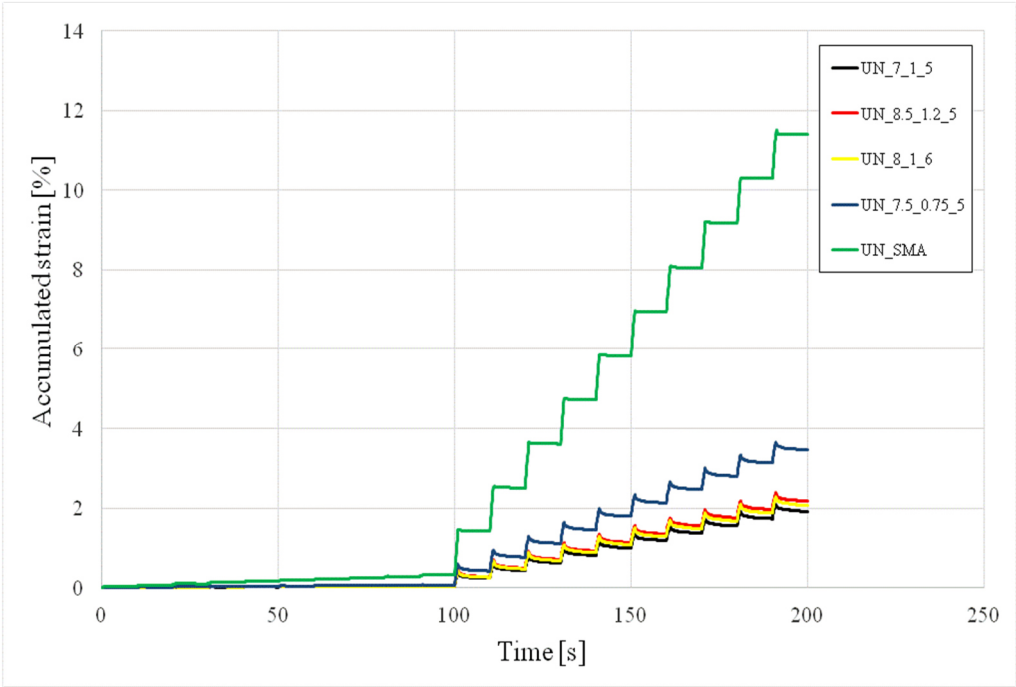

Figure 6.15 MSCR test results at @58°C for the mastics made with the unmodified bitumen.

Table 6.21 shows the results in terms of accumulated strain at the end of 10th cycle at 0.1 and 3.2 kPa. For both shear stress levels, the accumulated strain of the UN_SMA mastic is one order of magnitude higher than those of the mastics containing both limestone filler and crumb rubber. It is also evident the crumb rubber effect at 3.2 kPa. For the UN_7.5_0.75_5 mastic the accumulated strain from 0.1 kPa to 3.2 kPa is 60 times higher, compared to the other three mastics for which there is an increasing deformation 50 times higher.

Table 6.21 Accumulated strain values at the end of 10th cycle at 0.1kPa and 3.2kPa for the mastics made with the Unmodified bitumen.

Mastic Name Code	**Temperature 58°C**	
	0.1 kPa	**3.2 kPa**
	Accumulated Strain 10th cycle [%]	**Accumulated Strain 10th cycle [%]**
UN_7_1_5	0.03	1.92
UN_8.5_1.2_5	0.04	2.17
UN_8_1_6	0.04	2.17
UN_7.5_0.75_5	0.06	3.46
UN_SMA	0.30	11.4

Table 6.22 shows the average percentage of recovery of the five mastics under 0.1 and 3.2 kPa shear load at the test temperature of 58°C. The UN_8_1_6, UN_7_1_5 and UN_8.5_1.2_5 mastics attain an average recovery (%) higher than the UN_7.5_0.75_5 and UN_SMA; in particular, the average recovery of these mastics in close 30% at 0.1 kPa and 16% at 3.2 kPa. At the highest shear stress level the mastics containing only limestone filler has no recovery. Comparing the UN_8_1_6 (6.67% of rubber by mass) and UN_7.5_0.75_5 (5.66% of rubber by mass) mastics it can be stated that a 1% more rubber inside increases the recovery at both shear stress levels.

Table 6.22 Average percentage of recovery at 0.1 and 3.2 kPa for the mastics made with the Unmodified bitumen.

Mastic Name Code	Temperature 58°C	
	0.1 kPa	3.2 kPa
	Average % recovery [%]	Average % recovery [%]
UN_7_1_5	28	14
UN_8.5_1.2_5	27	14
UN_8_1_6	30	16
UN_7.5_0.75_5	20	9
UN_SMA	2	0

As shown in chapter 3 the creep compliance J_{nr} parameter is a measure of the non-recoverable behavior of the bitumen/mastics caused by creep-recovery cycles. The J_{nr} values were calculated for the five mastics under 0.1 and 3.2 kPa shear stresses at 58°C. The UN_8_1_6, UN_7_1_5 and UN_8.5_1.2_5 mastics have lower values of non recoverable compliance at both shear stresses, showing less sensitivity of these three mastics to stress increasing. Despite the limestone filler presence in the last mastic is 4% less than the others two (34% by mass for UN_8.5_1.2_5, 38.5% by mass for UN_7_1_5 and 40% for UN_8_1_6), the 1% crumb rubber more than UN_7_1_5 and the 1.5% of crumb rubber more than UN_8_1_6, make the mastic less susceptible to permanent deformations. The UN_SMA mastic has the highest values of J_{nr} under all test conditions, it is once again proven that the absence of rubber increases the potential rutting sensitivity.

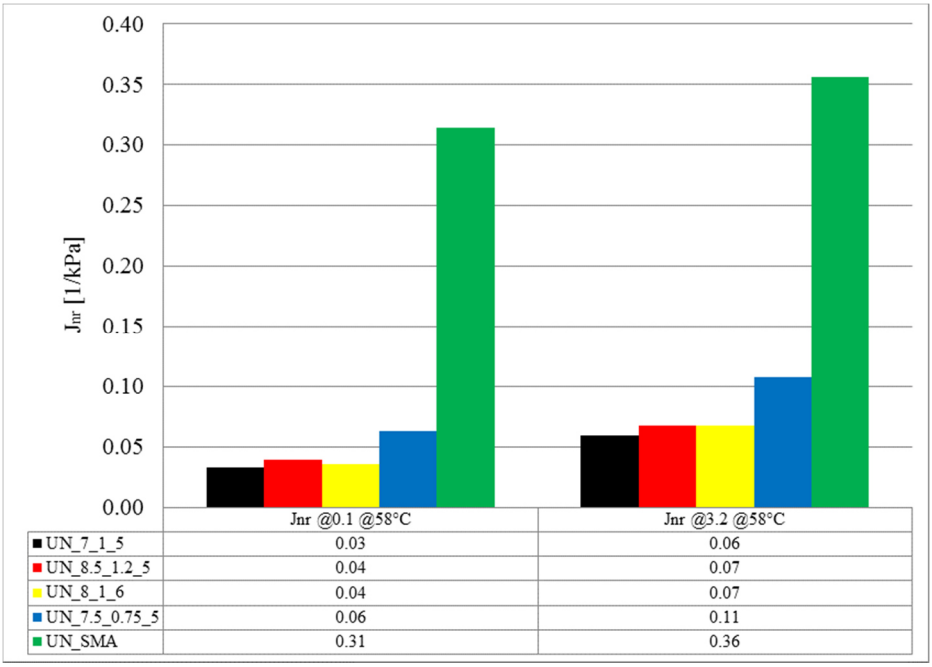

	Jnr @0.1 @58°C	Jnr @3.2 @58°C
UN_7_1_5	0.03	0.06
UN_8.5_1.2_5	0.04	0.07
UN_8_1_6	0.04	0.07
UN_7.5_0.75_5	0.06	0.11
UN_SMA	0.31	0.36

Figure 6.16 Non-recoverable compliance at 0.1 kPa and 3.2 kPa for the mastics made with the Unmodified bitumen.

6.6.4.3 Mastic made with ZERO BITUMEN

Figure 6.17 shows the test results at the temperature of 58°C related to the mastics made with the *Zero* bitumen. The Z_8.5_1.2_5 mastic has accumulated less deformation at the end of the 10 cycles at 3.2 kPa. Among the mastics containing both limestone filler and crumb rubber, the mastic that have the highest concentration percentage of rubber (8.16% by mass) has the lowest values of accumulated strain at both shear stress levels. The A_SMA (58% of limestone filler by mass, 0% rubber) has accumulated the highest strain percentage and among the mastics containing both limestone filler and crumb rubber, the A_7.5_0.75_5 mastic containing less crumb rubber (5.5% by mass) shows the greatest accumulated strain. This differences are exalted at 3.2 kPa shear stress level at which the crumb rubber transmits its elastic properties to the mastics.

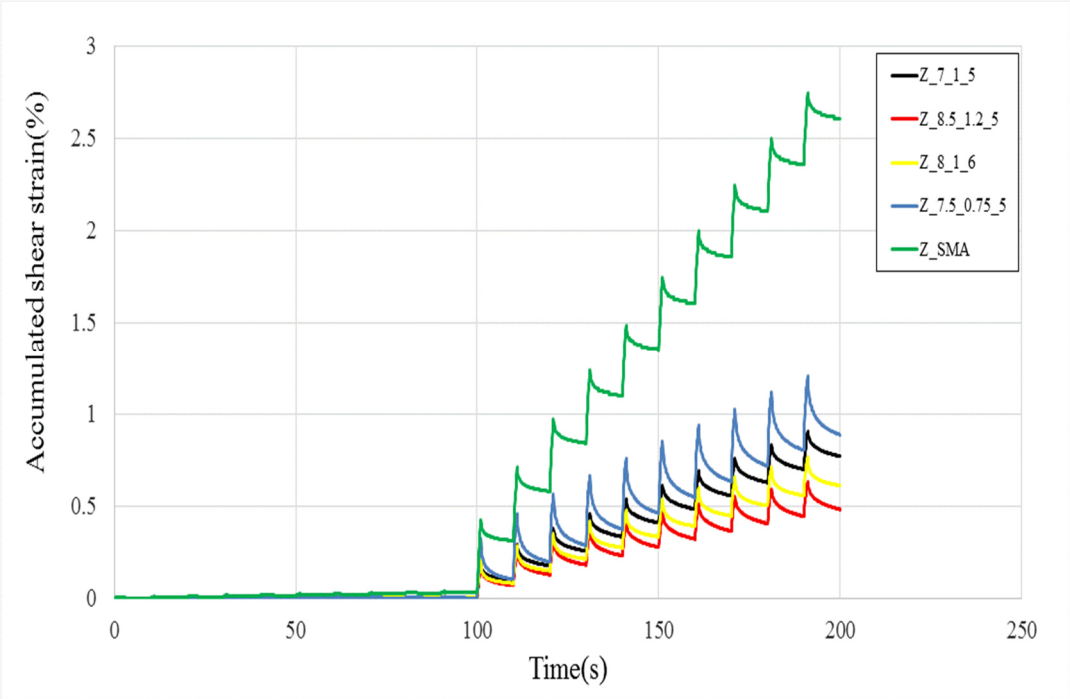

Figure 6.17 MSCR test results at @58°C for the mastics made with the Zero bitumen.

At the shear stress level of 0.1 kPa the mastics containing both limestone filler and crumb rubber have accumulated, at the end of 10th cycle, the same strain (range between 0.002 and 0.005%) (Table 6.23). At 3.2 kPa the 8.16 % of rubber concentration acts in response to stresses such as is shown in Tables 6.23 and 6.24. However, as analyzed from the master curves, in the Z_8_1_6 mastic the 40% of limestone filler increases the mastic stiffness, obtaining, by MSCR test, that this mastic has the second best percentage of accumulated deformation.

Table 6.23 Accumulated strain values at the end of 10th cycle at 0.1kPa and 3.2kPa for the mastics made with the Zero bitumen.

Mastic Name Code	**Temperature 58°C**	
	0.1 kPa	**3.2 kPa**
	Accumulated Strain 10th cycle [%]	**Accumulated Strain 10th cycle [%]**
A_7_1_5	0.005	0.85
A_8.5_1.2_5	0.002	0.50
A_8_1_6	0.005	0.60
A_7.5_0.75_5	0.005	1.40
A_SMA	0.030	2.00

The phase angle reduction analyzed in the FS test, at high temperatures, is visible in terms of % recovery and accumulated deformation in MSCR test. Among the mastics

made with the *Zero* bitumen, Z_SMA highlights the lowest percentage of recovery at 3.2 kPa. The Z_8.5_1.2_5 and Z_8_1_6 (mastic with lowest phase angle values at high temperaures) have the highest recovery percentages at both shear stress level. As described on linear analysis, this result confirms that the limestone filler and crumb rubber action increases both stiffness and elastic mastic response at the high temperatures.

Table 6.24 Average percentage of recovery at 0.1 and 3.2 kPa for the mastics made with the A Bitumen.

Mastic Name Code	Temperature 58°C	
	0.1 kPa	3.2 kPa
	Average % recovery [%]	Average % recovery [%]
UN_7_1_5	61	27
UN_8.5_1.2_5	87	32
UN_8_1_6	61	29
UN_7.5_0.75_5	61	25
UN_SMA	40	20

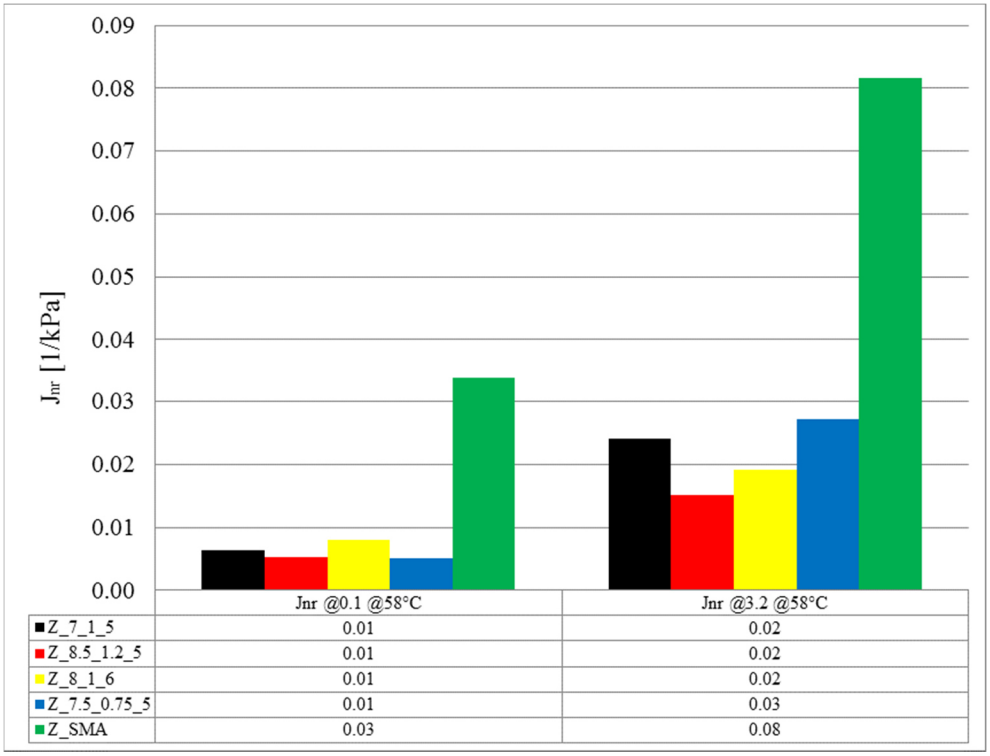

Figure 6.18 Non-recoverable compliance at 0.1 kPa and 3.2 kPa for the mastics made with the Zero Bitumen.

6.6.4.3 Mastic made with "A" BITUMEN

Figure 6.19 shows the test results at the temperature of 58°C related to the mastics made with the *A* bitumen. The A_8.5_1.2_5 mastic has accumulated less deformation at the end of the 10 cycles at 3.2 kPa. Among the mastics containing both limestone filler and crumb rubber, the mastics that have the highest concentration of crumb rubber (8.16% by mass) has the lowest values of accumulated strain at both shear stress levels. Also in this analysis it can be noticed that the A_SMA (58% of limestone filler by mass, 0% rubber) has accumulated the highest strain percentage and among the mastics containing both limestone filler and crumb rubber, the A_7.5_0.75_5 mastic containing less crumb rubber (5.5% by mass) shows the greatest accumulated strain percentage. This differences are exalted at 3.2 kPa shear stress level at which the crumb rubber transmits its elastic properties to the mastics.

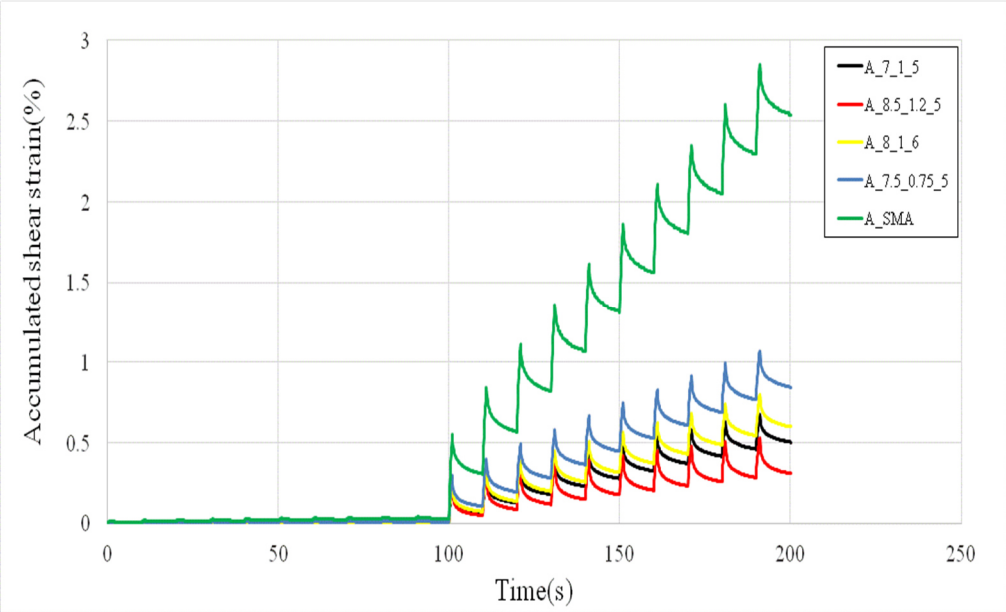

Figure 6.19 MSCR test results at @58°C for the mastics made with the A bitumen.

These results confirm the analysis made in the visco - elastic range through the Frequency sweep test. In the linear analysis for the mastics containing both limestone filler and crumb rubber it is recorded the same response with accumulated strains ranging between 0.002 and 0.007% (Table 6.25); with the increase of the shear stress the presence of an higher percentage of rubber acts in response to stresses as is shown in Table 6.25-6.26.

Table 6.25 Accumulated strain values at the end of 10th cycle at 0.1kPa and 3.2kPa for the mastics made with the A bitumen.

Mastic Name Code	Temperature 58°C	
	0.1 kPa	3.2 kPa
	Accumulated Strain 10th cycle [%]	Accumulated Strain 10th cycle [%]
A_7_1_5	0.005	0.50
A_8.5_1.2_5	0.002	0.30
A_8_1_6	0.005	0.50
A_7.5_0.75_5	0.007	0.85
A_SMA	0.030	2.54

As highlighted in the previous paragraphs the crumb rubber action increases the influence of the polymer modification. The phase angle reduction analyzed in the FS tests, at high temperatures, is visible in terms of recovery (%) and accumulated deformation in the MSCR tests. The A_SMA mastics made with the A bitumen, shows a 17% of recovery at 3.2 kPa compared to a 0% of the UN_SMA because of the presence of SBS in the bitumen matrix. This result highlights the rubber action that has increased the SBS polymer performances, ranging between 50 and 70% of the elastic recovery of the mastics. The J_{nr} values were calculated for the five mastics under 0.1 and 3.2 kPa shear stresses at the test temperatures at 58°C are shown in figure 6.20. The UN_8.5_1.2_5 mastics have lower values of non recoverable compliance at both shear stresses, confirming a reduced sensitivity of this mastics to permanent deformations. The mastic A_7.5_0.75_5 (5.66% by mass of rubber) shows the highest J_{nr} values among the mastics containing both filler types. The A_SMA mastic has the highest values of J_{nr} under all test conditions, it is once again proven that the absence of rubber increases the potential rutting sensitivity.

Table 6.26 Average percentage of recovery at 0.1 and 3.2 kPa for the mastics made with the A Bitumen.

Mastic Name Code	Temperature 58°C	
	0.1 kPa	3.2 kPa
	Average % recovery [%]	Average % recovery [%]
UN_7_1_5	61	35
UN_8.5_1.2_5	87	54
UN_8_1_6	61	36
UN_7.5_0.75_5	61	31
UN_SMA	40	17

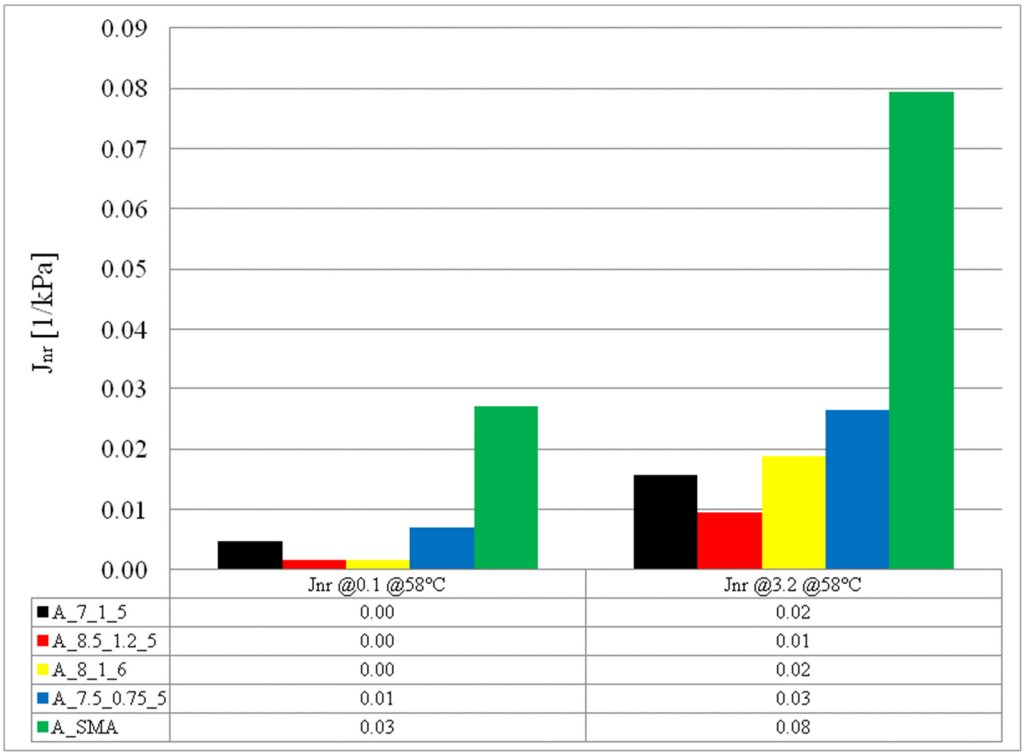

Figure 6.20 Non-recoverable compliance at 0.1 kPa and 3.2 kPa for the mastics made with the A bitumen.

6.6.5 DEM results

6.6.5.1 Frequency Sweep Test Results

In Figure 6.19 are shown the Z_SMA and Z_8.5_1.2_5 G* Master Curves obtained from DEM simulations. Master curves from DEM data confirm the laboratory test. In particular the differences between the mastics containing the fine crumb rubber and the Z_SMA containing only limestone filler are evident. This is the mastic that have

the lowest G* values at high frequencies and highest G* values at high frequencies. On the contrary, at the high temperatures, the mastic containing rubber shows a better response to shear stresses, attaining moduli values higher than Z_SMA. At high frequencies the crumb rubber properties reduce the mastic stiffness; at low temperature this mastic is less rigid than the mastic containing only limestone filler.

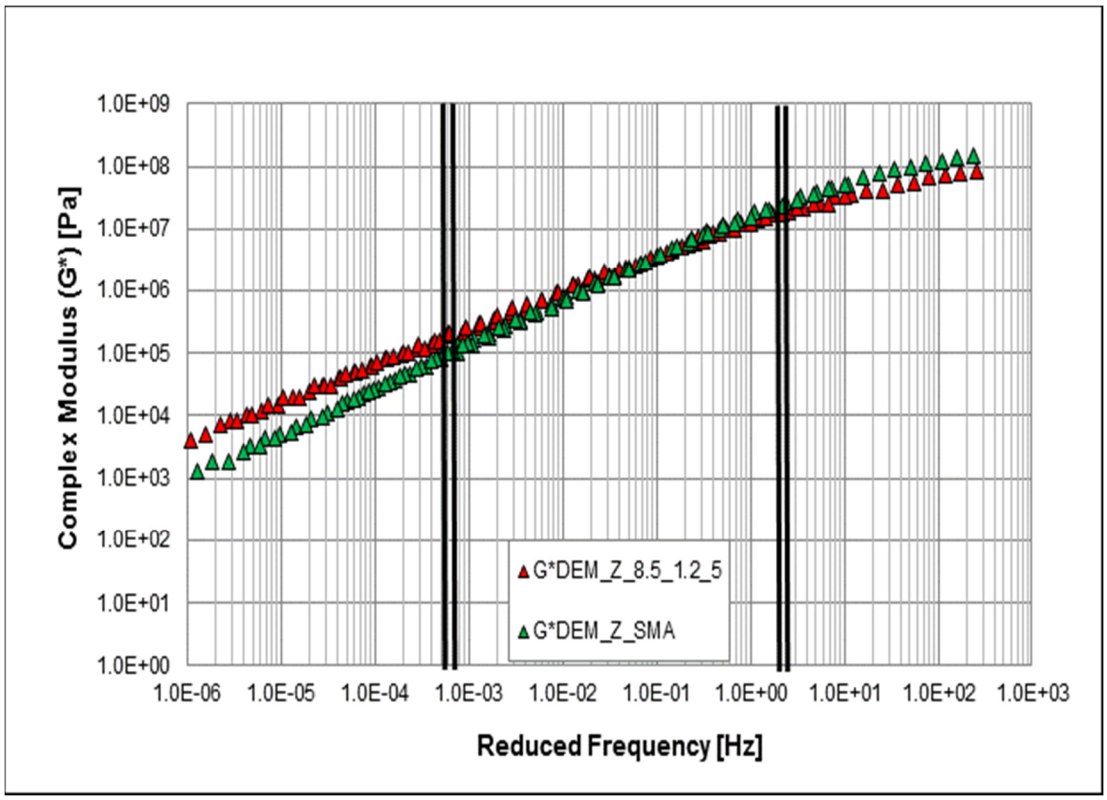

Figure 6.21 Z_SMA and Z_8.5_1.2_5 3D DEM G*Master Curve comparison.

The phase angle Master Curves also confirms the laboratory results as shown on figure 6.22. At the high temperatures, the elastic response of the mastic containing rubber increases, exalting significantly the elastic behavior given by the polymer in all range frequencies. At medium and low temperatures the stress response of mastics containing rubber shows phase angles values lower than the δ values of mastics containing more filler.

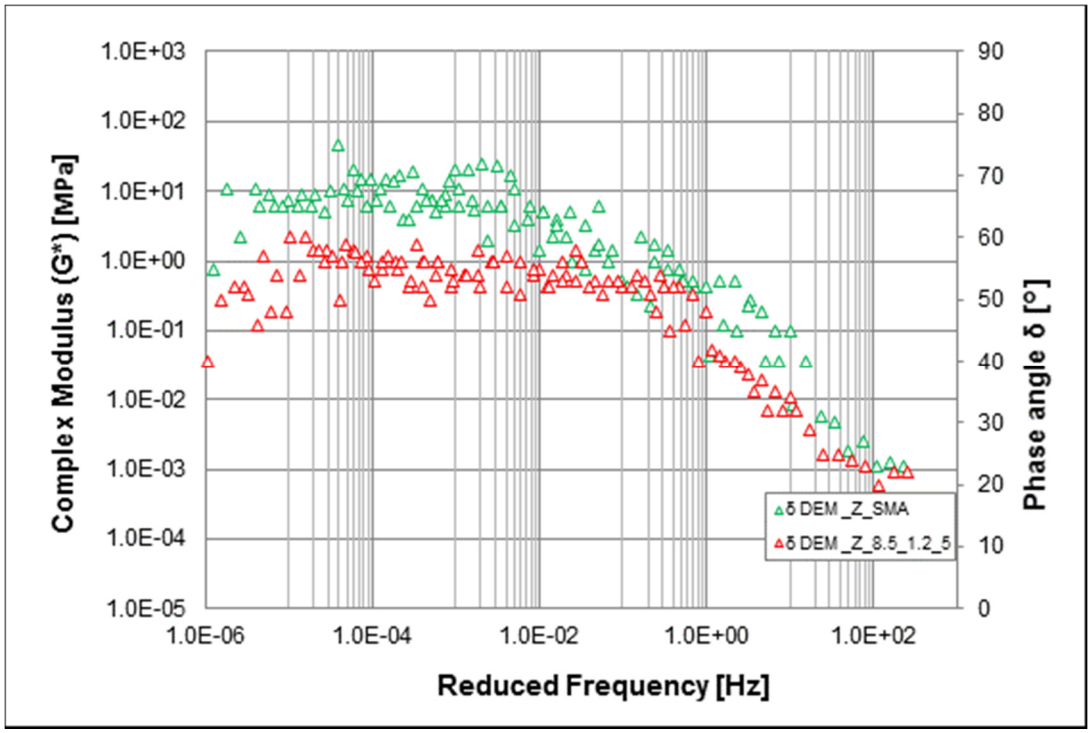

Figure 6.22 Z_SMA and Z_8.5_1.2_5 3D DEM δ Master Curve comparison.

Contact forces have been evaluated inside the Z_SMA and Z_8.5_1.2_5 modeled samples at the end of the sweep test at different temperatures (10°C, 30°C, and 60°C). The applied shear stresses increase the shear contact forces distribution inside the specimen and showing higher values than normal ones. As shown in Table 6.27, as the temperature increases, the maximum shear contact force inside the sample increases. While at 10°C and 30°C the maximum shear contact force inside the Z_SMA and Z_8.5_1.2_5 specimens are very similar, increasing the temperature the difference between the two mastics behavior increases. The maximum shear contact force of the Z_8.5_1.2_5 sample, in particular, are always higher than the Z_SMA one, and the relative difference (Δ) increases passing from 30°C to 60°C. This trend confirms that at high temperatures both limestone filler and crumb rubber improve the sample stiffness and the mastic resistance to permanent deformations.

Table 6.27 Maximum shear contact force inside the mastic sample [$*10^{-3}$ N/m]

Temperature [°C]	**10**	**30**	**60**
Z_SMA	2.809	6.173	11.357
Z_8.5_1.2_5	2.477	8.138	17.323
Δ	0.332	-1.965	-5.966

For each mastic, as the temperature increases, the total number of spheres displacements inside the sample increases. The spheres displacements, in particular, are evaluated in a Cartesian coordinate system, with:

- the origin in the centre of the upper horizontal plane of the model, which simulates the oscillating plate (chapter 4);
- the z direction coincident to the vertical axis of symmetry of the sample, pointing to the lower plate (chapter 4).

Displacements are calculated at the end of the sweep test at different temperatures (10°C, 30°C, 60°C). As shown in Table 6.28, for the same mastic, as the temperature increases, the maximum and minimum displacements of the particles in x, y and z directions increase. In terms of displacement it is also visible the shear stress action in terms of horizontal spheres movement, higher than the normal one.

Table 6.28 Particles displacement of Z_SMA and Z_8.5_1.2_5 models in x y z direction [mm].

Temperature [°C]	Mastic	xdisp min	xdisp max	ydisp min	ydisp max	zdisp min	zdisp max
10	Z_SMA	3.85E-05	0.9500	3.79E-05	1.10	6.00E-07	0.11
	Z_8.5_1.2_5	4.02E-05	1.0050	3.95E-05	1.19	8.00E-07	0.13
30	Z_SMA	4.85E-05	1.5000	4.50E-05	1.40	3.00E-06	0.30
	Z_8.5_1.2_5	4.30E-05	1.3000	4.40E-05	1.35	2.00E-06	0.20
60	Z_SMA	6.00E-05	2.1000	5.60E-05	2.20	7.00E-06	0.80
	Z_8.5_1.2_5	4.70E-05	1.7000	4.50E-05	1.80	5.00E-06	0.50

Comparing the Z_SMA and Z_8.5_1.2_5 specimens, for each temperature, in terms of horizontal displacement, the Z_8.5_1.2_5 shows larger spheres displacements than the Z_SMA at low temperatures. This trend is inverted as the temperature increases; at 30 and 60°C the horizontal displacement of mastic containing only limestone filler are larger than the mastic containing both components. So the master curve trend, which shows that Z_8.5_1.2_5 is stiffer than Z_SMA at high temperature, and less fragile at low temperature, is confirmed by the displacements of the spheres of the two models.

6.7 Mortar System

Mortar is the blend of the binder, limestone filler, small-size aggregate (sand) and additive (such as crumb rubber). The role of mortar is important to understand the behaviour of the fine particles (limestone filler and crumb rubber) with sand-size aggregates and binder. To investigate this role samples with normalized sand-size aggregates (below 2mm) were made, starting from a typical Stone Mastics Asphalt (SMA) grading curve as a reference, and normalizing the aggregates passing the 2 mm sieve.

6.7.1 Mortar Design

6.7.1.1 Fine aggregates normalization

The A Bitumen (PWmB) was used for producing the mortar samples. The crumb rubber and the limestone filler are the same used for all the mastics. Bardon Hill Quarry dust (Fine igneous aggregates) was used for mortar blending. A traditional SMA grading curve has been normalized on the particle percentages below 2mm to find the mortar grading curve. The total passing at sieve 2[mm] was considered equal to 100% and consequently, the other sieves have been normalized. Bitumen and crumb rubber percentages were then calculated on the aggregates weight. Passing Fine Aggregate Normalized (i) below 2[mm] has been calculated from the following formula:

$$\text{Passing Fine Aggregate Normalized (i)} = \text{Total passing (i) [mm]} \times \frac{100}{\text{Total passing [2mm]}} \quad (6.9)$$

Table 6.29 and Figure 6.23 show the normalized SMA grading curve for mortar design.

Table 6.29 Normalized SMA grading curve.

Sieve Size [mm]	Total Passing [%]	Passing [%] Normalized [2mm]
40	100	
31	100	
20	100	
16	100	
14	100	
12.5	100	
10	100	
8	97.5	
6	82.8	
4	40.1	
2	24.8	100.00
1	19.8	79.84
0.5	16.8	67.74
0.25	13.4	54.03
0.125	10.9	43.95
0.063	9	36.29

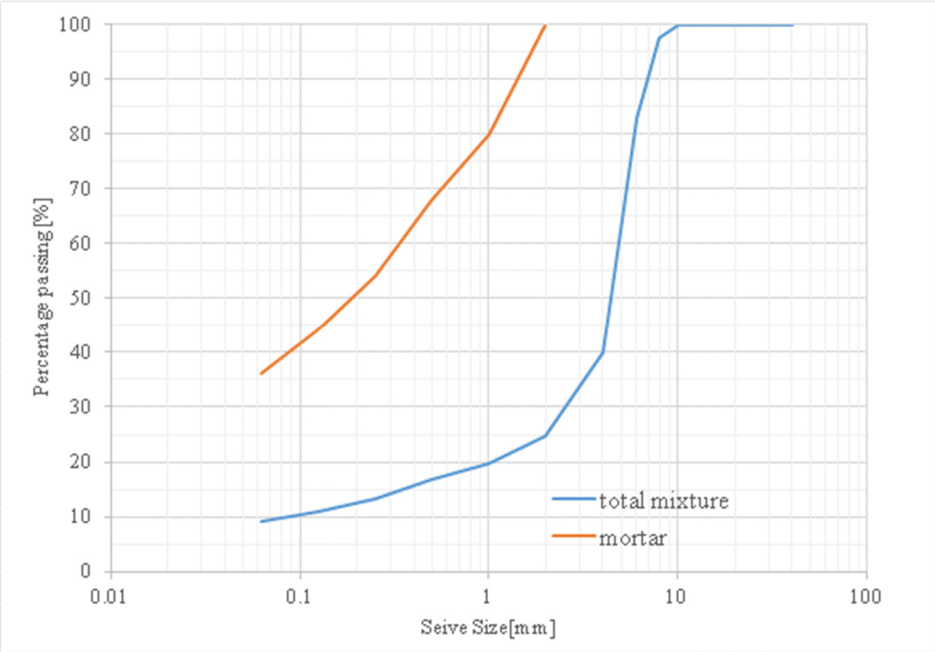

Figure 6.23 Total mixture and mortar grading curves.

6.7.1.2 Bitumen, Rubber and Filler normalization

For mixing a mortar with the right percentage of bitumen, a normalized percentages of the bitumen (and Rubber) is needed, therefore the percentages of Bitumen and Rubber have been also normalized;

$$B_{FA} = B_A \times \frac{100}{\text{Total passing[2mm]}} \tag{6.10}$$

$$R_{FA} = R_A \times \frac{100}{\text{Total passing[2mm]}} \tag{6.11}$$

$$F_{FA} = F_A \times \frac{100}{\text{Total passing[2mm]}} = \text{passing normalized[0.063 mm]} \tag{6.12}$$

where:

B_{FA} = Bitumen % on Fine aggregates

R_{FA} = Rubber % on Fine aggregates

F_{FA} = Filler % on Fine aggregates

B_A = Bitumen % on Total aggregates

R_A = Rubber % on Total aggregates

F_A = Filler % on Total aggregates

Finally, normalizing all the components the mortar mixture percentages were found as follows:

$FA_{FA}(i-j)$ = Normalized Fine Aggregates retained between sieves$(i-j)$ %(except filler)

$FA_m(i-j)$ = Fine Aggregates retained between sieves$(i-j)$ %(except filler) on mortar

$$B_m = \frac{B_{FA}}{\sum FA_{FA}(i-j)+F_{FA}+B_{FA}+R_{FA}} \tag{6.13}$$

$$R_m = \frac{R_{FA}}{\sum FA_{FA}(i-j)+B_{FA}+R_{FA}+F_{FA}} \tag{6.14}$$

$$F_m = \frac{F_{FA}}{\sum FA_{FA}(i-j)+B_{FA}+R_{FA}+F_{FA}} \tag{6.15}$$

$$FA_m(i-j) = \frac{FA_{FA}(i-j)}{\sum FA_{FA}(i-j)+B_{FA}+R_{FA}+F_{FA}} \tag{6.16}$$

6.7.1.3 Mortars Combinations

The same combinations used in mastic have been used to create the mortars. The amount of limestone filler, bitumen and crumb rubber were normalized using the described normalization method.

Table 6.30 Mortar percentage composition.

A BITUMEN				
Mortar Name Code	**%Bitumen**	**%Rubber**	**%Filler**	**%Fine Aggregates**
MoA_7_1_5	23.73	3.39	16.95	55.93
MoA_8.5_1.2_5	27.24	3.85	16.03	52.88
MoA_8_1_6	26.23	3.28	19.67	50.82
MoA_7.5_0.75_5	25.21	5.65	16.81	55.46
MoA_SMA	42.31	0.00	28.66	50.32

6.7.2 Mortar Preparation

Maximum densities for all mortars have been found using the density of the materials shown in Table 6.31.

Table 6.31 Mortar components density.

Material	**Density [g/cm^3]**
Bitumen	1.030
Limestone Filler	2.500
Rubber	1.000
Bardon Hill dust	2.800

The maximum density and target density have been found using 2% air void.

Table 6.32 Mortar target density.

Mortar sample	**Target Air void**	**Maximum density [kg/m^3]**	**Target Density [kg/m^3]**
MoA_7_1_5	2%	1880	1842
MoA_8.5_1.2_5	2%	1800	1764
MoA_8_1_6	2%	1826	1789
MoA_7.5_0.75_5	2%	1868	1831
MoA_ SMA	2%	2000	1960

Mortar samples were made using normalized percentages of the fine aggregates, rubber and bitumen based on mass of aggregates. Fine aggregates were stored in oven

overnight at 160 °C to reach the dry condition needed for mixing. Mortar samples have been made at about 160 °C by hand mixing. Temperature was controlled regularly during mixing. First the fine aggregates were poured into the mixing pot, then the bitumen was added and after few minutes the rubber was added to the mixture.

Figure 6.24 Mortar mixing process.

The obtained mortar was mixed for 5 minutes. The mould described in Table 6.33 was used to make the mortar samples:

Table 6.33 Mould description.

Mould	Sample Shape	Diameter [mm[	Height [mm]
Solid Fixture Mould	Cylinder	12.3	50

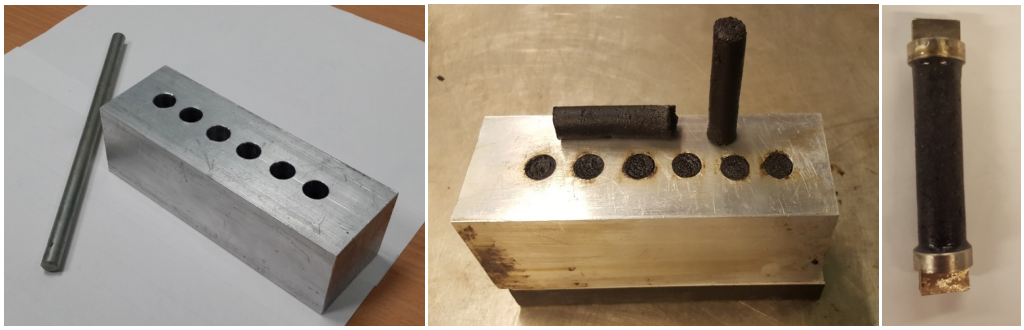

Figure 6.25 Mould and mortar samples extraction.

The mortars have been extracted and stored in 5° C. Table below shows the sample densities and internal air voids.

Table 6.34 Mortar samples density.

Mortar Sample	Weight [kg]	Air void [%]	Density [kg/m^3]	Target Density [kg/m^3]
MoA_8.5_1.2_5	0.56	2.14	1806	1764
MoA_7_1_5	0.59	1.04	1872	1842
MoA_7.5_0.75_5	0.57	1.83	1863	1831
MoA_8_1_6	0.58	1.90	1832	1789
MoA_SMA	0.64	2.12	2022	1960

6.8 Mortar Testing Programme

6.8.1 Test Equipment and Sample Preparation

The **Kinexus – Malevern** DSR (Figure 6.26) Dynamic Shear Rheometers (DSR) has been used to measure the mortar rheological properties.

Figure 6.26 Kinexus – Malvern rheometer.

Mortar samples have been tested using Solid Fixture configuration for torsional loading. The Kinexus uses an active hood for reaching the required temperature in the chamber. The Peltier Cylinder cartridge for the Kinexus rheometer provides multifunctional configuration options to meet the temperature (Figure 6.27).

Figure 6.27 Kinexus – Malvern temperature chamber.

The samples were left at the room temperature (25°C approximately) from the store room (5°C) for an hour before conditioning to avoid sudden variation in the sample temperature. The conditioning was applied for an hour before commencing the test. A

sufficient amount of instant adhesive glue has to be placed on the disposable plate and sample surfaces on both sides. To ensure satisfactory bond additional glue sited around the circumference of the sample edges and plates. 10 minutes were allowed for the glue to stiffen enough (Elnasri 2014). The sample has been clumped to the solid fixture by two bolts before installing the system inside the device (Figure 6.28).

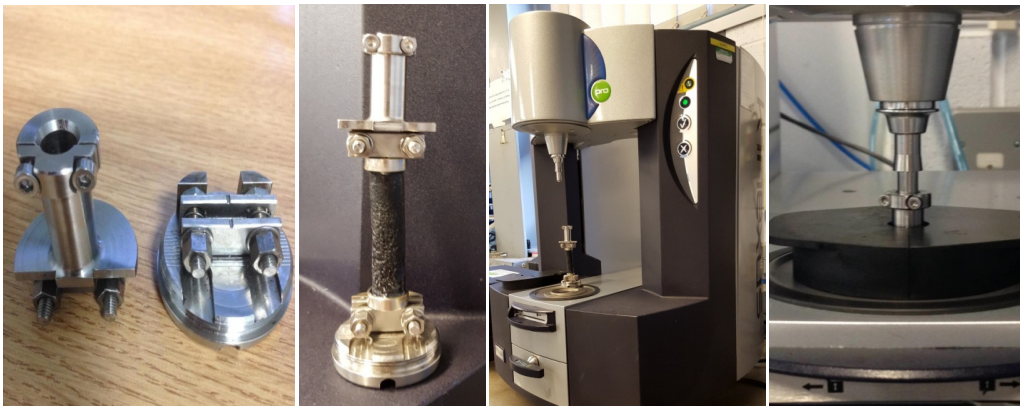

Figure 6.28 Mortar samples installation.

6.8.2 Frequency Sweep Test

Dynamic mechanical analysis, using oscillatory tests, was performed on the five mortars to determine their rheological properties. The tests were performed under controlled strain, and the strain amplitude was limited within the Linear ViscoElastic (LVE) response of the samples. In particular a strain level of 0.0065 % has been imposed. Data were obtained from frequency sweep tests between 0.01 and 10 Hz, conducted between 10°C and 60°C. The solid fixture configuration with a cylindrical sample of 12.3 mm of diameter and 50 mm of height was adopted in all temperature range. The sample was conditioned for 30 minutes for each temperatures in order to reach the internal temperature equilibrium. Also for this configuration the rheological parameters obtained were the complex shear modulus G* and phase angle δ.

6.9 Mortar Test Results and Discussion

6.9.1 Master Curves

The mortar master curves were built applying the temperature-time superposition principle and the WLF theory. The TTS principle is valid also in the case of bituminous mortars, as demonstrated by the continuous master curves trends. As shown in Figures 6.29-6.30-6.31-6.32-6.33 the mortar master curves in terms of G* are parallel to those of mastics. This result confirms that the proportion of the single components within the mortar has been correctly designed and that the rheological behavior of the mortar (master curve slope) is related to the rheological behavior of the mastic. The stiffness increase between mortar and mastics is because of the skeleton presence given by the combined action of the lytic fine aggregates and the limestone filler. In fact, as can be seen in Figures 6.29-6.30-6.31-6.32-6.33, in the case of mortar with the highest percentage of filler, the horizontal asymptote at high temperatures is accentuated; the limestone filler decreases the deformation susceptibility of the mixtures at high temperatures. The elastic response of bituminous mortar containing both limestone filler and crumb rubber is analogous to that of mastics at high temperatures. The MoA_SMA is the only mortar that show an elastic behavior higher than the corresponding A_SMA mastic. At medium and low temperatures the mortar shows higher elastic response than that of the mastics. If in fact in the case of bituminous mastics at low temperatures the phase angle values are between 30 and 40 ° in the case of the mortar the phase angle values are between 25 and 35°. This may be due to the fine aggregates skeleton that increases the mortar elastic behavior. In Table 6.35 the complex modulus rate increasing from mastics to mortar master curves are reported. The MoA_8.5_1.2_5 mortar with the highest bitumen percentage has the highest stiffness average percentage increase. The mortar with lowest bitumen percentage (MoA_SMA, MoA_7_1_5 and MoA_7.5_0.75_5) have the lowest G* average percentage increase. The MoA_SMA and the MoA_8_1_6 show the highest percentage stiffness increasing at low frequencies, confirming the limestone filler action at the high temperatures. In Table 6.35 are reported the complex modulus rate increasing from mastics to mortar master curves. The MoA_8.5_1.2_5 mortar with the highest bitumen percentage has the highest stiffness average percentage increasing. The mortar with the lowest bitumen percentage (MoA_SMA, MoA_7_1_5 and

MoA_7.5_0.75_5) have the lowest G* average percentage increase. The MoA_SMA and the MoA_8_1_6 show the highest percentage stiffness increasing at low frequencies, confirming the limestone filler action at the high temperatures.

Table 6.35 Mortar complex modulus rate increasing.

Mortar Sample	Low Frequencies	Medium Frequencies	High Frequencies
	Stiffness Increasing [%]	Stiffness Increasing [%]	Stiffness Increasing [%]
MoA_8.5_1.2_5	92	95	95
MoA_7_1_5	90	91	85
MoA_7.5_0.75_5	93	92	89
MoA_8_1_6	96	93	94
MoA_SMA	94	91	88

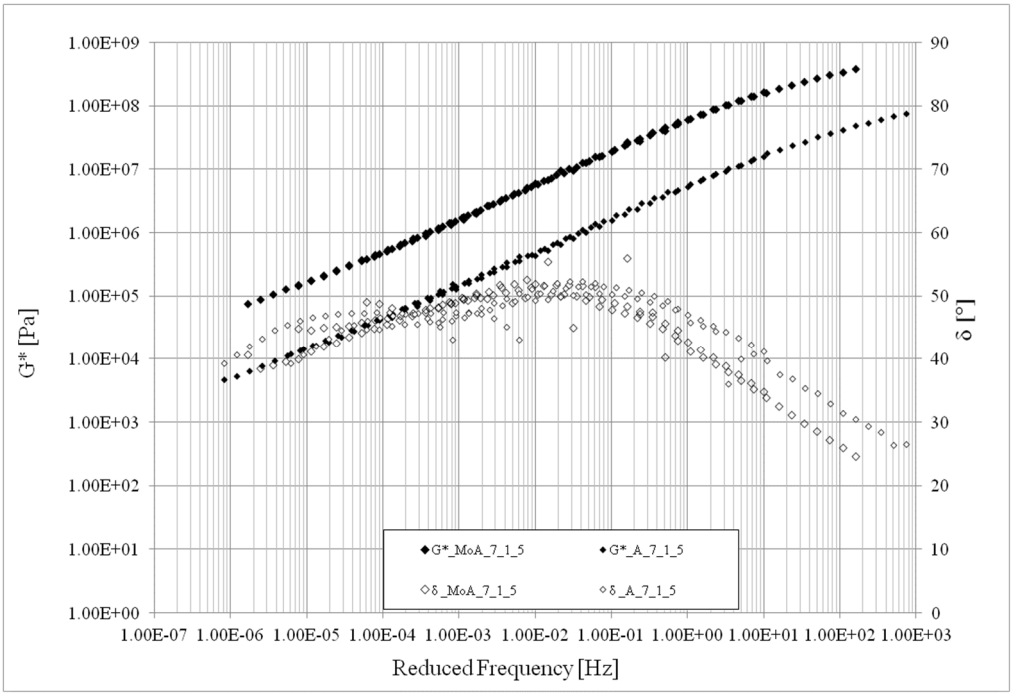

Figure 6.29 MoA_7_1_5 Mortar and A_7_1_5 mastic master curves comparison.

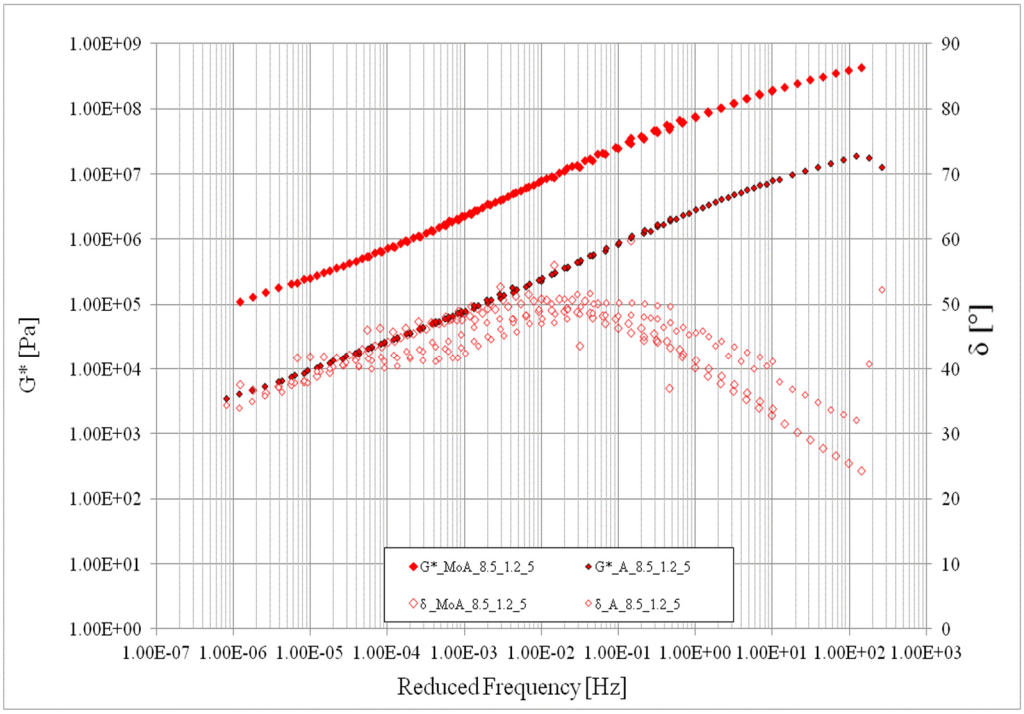

Figure 6.30 MoA_8.5_1.2_5 Mortar and A_8.5_1.2_5 mastic master curves comparison.

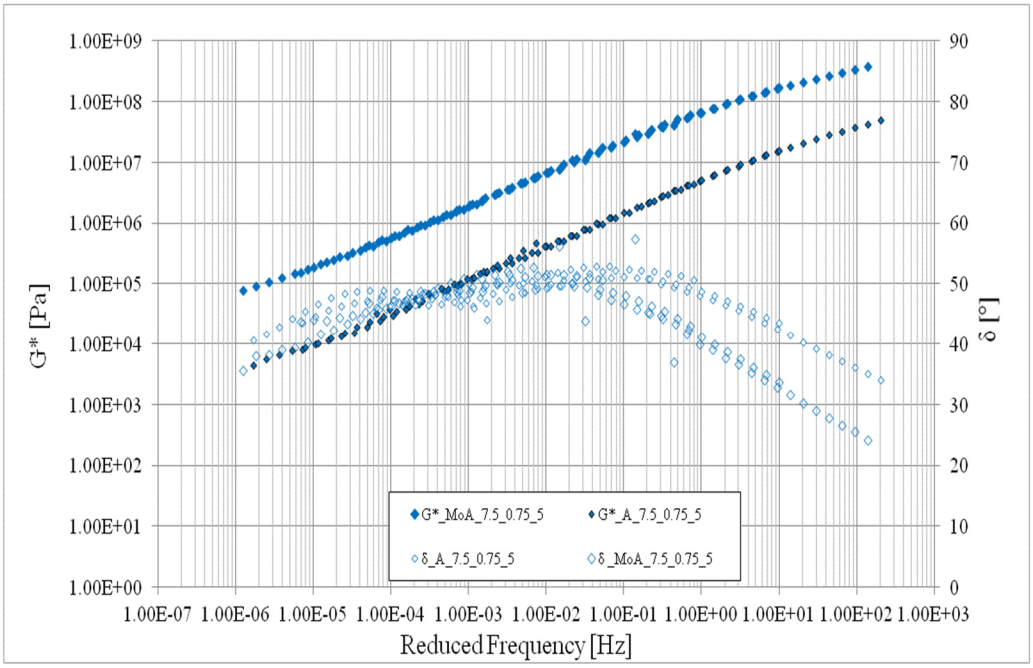

Figure 6.31 MoA_7.5_0.75_5 Mortar and A_7.5_0.75_5 mastic master curves comparison.

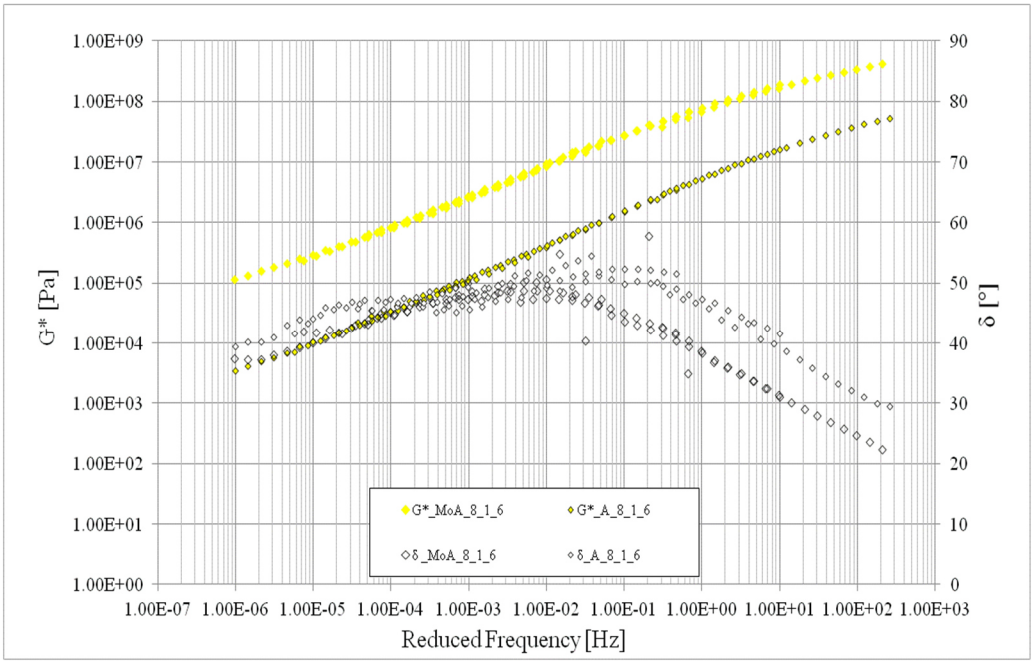

Figure 6.32 MoA_8_1_6 Mortar and A_8_1_6 mastic master curves comparison.

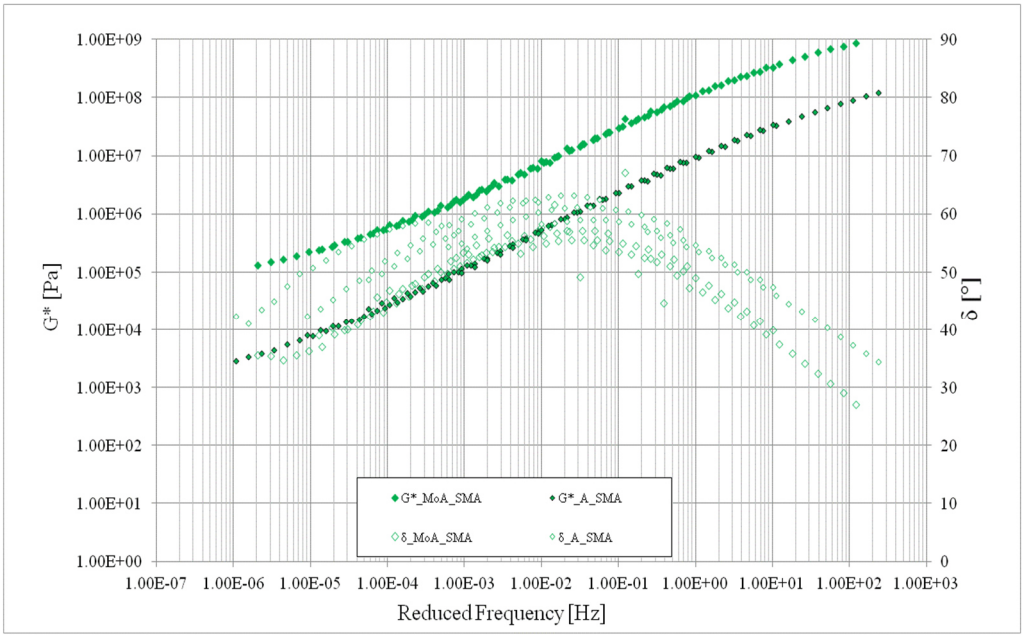

Figure 6.33 MoA_SMA Mortar and A_SMA mastic master curves comparison.

Figure 6.34 shows the mortar samples G* master curves comparison. At low frequencies (high temperatures) MoA_8_1_6, MoA_8.5_1.2_5 and MoA_SMA mortars have the highest values of complex modulus G*. However, it is necessary to distinguish the action of the individual components within each mortar. In the case of MoA_SMA, the presence of the highest proportion of limestone filler (28.66% by

mass) increases the cohesion between the fine aggregate and the bitumen, creating, at high temperatures, a matrix that is solid, homogeneous and resistant to torsion stresses. For the mortars containing both limestone filler and fine crumb rubber, the MoA_8_1_6 (50.82% by mass of fine aggregates, 19.67% by mass of limestone filler, 28.3% by mass of rubber, 26.23% of bitumen) and MoA_8.5_1.2_5 (52.88% by mass of fine aggregates, 3.16% by mass of limestone filler, 3.85% by mass of rubber, 27.24% of bitumen) have the same complex modulus and higher than those of the other studied mastics. However in the first case, the highest limestone filler percentage creates a strong cohesive bond with the fine aggregates fraction at high temperature; in the second case the 1% bitumen more and the 2% fine aggregates more, increasing the mortar stiffness at low frequencies in spite of 3.65% limestone filler reduction. MoA_7_1_5 and MoA_7.5_0.75_5 have the lower complex modulus. Both mastics have the highest percentage of fine aggregates (56% by mass), and the lowest bitumen percentage, 25 and 24% respectively. The lower specific surface of the fine aggregates and the low bitumen percentage affects the mortar cohesion, reducing its stiffness at high temperatures. At medium and high frequencies all the mortars containing both limestone filler and rubber tend to the same of complex modulus value. The MoA_SMA with only limestone filler showed the stiffer behavior, and consequently more fragile at low temperatures. The rubber powder therefore acts mainly at low temperatures reducing the stiffness of the mortar. As showed on Figure 6.35, all the studied mortars show a continuous trend of the phase angle, with a descending arm at high temperatures. At low frequencies mortars stress response is perfectly visco-elastic (δ=45°). At medium and high frequencies there are the main differences between the mortars containing both crumb rubber and limestone filler and MoA_SMA. For the mortar containing both limestone filler and crumb rubber the phase angle varying from a minimum value of 25° to a maximum value of 50°. For the mastic containing only limestone filler, the phase angle range is between a minimum of 25° and a maximum of 60°. From the analysis of the phase angle trend and Black diagram (Figures 6.35-6.36) it is evident that the crumb rubber works mainly at low temperatures if compared to the limestone filler that increases the torsion stress response of mortar at high temperatures.

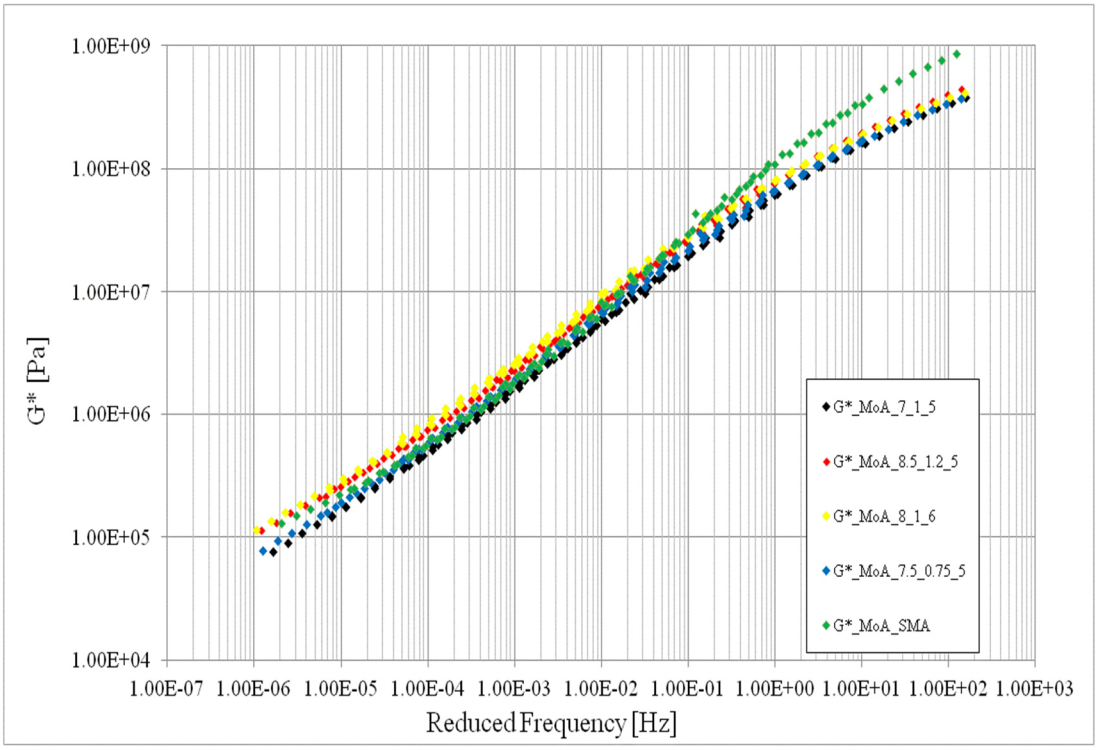

Figure 6.34 Mortar samples G*master curves comparison.

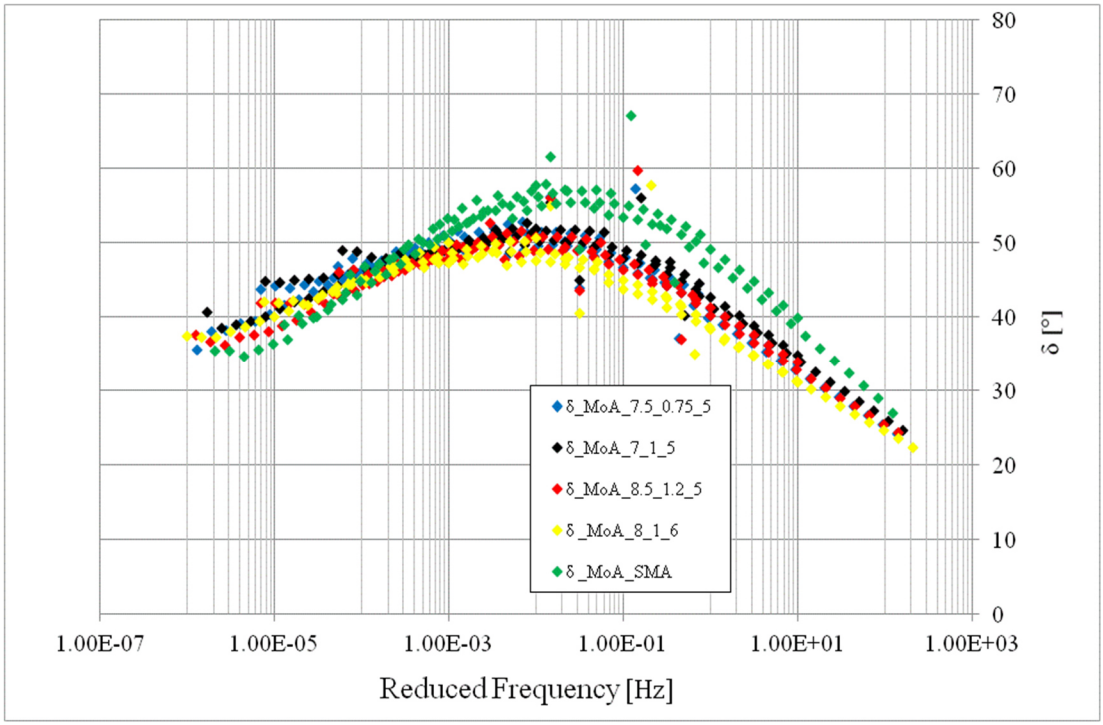

Figure 6.35 Mortar samples δ master curves comparison.

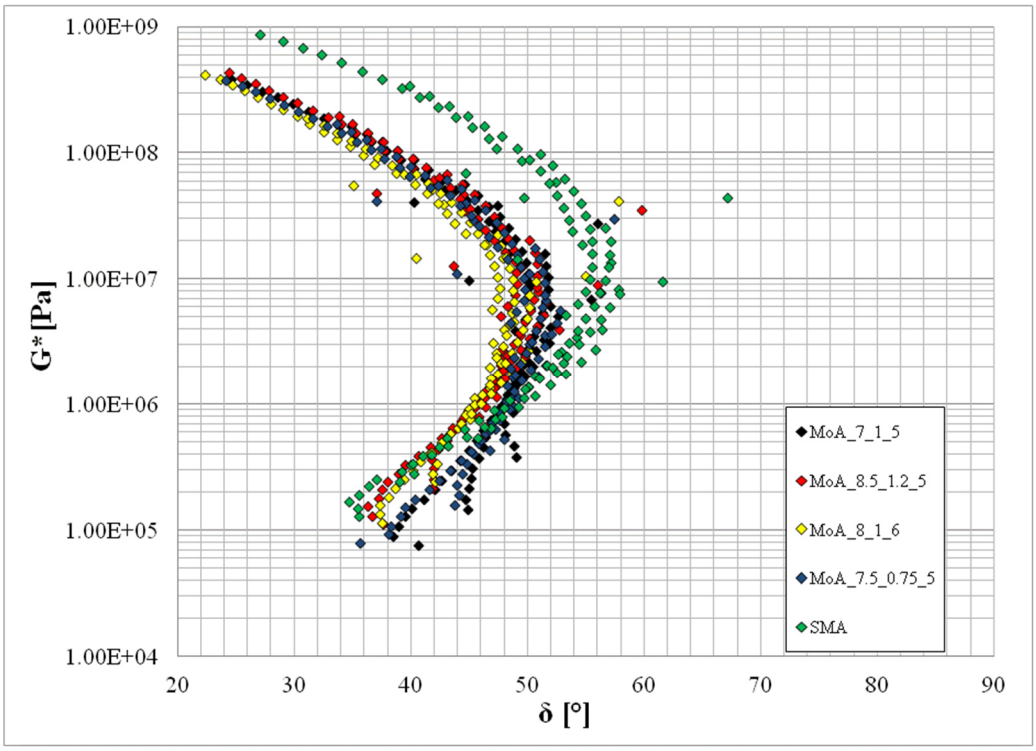

Figure 6.36 Mortar Balck Diagram

6.10 Summary

The main objective of this study is to evaluate the rheological properties of mastics and mortars containing crumb rubber and limestone filler, and find the optimum percentages of the components for the asphalt mixture increasing permanent deformations resistance. In particular:

- the interaction between fine crumb rubber and limestone filler, gives more stiffness to the mastics, reduces phase angles values and raises the rutting parameter; the fine crumb rubber used as filler reduces mastic thermo-sensitivity;
- on mastics with highest limestone filler amount G* values increases in all range frequencies. This effect continuous in mortar combination as well, at high temperatures, in correspondence of which the filler presence increases the permanent deformation resistance;
- in terms of MSCR results, the mastics containing both limestone filler and crumb rubber exhibits the lowest accumulated strains values at the end of load cycles. This results reflects the J_{nr} results on mastics containing rubber as part of active filler. The rubber presence increase the mastic recovery;
- polymer modified bitumen plays a significant role especially when the polymer modification is enhanced by the base bitumen characteristics; the fine crumb rubber elastic behavior is exalted with the polymer modified bitumen;
- the mortar master curve slope validates the mix design. The rheological behavior is depending on mastics matrix, the coarse aggregate increase the stiffening uniformly, the fine crumb rubber and limestone filler contribute to change the master curve slope;
- the 3D DEM model has given more information to understand the internal mastic behavior, confirmed the shear stress response increasing for the mastic containing rubber.

CHAPTER 7 – CONCLUSIONS AND RECOMMENDATIONS

The research presented in this thesis was based on three main topics:

- *Validation methods for the rheological characterization of cold bituminous mastics*
- *Identifying 3D Discrete Elements Particles models that are able to reproduce rheological tests in the Linear Visco-Elastic range*
- *Rheological study of bituminous mastics containing reclaimed filler from industrial wastes and by-products.*

7.1 Validation methods for the rheological characterization of cold bituminous mastics.

It was proven that rheological tests with the DSR in the study of cold bituminous mastics provide consistent results and that the principles behind the linear analysis of hot bitumen is valid also for that type of material. In particular, the mastics tested within the linear viscoelastic range exhibited a simple thermo-rheological behavior, as derived from the study of complex modulus and phase angle master curves. The time-temperature superposition principle (TTS) was applied. and results were represented by continuous curves in the Black Diagrams.

The creep tests carried out in various test configurations were confirmed also for the mastics, to be useful for the assessment of the rutting phenomenon of asphalt pavements at high temperatures. Correlating the J_{nr} and the recovery percentage parameters allowed to study the mastics sensitivity to permanent deformations. The obtained results show sufficient reproducibility of RCR and MSCR tests on mastics. For these testing procedures it can be stated that the 3.2 kPa could be not sufficient to conduct a non-linear analysis in terms of deformations, in particular if the mastics exhibit high recovery rates.

The dynamic tests conducted on mastics also permitted to better understand the role of mineral fillers in the mixtures, validating the multiscale approach through which it was possible to evaluate the interaction between bitumen and filler and consequently its effects on the asphalt mixtures stiffness In particular, based on the performed rheological analysis and the investigated volumetric proportions, it can be stated that,

in the cold mix design process, cement could be partly replaced with limestone filler, increasing the performance of the mixture related to the phenomenon of permanent deformations at high temperatures.

7.2 Identifying 3D Discrete Elements Particles models that are able to reproduce rheological tests in the Linear Visco-Elastic range.

3D Discrete Element Particles models to reproduce DSR Frequency Sweep Test on LVE range was developed. The mastic specimen was modeled through spherical particles for which radius, density, friction coefficient and temperature were defined. The contact particles parameters was defined through the Burger's viscoelastic model, with a calibration procedure based on laboratory testing data. The DSR metal plates were schematized by means of two horizontal walls, for which a linear elastic stiffness model was also defined. The sinusoidal load was simulated imposing angular speed with a sinusoidal trend to the top of the wall. The obtained results in terms of contact forces and particles displacements were compared with laboratory data. There is very good correlation between model and laboratory results and it can be affirmed that the use of DEM method to model dynamic test on mastics is successful in predicting, both quantitatively and qualitatively, the mastics complex modulus and the phase angle. Moreover, the micro-scale analysis is suitable to capture the real time-dependent behavior of asphalt binder and to predict its performance through the study of its internal interaction. Contact forces and displacements obtained by the simulation tests have given useful information about the filler-bitumen interaction in terms of stiffening effects.

7.3 Rheological study of bituminous mastics containing reclaimed filler from industrial wastes and by-products.

7.3.1 Fillers from waste bleaching clays

The effects on the rheological properties of bituminous mastics made with two waste bleaching clays, obtained from two different industrial processes, was here studied. Mastics with traditional limestone filler were made as reference to compare the rheological results. All the rheological test validated on cold mastic studies has been applied. From the analysis of mastics master curves it can be stated that the substitution of the limestone filler with the proposed bleaching clays fillers is significantly effective on altering their rheological behavior. In particular, the study at the mastic scale

confirmed that the digested bentonite increases the bitumen stiffness, while the spent bentonite filler softens the mastic by a considerable amount. The high specific surface area, and the high Rigden voids percentage, transmit to the digested filler good properties in terms of bitumen interaction. The RCR and MSCR tests results confirms that this filler increases the mastic resistance to permanent deformations. Furthermore, the residual oil in the spent bentonite filler is evidently interacting with the bituminous phase. This filler reduces the mastic stiffness in all the frequency range and the J_{nr} analysis confirms that the non recovered deformations are increasing in the mastic containing the spent bentonite.

Positive aspects related to the possible use of these mastics in road bituminous pavements are referred to the fact that the mastic containing the oily filler does not reach the glassy modulus at high frequencies (low temperatures) and that the mastic obtained with the digested bentonite is stiffer than the mastic with traditional filler at high temperatures (low frequencies).

The overall rheological analysis confirms that the fillers obtained as residual of Bio-Gas production appears to have more positive effects on the mastic of an HMA and this is mainly due to the stiffening power of this digested bleaching clay; nevertheless some positive aspects of the use of filler from bleaching plants process may be capitalized on the production of bituminous sealants or membranes were high percentages of fillers are used.

7.3.3 Crumb Rubber Filler from ELTs

The effects of fine crumb rubber from ELTs, used as active filler on SMA surface layers was investigated. The interaction between fine crumb rubber and limestone filler, provides the mastics with more stiffness, reduces the phase angles values and the MSCR rutting parameter. Also, the fine crumb rubber used as filler reduces the mastic thermo-sensitivity, emphasizing the polymer modification benefits within the bitumen.

The multiscale analysis on bituminous mortars confirms that the mixtures rheological behavior depends on the mastics internal components. The fine rubber influenced the rheology increasing the elastic properties ,while the limestone fillers increased the mixture stiffness at high temperatures. The improvement of the characteristics of SMA

asphalt mixtures containing rubber modified by ELTs during production, installation and operation, required a careful study of fine rubber proportion with the mixtures.
In terms of mix design it can be stated that the mixtures containing 8% of bitumen, 1% of fine crumb rubber and 6% of limestone filler on weight of aggregates could be suggested to combine the rubber elastic properties and the limestone filler stiffening power. In terms of mixture production the use of PmWB permits to use the fine rubber reducing the mixing temperatures (160°C temperatures mixing) and consequently the environmental externalities generated heating the rubber at temperatures higher than 180°C. The here developed solution, subjected to experiments described in the experimental section, confirm the feasibility of mixing a fine rubber powder system together with a modified bitumen of high workability and aggregates. The process allows the elimination of the commonly used fibers and enables the production at reduced temperatures, with all the environmental benefits that this entails, especially in the coating phase.

REFERENCES

Chapter 2 - LITERATURE REVIEW: MATERIALS

Paliukaite M., Vaitkusa A., Zofkab A. (2014) "Evaluation of bitumen fractional composition depending on the crude oil type and production technology", The 9th International Conference "ENVIRONMENTAL ENGINEERING" 22–23, Vilnius, Lithuania SELECTED PAPERS. eISSN 2029-7092 / eISBN 978-609-457-640-9.

Didier L. (2009). "The colloidal structure of bitumen: Consequences on the rheology and on the mechanisms of bitumen modification", Advances in Colloid and Interface Science. Vol.145, pp. 42–82.

Mazzotta F. (2012). "Studio reologico avanzato di bitumi modificati ed additivati: proposta di una nuova procedura di aing". Tesi di Laurea Magistrale, in Costruzione di Strade Ferrovie e Aeroporti M. Scuola di ingegneria e Architettura. Università di Bologna.

Liao M.-C. (2007). "Small and Large Strain Rheological and Fatigue Characterisation of Bitumen-Filler Mastics". PhD Thesis, School of Civil Engineering. University of Nottingham.

Traxler, R.N. and Miller, J.S. (1936). "Mineral Powders, Their Physical Properties and Stabilizing Effects", Proceedings of the Association of Asphalt Paving Technologies, Vol. 7.

Tunnicliff D.G. (1962). "A Review of Mineral Filler", Journal of the Association of Asphalt Paving Technologies, Vol. 31, pp. 119-147.

Anderson D.A., Goetz W.H. (1973), "Mechanical behavior and reinforcement of mineral filler-asphalt mixtures". Proceedings of the Association of Asphalt Paving Technologists. Vol.42, pp.37-66.

Faheem A. F., Bahia H.U., Yang S-H, and Al-Qadi I. (2012) Evaluation of Rigden Fractional Voids Test Method and the Relation to Mastic Viscosity. Transprt Research Board (TRB), Washington, U.S.

Faheem, A., and Bahia, H. (2009). "Conceptual phenomenological model for interaction of asphalt binders with mineral fillers." J. Assoc. Asphalt Paving Technol., Vol. 78, pp. 679–720.

Faheem, A., Wen, H., Stephene, L., and Bahia, H. (2008). "Effect of mineral filler on damage resistance characteristics of asphalt binders." J. Assoc. Asphalt Paving Technol., Vol.77,pp. 885–908.

Liao M.C., Chen J.S. and Tsou K.W. (2012)"Fatigue Characteristics of Bitumen-Filler Mastics and Asphalt Mixtures" J. Mater. Civ. Eng.24:916-923.

Mogawer WS, Stuart KD (1996), "Effects of mineral fillers on properties of stone matrix asphalt mixtures". Transportation Research Record 1530, Transportation Research Board, National Research Council, Washington DC, USA. TBR 86-94.

Puzinauskas VP (1969) "Filler in asphalt mixtures". The Asphalt Institute Research Report 69-2, Lexington, Kentucky.

Kallas BF, Puzinauskas VP (1967), "A study of mineral fillers in asphalt paving mixtures". Proceedings of the Association of Asphalt Paving Technologists 36:493-528.

Kandhal P.S., Parker F. (1998), "Aggregate tests related to asphalt concrete performance in pavement". NCHRP Report 405, Transportation Research Board, National Research Council, Washington DC, USA.

Kandhal PS (1981), "Evaluation of bag house fines in bituminous paving mixtures". Proceedings of the Association of Asphalt Paving Technologists Vol. 5, pp.150-210.

Muniandy R., Aburkaba E. and Taha R. "Effect of Mineral Filler Type and Particle Size on the Engineering Properties of Stone Mastic Asphalt Pavements". TJER 2013, Vol. 10, No. 2, pp.13-32.

Elnasri M. (2014) "From binder to mixture; multiscale permanent deformation behavior" Ph.D. Thesis, Department of Civil Engineering, University of Nottingham, United Kingdom.

Deshpande, V. & Cebon, D. (1999). Steady-state constitutive relationship for idealised asphalt mixes. Mechanics of materials, 31, 271-287.

Deshpande, V. & Cebon, D. (2000). Uniaxial experiments on idealized asphalt mixes. Journal of Materials in Civil Engineering, 12, 262-271.

Ghaffarpour Jahromi S., Khodaii A. (2009)"Effects of nanoclay on rheological properties of bitumen binder" Construction and Building Materials Vol. 23 pp. 2894–2904.

Grim RE. "Physical-chemical properties of soils clay minerals". J Soil Mech Found Div ASCE 1959;85.

Chen M., Lin J., Wu S. (2011). "Potential of recycled fine aggregates powder as filler in asphalt mixture Construction and Building Materials". Vol. 25, pp. 3909–3914.

Chen M-Z., Lin J., Wu S., Liu G. (2011). "Utilization of recycled brick powder as alternative filler in asphalt mixture Construction and Building Materials. Vol.25, pp. 1532–1536.

Melotti R., Santagata E., Bassani M., Salvo M., Rizzo S. (2013). "A preliminary investigation into the physical and chemical properties of biomass ashes used as aggregate fillers for bituminous mixtures". Waste Management. Vol. 33 pp.1906–1917.

Charamia, Equbalali, Joe A. Cano, and Russell N. Schnormeier.(1991) "Twenty Year Study of Asphalt-Rubber Pavements in the City of Phoenix, Arizona." Presented at the 70th Annual Meeting of the Transportation Research Board, Washington, DC.

Tataranni P., (2012).“Applicazione sperimentale del polverino di gomma nella tecnica di riciclaggio a freddo con emulsione bituminosa e cemento: confronto tra polverino tradizionale e criogenico”. Tesi di laurea in Ingegneria Civile, Università di Bologna.

Viola P., (2013)“Caratterizzazione avanzata in laboratorio di materie prime secondarie rigenerate o stabilizzate con emulsione di bitume e leganti cementizi ”, Dottorato di ricerca in Ingegneria geomatica e dei trasporti, Università di Bologna.

Antunes I., Giuliani F., Sousa J.B., Way G.“Asphalt Rubber: bitume modificato con polverino di gomma di pneumatico riciclata”, Università degli studi di Parma.

Ecopneus in collaborazione con politecnico di Torino, “L’impiego di prodotti da Pneumatici Fuori Uso nelle pavimentazioni stradali”.

Dondi G., Tataranni P., Pettinari M.., Sangiorgi C., Simone A., Vignali V.(2014). “Crumb Rubber in cold recycled bituminous mixes: Comparison between Traditional Crumb Rubber and Cryogenic Crumb Rubber”. Construction and Building materials. Vol.68, pp. 370-375.

Chen, J.S. and Peng, C.H. (1998). “Analyses of Tensile Failure Properties of Asphalt-Mineral Filler Mastics”, Journal of Materials in Civil Engineering. Vol. 10, No.4, pp.256-262.

Chapter 3 - LITERATURE REVIEW: METHODS

Merusi F. (2009), “Metodi reologici avanzati per l’analisi del comportamento dei bitumi stradali negli stati critici di esercizio”, Tesi di Dottorato in Ingegneria Civile, Università degli studi di Parma.

Dalmazzo D.(2008), “Caratterizzazione reologica del danneggiamento per fatica e dell’autoriparazione dei leganti bituminosi”, Tesi di Dottorato in Ingneria Civile, Università delle Marche.

Yusoff N.I., Montgomery T. Shaw, Airey G.D. (2011) “Modelling the linear viscoelastic rheological properties of bituminous binders”. Construction and Building Materials. Vol.25, pp. 2171–2189.

David Anderson, Mihai Marasteanu. (2010) “Continous model for characterizing linear viscoelastic behavior of asphalt binder”. ISAP Workshop on Asphalt binders and mastics, Settembre.

Anderson, D.A., Christensen, D.W., Bahia, H. U., Dongre, R., Sharma, M. G., Antle, C. E. and Button, J. (1994). “Binder Characterization and Evaluation, Volume 3:

Physical Characterization", SHRP-A-369, Strategic Highway Research Program, National Research Council, Washington, DC, United State.

Airey, G.D. (1997). "Rheological Characteristics of Polymer Modified and Aged Bitumens", Ph.D. Thesis, Department of Civil Engineering, University of Nottingham, United Kingdom.

Kim Y-R. and Little D.N. (2005). "Development of specification-type tests to assess the impact of fine aggregate and mineral filler on fatigue damage". Report 0-1707-10. Project No. 0-1707. Research name: Long-Term Research on Bituminous Coarse Aggregate.

Shafabakhsh G.H. and Sadeghnejad Y.S. (2014). Case study of rutting performance of HMA modified with waste rubber powder. Case Studies in Construction Materials Vol.1, pp. 69–76.

Huang YH. (1993) Pavement analysis and design. USA: Prentice Hall, University of Kentucky.

Esmail M. Kabbashi A. and Ayop M.B. (2014) Rutting Performance Of Hot Mix Asphalt (HMA) during 60 degree temperature. nternational Journal of Humanities and Social Science Invention. ISSN (Online): 2319 7722, ISSN (Print): 2319 –7714. pp. 35-40.

Philips, M.C. and Robertus, C. (1996). "Binder Rheology and Asphaltic Pavement Permanent Deformation; the Zero-Shear-Viscosity", No.5134, Euroasphalt & Eurobitume Congress.

Anderson, D.A., Christensen, D.W. and Bahia, H. (1991). "Physical Properties of Asphalt Cement and the Development of Performance-Related Specifications",Journal of the Association of Asphalt Paving Technologists, Vol. 60, pp. 437-532.

Collop, A.C., Airey, G.D. and Khanzada, S. (2002). "Creep Testing of Bitumens Using the Dynamic Shear Rheometer", the International Journal of Pavement Engineering, Vol.3 (2), pp. 107-116.

Clopotel, C.S. & Bahia, H.B (2012). Importance of Elastic Recovery in the DSR for Binders and Mastics. Engineering Journal. Vol. 16(4), pp. 99–106.

NCHRP 459, (2001). Characterization of Modified Asphalt Binders in Superpave Mix Design. Transportation Research Board.

AASHTO M-320. Standard specification for performance – graded asphalt binder.

Federal Highway Administration (FHWA)-HIF-11-038, (2011).The Multiple Stress Creep Recovery (MSCR) Procedure.

Calvetti F. (2003). "Limitations and perspectives of the micromechanical modeling ofgranular materials". Mathematical and Computer Modelling, Vol. 37, pp. 485-495.

Jing L. (2003). "A review of techniques advances and outstanding issues in numerical modeling for rock mechanics and rock engineering". International Journal of Rock & Mining Sciences, vol. 40, pg. 283-353.

Giulia Manganelli G. (2013). "Studio numerico e sperimentale delle miscele di aggregati per i conglomerati bituminosi", Tesi di dottorato in Ingegneria Geomatica e dei Trasposti, Università degli Studi di Bologna.

Dondi G, Vignali V, Pettinari M, Mazzotta F, Simone A, Sangiorgi C. (2014)"Modeling the DSR complex shear modulus of asphalt binder using 3D discrete element approach". Constraction and Building Materials;vol. 54:236–46.

Dondi G, Simone A, Vignali V.(2012)"Micromechanical modelling of aggregate–aggregate interactions with distinct particle element method for virtual laboratory simulation". Proceedings of 11th International Conference on Asphalt Pavement, august 1-6, Nagoya, Japan.

Abbas A. (2004)"Simulation of the micromechanical behavior of asphalt mixtures using the Discrete Element Method". Doctor of Philosophy in Civil Engineering, Washington State University, Department of Civil and Environmental Engineering.

Baumgaertel M, Winter HH.(1989) Determination of discrete relaxation and retardation time spectra from dynamic mechanical data. Rheologica Acta; 28(6):511–519.

You Z, Buttlar WG.(2006)"Micromechanical modeling approach to predict compressive dynamic moduli of asphalt mixture using the distinct element method". Transportation Research Record. Transportation Research Board, Washington, D.C.; 1970:73-83.

Kim H, Buttlar WG.(2005) Micro mechanical fracture modeling of asphalt mixture using the discrete element method. Journal of the Association of Asphalt Paving Technologists; 74:209–223.

Kim H, Buttlar WG, Partl M. (2008) Investigation of fracture toughening mechanisms of asphalt concrete using the clustered discrete element method. 8th Swiss Transport Research Conference.

Kim H, Buttlar WG. (2009)"Micromechanical fracture modeling of asphalt mixture using the discrete element method". Advances in Pavement Engineering.

Collop AC, McDowell GR, Lee Y.(2004) Use of the distinct element method to model the deformation behavior of an idealized asphalt mixture. The International Journal of Pavement Engineering; 5(1):1–7.

Collop AC, McDowell GR, Lee YW. (2006).Modeling dilation in an idealised asphalt mixture using discrete element modeling. Granular Matter; 8(3)(4):175–184.

Collop AC, McDowell GR, Lee Y. (2007) "On the use of discrete element modelling to simulate the viscoelastic deformation behaviour of an idealized asphalt mixture". Geomechanics and Geoengineering; 2(2):77-86.

Abbas A, Masad E, Papagiannakis T, Shenoy A.(2005) "Modelling asphalt mastic stiffness using discrete element analysis and micromechanics-based models". The International Journal of Pavement Engineering; 6(2):137–146.

Dai QL, You Z. (2007)"Prediction of creep stiffness of asphalt mixture with micromechanical finite element and discrete element models". Journal of Engineering Mechanics; 133(2):163-173.

You Z, Adhikari S., Dai Q. (2008) "Three-dimensional discrete element models for asphalt mixtures". Journal of Engineering Mechanics; 134(12).

Masad E, Mahmoud E, Nazarian S. (2009)"Discrete element analysis of aggregate variability, blending, and fracture in asphalt mixture". Proceedings of the 8th International BCR2A'09 Conference; 367-376.

Mahmoud E, Masad E, Nazarian S. (2010)"Discrete element analysis of the influences of aggregate properties and internal structure on fracture in asphalt mixtures". Journals of materials in civil engineering; 22(1):10-20.

Wu J, Collop AC, McDowell GR. (2011)"Discrete element modeling of constant strain rate compression tests on idealized asphalt mixture". J. Mater. Civ. Eng.; 23(1):2–11.

Dondi G, Bragaglia M, Vignali V. (2005)"Bituminous mixtures simulation with distinct particle elements method". Proceedings of the 3rd International Congress SIIV, 22–24 September, Bari, Italy,

Dondi G, Bragaglia M, Vignali V. (2007)"Flexible pavement simulation with Distinct Particle Element Method", IV International Congress SIIV, 12-14 September, Palermo, Italy,.

Abbas A., Masad E., Papagiannakis T., Shenoy A. (2007)"Micromechanical modelling of the viscoelastic behavior of asphalt mixtures using the discrete-element method". International Journal of Geomechanics; 7(2):131-139.

Liu Y, You Z. (2008)"Simulation of cyclic loading tests for asphalt mixtures using user defined models within discrete element method". Proceedings of the GeoCongress, ASCE, Reston, Va; 742–749.

Liu Y, Dai Q, You Z. (2009)"Viscoelastic model for discrete element simulation of asphalt mixtures". Journal of Engineering Mechanics; 135(4):324-333.

Chen J, Pan T, Huang X. (2011)"Discrete element modeling of asphalt concrete cracking using a user-defined three-dimensional micromechanical approach". Journal of Wuhan University of Technology-Mater.

Adhikari S, You Z. 3D (2010) "Discrete element models of the hollow cylindrical asphalt concrete specimens subject to the internal pressure". International Journal of Pavement Engineering; 11(5):429–439.

Chpater 4 - RHEOLOGICAL AND 3D DEM CHARACTERIZATION OF TRADITIONAL BITUMINOUS MASTIC: METHODS VALIDATION

Vignali V., Mazzotta F., Sangiorgi C., Simone A., Lantieri C., Dondi G. (2014). Rheological and 3D DEM characterization of potential rutting of cold bituminous mastics. Construction and building materials Vol.73, pp.339-349.

Dondi G., Mazzotta F., Sangiorgi C., Pettinari M., Simone A., Vignali V. & Tataranni P., (2014). Influence of Cement and Limestone Filler on the Rheological Properties of Mastic in Cold Bituminous Recycled Mixtures. 3rd ICTI, Internat. Conf. on Transportation Infrastructure, Pisa, April 22-25.

Hammoum F, De la Roche C, Piau JM, Stefani C.(2002) "Experimental investigation of fracture and healing of bitumen at pseudo-contact of two aggregates". Proceedings of the 9th International Conference on Asphalt Pavements, Copenhagen.

Kose S, Guler M, Bahia HH., Masad E.(2000) Distribution of strains within asphalt binders in HMA using imaging and finite element techniques. Transportation Research board, 79th Annual Meeting, Washington.

Abbas A. (2004) "Simulation of the micromechanical behavior of asphalt mixtures using the discrete element method". Doctor of philosophy in civil engineering, Washington state university, Department of civil and environmental engineering.

Chapter 5- RHEOLOGICAL CHARACTERIZATION OF BITUMINOUS MASTICS CONTAINING WASTE BLEACHING CLAYS

Sangiorgi C, Tataranni P, Simone A, Vignali V, Lantieri C, Dondi G (2014) "Waste bleaching clays as fillers in hot bituminous mixtures". Construction and Building Materials 73: 320–325.

Mazzotta, F., Sangiorgi, C., Vignali, V., Lantieri, C., Dondi, G. (2016). Rheological characterization of bituminous mastics containing waste bleaching clays. RILEM Bookseries Vol 11, pp.595-606. Presentato 8th Intern.RILEM SIB Symposium Testing and Characterization of Sustainable & Innovative Bituminous Materials, Oct 7-9, 2016 – Ancona, ITALY.

Liao M.-C. (2007). "Small and Large Strain Rheological and Fatigue Characterisation of Bitumen-Filler Mastics". PhD Thesis, School of Civil Engineering. University of Nottingham.

Vignali V., Mazzotta F., Sangiorgi C., Simone A., Lantieri C., Dondi G. (2014). Rheological and 3D DEM characterization of potential rutting of cold bituminous mastics. Construction and building materials Vol.73, pp.339-349.

Dondi G., Mazzotta F., Sangiorgi C., Pettinari M., Simone A., Vignali V. & Tataranni P., (2014). Influence of Cement and Limestone Filler on the Rheological Properties of Mastic in Cold Bituminous Recycled Mixtures. 3rd ICTI, Internat. Conf. on Transportation Infrastructure, Pisa, April 22-25.

Elnasri M. (2014) "From binder to mixture; multiscale permanent deformation behavior" Ph.D. Thesis, Department of Civil Engineering, University of Nottingham, United Kingdom.

APPENDIX A

Dynamic Shear Rheometer - Bohlin Gemini 200

Dynamic Shear Rheometers – Bohlin Gemini 200 (DSRs), supplied at Nottingham Transportation Engineering Centre (NTEC) was used to measure the rheological characteristics of bituminous mastics obtained adding fine crumb rubber and limestone filler. The principles involving in dynamic shear rheometry testing and dynamic mechanical analysis have been reviewed in Chapter 3. In this investigation, a Bohlin Gemini 200 Dynamic Shear Rheometer having a torque range between 0.5 (μN·m) and 200 (mN·m) was used for measuring the rheological parameters through Frequency Sweep Test. This DSR is a controlled stress and strain instrument, which either applies a stress to a specimen and thus measures a resultant displacement or applies a displacement to a specimen and thus measures a resultant stress. The principal component of this rheometer is schematically shown in Figure A.1. A constant motor in the rheometer works by a drag cup system. An angular position sensor detects the movement of the measuring system attached to the shaft. The software converts the applied torque to a shear stress when displaying data, and the reading from the position sensor is converted to a shear strain (Liao 2007).

Figure 1.A Bohlin Gemini 200 device

A water bath temperature control system was used with the Bohlin Gemini 200 DSR. A bituminous sample was submerged in the circulating water bath during testing. Small Strain Rheological Analysis between 0°C and 85°C less compared to Peltier and ETM (extended temperature module) temperature controlled system. The temperature controlled system is capable of maintaining a temperature to within 0.1°C.Three types of test geometry used for the DSR testing include 25-mm standard diameter parallel plate geometry, 8-mm diameter standard parallel geometry and 8-mm diameter thick shaft parallel plate geometry. It is essential to select spindle geometry (upper plate) for DSR testing on bituminous binders due to the effect of spindle compliance on rheological measurements when testing stiff binders. Anderson et al. (1994) suggested that 25-mm standard parallel plates should be used as the complex modulus ranges from 103 to 105 Pa, and 8-mm standard parallel plates should be used as the complex modulus ranges from 105 to 107 Pa (above the complex modulus of 107 Pa, torsion bar test is suggested to be used). The 8-mm thick shaft spindle is suggested to be used as the complex modulus is above 106 Pa (Bohlin DSR Manual).

Dynamic Shear Rheometer – Anton Paar MCR 302 – Anton Paar Smart Pave 102

Figure 2.A shows the rotational Rheometer Physica MCR 302 Anton-Paar supplied to the DICAM laboratory - Section Roads, used for the test mastics validation methods described on chapter 4, for the rheological characterization of mastics containing waste bleaching clays and for the MSCR test on mastic containing both limestone filler and crumb rubber.

Figure 2.A Anton-Paar MCR 302

In Figure 3.A DSR- Anton Paar Smart Pave 102 is shown.

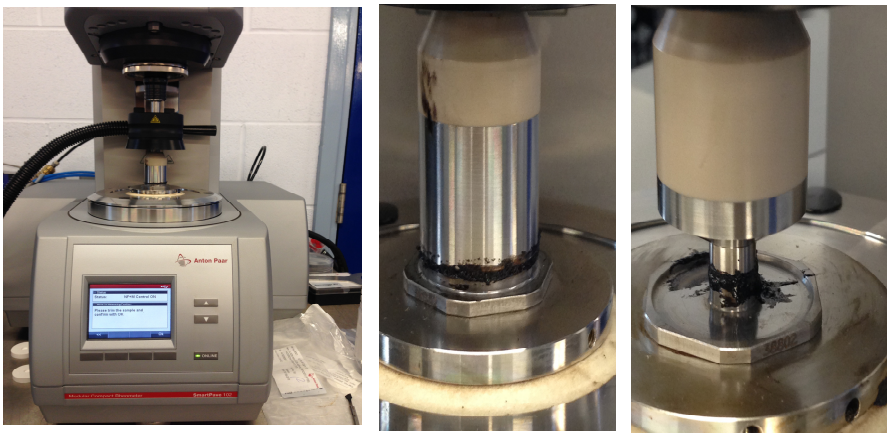

Figure 3.A Anton Paar Smart Pave 102

For both rheometers the measuring head are placed the electric motor, the bearing air and the optical encoder. All mechanical and electronic parts, such as the engine, the air bearings, the electronic control unit and the supporting structure, are incorporated in a single unit. Thanks to this configuration reduces the overall size and simplifies the instrument installation. The structure is extremely rigid, in order to optimize the mechanical and thermal stability. Together with the synchronous motor, the air bearing

used is very rigid and is equipped on the inside of a sensor able to monitor the normal stress. This system, specially developed, measuring the normal internal to the bearing efforts by identifying the normal movement of the same which is thus automatically mapped to 360°, eliminating the torque generated by turning unwanted effects at very low levels, greatly increasing accuracy and stability. The air bearing supports synchronous motor which has the task to enforce and control the torque on the motor shaft, characterized by a resolution of less than 0.002 μNm and a maximum applicable torque of 200 mNm. The motor is constituted by permanent magnets mounted on a small rotor capable of generating a constant magnetic field. The rotor surrounded by the stator comprising windings, synchronously rotates with respect to the generated magnetic field, ensuring a fast response and devoid of the system delays. It appears therefore possible to adjust the value of the torque in a simple and fast, being linearly related to the amount of current flowing through the stator. In contrast to induction motors, the magnetic field of the rotor in the synchronous motor does not change, since it does not present the problem of eddy currents that may generate heating and thus alter the characteristics of the engine. The linear response coupled to an advanced electronic control allow the system to operate in the rotation and deformation speed control. The optical encoder is used to measure the angular deflections; in combination with the Direct Strain Oscillation method (DSO), specially developed, they control the deformation oscillatory below 0.1 μrad. The Toolmaster TM system allows the recognition of the measurement systems and the fully automatic system configuration, as soon as these are ciollected. Each measuring system contains in its interior a chip on which are stored geometric coefficients and calibration, automatically transferred and managed by the software. The available allows a very accurate temperature control instrument, with minimal thermal gradients that can be monitored by means of suitable calibration of sensors due to the advanced Peltier system PTD 200. The temperature range is between -40° C and 200 °C. The system consists of a plate and a hood equipped with Peltier elements directly controlled by the rheometer. The combined control of the temperature from the top and from the bottom allows to minimize thermal gradients within the tested specimen. The hood can be raised to allow easy access to the sample. The Peltier cell is basically a heat pump solid state, by the appearance of a thin plate crossed by current; a face absorbs heat while the other makes

it. The direction in which the heat is transferred depends on the direction of the applied current. The principle of operation is simple: by passing a direct voltage through two conductors of different material, heat is absorbed from one side (side "cold"), and the other part is transferred ("hot" side). The two conductors, of N type and P type, are connected by a copper slat. If you apply to the N-type conductor and a positive voltage to the conductor of the P type a negative voltage, the upper part of the blade will cool down, while the lower one will heat. By reversing the voltage of the thermal energy shift it will also be reversed. Due to the high thermal susceptibility to viscoelastic behavior of the materials, with decreasing test temperature (and the increase of the stress rate) greatly increases the stiffness of the specimen and can reach such values as to cause the occurrence of drawbacks related to the deformability of some of the measuring instrument components. One then speaks of machine compliance, ie the onset of measurement anomalies due to the fact that the stiffness of the material has exceeded that of the machine. When the temperature conditions are particularly severe must then check that this limit is not exceeded in order to avoid misinterpretation of test results. This anomaly is explained by comparing the torsional stiffness of the specimens (dependent on temperature and / or frequency) with that of the rheometer, assumed for simplicity independent. When operating at high temperatures (or low frequency), the measures are acceptable as the stiffness of the machine turns out to be much higher than that of the samples and therefore has no influence on them. When instead it operates at lower temperatures and / or higher frequencies, the deformability of the specimen is close to that of the system and the measures completely lose their meaning: this is because the deformation transducer begins to measure, together with their deformations of the sample also those of the machine, linked in particular to the torsional deformation of the shaft of transmission of loads.